DEVELOPMENT OF IMPROVED MATHEMATICAL MODELS FOR THE DESIGN AND CONTROL OF GAS-FIRED FURNACES

Sara Alexandra Chanoca Correia

A submission presented in partial fulfilment of the
requirements of the University of Glamorgan/Prifysgol Morgannwg
for the degree of Doctor of Philosophy

December 2001

To
Mum, Dad and Lili

"You can pray for anything and if you believe....it's yours" Mark 11:24

ABSTRACT

Mathematical models based on the zone method for radiation analysis have been frequently employed to evaluate the performance of a variety of furnaces and other high temperature systems. Generally in these systems the dominant mode of heat transfer is radiation so that prediction of the thermal performance requires accurate calculation of the radiative transfer. This can be achieved by using the zone method in which the furnace enclosure is subdivided into a number of zones. Applications of the zone method, however, have been generally confined to over-simplified furnace geometries and steady-state operating conditions. In addition combustion is usually simplified, for example, by assuming nozzle mix burners where combustion is virtually complete within the burner. Moreover, the combustion products flow patterns have generally been simplified due to lack of realistic data on the overall flow in the furnace chamber. Furthermore, little is known with regard to the effect of the number and arrangement of the gas zones, adopted to represent the enclosure, on the overall accuracy of the predictions.

This present study aims to improve the applicability of zone models by overcoming some of the current limitations. For this reason both steady-state and transient operating conditions have been simulated using zoning arrangements ranging from simple long furnace models to more sophisticated multi-dimensional models. Information on the inter-zone mass flows and mixing patterns were obtained by means of an isothermal computational fluid dynamics (CFD) calculation and it was considered that this technique can provide sufficiently realistic representations of the overall flow of combustion products and heat release distribution inside the enclosure. The isothermal CFD

simulations, which were tested for grid independence and compared where possible to data from closely related problems, were capable of simulating the furnace flow and mixing patterns for a variety of burner characteristics.

The zone models were then used to investigate both the transient and steady-state thermal performance of a metal reheating furnace producing steel bars at a nominal discharge temperature of 1250°C. The effect of different zone sizes was demonstrated by varying the number of gas zones from 7 to 50 with a corresponding variation in the number of surface zones from 37 to 147. It was found that changes in the number of zones employed in the calculation could significantly alter the model predictions. Results from simpler long furnace models were compared to those obtained from more complex two-dimensional arrangements and it was shown that the use of simplified versions can lead to substantial differences in the predictions. As a result relatively fine subdivisions should be employed in regions where the flow and temperature variations are likely to be important, for example, in the near burner region. In general the use of finer zone subdivisions resulted in improved predictions albeit at the expense of additional computational time. Nevertheless, the computational effort remained competitive when compared with other alternative furnace simulation methods. The steady-state models were used to predict the discharge temperatures within the steel bars, as well as the furnace thermal performance, for a range of production rates. The transient models concentrated on predicting fuel usage, heating rates and load temperatures following a cold start-up of the furnace. In addition the transient models were used to study a period of prolonged operation.

A two-dimensional (2D) zone model was then employed to assess the influence of changes to the burner geometry including burner diameter and orientation as well as position. Furnace control was investigated by studying the effects of changes in the roof set point temperature, which is used to control the thermal input to the burners as well as by varying the position of the control sensor relative to the burners. The effect of increasing the length of the furnace to provide stock preheating was also examined. The 2D zone model was also employed to simulate other changes in the design and operation of the furnace such as the use of alternative refractory constructions and combustion air preheating equipment. The zone models were then modified to incorporate diffusion flames where combustion progresses along the furnace length. CFD calculations were employed to determine mixing rates between gas and air streams and hence heat release

rates. Two flames were studied corresponding to two different levels of excess air. Comparisons of the predictions with those for the equivalent nozzle mix cases illustrate the importance of modelling combustion heat release since it can lead to considerable variations in the heat flux profile and hence overall furnace behaviour.

Overall the potential for the use of zone models for furnace design and control purposes has been demonstrated under both steady-state and transient operating conditions. The method is sufficiently flexible to handle a range of geometries and heating cycles. The relatively short computing times, even for a relatively large number of zones, means that they are potentially suitable for online process control.

ACKOWLEDGEMENTS

I would like to express my gratitude to my Director of Studies, Professor John Ward, and my second supervisor, Dr. João Alves e Sousa, for their guidance and encouragement during the course of this work. Mr. Tony Evans should also be thanked for helping with the diagrams and for scanning images. In addition my heartfelt thanks are due to my family for their love, encouragement and constant prayers and finally I am grateful to my friends who offered companionship and constant support and have made my life throughout the PhD period more enjoyable.

TABLE OF CONTENTS

LIST OF FIGURES

LIST OF TABLES

NOMENCLATURE

A	Surface Area	m^2
a,b,c etc.	General correlation coefficients	
a_g, $a_{g,n}$	Weighting coefficient in mixed grey gas model	
C	Fuel mixture fraction	
C_p	Specific heat at constant pressure	$J\ kg^{-1}\ K^{-1}$
C_r	Thermal contact resistance	$m^2\ K\ W^{-1}$
CV_{net}, CV_{gross}	Calorific value of fuel (ref. 288K)	$MJ\ m^{-3}$
C_μ	Constant in equation 4.4 (=0.09 in k-ε model)	
d,D	Characteristic length , Turbulence dissipation length	m
E	Total hemispherical black emissive power	$W\ m^{-2}$
f	Fractional amount of fuel flow rate	
F	Proportion of maximum firing rate	
F_{ij}	View or configuration factor	
$\overline{g_i g_j}$	Gas-gas direct exchange area	m^2
$\overline{g_j s_i}$	Gas-surface direct exchange area	m^2
$\overline{G_i G_j}$	Gas-gas total exchange area	m^2
$\overrightarrow{G_i G_j}$	Gas-gas directed flux area	m^2
H	Incident radiation	W
h	Heat transfer coefficient	$W\ m^{-2}\ K^{-1}$

$H(T)$	Specific enthalpy at temperature T	J kg^{-1}
I	Radiation intensity	W m^{-2} sr^{-1}
$\mathbf{I}$	Identity matrix	
K	Radiation attenuation or extinction coefficient	m^{-1}
k	Thermal conductivity	W m^{-1} K^{-1}
k	Turbulence kinetic energy	m^2 s^{-2}
k_g	Grey gas absorption coefficient	m^{-1} atm^{-1}
k_s	Scattering coefficient	m^{-1} $(kg\ m^{-3})^{-1}$
L	Beam length	m
L_f	Flame length	m
m	Mass flow rate	kg s^{-1}
M	Mass	kg
p	Partial pressure	N m^{-2}
P_b	Proportional band	
q	Heat flux	W m^{-2}
Q	Heat transfer or release rate	W
r	Path length	m
$\vec{s}'$	Direction of radiation beam in equation 2.1	m
$\overline{s_i s_j}$	Surface-surface direct exchange area	m^2
S	Source term in equation 4.1	
$\overline{S_i G_j}$	Surface-gas total exchange area	m^2
$\overline{S_i S_j}$	Surface-surface total exchange area	m^2
$\overrightarrow{G_i S_j}$	Gas-surface directed flux area	m^2
$\overrightarrow{S_i S_j}$	Surface-surface directed flux area	m^2
t	Time	s
t_d	Turndown ratio	
T	Temperature	K
u,v	Velocity in x, y directions	m s^{-1}
V	Volume	m^3
W	Leaving radiation	W
x,y,z	Coordinate directions	m

Greek Symbols

α	Absorptivity	
δ,Δ	Interval	
ε	Emissivity	
ε	Dissipation rate	$m^2\ s^{-3}$
ϕ'	Fluctuating component of variable ϕ	
ϕ	Dependent conserved variable in equation 4.1	
Φ	Phase function	
Φ	Mean component of variable ϕ	
Γ	Diffusion coefficient	
η_{eff}	Recuperator effectiveness	%
φ	Fraction of fuel burnt	
λ	Wavelength	μm
μ	Dynamic viscosity	$N\ s\ m^{-2}$
θ	Angle	rad
ρ	Density	$kg\ m^{-3}$
ρ	Reflectivity	
σ	Stefan-Boltzmann constant ($=5.6687x10^{-8}$)	$W\ m^{-1}\ K^{-4}$
τ	Transmissivity	
ω	Wavenumber	m^{-1}
Ω	Solid angle	sr

Subscripts

ad	Adjacent
b	Blackbody
conv	Convection
cp	Combustion products
enth	Enthalpy
e	Eastbound cell face
eq	Equivalent
E	Eastbound node

g	Grey gas, gas
G	Fuel gas
HT	Heat release
i,j	Surface and/or gas zone
inl	Inlet
λ	Spectral
n	Node
N_s	Number of surface elements
P	Mid-point node
s	Surface, scattering
rad	Radiation
t	Turbulent
w	Wall
w	Westbound cell face
W	Westbound node
x	Local value
∞	Ambient

Superscripts

1	Value at time $t+\Delta t$
0	Value at time t

CHAPTER ONE

INTRODUCTION

1.1 Background

Gas-fired furnaces have been used in manufacturing industry for many decades despite incomplete understanding of the complex processes occurring in these systems. Early developments in furnace technology were primarily concerned with increasing production and improving reliability while fuel economy was often of secondary importance. However since the oil shocks of the 1970s, energy efficiency has improved considerably in response to energy price increases, supply uncertainties and to some extent to government policies. From that time on improvements in gas-fired equipment for industrial heating purposes were mainly driven by fuel cost and focused on the efficient use of natural gas whilst improving product quality and increasing production. At present a growing awareness of the detrimental impact of energy production and use on the environment and a consequent recognition of the need for energy conservation has put further pressure on the need to enhance furnace efficiency whilst reducing pollution at a minimal cost. Conservation of existing fuel resources is also a consideration in the drive for optimisation of industrial combustion processes. Thus, there is a strong incentive to develop and install the best available cost-effective technologies to reduce energy requirements and associated emissions.

1.2 Industrial Furnaces

Furnaces, such as the one shown in Figure 1.1, are devices commonly used in the industrial sector for a variety of heating applications and their use represents an important part of the overall production process. They usually involve initial combustion of a fuel and subsequent transfer of energy from the combustion products to the load in the furnace.

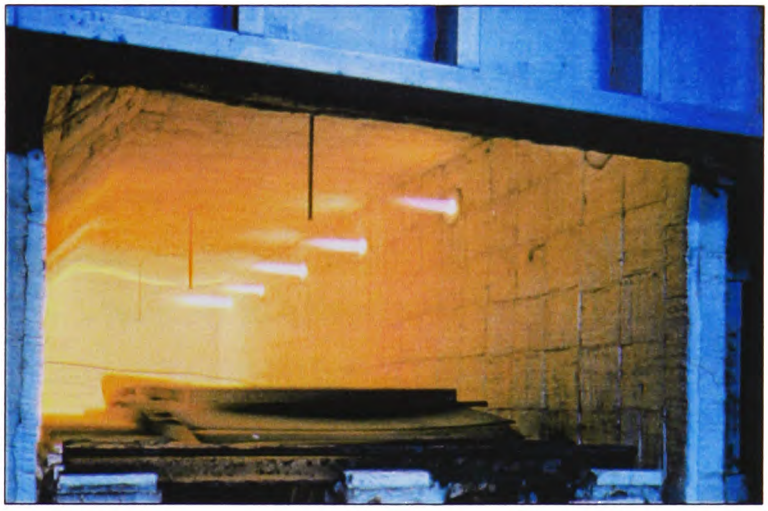

Figure 1.1 Gas-Fired Metal Reheating Furnace

Because of the relatively high temperatures encountered, furnace chambers are generally refractory lined to reduce heat losses. They contain either a refractory hearth or metallic supports to hold the load which can be moved along the furnace. These high temperature systems generally rely upon burners to heat up and maintain the temperature in the chamber and may be operated continuously or in an intermittent fashion. Inappropriate operation or design of a furnace will be reflected in reductions in the efficiency and poor quality of the final product. It is therefore necessary to understand the underlying processes central to these combustion systems to determine accurately the rates of heat transfer and hence to predict their performance.

The diversity of heating processes used in manufacturing industry and hence the specific requirements of each process have led to the development of a variety of furnaces tailored to particular duties. The efficiency of these combustion systems is highly influenced by design and operating parameters. The optimisation of the design over a wide range of conditions will assist designers in meeting the demands of increased unit capacity, improved thermal performance and reduction of the problems

associated with combustion generated pollution. Thus, in metal reheating furnaces where stringent metallurgical requirements must also be satisfied, additional pressure is placed on operators trying to make the best compromise between the often contradictory objectives of improved product quality, enhanced furnace productivity and energy savings.

1.3 Prediction of Furnace Performance

Combustion of fossil fuels is still the most important process to provide the energy supplies for society, although it is also responsible for the release of unwanted pollutants which affect our environment. However, the last few decades have seen a significant advance in the development of combustion processes that simultaneously save energy whilst reducing harmful effects on the environment. Nevertheless, global climate change as a result of emissions of so-called greenhouse gases, particularly carbon dioxide generated by combustion of hydrocarbon fuels, is a major issue that is attracting considerable concern. These latter emissions can be reduced by using natural gas. Consequently, as a result of this and considerations such as reduced cost and ease of use there has been a shift towards the use of more hydrogen-rich fuels (such as natural gas), away from dirtier fuels such as coal and this trend is likely to remain for some time.

Whilst the use of natural gas can lead to lower carbon dioxide emissions other pollutant gases such as various oxides of nitrogen, NOx can still be a problem. High temperature processes tend to run at low thermal efficiencies unless high combustion air preheats are employed. This however leads to high flame temperatures with consequent high rates of NOx formation. Thus the strongest challenge facing combustion engineers today relates to the "potential incompatibility" between improved energy savings (which require high air preheat temperatures) and the resultant high NOx levels. The need to improve efficiency whilst simultaneously reducing NOx emissions has led to the development of new technologies such as "flameless oxidation" [1]. Accurate prediction of furnace behaviour can assist in introducing these new technologies. The problem of predicting furnace performance is complicated because of the interactions of the fundamental mechanisms of heat transfer, aerodynamics and combustion which are involved. However, undertaking measurements on the actual plant or on a pilot-scale prototype is difficult and expensive so that mathematical modelling is an attractive cost-effective technique.

In the past, natural gas fired furnace design was often empirical and relied to a large degree upon the experience results from previous designs. A natural evolution in furnace design has therefore ensued. Physical modelling, using small-scale, ambient temperature, isothermal models have provided useful information on the flow-related characteristics of furnaces [2]. However, due to the impossibility of complying with all the necessary physical similarity criteria, only partial simulation of the real process is possible and in particular radiation heat transfer predictions cannot be obtained with these models.

Consequently, there has been considerable interest in developing mathematical models for control and design of industrial furnaces. These developments have also been aided by the increased power of computing systems so that mathematical modelling is widely used as a fundamental tool in the design and assessment of furnaces. Thus, advances in computer hardware and software have led to the introduction of models for prediction of heat transfer and pollutant emissions from both individual burners and furnaces. These models can also be employed for control purposes.

A large spectrum of heating processes, including reheating, heat treatment, melting of metals and glass can benefit from the application of computational modelling techniques. Thus, for example, models can be used to predict the thermal performance of a plant e.g. the fuel consumption and thermal efficiency. In addition the mathematical models can be employed to assess the quality of the final heated product by providing quantitative data for the load temperature uniformity and history.

Other typical applications of furnace simulation models include prediction of furnace start-up characteristics and pollutant formation and emission. The effect of furnace control parameters such as optimisation of the temperature set point, selection of the location of the set point sensor and analysis of different control strategies during changes in the production process can also be studied.

Over the years many different mathematical methods have been proposed, tested and refined to describe the thermal behaviour of furnaces and other combustion systems. In terms of radiative transfer, a furnace is an enclosure containing an absorbing, emitting and possibly scattering medium in which there is heat generation. Because thermal radiation is the dominant mechanism of heat transfer in most high temperature heating plant, rigorous calculation of the heat transfer in such a system can

only be undertaken from detailed information on the various physical and chemical processes present on the system. Since all these phenomena take place simultaneously, complete solution is possible only if they are simulated together. However, accurate treatment of the problem is very difficult because of the complexity of the governing equations and in some cases because of incomplete knowledge of the fundamental physical nature of the processes. This has led to the development of mathematical models with different levels of sophistication to cope with different applications.

These models can generally be divided into two groups. The first group, based on computational fluid dynamics (CFD) techniques, solves the differential equations describing the transport of heat, mass and chemical reaction as well as incorporating a turbulence model and requires considerable time and expertise. These models are particularly suited to prediction of flows and pollutant formation. However, in many cases the calculation of radiative heat transfer is considerably simplified. The second group is often based on the zone method of radiation analysis and involves simplification of the flow fields. These latter models generally require shorter computing times and can be adopted to investigate transient furnace operation. The adoption of a particular type of model will depend upon the nature of the application, the degree of accuracy required and available computer facilities.

1.4 Energy Utilisation in Metal Reheating Furnaces

Metal reheating furnaces are used throughout the industrial sector to heat slabs, billets, etc. to a temperature suitable enough to allow subsequent hot forming to be carried out. They are further employed for the metallurgical heat treatment of metal products. This project is concerned with a steel reheating furnace whose fundamental purpose is to provide steel bars at a suitable temperature resulting in the production of acceptable and consistent quality material. Steel reheating processes take place generally in the range of 1150°C to 1300°C. The reheating process is known to be one of the major energy consuming steps in the production of metals. In the UK this process consumes about 32.6 PJ, of which continuous reheating furnaces use 28.6 PJ with natural gas being the main fuel of choice. Fuel costs are reported to exceed £80 million/year (in 1994 prices) [3] and yet only 30-40% of the supplied energy is often utilised within the furnace. The efficiency of reheating furnaces undertaking similar

duties is usually measured in terms of their specific energy consumption, which expresses the amount of energy consumed per tonne of throughput.

The high temperatures encountered in steel reheating processes leads to relatively high specific energy consumptions. Reported values range from 1.13 GJ/tonne to 10.99 GJ/tonne [4] for reheating furnaces with values differing according to the specific requirements of each process and working patterns. The major cause of furnace inefficiency is the loss of energy in the waste gases but other losses to the furnace structure and surroundings can also occur. Therefore, energy saving techniques such as combustion air preheating offer significant benefits to recover energy from the waste gases. The UK government has a commitment to reduce the emissions of CO_2 and other greenhouse gases to below 1990 levels by 2010 and has placed greater emphasis on energy efficiency programmes. The Energy Efficiency Best Practice Programme (EEBPP) is one of such programmes that aims to generate and spread good practice in energy efficiency. Under this programme guides and case studies have been published to help users of furnaces to save energy.

As an illustrative example, Good Practice Case Study 322 [5] reports on the improvement in energy utilisation as a result of a combination of measures on a heat treatment furnace.

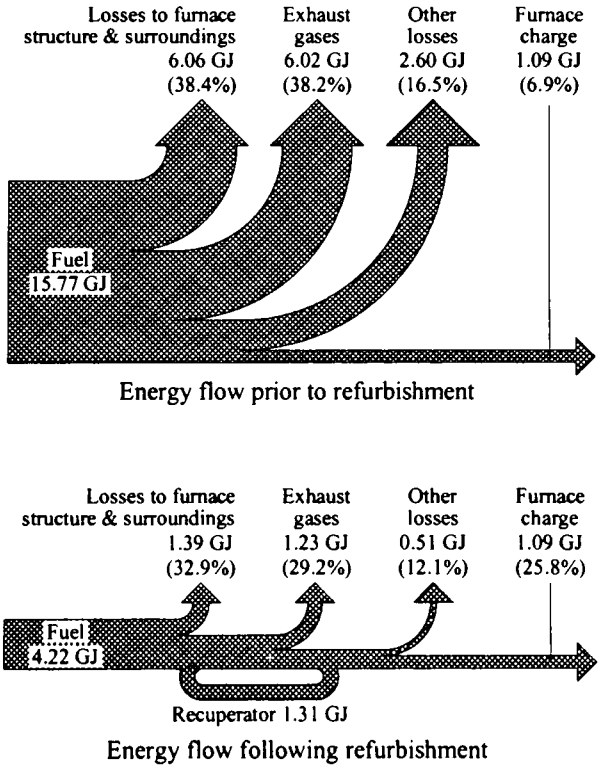

Figure 1.2 Comparison of Furnace Energy Use Before and After Modification [5]

Installation of recuperative burners saved approximately 30% with a similar saving resulting from the adoption of improved burner controls. Finally the use of low thermal mass linings also gave substantial reductions, so that a total fuel saving of over 70% was achieved. To illustrate the energy savings obtained an energy flow diagram (known as Sankey diagram) of the heat treatment furnace is presented in Figure 1.2. In addition to saving energy and reduced manning requirements, the modifications to the furnace also improved product quality.

1.5 Motivation for the Current Project

As mentioned previously much effort has been expended on developing methods to predict the difficult processes found in combustion systems. Thus, for example, in addition to the traditional zone and Monte Carlo methods for calculating radiative heat transfer, several alternate methods such as the Discrete Transfer, Discrete Ordinates and Finite Volume techniques (which are particular suited for use in CFD models) have been developed. Publications abound on applications of these methods to reheating or melting furnaces but many of these studies are often restricted to relatively simple geometries and steady-state operation. These conditions are often not found in practical industrial environments since many furnaces operate in a transient fashion.

Therefore, the initial motivation for this work was to develop a model, which offers the potential to analyse the non-steady state behaviour of a metal reheating furnace. This can be important since, for example, many furnaces consume considerable amounts of fuel when starting-up from cold. It is also necessary to simulate transient operation if models are employed for control purposes. A further requirement of reheating furnace models is the ability to predict load temperature-time histories since temperature uniformity within the steel bars is an important consideration in determining the quality of the final product.

Models based on the zone method are a promising technique in this application since they provide the ability to simulate non-idealised transient operating conditions such as varying production patterns, cold start-ups and intermittent production delays. These zone models are relatively simple to run and have short computing times and have been shown over many years to give accurate predictions. They are particularly effective as a tool to evaluate the influence of parametric changes on the overall heat transfer and furnace performance in what-if type analysis. They do however suffer from limitations, the most important of which is the inability to calculate the fluid flow,

mixing and chemical kinetic processes governing combustion and hence pollutant formation. This together with the ongoing increase of computer capability and demand for ever more detailed investigations into combustion systems to satisfy both environmental and efficiency requirements have resulted in many of the published studies employing complex CFD models albeit with the limitation of steady-state simulation.

In the quest for more efficient and cleaner systems, a number of technologies have emerged in recent years. One such development is "flameless oxidation" where very low NOx levels are achieved even with high levels of combustion preheated air. The most striking factor about this technology is that relatively uniform temperatures are reported within the furnace chamber and this can approximate to a well-stirred reactor. Thus, it is likely in this situation that relatively simple zone models can provide good estimations of furnace performance. Overall there is still considerable potential for the use of zone models so that this type of simulation is employed in the current study.

1.6 Objectives and Structure of the Thesis

This current project is primarily aimed at developing a multi-dimensional zone model capable of handling the transient operation of a gas-fired furnace for heating metal bars prior to hot forming. In this type of equipment temperature uniformity is critical and the temperature-time curve of the load must be strictly controlled. In addition, most of these systems are operated intermittently so that the fuel consumed to achieve a working temperature following a cold start may often be a significant proportion of the overall energy consumption. As far as possible, the model should have relatively short computing times whilst retaining a high accuracy. The model will then be used to investigate the effects of changes in furnace design, control and operating parameters.

Most previously developed transient zone models have been restricted to so-called single gas zone versions or alternatively long furnace models (LFM) in which the length of the furnace chamber is split into a series of zones. This restriction is relaxed in the current work since both the length and height of the chamber is subdivided. The effect of zone size on the predicted thermal performance will be examined by comparing a series of increasingly refined zone arrangements.

Previous zone models have mainly been concerned with nozzle mix burners (i.e. situations where combustion is complete within the burner) although some furnaces are

end-fired by long diffusion flames. In this case heat due to combustion is gradually released along the length of the flame and this can significantly affect the heat transfer in these systems. Past models based on the long furnace assumption were found to underestimate the flame radiation due to lower predictive flame temperature. In some cases allowance was made for two temperature levels at each longitudinal zone, one for the flame jet and the other for the surrounding combustion products which adjusted the radiative heat transfer in the right direction [6]. This latter approach, however, does not provide a rigorous representation of a confined flame. Consequently, this project aims to extend the application of the models to include heat transfer from long diffusion flames. The model can take into account changes in flame length and combustion profile and incorporates improved representation of the thermal radiation from the flame hot core by employing a larger number of zones to represent the flame. Comparison of a nozzle mix model with a diffusion flame model will be made to determine the significance of combustion heat release on the overall performance of the furnace.

The zone model, which involves a series of energy balances, requires data concerning the flow field and combustion pattern within the furnace. Physical modelling and empirical correlations can be employed to supply this information. In particular, the use of ambient temperature, isothermal models is a well-established technique which appears to provide reliable information on flow related behaviour of a wide range of both high and low temperature heating plant [2]. Isothermal modelling has, for example, been employed for flow visualisation studies in intermittent kilns and the acid/alkali isothermal technique[1] has been particularly useful to study flames in glass tanks [7, 8] and cement kilns [9]. It can thus be concluded that isothermal studies provide reasonable information on flows in non-isothermal systems. Consequently, the use of isothermal ambient temperature computational fluid dynamics (CFD) models in this thesis is appropriate to simulate the flow and mixing process providing adequate scaling and similarity criteria are considered. This combination of relatively simple CFD and zone models has not been much exploited in the past and is a novel feature of the current work. The use of this type of approach offers considerable potential since it retains the advantages of both types of models.

[1] The technique simulates the mixing in the flame by using dilute solutions of an acid and alkali together with an indicator to represent the fuel and the air respectively. After mixing, the coloured indicator becomes clear and the result is a visual representation of the flame.

The structure of the remaining chapters is now outlined.

Chapter 2 introduces the subject of mathematical modelling followed by a detailed description of the common methods used for the calculation of radiative heat transfer in furnaces and combustion systems. Their advantages and disadvantages are outlined and the application of these methods to combustion processes is reviewed. In particular a critical review of the published literature on zone models and their applications is also presented.

Chapter 3 describes the principles and overall formulation of the zone method and leads on in the remaining chapters to the development and application of the two-dimensional models.

Chapter 4 provides a detailed description of the transient zone models developed for both the nozzle mix and diffusion flame burners to simulate the performance of a gas-fired metal reheating furnace. It includes a description of the overall computer structure and the sequence of operations to obtain flow data, radiation exchange factors and zone calculations.

Chapter 5 presents the preliminary studies carried out with the CFD model to test the validity of the predictions. The model is tested for grid independence and, where possible, comparisons are made with previously published studies.

Chapter 6 examines the effect of zone size and arrangement on the accuracy of the predictions and also on the computational time.

Chapter 7 discusses the application of two-dimensional nozzle mix burner models to examine the effect of burner characteristics, the operation of the control system and the use of different insulation materials on the predicted thermal performance of the furnace during the initial start-up from cold and for prolonged production periods. A number of energy saving techniques are also simulated to illustrate the opportunities for improvement in furnace design.

Chapter 8 investigates the use of steady-state two-dimensional zone models to simulate continuous operation and assess changes in furnace design and control.

Chapter 9 extends the application of multi-zone models to long diffusion flames by including combustion heat release. Isothermal CFD computations are used to simulate flows and estimate flame lengths and heat release profiles. The modified zone models are then employed to predict the performance of a metal reheating furnace when starting

up from cold and, in particular, the influence of flame length and heat release distribution.

Chapter 10 draws the overall conclusions from this work with respect to the transient and steady-state multi-dimensional zone models developed. Conclusions are also drawn regarding the application of isothermal CFD computations to predict flow and mixing patterns. Finally recommendations for further research are proposed.

1.7 Heat Transfer in Gas-Fired Furnaces

The zone model relies on accurate calculation of heat transfer so that it is relevant to review the main ways heat is transferred in a gas-fired furnace at this stage. A simple box type furnace comprising refractory lined surfaces with the stock occupying the hearth is shown schematically in Figure 1.3. The furnace is usually fired by one or more gas burners and the combustion products are flued out through an exhaust duct.

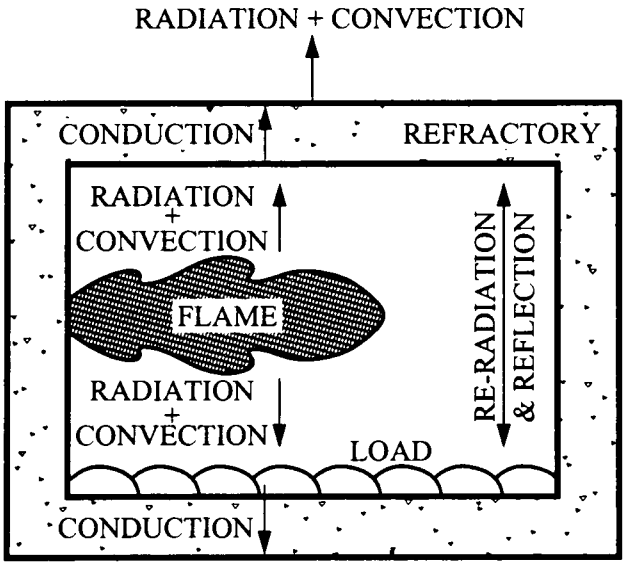

Figure 1.3 Heat Transfer Mechanisms

Despite the relatively low flame emissivity, radiation is usually the dominant mode of the heat transfer (>90%) in a gas-fired furnace. However, on occasions high rates of convective heat transfer may be obtained by promoting high velocities within the hot combustion products flowing over the load. Once the thermal energy is transferred to the solid surfaces, conduction within these surfaces becomes important and must be taken into account in the subsequent redistribution of energy.

Heat is transferred to the stock and furnace lining directly by radiation and convection from the flame and hot combustion products. At the lining surface the thermal radiation can follow three distinct paths, in that some of the incident energy will be reflected back into the enclosure, whilst the remainder is absorbed within the lining. Part of this absorbed component is re-radiated back into the furnace chamber whilst the remainder is conducted into the lining. As the stock heats up, energy can be lost by conduction into the hearth whilst in the case of the refractory walls and roof heat is lost to the surroundings by convection and radiation from the outside wall of the furnace. The overall heat transfer analysis of a furnace is thus complicated because these interacting mechanisms are dependent on the furnace geometry, surface properties and on the ability of the combustion products to absorb and emit radiation.

The emissivity and absorptivity of a natural gas flame is mainly governed by the emission and absorption from carbon dioxide and water vapour molecules and is usually referred to as non-luminous radiation. This non-luminous gaseous emission and absorption does not extend continuously over the whole range of wavelengths associated with thermal radiation, unlike that of solid surfaces. Instead, it is restricted to discrete regions of the wavelength spectrum and exhibits non-grey characteristics. So-called luminous radiation is, however, generally associated with oil and coal flames and is governed by the emission and absorption characteristics of solid particles in the flame. The presence of these particles enhances the emissivity and absorptivity of the flame by emitting radiation at all wavelengths.

The contribution from the energy reflected and re-radiated from the lining to the rate of heat transfer to the load depends on the radiation properties of the flame, refractory and stock surfaces. Thus, with a non-luminous flame, the clear windows in the spectrum allow some of the re-emitted radiation from the wall and roof to pass unattenuated to the load. With luminous radiation over all wavelengths this re-radiated component is attenuated so that a greater proportion of radiation arriving at the load ensues from the flame itself. Luminous flames also have a higher emissivity and this leads to enhance direct radiation from the flame.

Due to the small contribution of convection to the total heat transfer in high temperature furnaces, a crude estimation of this mode of heat transfer is usually sufficient. Consequently, existing heat transfer correlations for duct flow can be readily employed, although in practice many furnace flow patterns differ significantly. In cases

where more accurate estimates of convection are necessary and the relevant correlations do not exist, estimates can be obtained from isothermal physical modelling [2].

Conduction in the furnace lining dictates the rate of heat loss through the insulation. In intermittently operated furnaces these "insulation losses" comprise both the stored thermal energy in the lining as well as conductive heat loss through the lining. For continuously operated furnaces, a steady-state conduction calculation suffices to determine the heat loss through the refractories and these losses can be minimised by selecting an appropriate thickness of refractory. Storage losses are quite significant in furnaces operating in a transient regime due to the considerable amount of energy the structure must absorb to achieve thermal equilibrium when started from cold. Conduction within the load inevitably causes the interior to lag in temperature behind the exposed top surface. The magnitude of the lag is dependent on the thermal conductivity and thickness of the load and can thus affect the overall heating time and temperature uniformity within the load.

The next chapter now deals in greater detail with methods for calculating radiation heat transfer in furnace enclosures.

References

1. Weber, R., Verlaan, A.L., Orsino, S., Lallemant, N., *On emerging furnace design methodology that provides substantial energy savings and drastic reductions in CO2, CO and NOx Emissions.* J. Inst. Energy, 1999. **72**(September): p. 77-83.
2. Rhine, J.M., Tucker, R.J., *Modelling of Gas-Fired Furnaces and Boilers and Other Industrial Heating Processes*, 1991, London: McGraw-Hill.
3. *Continuous Steel Reheating Furnaces: Specification, Design and Equipment*, in *Good Practice Guide 76.* 1994, EEBPP, ETSU: UK.
4. *Energy Consumption in Continuous Steel Reheating Furnaces*, in *Energy Consumption Guide 74.* 1999, EEBPP, ETSU: UK.
5. *An efficient small batch heat treatment furnace*, in *Good Practice Case Study 322.* 1996, EEBPP, ETSU: UK.
6. Faber, A., Michelfelder, S., *A one-dimensional mathematical model for the calculation of heat flux distributions in furnaces with substantial external recirculation*, in *Report No. G 04/a/8.* 1976, IFRF: IJmuiden.

7. Fricker, N., Page, M.W., Chew, J.W., *Combustion and heat transfer in reverberatory glass melting furnaces.* in *IFRF 5th Members Conf.,* May 1978. Holland.
8. Inman, C., *The use of simple isothermal model as a guide to flame behaviour in a glass furnace.* J. Inst. Fuel, 1969. **42**(December): p. 451-454.
9. Ruhland, W., *Investigation of flames in the cement rotary kiln.* J. Inst. Fuel, 1967. **40**(February): p. 69-75.

LITERATURE REVIEW

2.1 Overview

A great deal of effort has been expended towards the development of tools for solving radiative heat transfer problems in participating media. This interest in mathematical modelling partially stems from the need to improve our understanding of the complex interrelated phenomena governing combustion systems. In these systems high temperatures are encountered and therefore radiation heat transfer prevails. The overall driving forces include the need to improve energy conservation, environmental performance, product quality and safety of industrial systems. Because of the complicated nature and importance of the radiative transfer mechanisms, a large number of publications dedicated to radiation fundamentals and their use in modelling industrial appliances have appeared over the years, see for example Hottel and Sarofim [1], Siegel and Howell [2], etc. The purpose of this chapter is thus not to cover every single application. Rather, it is intended to describe and compare the common solution methods and to critically evaluate the relevant studies carried out to date on furnace modelling, whilst stressing the limitations of the various approaches. Emphasis will be placed on the zone method which is one of the few techniques capable of handling the transient operation of practical systems such as metal reheating furnaces. Finally, the scope for further progress in zone modelling is highlighted.

2.2 Mathematical Modelling

Since it was first recognised as an important mechanism of heat transfer in furnaces in the 1920s, thermal radiation has been extensively explored in order to assess furnace performance. Consequently, mathematical modelling has played a vital role in that it provides an effective means to investigate, in advance, the performance of proposed equipment as well as the consequences of any changes in the design, operation or control of existing plant. Prediction methods that can adequately describe radiative heat transfer have gradually become more available to furnace designers and operators. Today's requirements for more reliable, cost-effective, well controlled, environmentally friendly and highly efficient industrial processes have placed greater emphasis on modelling. The methods should not only be capable of providing more accurate estimations of radiative heat transfer but also have a high level of generality and applicability.

Designs based upon past experience and empirical methods have proved to be inadequate for the necessary current level of refinement. The ability to accurately model radiative transfer allows detailed analysis of the heat transfer in high temperature systems where experimental test data is often too difficult, time-consuming or prohibitively expensive to obtain. Furthermore, the greater availability, speed and capacity of computers together with developments in numerical analysis techniques have resulted in more efficient practical design tools. However, experiments are still required to provide extensive validation of these models to ensure the reliability of the predictions. Consequently, numerical and experimental approaches are complementary and investment in mathematical models is continuing to increase.

The use of mathematical models to predict furnace performance has proven to be a useful tool and is now employed in many industrial applications. They can be used to investigate the design of new or existing plant and can be used to assess a range of techniques for improving production, energy efficiency and product quality. Another application is in the optimisation of operating conditions and the definition of control strategies where set points can be carefully selected to meet the specific constraints of a particular process. More recently, applications have extended to on-line plant control where the furnace models act as the "software sensor". Therefore, a variety of models exist to cope with these different applications.

The advent of more powerful computers has led to a greater level of sophistication in the models. A rigorous 3D model of a furnace should include chemical kinetics, flow and turbulence modelling, thermodynamics, convective and radiative heat transfer and conduction into the stock and furnace walls so that it reflects the actual process as closely as possible. In this case complete solution can only be obtained by simultaneous solution of a range of sub-models, since the nature of the interaction of the physical processes makes them interdependent. At the present time there are models, see for example [3], which attempt to partially represent all these processes. However, further validation is required to prove their adequacy. In addition, these models involve large computing times and storage requirements and provision of the appropriate input information is a complex task requiring considerable expertise. Consequently, these large complicated models are not generally suitable for design and control purposes at present.

The numerical simulation of the thermal performance of a furnace embodies a set of mathematical equations. Unfortunately, combustion systems are defined by integro-differential equations which are time consuming to solve. It is left to the mathematical modeller to make the appropriate simplifications in order to arrive at a tractable problem. Since no singular general solution exists which would be equally applicable to different systems, several distinct methods have been developed throughout the years. The choice of a particular method to be adopted depends on the problem considered and the available computer facilities.

2.3 Radiative Transfer in Combustion Systems

All materials as a result of the molecular and atomic oscillations associated with their internal energy emit radiation. To describe the nature of this radiative transport two independently formulated theories have appeared. The quantum model views radiation as the propagation of a group of particles called photons while the classical electromagnetic wave model views it as the propagation of electromagnetic waves. However, the phenomenon of radiation is intrinsically linked to direction and wavelength so that in this context a ray is described as the intensity of energy travelling in a direction per unit solid angle and per unit wavelength.

2.3.1 The Radiative Heat Transfer Equation

The equation governing the transfer of radiant energy in participating media can be derived by applying an energy balance on a small volume element in the medium taken along the direction of a pencil of rays as represented in Figure 2.1.

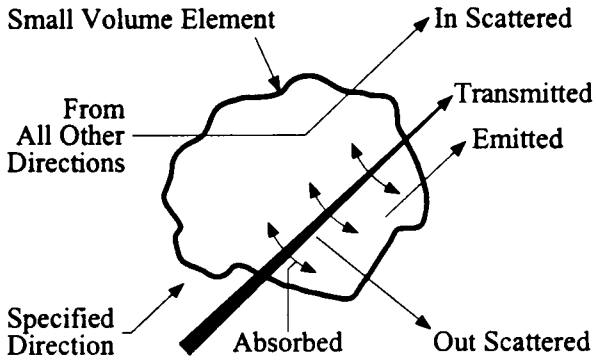

Figure 2.1 The Radiant Energy Balance

Radiation travelling through an elementary volume within a participating medium is therefore increased by emission and in-scattering from other directions and attenuated by absorption and out-scattering into other directions. Considering a small volume element in an absorbing, emitting and scattering medium in local thermodynamic equilibrium and a pencil of rays of wavelength λ travelling within the solid angle $d\Omega$ about the direction $\vec{s}$, the net change in radiation intensity per unit length along the defined path can be written as [4]:

$$\frac{dI_\lambda}{ds} = -(\kappa_\lambda + \kappa_{\lambda s})I_\lambda + \kappa_\lambda I_{b\lambda} + \frac{\kappa_{\lambda s}}{4\pi}\int_0^{+\infty}\int_0^{4\pi}\Phi(\vec{s}' \to \vec{s}; \lambda' \to \lambda)I'_\lambda(\vec{s}')d\Omega' d\lambda' \qquad (2.1)$$

In this expression I_λ is the spectral radiation intensity, $I_{b\lambda}$ is the spectral radiation intensity for a blackbody, κ_λ is the spectral absorption coefficient of the medium, $\kappa_{\lambda s}$ is the spectral scattering coefficient and $\Phi(\vec{s}' \to \vec{s}; \lambda' \to \lambda)I'_\lambda(\vec{s}')d\Omega' d\lambda'/4\pi$ represents the probability that radiation of wavelength λ' travelling in the direction $\vec{s}'$ and confined within the solid angle $d\Omega'$ is scattered into the direction initially considered. Equation 2.1 allows for the contributions from the various processes of absorption, emission and scattering in that on the right hand side the first term represents the

reduction in radiation intensity due to absorption within the volume and scattering into other directions, the second term describes the increase in intensity due to emission from the volume and the last term accounts for the increase in intensity due to scattering, into the specified direction, of radiation arriving at the volume from all other directions. Equation 2.1 is an expression of the energy conservation law applied to a pencil of rays travelling through a small volume element in the medium and is commonly known as the *Radiative Transfer Equation (RTE).*

To determine the radiative transfer within the entire enclosure one equation should be solved at each point within the volume and on the surrounding surfaces. Because all directions and wavelengths need to be considered, two inherent complexities emerge when handling radiative problems. Firstly, the resultant set of equations is integro-differential in nature and therefore extremely difficult to solve analytically and secondly there is a difficulty associated with the evaluation of the spectral radiative properties of the combustion products and surfaces. These latter properties pose a particular problem with gases, especially those with asymmetric molecular structures, because of the strong spectral variations of their radiative properties in comparison with other participating media such as particulates or droplets.

2.3.2 Solution Methods

Exact analytical solutions of the integro-differential radiative transfer equation are available but most of them refer to simple one-dimensional cases or assume uniform radiative properties [5]. However, most furnace systems are multi-dimensional and contain combustion products with spectrally dependent properties so that it can be seen that this type of solution is not practical for engineering purposes. Consequently, simpler approaches are needed to tackle radiation problems. These results in simpler cases are, nevertheless, useful for testing the accuracy of approximate radiation models.

To adequately simulate radiative heat transfer, a model may have to account for the effects of complex enclosure geometry and spectral radiative properties in the participating media. Anisotropic scattering, which has been receiving increasing attention, may also be accounted for in some cases because of its importance in systems where particulate matter in the form of ash and soot is present. The ideal model should be sufficiently accurate, computationally efficient in terms of time and storage requirements, flexible, easy-to-apply, compatible with other numerical schemes used for solving combustion related phenomena and above all capable of realistic representation

of time dependent processes since many combustion systems operate in a transient fashion. Therefore, due to the intrinsic complexities in describing both the physical and mathematical aspects of the radiative transfer problem in furnaces and combustion chambers, a number of simplifications have been introduced in the past in an attempt to aid the solution of the RTE. This has resulted in a variety of solution methods.

There are two different approaches commonly used to model combustion systems. One due to Hottel and Cohen [6] and the other initially followed the work of Patankar and Spalding [7]. The first model (commonly known as the zone method) is based on the division of the surfaces and gas volume in the combustion chamber into zones and the evaluation of the mutual exchange of heat and mass between these zones. The second model is based on so-called computational fluid dynamic (CFD) techniques which solve the flow and heat transfer equations in an efficient way. This latter model has been directed towards a fundamental prediction of the flow and mixing under turbulent conditions and involves less rigorous calculation of radiation heat transfer, whereas zone models in general provide accurate estimates of radiation but involve simplification of fluid flow aspects. Generally these two approaches have been used in different applications. The heat balance method of Hottel and Cohen [6] has been successfully applied as a design tool to a wide range of high temperature combustion systems such as furnaces for reheating and melting of metals [8] and boilers [9], whereas the CFD models [7] have largely been applied to model individual burners [10], pollutant emissions and the steady-state behaviour of industrial boilers [11]. Both approaches require the solution of the RTE.

There are several techniques available for solving this equation as documented for example in Viskanta and Mengüç [12], Howell [13], Rhine and Tucker [14], Modest [15] and Carvalho and Farias [4]. They can be grouped into three main categories namely: zone, probabilistic and flux methods.

Zone Methods were the first numerical procedure employed to model engineering radiative heat transfer. The model was first introduced by Hottel and his co-workers in 1958 [6] and since then a number of improvements have extended the capabilities of the original formulation. The method is essentially an energy transfer technique which attempts to determine accurately the radiant heat exchange in a enclosure. The method provides an integral mathematical description for the problem of radiation heat

exchange in enclosures in which the RTE is transformed into a set of algebraic equations by casting the formulation in terms of radiative energy balances.

The model, which is well documented in Hottel and Sarofim [1], basically discretises the nonisothermal enclosure and gas to give a finite number of isothermal surfaces and gas volumes with constant radiative properties, see Figure 2.2. Surface zones are considered to be diffuse grey emitters. Depending on the number and arrangement of the zones subdividing the enclosure, a number of models of varying complexity can be obtained. These range from simple single gas zone versions to long furnace models (in which the furnace volume is subdivided longitudinally) and finally to multi-dimensional zone models. The computation of radiation then follows several stages. Firstly, the direct exchange areas between all zone pairs are calculated followed by the total exchange areas which take into account multiple diffuse reflections at the various surfaces. These are modified in turn to yield the directed flux areas which allow for the non-greyness of the combustion products. These calculations are performed for all pairs of zones, that is, surface-surface, surface-gas and gas-gas. An energy balance is then formulated for each surface and gas zone in turn including convection and conduction if appropriate.

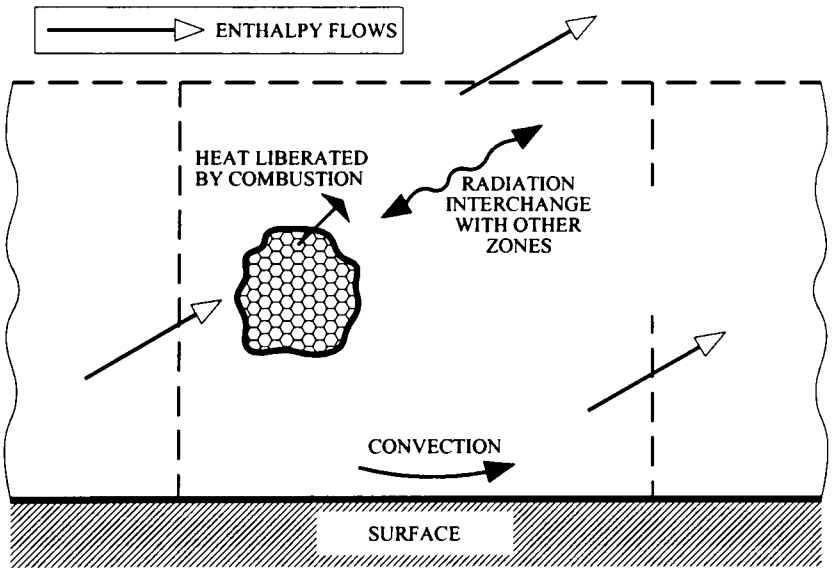

Figure 2.2 The Zone Method

The flow and combustion patterns must also be available in order to estimate the contributions to the overall energy balances due to combustion and sensible enthalpy

exchange for each zone. The resulting energy balance equations are non-linear and have to be solved iteratively for temperatures and hence heat fluxes.

A major task in applying the method is the calculation of the exchange areas since they are complicated functions of the optical properties and geometric configuration of the zones. However, providing that the radiative properties are accurately known and a sufficient number of zones are chosen, the method is considered to give an "exact" solution of the radiation interchange in enclosed systems [14]. Although the method is over 40 years old, the concept is elegant, simple and above all capable of solving many practical problems. Therefore, the method has enjoyed success and is recognised by furnace designers as one of the most rigorous, reliable and tested numerical methods for calculation of thermal radiation.

The method is limited, however, by the difficulty in coupling the zone radiative procedure with fluid flow calculations due to the different solution algorithms and hence incompatibility of the grid sizes required. In terms of computational effort, the method is sometimes seen as expensive particularly when adopted to model complicated geometries where numerous radiative factors must be determined and stored. This restriction can, however be removed by employing a "once-only", offline Monte Carlo technique to provide the temperature independent radiative factors for later use by the zone model. More recently Charette *et al.* [16] employed a new method of solution, the so-called Imaginary Planes method, which is an approximation to the zone method but it is of an order of magnitude faster. This technique works in the same fashion as the zone method but imaginary planes are introduced to link adjacent volume zones. The directionality and global nature of the radiation exchange in the enclosure are not represented correctly, however, and the calculations are thus likely to be less accurate than those which can be achieved with a full zone calculation. Applications of the zone method to simulate radiative systems are numerous and include multi-dimensional systems and transient processes and are reviewed later in this chapter. Such models have sometimes accounted for the non-grey character of the atmosphere but only rarely have they been coupled together with CFD flow calculations. A more complete description of the mathematical formulation of the zone method and its various uses can be found in an excellent monograph by Rhine and Tucker [14].

Probabilistic Models are a class of numerical techniques based on variants of the Monte Carlo approach which was first developed for solving problems in the field of

nuclear physics. In 1964, Howell and Perlmutter [17] reported the first applications to radiative heat exchange problems. The Monte Carlo method is a statistical approach that in contrast to other conventional techniques (which typically rely on various degrees of approximation for solving the relevant equations) works by directly simulating the behaviour of a real process by sampling distributions generated by random numbers. For thermal radiation applications this implies following the history of a statistically meaningful random sample of photons from their emission until their final absorption in the system. The radiative behaviour of the system is then estimated from the average behaviour of the photons.

With the Monte Carlo approach, random numbers are employed to generate probability distributions for the location of the origin of a photon and its direction of emission, scattering direction, probability of reflection from a surface and reflection direction. The random selection takes into account the radiative properties of the surfaces and medium. The heat balances for the surfaces and gas are then related to the number of photons absorbed and those emitted. Usually a high number of photons is used, with the accuracy increasing as this number increases.

The method is particularly relevant for solving problems involving complex geometries and real gases where the use of other techniques can become extremely involved. The Monte Carlo method simulates the actual mechanism of radiative transfer rather than attempting to solve the RTE, so that all important effects can be included without too much difficulty and there is little need for significant approximations and this is the major feature. Because of its statistical nature, the results produced by the method will generally fluctuate randomly around the real exact solution. As the number of photons tracked in the simulation is increased these fluctuations will decrease so that for very large numbers of photons the method should approach the exact solution.

The Monte Carlo approach is a flexible technique and provides results which can be highly accurate although the results are always subject to some statistical error. The main drawbacks are the heavy demand for computer time particularly when large numbers of photons are simulated and, as with the zone method, the difficulty of integrating it with flow algorithms. With the continuous improvement in computing systems the first disadvantage is, however, rapidly being reduced. The Monte Carlo method has thus been widely applied to many practical problems involving high temperature complex multi-dimensional systems with participating media such as those

found, for example, in the field of space technology and industrial furnaces. Howell [18] has provided a comprehensive review of the method and its application to heat transfer problems with an emphasis on thermal radiation.

Flux Models also termed differential approximations, are an alternative to the more classical zone and Monte Carlo approaches in that the RTE is simplified by assuming the intensity of radiation can be discretised into a finite number of directions. This procedure transforms the RTE into a set of differential equations easily solved by a standard finite-difference technique. The method was first applied as a one-dimensional solution to problems in astrophysics [19] and only later was it developed for solving thermal radiative transfer problems. Flux methods are based on the simultaneous solution of a set of discrete directions spanning the total solid angle range so that the radiation intensity is uniform over each solid angle.

There are many types of flux methods available and they can be classified according to the different number of subdivisions chosen for the solid angle and also by the mathematical treatment adopted to obtain the radiative fluxes. Examples of the first classification are the simple two-flux models and their extensions to four-flux and six-flux versions (also called multi-flux methods) [20, 21], whereas more sophisticated treatments include the Discrete Ordinate method (DOM) [22], the Spherical Harmonics method [12, 23] and the Finite Volume method (FVM) [24].

All these methods involve some kind of approximation or assumption to simplify the RTE. For example, the discrete ordinate or S_N method approximates the angular integrals of intensity by quadrature summed over the ordinate directions. It further assumes that the intensity of radiation is constant within each discrete direction. Control volume formulations are then used to spatially discretise the resultant set of partial differential equations. The higher the number of discrete directions, the closer the solution approaches exactness. In the Spherical Harmonics or P_N method, the angular distribution of intensity is approximated by a finite series of spherical harmonics. The method is elegant but computationally tedious and the accuracy increases with the order of the approximation N. The FVM is another kind of DOM which differs only in the way the angular discretisation is performed. In this former method the angular domain is divided into a set of discrete directions over the entire solid angle, and the radiative intensity is assumed constant within each discrete angle. However, the key step of this method is the integration of the RTE over each control volume and each solid angle into

which the domain is subdivided. In all of these methods there is an attempt to reduce the computational time by simplifying the rigorous representation of the radiation mechanism.

Flux methods are economic when complete solutions to problems involving flow and radiation transfer are required because the radiation analysis involves partial differential equations which can conveniently be solved simultaneously with the equations describing the flow field. The radiative intensity is primarily related to conditions at nearby locations, and not to conditions at all other more distant positions, and this greatly reduces the computational burden. The greatest weakness of flux methods is the so-called ray effects which are caused by the crude approximation used for the angular distribution of the radiation intensity. Since radiation is only allowed to travel along discrete directions, it is possible for a localised radiation source to remain unseen by a point receiver unless the source lies along an ordinate direction. There is, therefore, no connection between the radiation fluxes in the coordinate directions. Improved accuracy can, however, be obtained at the expense of computational economy by increasing the number of subdivisions of the solid angle (i.e. increasing the number of discrete emission directions).

Improved versions of the method have been introduced to account for the coupling of the fluxes [25]. Other important features such as the non-greyness of the medium and anisotropic scattering have also been easily included. The methods have been applied to a wide variety of multi-dimensional and non-grey problems where fluid dynamics and radiative transfer are both of significant importance and therefore a compatible approach is required. Viskanta and Mengüç [12] have presented a comprehensive review of flux methods including the development of the technique and its application.

Hybrid Models It can be seen from the previous discussion that to date there are no ideal methods for solving the radiative heat exchange in enclosures. In one way or another all available methods suffer from limitations as a result of the assumptions which are employed to simplify the complex integro-differential equation describing the radiation phenomenon.

The zone approach approximates the spatial variation rather than the directional behaviour by subdividing up an enclosure into finite, isothermal zones. Although the method is capable of providing an "exact" solution, its implementation as part of a complete prediction procedure is restricted firstly because it is relatively incompatible

with the finite-difference techniques used to determine the flow fields and secondly because the resultant computational effort would be excessive. The method also requires information for inter-zone radiative exchange factors and the calculation of these can further require substantial computer resources if large numbers of zones are used. However, even with these inherent limitations, the method remains attractive in many applications because of its simplicity and generality and also because of its ability to economically simulate transient operation once the exchange factors have been determined on a once-off basis, off-line. Moreover, in general the computational efficiency of the zone method is higher than that of the direct alternatives [4].

Probabilistic methods are also known to give "exact" answers. These methods, which trace the history of a pencil of rays as they travel within an enclosure, are particularly suited for handling furnaces of complex geometry. However, as with the zone method, it is difficult to integrate them with fluid flow algorithms. In addition there can be a heavy demand on computer time and because of the nature of the technique the results are always affected by statistical error.

Another alternative is the use of flux methods although these involve coarse directional approximations for the radiation intensity or require complicated mathematical manipulations to reduce the equations to a form which is amenable to treatment by numerical methods. The resultant equations are partial differential in form and therefore can be readily integrated with CFD models. These flux methods are, however, less accurate and hence less reliable when compared to the zone and Monte Carlo methods due to the treatment of radiation as a local phenomenon.

The need for more flexible, accurate and economical methods for calculating radiation in a manner which can be coupled easily with the differential equations governing the fluid dynamics in an enclosure has led to the adoption of methods which attempt to combine the best features of the different models, i.e. the so-called hybrid models. For example zone models have been extensively used in combination with the Monte Carlo technique since this latter approach computes a priori the radiative factors required for the zone calculations [26, 27]. This substantially reduces the computational effort in the zone method calculations in complicated geometries although with a large number of zones the storage requirements can become considerable. Other investigators have coupled zone and flux methods [28] and the necessary equations were derived in the finite-difference form. This hybrid method, however, considers only the radiative

transfer between adjacent zones so that overall information about the directional distribution of radiation is lost. This approach, although computationally faster, can produce results which may not be sufficiently accurate.

The discrete transfer method originally formulated by Lockwood and Shah [29] is another alternative to the existing models which takes advantage of zone, Monte Carlo and flux model merits. In this method the enclosure is subdivided into a number of isothermal volume and surface zones with constant radiative properties and the RTE is solved iteratively for discrete pencils of rays directed between points on the enclosure walls at which the boundary conditions are known.

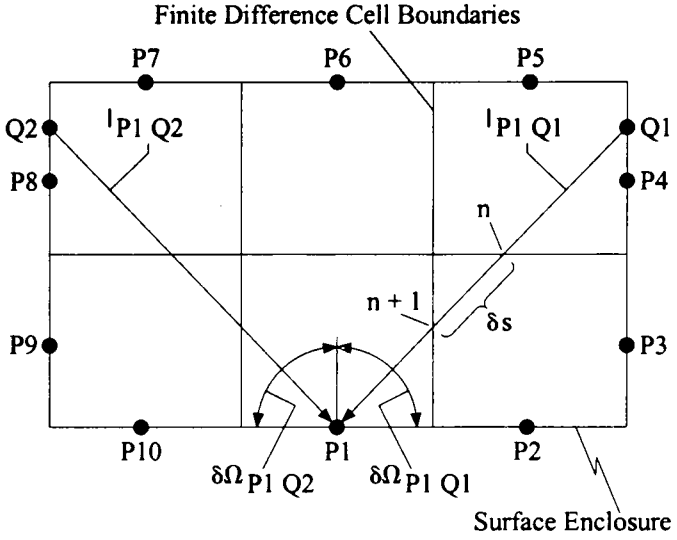

Figure 2.3 The Discrete Transfer Method

Thus for the mid point P_i of a surface zone i, the directions of the rays are chosen by subdividing an imaginary semi-hemisphere about P_i into a number of solid angles within which the intensity is assumed to be constant, see Figure 2.3. Unlike in the Monte Carlo method the directions of the rays are predefined instead of being randomly selected. The RTE is then used to derive a recurrence relationship which, for each prescribed direction, successively computes the intensity values at each of a series of n points at the boundaries of the volume zones crossed by the rays. The total incident radiation at a point P_i of a surface zone i is given by the sum of the contributions from all the rays reaching this point, whereas the total heat sources in the volume zones are obtained by adding the contributions from all rays intercepting the volume zone.

The method is said to be accurate, economical and flexible with regard to handling complicated geometries and for these reasons it has been employed to study complex

industrial problems such as the performance of glass melting furnaces [30, 31] and slab reheating furnaces [32]. A major disadvantage of the DTM is that usually the method does not satisfy completely the constraint of energy conservation and this is important if the method is to be used as part of a complete CFD procedure where the conservative finite volume method is often employed. The imbalance arises because the DTM assumes all incoming rays at a specific surface zone i to be condensed on the mid point P_i so that the solid angles associated with the leaving rays do not add up to 2π (i.e. total solid angle of a semi-hemisphere). The discrepancy is significant for coarse spatial and angular discretisations and decreases as the grid and solid angle distribution are refined. This limitation has, however, been tackled and there are DTM formulations satisfying the energy conservation principle [33]. In order to optimise the method, it is important to select the number of zones and rays to ensure that all zones are sufficiently covered whilst ensuring that the computational effort is not too great. The DTM can be readily incorporated with other sub-models in a full CFD prediction although results are still likely to be affected by the ray effect discussed previously for the flux methods.

2.3.3 Selection of the Modelling Technique in the Present Study

The whole process of selecting the most appropriate method from the wide variety of radiative solution techniques on hand is not always straightforward. Within their own particular limitations, all the methods are capable of solving the problem of radiation heat transfer in an enclosure. It is how well they can simulate a particular problem that must be examined in detail. This requires a systematic approach to look at the objectives of the particular study and at any special features of the process. These can then be related to the characteristics of the available models for solving radiative heat transfer or with exact solutions. Comparisons between the various methods for solving radiative heat transfer problems in participating media are available in the literature for simple test problems and for cases based on experimental data [4, 12, 23, 34-41]. Often the solutions from the zone and Monte Carlo methods are employed as benchmarks for comparison because in general these methods yield more accurate predictions.

According to the objectives listed in Chapter 1, the model to be adopted must predict accurately the heat flux to the load and hence the temperatures in a high temperature gas-fired metal reheating furnace. The model must be flexible, easy-to-apply, economic on computational effort and must be capable of dealing with the non-grey properties of combustion products since these can have a major influence on the

levels of radiation received by the surfaces. In addition, the model must also be suitable for prediction of the non steady-state behaviour of the furnace. Radiative transfer is normally the dominant mechanism of heat transfer in high temperature furnaces so that the proposed model must be capable of providing accurate predictions of this mode of heat transfer. Consequently, the zone method was chosen since the integral approach adopted in the method treats radiation in an enclosure in a global manner so that reliable estimates of radiative heat transfer can be obtained. If enough zones are chosen, it provides a substantially "exact" solution of the radiation interchange within the enclosure [14]. Flux models were eliminated in the present study because of their low accuracy in terms of radiation calculations and moreover, a full Monte Carlo implementation would have been computationally excessive. The zone model can also take into account the effects of different surface emissivities as well as the non-grey behaviour of the combustion products and can be applied in practical geometries. The ability to deal with complex geometries can be enhanced by using a Monte Carlo approach to calculate the radiative exchange factors. In addition, time-varying boundary conditions can easily be implemented in the zone models so that transient operation of the furnace can be simulated.

Other modelling techniques such as the use of the full CFD models already referred in section 2.2, attempt to provide a full description of the thermophysical processes involved in the furnace. However, their success depends on the sub-models used for simulating turbulence and the chemical kinetics in the flame. The sub-model used for radiation calculations in these CFD models is also often less accurate than a zone type analysis. Furthermore, large CFD models are extremely expensive on computing time due to the small grid size used and the simulation of transient furnace operation would involve repeated calculation of the already time-consuming CFD model. Thus, the use of CFD models in the present study was excluded because of their large computing demands and long running times. The major advantage of the zone model over the other methods is that the radiation exchange factors and flow/combustion calculations can be carried out separately from the main thermal computation so that a transient analysis is feasible. The zone model requires, as an input, information on the fluid dynamics of the hot furnace atmosphere. However, evidence exists that flow and combustion behaviour have little influence on the mechanism of radiation transfer, see Beer and Chigier [42] and Rhine and Tucker [14], so that it is possible to separate the radiation calculations

from a fluid dynamics simulation. Isothermal models, either physical or computational, can consequently be used to provide sufficiently accurate input data for the zone analysis.

2.4 Zone Modelling in Industrial Applications

The application of the zone method of analysis to furnace modelling and other industrial applications has been widely reported in the open literature. The various publications exhibit a great diversity, not only due to numerous types of systems which can be modelled but also according to the objectives of a particular study. This section is, therefore, intended to provide a critical evaluation of the relevant studies whilst stressing their limitations. Emphasis will be placed on furnace modelling, particularly the simulation of metal reheating furnaces, since this class of furnaces is the focus of this project. This overview is further aimed at demonstrating the current state of research regarding modelling of metal reheating furnaces and highlights areas for further development, some of which have been addressed in this project.

Zero-Dimensional Models The earliest models were so-called zero-dimensional formulations. These models which provide the basis for more complex furnace models are characterised by representation of the combustion chamber by a single gas zone of uniform temperature and composition radiating to one or more isothermal surfaces. In its simplest form, the gas is assumed perfectly well stirred so that there are no temperature gradients within the furnace chamber and the mean gas temperature is equal to the exhaust temperature. However, in practice the well-stirred assumption does not hold since the mean gas temperature is higher than the exit temperature. A further expression is therefore required to relate the mean gas and exhaust temperatures. The single gas zone model requires no information about the flow or the heat release and was initially devised to be amenable to hand calculations. The model does not provide information regarding the spatial distribution of heat flux or temperature, as it is only capable of predicting average values of those quantities.

At first, the model appears to be very simplistic and of restricted utility. However, Meunier and Cambier [43, 44] have shown that the model often suffices for prediction of the burner output during the heating cycle in a batch furnace and excellent validation has been obtained for heat treatment processes amongst others. Since the simple model has been able to economically predict the fuel consumption with a reasonable accuracy, it has been used to assess retrofitting applications.

Post and Hoogendoorn [45] have also shown that the well-stirred zone model gives a reasonable prediction of the heat transfer from the flame to the glass in a melting furnace. Because the simple model proved to be reliable and economic, it was further employed to investigate the influence of several parameters. Consequently, the same type of model was adopted by Wieringa *et al.* [46] to show that there is only a small increase in the heat transfer to the glass melt if the roof emissivity is increased and that this effect is even further reduced if a regenerator is installed. This later study took into account the spectral characteristics of the gas and refractory walls by using a statistical band model consisting of more than 300 wavelength bands. For regenerative furnaces, the simple model predicted fuel savings of 2-3% when the emissivity was increased from 0.4 to 0.95.

Well-stirred models have also been employed to study the effect of spectral radiation in steel furnaces. Docherty and Tucker [47] have used a single zone model to investigate the influence of wall emissivity on the transient performance of a batch furnace reheating steel slabs. The study tested the influence of the wall emissivity for both banded and grey furnace atmospheres. The results showed that increasing the wall emissivity for intermittent furnaces starting-up from cold results in a decrease of heat going to the slabs and consequently only slight reductions in fuel consumption could be achieved. This is illustrated in Figure 2.4 which plots the overall effect of wall emissivity on the predicted fuel consumption normalised to the value of consumption at 0.5 emissivity.

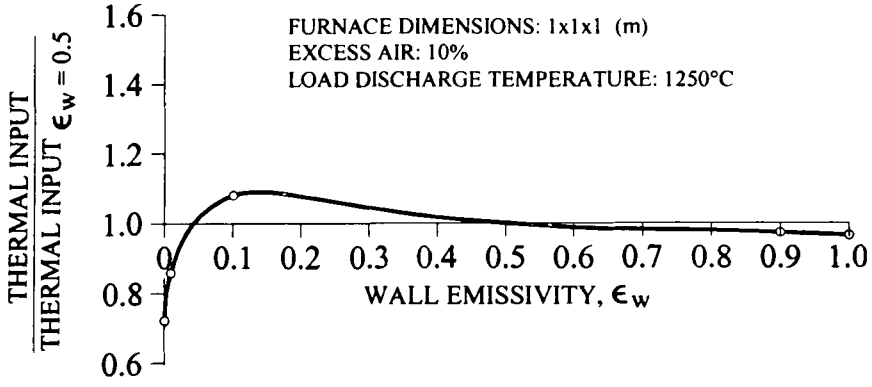

Figure 2.4 The Effect of Wall Emissivity on Predicted Transient Furnace Performance [47]

It can be seen that increasing the emissivity from 0.5 to 1 results in fuel savings of only 3% due to the higher rate of conduction heat loss into the furnace walls. At very

low emissivity values, however, fuel consumption is increased as the emissivity approaches 0.1 because of increases in heat absorption by the wall. For cases where the furnace atmosphere was grey, wall emissivity was shown to have no significant effect on the thermal performance.

In a similar investigation Elliston *et al.* [48] have also made use of a simple one-gas zone model to assess the effect of furnace linings on furnace performance. The spectral behaviour of the furnace gases was incorporated by using a banded model and they considered different types of furnaces operating under steady-state conditions. Their findings were validated against experimental work undertaken on a small test furnace and the measurements were in good agreement with the simple "well-stirred" model results. This study was then further extended by Alexander *et al.* [49] to include spectral data for the furnace linings and intermittent operation. For this study a multi-band model was used to represent the furnace gases (comprised of 15 bands). Results obtained from a small test furnace were in good agreement with the theoretical trends and the concept that low emissivity furnace linings can have advantages in the start-up period of furnaces operating in transient mode. The incorporation of spectrally dependent properties of the furnace linings was found to produce no significant effect in comparison to the general assumption of grey characteristics.

Applications of the simplest single gas zone model to boilers have also been reported by Guruz [50] who produced a generalised chart allowing rapid estimation of the total heat flux and exit temperature for any given firing rate in an oil-fired boiler. Comparison of predictions with measurements taken on two oil-fired boilers indicated the method could be used as first approximation providing radiation from soot particles was accounted for.

The simplicity of these models has benefits and in some cases they have undoubtedly produced useful design information, but in other situations it is exactly what the model ignores, i.e. non-uniformity of temperature and composition that the designer is striving to control and perhaps exploit. The results obtained from the models are limited since they are only capable of predicting the overall performance of a furnace. These simple models are thus particularly useful for investigating relative effects of changes in furnace variables. In fact, providing that the thrust of the burners is sufficient to ensure reasonably "well-stirred" conditions within a system, the assumption of assigning single values for the properties can sometimes be justified.

However, for estimating local behaviour (such as how gas and surface temperatures vary throughout the furnace) more complete models are required. Simple, single gas zone models may also find increasing application in so-called flameless oxidation systems. In these systems the gaseous fuel and air is introduced separately to avoid high peak flame temperatures and this results in relatively uniform temperatures and low NOx emissions within the furnace chamber.

One-Dimensional Models The so-called long furnace model (LFM) is an adequate representation of furnaces in which the length is much greater than the cross sectional dimensions. In this model the furnace is divided longitudinally into a series of well-stirred zones. The simplest approximation is to assume plug-flow as described in Hottel and Sarofim [1] although allowance can be made for recirculation [14] and axial transfer of radiation along the length [51].

Some of the early applications of zone models also included solutions of heat conduction within the load, see for example Fitzgerald and Sheridan [52, 53] who used a LFM to calculate the heat transfer to and temperatures within a slab heated in a gas-fired furnace. The model thus predicted the performance of the furnace and allowed modifications to be assessed in order to optimise the design and operation of the system. The results obtained were compared with measured temperatures from a hot model and whilst it was concluded that the quantitative predictions were of limited accuracy, suggestions were made regarding refinements to existing designs.

Later the same authors [8] made use of two different models, namely a LFM which was applied to a long rectangular furnace and a two-dimensional (2D) zone model which was used for a furnace with a sloping roof. This roof was represented in the model by a series of steps so that the furnace geometry was simplified. This simplification, which results in cubical gas zones and square surface zones, was necessary for determination of the exchange areas from data previously published by Hottel and Sarofim [1]. The solution procedure involved two stages: initially steady-state conditions were assumed and the resulting surface heat fluxes were then supplied to a one-dimensional transient conduction model which calculates the rate of temperature rise of the steel. Both models allowed for radiation interchange between zones and for variable thermal properties in the steel. Measured values of the flame emissivity were used with the furnace atmosphere assumed as grey. Comparison of predicted and measured steel temperatures in these two gas-fired pilot-scale, pusher

reheating furnaces showed that the method enabled the heat transfer to the steel and the distribution of temperatures to be predicted satisfactorily despite the crude zoning which was used and the assumption of grey behaviour, see Figure 2.5.

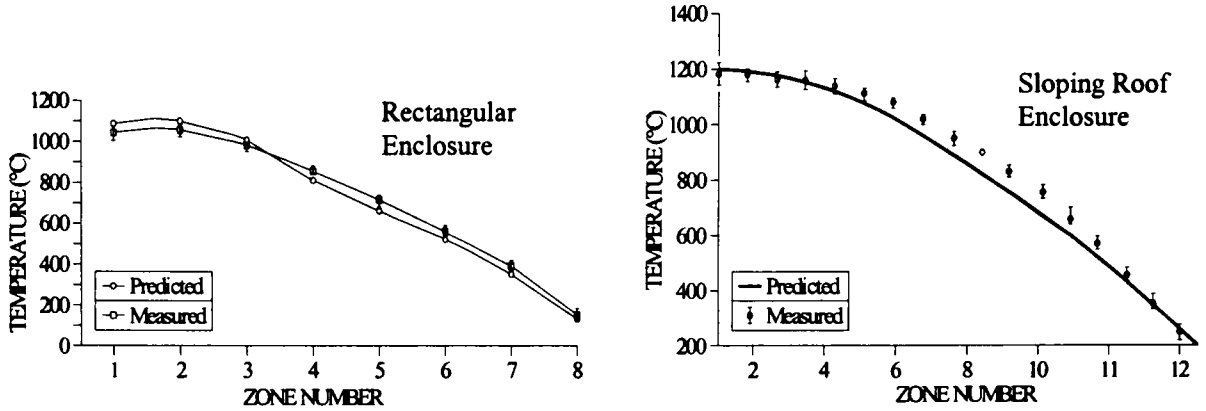

Figure 2.5 Comparison of Predicted and Measured Steel Temperatures for Two Different Furnace Geometries [8]

The linking of a transient conduction analysis in the stock to a furnace zone model has also been undertaken by Salter and Costick [54] for predicting the performance of a continuous reheating furnace producing slabs for hot rolling. The model simulated only half of the geometry by assuming symmetry between the top and bottom fired chambers. The model calculated the behaviour of each zone separately by assuming imaginary black planes divided the zones. The model considered only radiation heat transfer within the furnace and further assumed all surfaces as black and all refractory surfaces as adiabatic. The assumption of a grey atmosphere in the furnace enclosure was considered to be the principal cause for the inaccuracies in the findings when compared to measured data.

With the aim of simulating the steady-state operation of simple continuous furnace, Enemoto *et al.* [55] employed a LFM and validated it with measurements taken on a hot model. The furnace geometry was assumed to be asymmetric and the properties for the gas atmosphere were taken from simplified charts produced by Hadvig [56]. Convection was included in the heat transfer calculations and the results compared well with the experimental data for a number of different firing conditions and load absorptivities. Wall radiation was found to be the dominant parameter influencing the transfer of heat to the load. A similar application of a steady-state LFM was described by Chapman *et al.* [57] who conducted a parametric investigation of a continuous reheating furnace to identify the effect of design and operating parameters on the furnace thermal

performance including load and refractory emissivity and furnace height. They employed a more sophisticated sum-of-grey-gas model for the radiation properties of the combustion products. The predictions were, however, not validated against experimental data.

In another application to slab reheating furnaces, Fontana *et al.* [58] were able to predict three-dimensional temperature distributions within the slab and longitudinal temperature profiles along a box-shaped furnace. Axial radiation was neglected in the model and the flame was treated as separated gaseous zones with the flame emissivity and absorptivity derived from empirical relations. The model also took into account oxidation and decarburisation in the load during the heating process. Heat transfer between the underside of the slabs and the water-cooled supports was taken into account so that the formation of so-called skid marks (i.e. temperature depressions near the points of support) within the slabs was investigated. The effect of combustion air preheating on the furnace behaviour was also studied. This mathematical model was then integrated into an on-line computer system for control and optimisation of industrial furnaces. It complements the information received by data acquisition systems by predicting the load temperature profiles. The overall control system was successfully applied to walking beam reheating furnaces to optimise the heat supply distribution for any given set of specifications. It was also able to effectively supervise the plant operation by conveniently presenting relevant information to the various users regarding the operation, maintenance and quality control of the system.

In most of these previous studies plug-flow of the combustion products was assumed. However, Faber and Michelfelder [59] formulated a variation of a steady-state LFM for a rectangular furnace in which there is substantial recirculation of combustion products. The model differed from the usual one-dimensional LFM model by having two separate temperature levels in each of the longitudinal gas zones. Thus, the part of the zone corresponding to the hot core of the flame was allocated a temperature whilst the surrounding cooler recirculating combustion products were assumed to be at a lower temperature. The required information on flow and heat release patterns within the furnace chamber was provided by the use of appropriate sub-models.

Ceramic tunnel kilns have also been simulated by steady-state LFM. In contrast to reheating furnaces where radiation predominates, in tunnel kilns the heat transferred between the hot combustion gases and the ware is essentially by convection, with only a

small contribution from radiation However, due to the high temperatures involved an important role is played by radiation between the solid surfaces within the kiln. It is this mechanism that is responsible for equalising the temperatures and heat transfer rate around each piece of ware. Dugwell and Oakley [60] used two different transient conduction models. The first considered two-dimensional heat flow and temperatures in the ware whilst a simpler version considered only one-dimensional conduction into the ware. The model ignored any effects of axial radiation and, moreover, assumed a series of plug-flow regions interspaced by zones where burners and air inleakages were introduced. Estimates for the convective heat transfer coefficients in the kiln were obtained from experimental work on an ambient temperature small-scale model and the radiation treatment included the non-greyness of combustion products. In this steady-state analysis, the two-dimensional model was shown to provide good agreement for the measured temperature distribution within the ware whilst the simpler one-dimensional predicted the gas and kiln wall temperatures accurately, see Figure 2.6.

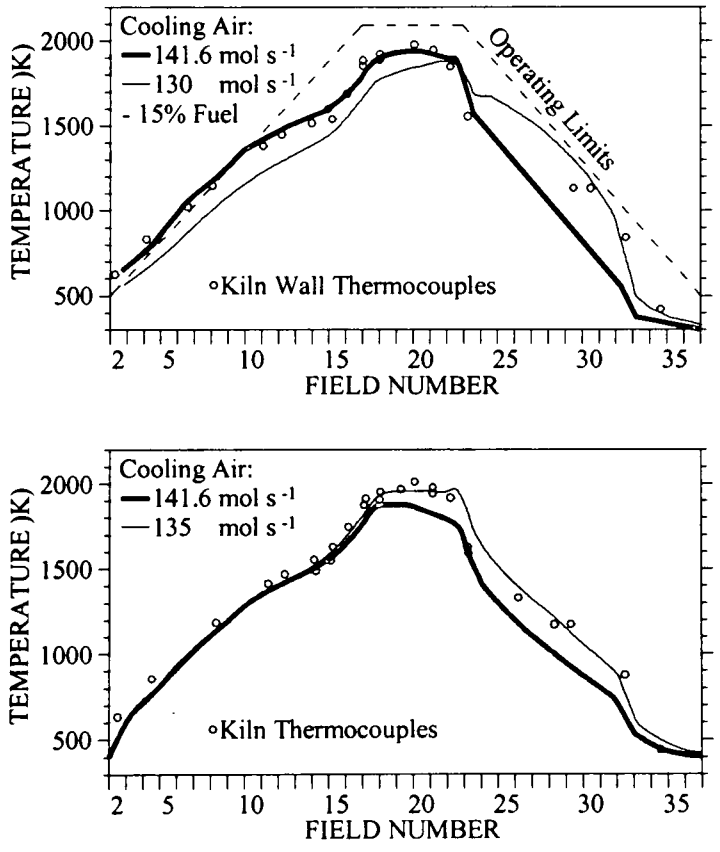

Figure 2.6 Comparison Between Predicted and Measured Kiln Wall and Ware Surface Temperature Profiles [60]

In a sophisticated model of a ceramic kiln [61] control loops were incorporated into the calculation procedure to optimise the thermal behaviour of the system. The model was therefore capable of simulating the real operation of a tunnel kiln and was used to estimate the influence of operating conditions on the fuel consumption. Plug-flow of the combustion gases was assumed but the distribution of these flows around and through the ware was determined by a hydraulic model which balances the pressures along the kiln. Conduction in the ware, furnace walls and cars was assumed to be one-dimensional. The steady-state behaviour of the kiln was determined by allowing the system to achieve this state from cold. The model was validated with measurements taken on a production plant and good agreement was achieved between the measured and computed load temperature profiles.

LFMs have also been used to predict the heat flux and temperature distribution in horizontal shell boilers. Thus, Lucas and Locket [62] employed a one-dimensional model mainly to predict the temperature of the combustion products as they go into the reversal chamber prior to the first convection pass so that the tube plate and tube end metal temperature could be calculated. The work was undertaken because of concerns, at the time, with regard to tube plate overheating in gas-fired shell boilers. They assessed the effect of firing different fuels over a range of conditions. In this work an initial "well-stirred" region was assumed close to the burners followed by a series of plug-flow zones along the length of the fire-tube. Finally a single "well-stirred" zone was used for the reversal chamber, see Figure 2.7.

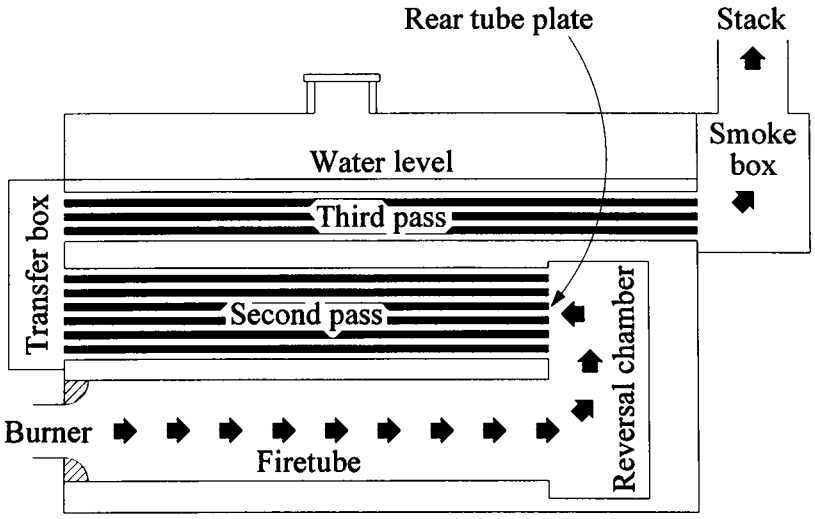

Figure 2.7 A Horizontal Shell Boiler

In principle the model allowed for the progress of combustion along the fire tube and was able to allow for the effects of flame characteristics by estimating the flame shape, heat release pattern and, in the case of luminous flames, the carbon concentration in each zone. Because of the lack of sufficiently accurate input data, much of the required values for these parameters were derived from experience and available empirical information. This model was validated for both oil and natural gas flames by comparing calculated heat fluxes and combustion products temperature at the exit of the fire tube with experimental values, see Figure 2.8.

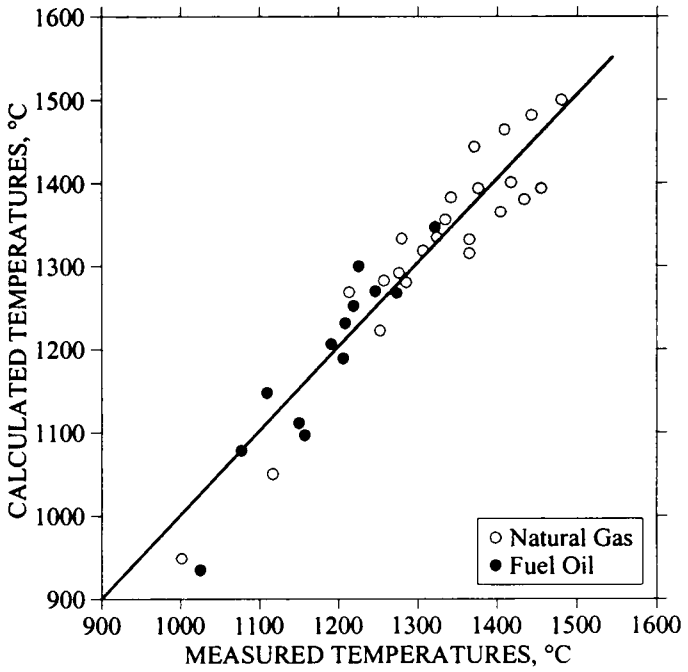

Figure 2.8 Comparison of Calculated and Measured Temperatures of the Combustion Products Leaving the Fire Tube [62]

A complete account of the comparisons made for this model was presented by Lucas and Toth [63]. The discrepancies between predictions and measurements on test rigs were found to be dependent on the estimates for the convective heat transfer near the burners. Thus, convective coefficients were obtained by mass transfer measurements on an ambient temperature small-scale model and resulted in improved predictions. This fire tube model did not account for inter-zone radiation and this may be responsible for some of the errors in the predicted overall heat transfer. Great care was taken to adequately zoning the fire-tube, i.e. fixing the length of the well-stirred region and elements of the plug-flow section, because this was found to alter the overall mixing pattern within the fire tube region and hence affect the calculated heat transfer and

exhaust temperatures. The furnace atmosphere was specified by a mixture of one clear and one grey gas [1].

Results showed that the tube end temperatures were insensitive to the type of fuel employed. Following this study the overall model was successfully applied to predict heat transfer rates and temperatures distributions in several different types of boilers since predicted fire tube gas exit temperatures were found to be relatively insensitive to the various assumptions and input data used.

Recently, Niu and Wong [64] described a simulation model which was capable of representing accurately the behaviour of a large water-tube boiler under different operational conditions. The model was made flexible enough to be adapted to other boiler systems with different configurations by introducing so-called modification factors. The combustion chamber was subdivided into 14 well-stirred sections along the height and plug-flow was assumed. Only steady-state operation was considered. The model was verified using test data and the results were within a reasonable error range, see Table 2.1.

Table 2.1 Comparison of Model Results with Experimental Data [64]

	Load=400MW		**Load=800MW**	
Items	Experimental	Predicted	Experimental	Predicted
Boiler Efficiency (%)	90.3	92.2	88.6	89.7
Preheated Air Δt (K)	193.1	185.6	242.2	224
Exit Flue Temperature (K)	420	443.1	417.4	452

In these previous studies described so far only steady-state operation of continuously operated furnaces was simulated. Steady conditions are, however, rarely achieved in many practical manufacturing environments where furnaces are operated in an intermittent fashion. In these situations considerable amounts of fuel can be used during the initial heating up part of the cycle so that the transient operation should be considered. Consequently, LFMs have been used by several authors to determine the transient performance of gas-fired reheating furnaces. Saimbi and Tucker [65] were the first investigators to use the zone method to simulate the thermal performance of furnaces operating under non steady-state conditions. Their zone model of a steel reheating furnace was linked to a transient conduction routine to determine the temperature distribution in the load.

The LFM made no allowance for axial radiation but the non-grey character of the furnace atmosphere was taken into account. The model, which was validated against measured performance data, was capable of predicting the furnace response from a cold start-up and also could take into consideration interruptions during production, see Figure 2.9. As a result the model was applied to evaluate energy saving measures such as improved insulation and working practices.

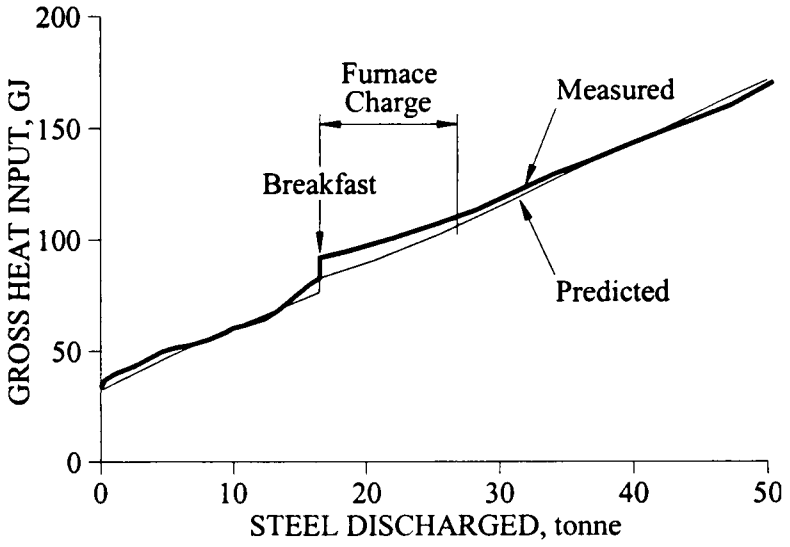

Figure 2.9 Comparison of Measured and Predicted Gas Consumption for a Pusher Reheating Furnace [65]

Tucker and Lorton [66] extended this previous research and compared the use of LFMs, with and without axial transfer of radiation, for both steady-state and transient cases. In both models, a one clear-two grey gases representation was used for the radiation properties of the combustion products. In the transient models, the temperature of the furnace was controlled by adjustment of the gas input rate. The results clearly demonstrated the importance of including axial radiation heat transfer for large values of the chamber height, particularly at high throughput conditions, see Figure 2.10. Simple LFMs are, therefore, likely to be less reliable for predicting the performance of heavily loaded furnaces with low rates of convective heat transfer. Nevertheless, the possible inaccuracy of these simple models has to be weighed against their computational advantages.

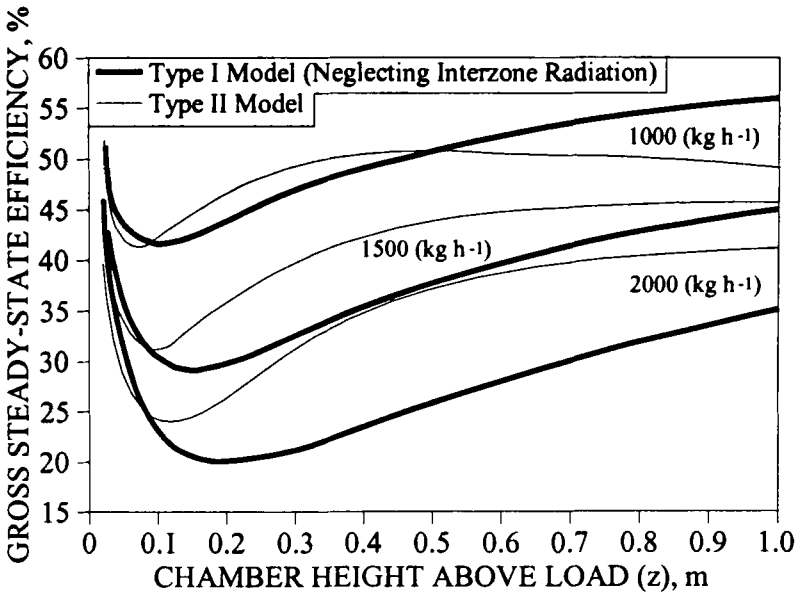

Figure 2.10 Comparison of Predicted Steady-State Efficiencies with and without Inter-Zone Radiation Included [66]

It was necessary in many previous investigations to simplify the furnace geometry because of difficulties in evaluating the appropriate radiation exchange areas by numerical integration. In some cases the values presented graphically by Hottel and Cohen [6] can be applied but these data are limited to square surface zones and cubical gas zones so that only geometrically simple systems, which can be built up from combinations of these shapes, can be represented. This restriction was, however, overcome by Tucker and Ward [67] who used a Monte Carlo technique to determine radiation factors in a LFM simulation of a slab reheating furnace. They included radiation exchange between all zones and demonstrated that over-simplification of the furnace enclosure can lead to substantial variations in the distribution of the heat fluxes along the length of the furnace with consequent errors in the predictions of the load temperature-time histories. This study also compared the values of direct exchange areas obtained with the Monte Carlo technique with values calculated by numerical integration. Although the exchange areas calculated using a Monte Carlo technique are likely to be less accurate (depending on the number of radiation beams used in the simulation) than those obtained by numerical integration, the percentage errors are normally only significant for distant zone pairs which play comparatively little part in the overall radiation process. As a result, these inaccuracies made little difference to the LFM predictions for a steel reheating furnace.

In a later publication [68] the same authors employed their Monte Carlo technique to derive the exchange areas to determine the performance of a gas-fired furnace for heating steel billets to a nominal discharge temperature of 1250°C under typical production conditions, including a cold start-up and various production delays. Longitudinal inter-zone radiation was incorporated in the model and simulation of the actual operation of the furnace was achieved by varying the natural gas input rate to maintain the temperature of the roof in the discharge end at a control set point of 1380°C, as occurred in practice.

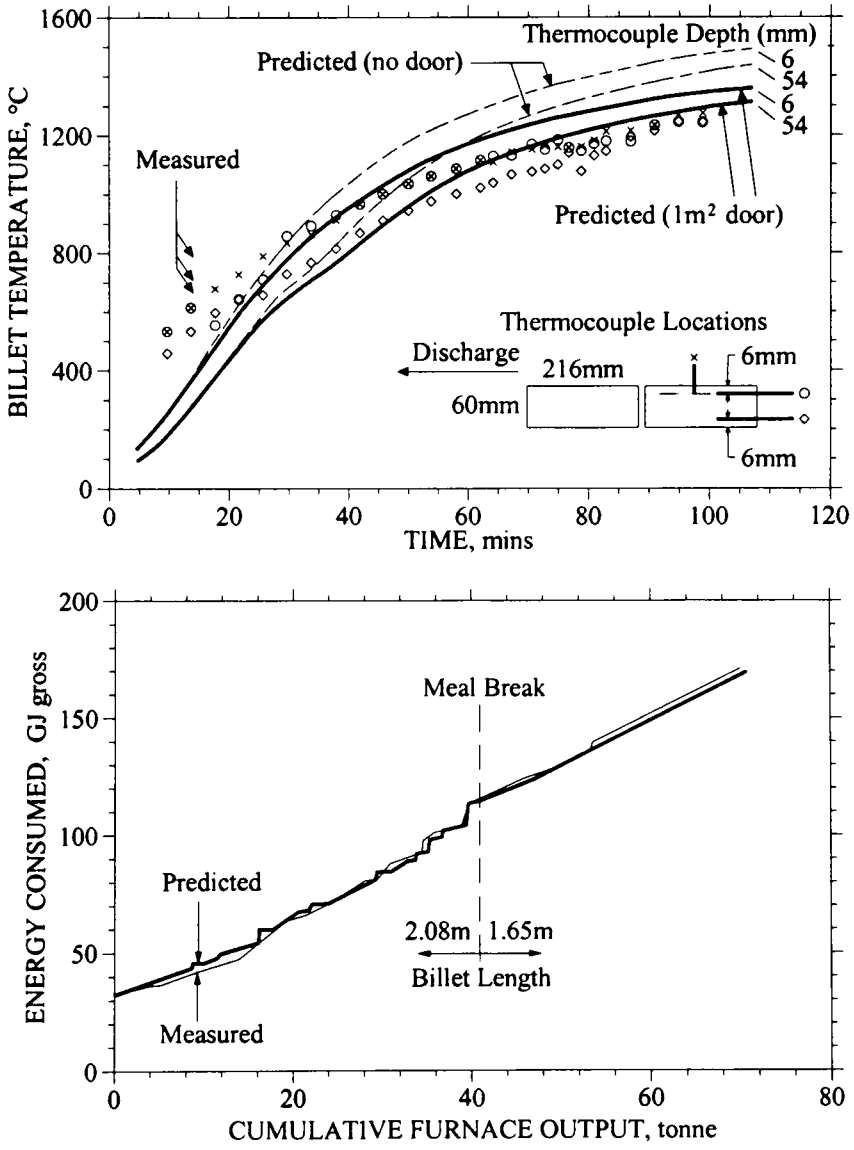

Figure 2.11 Predicted and Measured Discharge Billet Temperature and Energy Consumption [68]

The predicted gas consumption and discharge billet temperatures for both start-up and continuous operation were in good agreement with experimental measurements

undertaken on the production installation, provided that radiation losses through the open discharge door were considered, see Figure 2.11. It was further shown that an increase in the number of gas zones from 10 to 20 with a corresponding increase in the number of surfaces from 51 to 100, did not significantly improve the accuracy of the LFM. The model was then employed to investigate various energy saving options such as combustion air preheating and alternative control strategies.

Monte Carlo techniques are believed to be the optimum numerical method for computing exchange factors at present [69], despite slow and sometimes erratic convergence. Because exchange factors obtained by Monte Carlo methods are subject to statistical fluctuations, Vercammen and Froment [26] and Larsen and Howell [70] have both presented methods for normalising and smoothing these geometric factors so that they obey the required reciprocity and summation conservation relations. These procedures can be conveniently integrated into a zone model and have been shown to be effective and efficient. The applicability of the zone method was further enhanced by the development of a Monte Carlo based computer program, RADEX [71, 72], which was flexible enough to represent complex furnace geometries at an appropriate level of detail and this software code is employed in the present study.

The non-linear transient behaviour associated with many practical systems makes it difficult for the operator to efficiently control the process by means of classical control methods. The need to guarantee consistent product quality and reduced fuel consumption under non steady-state conditions has, therefore, led investigators to look at the alternatives of using furnace mathematical models to provide accurate information on the transient operation of the system for control purposes.

The use of mathematical models to provide on-line computer control of the transient behaviour of continuous reheat furnaces has been discussed by Halliday [73] who described a computer system which was able to continuously monitor and automatically adjust the operating conditions by using numerical models to provide computed temperatures as input to classical control loops. Good agreement between the predictions obtained with a transient LFM and the actual performance was reported for a range of furnace sizes. Michotte and Bretton [74] have also addressed the problem of controlling the dynamic behaviour of reheating furnaces and emphasised the importance of employing transient numerical simulators as "software sensors" for monitoring the temperatures of the slabs.

Previously, Herapath and Peskett [75] developed a computer control system and used a simplified one-dimensional plug-flow zone model to predict the load temperatures to ensure consistent performance. The simplified transient zone model assumed volume zones separated by imaginary surfaces for which the incident radiation was taken as equal to the leaving radiation. This procedure requires substantially fewer exchange factors than a full zone computation because only those between the real and imaginary surfaces are necessary. However, because the leaving radiation from an imaginary boundary was assumed to be diffuse, the directionality and global nature of radiation exchange in the enclosure was improperly represented. It should also be emphasised that the proposed control system was only simulated and was not implemented in practice.

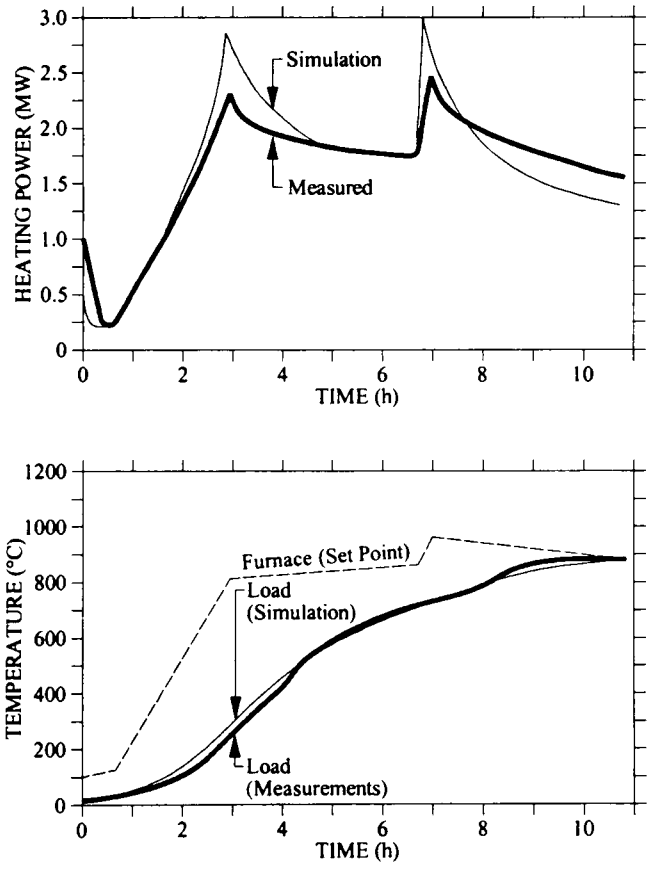

Figure 2.12 Validation of the Firing Curve and Load Heating Profile for a Heat Treatment Furnace [76]

Meunier and Cambier [76] have also used a simple non-steady LFM (ignoring longitudinal radiation) for the optimisation of a batch bell type furnace for coil annealing. The stack of sheet coils was placed under a protective cover and heated in an inert atmosphere which was circulated by a fan. The model was able to simulate a

complete heating-cooling cycle and was validated against several test measurements, see Figure 2.12.

Both the coil temperatures and fuel flow rates were predicted with reasonable accuracy by the zone model which was then combined with a control loop which was used to select the optimal set point temperature schedule at any time in the process.

Yu [77] also employed a transient LFM to study the behaviour of tunnel kilns firing refractory or ceramic ware. The model is similar to the one described by Dugwell and Oakley [60] but in addition accounts for the dynamic characteristics of the furnace. He investigated the effects of different firing cycles and lining materials on the fuel consumption, temperature distributions and heat storage rates of both the ware and kiln lining. The fuel consumptions and heat losses were in good agreement with reported measurements from other kilns.

It can be seen that so-called long furnace or one-dimensional models are more realistic in most circumstances than zero-dimensional ones and especially when "tuned" for a particular furnace can provide reliable estimations of the efficiency of the process. More information has to be supplied by the LFM user than for the simpler models. This can, however, usually be obtained without much difficulty, e.g. plug-flow of combustion products is often assumed. The benefits of using a LFM, such as improved efficiency and better control of the load, may be significant and cost effective. However, in some furnaces substantial variations in temperature and composition of the gases can occur across both the height and width of the system in addition to these in a longitudinal direction. Consequently, multi-dimensional models have been used when both longitudinal and cross-sectional variations in temperature are expected to be important.

Multi-Dimensional Models The procedure of splitting the combustion chamber into zones can obviously be applied, if appropriate, in three dimensions and in a full zone model the subdivisions can occur in the main flow and both cross-stream directions. Because of the computational effort required relatively few examples have been reported regarding two and three-dimensional models and most of these have been limited to steady-state cases.

Many practical combustion systems are axi-symmetrical in geometry. In these cases two-dimensional models can provide suitable analysis for predicting performance. Johnson and Beer [78, 79] used a 2D model to predict temperature and heat flux

distributions in the IJmuiden furnace of the International Flame Research Foundation (IFRF). This study extended the zone method to include luminous flame radiation. The furnace atmosphere was represented by a weighted sum of grey gases and included the effect of soot radiation by representing the gas/soot mixture attenuation coefficient as a sum of the individual coefficients of the gas and soot. Validation of the method was performed and good agreement between predictions and detailed measurement data was found see, for example, Figure 2.13 which compares predicted and measured cumulative heat absorptions for both oil and gas flames and Figure 2.14 which shows the heat absorption distribution for a gas flame.

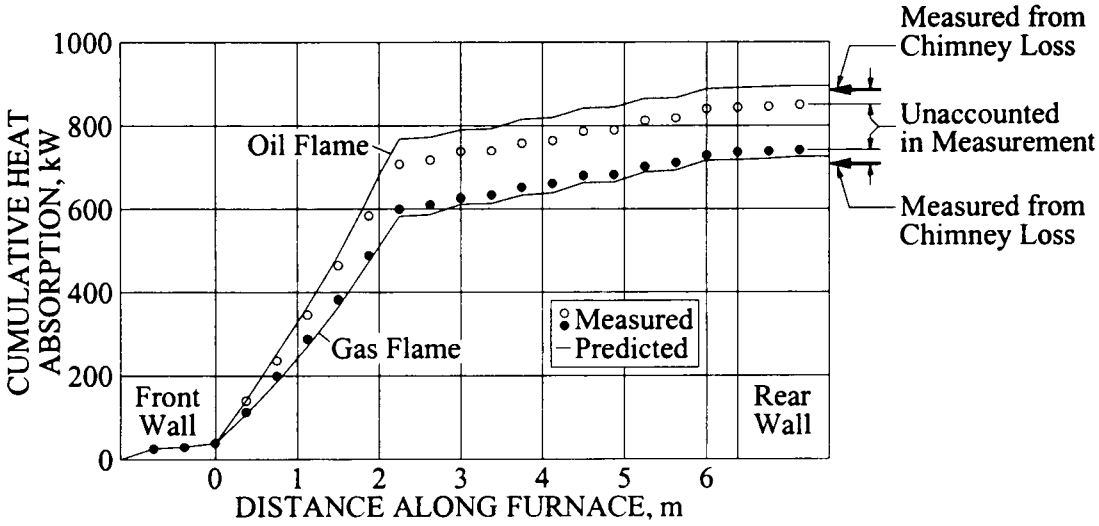

Figure 2.13 Comparison of Cumulative Heat Absorptions along a Furnace [79]

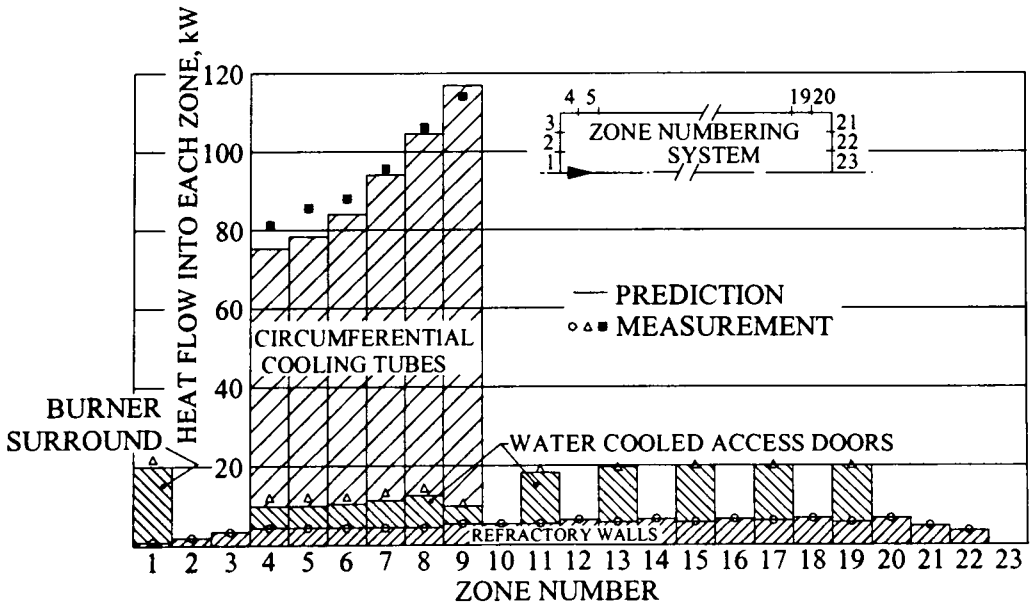

Figure 2.14 Comparison of Predicted and Measured Distributions of Heat Absorption in a Furnace for a Gas Flame [79]

Steward and Tennankore [80] also presented a 2D mathematical simulation of a cylindrical combustion chamber. However, their study combined the zone analyse with a finite difference solution for the flow equations. Initially a relatively fine grid was used to subdivide the enclosure and the equations of motion, conservation of energy and mass fraction were written for every node to yield the flow field and heat release rates within the chamber. The zone method was then used to supply the net radiation transfer for the source term in the energy equation. The combustion products were assumed to be a mixture of three grey gases and one clear gas and the appropriate exchange factors were computed by a Monte Carlo technique. Because the subdivision used for the zone method is much larger than the corresponding flow field grid, the zone temperature was taken as the average of the fourth power of the temperature over the nodes within the zone. However, relatively poor agreement was found between the predictions and experimental data from a test model and this was attributed to the simplifications introduced in the combustion and turbulence sub-models.

Other applications concerning the use of multi-dimensional models have generally employed a simplified approach which utilises the Imaginary Planes Method (IPM) to link adjacent volume zones. With this method the direct radiation transfer between all zones is simplified by determining the radiative fluxes crossing the imaginary planes (the incident flux on one-side of the plane is assumed to leave the other side). The method assumes that each volume zone has a direct view only of its boundaries (including the imaginary planes), so that total exchange areas are not required. Its major shortcoming is that the directional nature of the radiative interchange is "lost" at the imaginary planes, since beams of radiation are not allowed to travel freely throughout the furnace.

The technique has been employed extensively by Charette and his co-workers. Applications range from 2D steady-state models [16] through to a 3D steady-state case [81]. In addition, they developed a 3D transient model [82] and also extended the technique to cylindrical geometries [83] and integrated their IPM model with a CFD procedure for calculating the fluid dynamics within the chamber [84].

In all the above studies a Monte Carlo technique was employed for the calculation of the direct exchange areas and in some cases the combustion gases were assumed to be grey. In none of them have the predictions been compared with actual measurements although good agreement was claimed between the results obtained from the IPM

model and those from a full zone calculation. The IPM is basically a simplified version of the zone analysis so that the computational time is reduced. For a simple one gas zone case the two methods are identical. It is only when the number of subdivisions increases that they start to diverge from each other in that the IPM can lose accuracy as indicated in Charette *et al.* [39].

Li *et al.* [85] starting from assumed temperature profiles for the furnace combustion gases have used a 2D zone model to calculate the heat flux distribution at the surface of the slab in a pusher type reheating furnace. They investigated the formation of skidmarks, i.e. temperature depressions in the slab above the points of support. In this analysis, the shadowing effect of the skidrail structure was taken into account. Transient conduction within the slab was assumed to be two-dimensional by neglecting this mode of heat transfer in the longitudinal direction. The furnace gases were simulated using a one clear-two grey gas model. Radiative shadowing of the slab bottom surface was identified as the dominant factor in the formation of skidmarks in this reheating furnace.

Beltagui *et al.* [86] obtained a detailed set of experimental heat transfer data (heat flux distributions and overall heat transfer) in a gas-fired cylindrical furnace to validate the predictions of a 2D zone model of the system. The flow field, heat release and convection information required by the zone analysis were specified by means of simple models and empirical formulae. Predicted results were in good agreement with the measurements despite the crude input assumptions, see Table 2.2.

Table 2.2 Measured and Predicted Main Variables [86]

Test No.	*Fire Rate (kW)*	*Excess Air (%)*	*Swirl No.*	**Experimental**		**Predicted**	
				Flue gas Temperature (°C)	Efficiency (%)	Flue gas Temperature (°C)	Efficiency (%)
1	*400*	*5*	*0*	671	63.7	748	61
2	*400*	*5*	*0.45*	627	65.8	578	70.3
3	*400*	*5*	*0.9*	592	68.6	497	74.8
4	*400*	*5*	*2.3*	524	74.8	401	80
5	*400*	*20*	*0*	661	61	684	60.1
6	*400*	*20*	*2.3*	560	70.8	376	78.1
7	*300*	*5*	*0*	620	64.7	681	64.6
8	*300*	*5*	*2.3*	455	74.7	348	82.1

A different application was reported by Jenkins and Moles [87] who used a zone model to assess the performance of a large cylindrical, axially-fired, rotary kiln. Their steady-state model accounted for the non-grey character of the combustion products by employing a one clear-two grey gases approach and included allowances for the presence of soot and dust particles.

Local variations in the concentration of the furnace atmosphere were also taken into account in the calculation of the required radiative factors. In addition, the model included convection and the effect of dissociation of the combustion products at high temperature. Measurements of the concentrations of CO_2 downstream from the burner were employed to estimate the heat release patterns in the kiln. The required combustion products flow patterns were derived from available information for enclosed jets [88]. The mathematical model was tested against measurements obtained in a real rotary kiln and the predictions of gas and refractory temperature profiles were generally in satisfactory agreement with the practical data, see Figure 2.15.

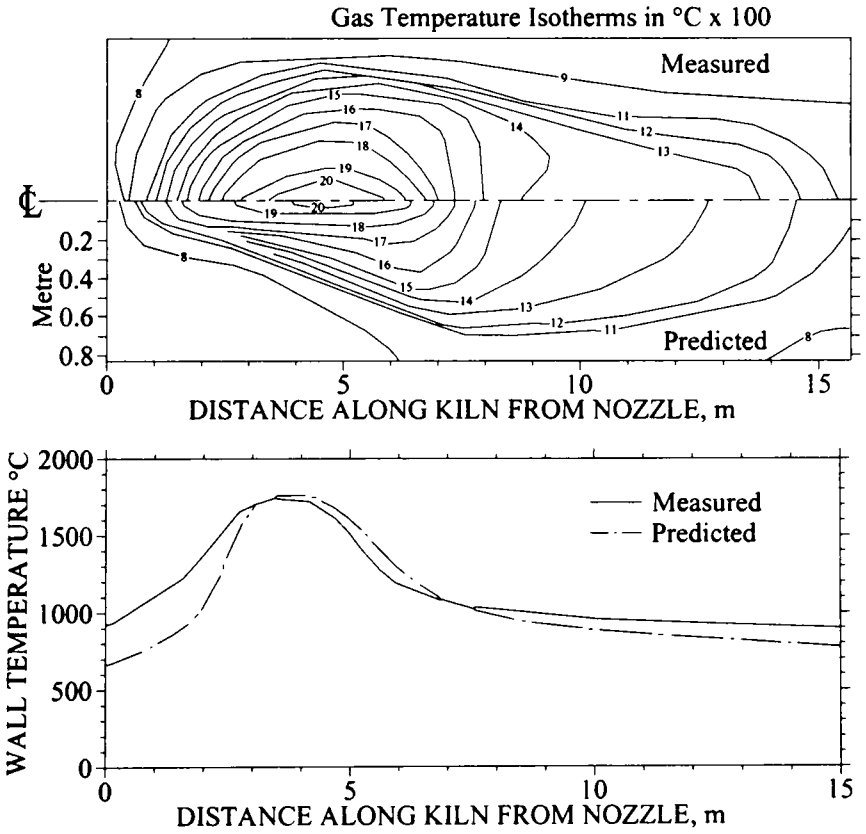

Figure 2.15 Comparison of Predicted and Measured Gas and Wall Temperature Profiles in a Cement Kiln [87]

Many furnaces are not axy-symmetric so that in order to describe properly the temperature and composition distributions within these systems reference must be made to three spatial coordinates. In 1990, Omori *et al.* [89] described a 3D zone model for the analysis of the radiation exchange inside a room with people and furniture. The study was aimed at improving the design of radiant heating/cooling systems to provide an improved temperature distribution inside buildings and therefore a more comfortable environment. Radiation factors were calculated by a Monte Carlo technique and the radiant analysis looked at the interaction between heating devices, walls and windows and the resultant impact on the thermal comfort of the occupants. Significant temperature asymmetry was found around people near exposed walls and windows. This non-uniformity can, however, be reduced by adding insulation to the walls and installing double glazing. In a later publication [90], the same authors have developed a three-dimensional heat transfer analysis to describe the interactions between fluid flow, combustion and radiation in a steel reheating furnace operating under steady-state conditions. The resultant hybrid model uses the zone method to solve the radiative heat transfer, the Monte Carlo method to determine the required direct exchange areas and a CFD package to obtain the flow and combustion patterns. The combustion gases were taken as grey and the thermal properties of the walls were assumed to be invariant and independent of temperature throughout the calculation. The predicted steady-state furnace gas and wall temperatures and load heat flux distribution followed expected trends but no comparisons were made with experimental data.

Heidekker *et al.* [27] developed a three-dimensional zone/Monte Carlo method to compute radiative heat transfer in systems which can be represented by non-orthogonal curvilinear grids and thus extended the applicability of the zone method to more complex geometries. The method was applied to two different complicated geometries. Non-uniform gas properties and shadowing effects were taken into account in the radiation space which contained a grey gas at a specified temperature. The predictions were compared with a Discrete Transfer solution of the same cases. The differences between the two methods were relatively small for the surface heat fluxes and slightly higher, although still acceptable, for the volumetric radiation from the gas. Despite having relatively long computer times, the method allows radiation to be calculated using the same grids as those used to solve fluid flow problems.

Another 3D hybrid model, this time combining a six flux model with a zone analysis was described by Sasse *et al.* [28] for calculating the radiative transfer in enclosures containing a participating medium. The method is similar to the approach of Charrete *et al.* [16] in that it only allows radiative transfer between adjacent zones so that calculations can be performed from zone to zone. The imaginary planes separating the gas zones effectively collect the radiation from a given zone and re-emit it diffusively to the neighbouring zone. For each zone a system of six relationships are written in terms of the flux densities. This hybrid model yielded in some cases better predictions than the standard common six-flux model. As the number of subdivisions increases so will the difference between the models increase. The inaccuracies were partly a result of the use of imaginary planes in that the directionality of the radiation exchange is lost. To improve the method the authors introduced a correction to allow for the directional characteristics of the radiation leaving the imaginary planes and demonstrated that improved accuracy can be achieved in comparison with the standard IPM and six-flux models.

The zone method for radiation analysis has also been applied to simulate the steady-state behaviour of industrial waste incinerators, see Olsommer *et al.* [91] who employed a 3D model to investigate the plant under "off-design" conditions. The zone method was particularly applicable since heat exchange in the main section of the incinerator occurs primarily by radiation because of the high gas temperatures which are involved. The combustion atmosphere was represented by a weighted sum of grey gases and included allowances for soot particles because of the high concentrations which are present in this type of plant. Two methods were tested to calculate the radiation factors, and it was found that numerical integration provided better results than the Monte Carlo technique. The model was validated with measurements taken on an actual waste incinerator plant and the predictions of the combustion products temperatures were found to agree quite well with the measurements with a maximum error of 6%, see Figure 2.16. This thermal model was then coupled with a thermodynamic model of the incinerator/boiler arrangement to predict the steam production at both full and off load conditions [92].

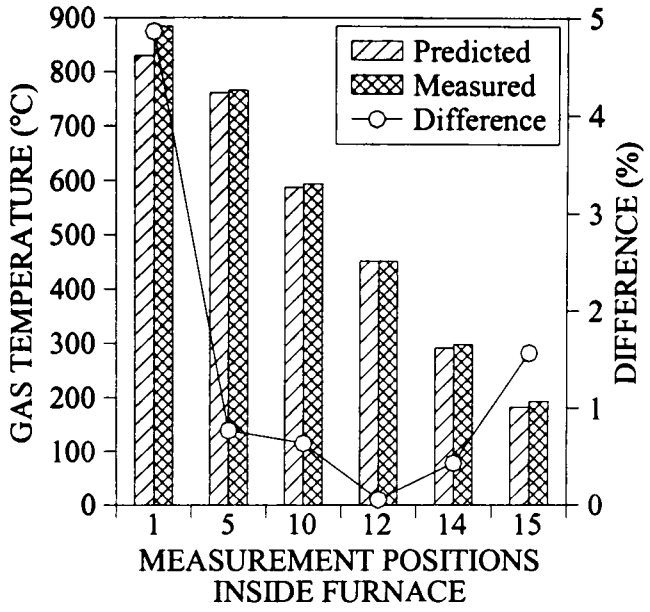

Figure 2.16 Gas Temperature Validation [91]

A number of publications also report the application of the zone method to large utility water-tube boilers. Anson [9] investigated the heat transfer distribution in an oil-fired boiler and used measurements of the flame emissivities and temperatures on the boiler as input data for the 3D zone model. The model calculated the distribution of heat fluxes in an attempt to avoid overheating of the tubes as a result of converting the system from coal to oil firing. Calculated heat fluxes were found to agree within about ±20% of those measured. Steward and Guruz [93] described a 3D mathematical simulation of the heat transfer in a large boiler and have demonstrated that predictions of the wall heat flux distribution can be obtained using data normally available to the operator. In all these studies the accuracy of the predictions was strongly affected by the uncertainties in the input data particularly of the flow, heat release patterns and radiative properties of the gaseous atmosphere. Nevertheless, in some cases simplified treatment of flow and combustion patterns was appropriate providing that soot radiation was adequately represented.

Simulations of the transient operation of furnaces using multi-zone models appears to have been restricted to the works of Charette *et al.* [81], Sousa *et al.* [94, 95] and Ward *et al.* [96]. As previously mentioned the first study used the simplified method of imaginary planes with its inherently incorrect representation of the directionality and global nature of the radiation exchange in the enclosure. Consequently, the results are likely to be less accurate than those achieved with a full zone model. Moreover, Charette and his co-workers did not make any comparisons with experimental data.

Sousa *et al.* [94, 95], on the other hand, were able to compare their predictions with experimental measurements for a gas-fired heat treatment furnace. The furnace geometry was relatively simple so that they were able to combine a LFM with a single gas zone representation of the upper part of the furnace chamber. A flexible computer code, RADEX [97], was used to generate the exchange area information so that the often applied restriction of simplifying the chamber geometry was avoided. The measured and predicted fuel consumptions were in good agreement and the model was also able to predict accurately the stock temperature-time histories for both hot and cold start-up conditions, see for example Figure 2.17.

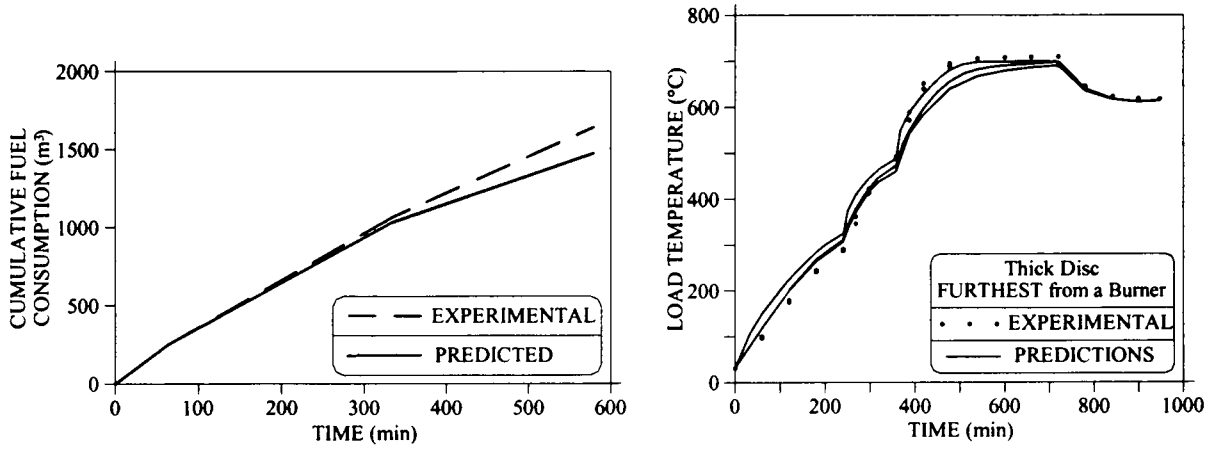

Figure 2.17 Comparison of Predicted and Measured Fuel Consumption and Load Temperature for a Gas-Fired Heat Treatment Furnace [94]

Although adequate predictions of transient performance can in some cases be obtained with a long furnace model, this may not be appropriate when the flows differ substantially from a plug-flow situation. Consequently, Ward *et al.* [96] have illustrated the advantages of using a more rigorous zoning arrangement of a gas-fired metal reheating furnace by comparing a 2D model with a LFM. The simulated furnace was similar to a scaled-up version of the system originally described by Fitzgerald and Sheridan [8] since these authors presented information on the flow patterns in the furnace chamber. These patterns were then used to estimate the inter-zone enthalpy flows in the 2D model. Comparisons of the start-up periods and fuel consumptions for the two models are presented in Table 2.3 and clearly show that the LFM representation may not always be appropriate.

Table 2.3 Comparison Between the Two-Dimensional Multi-Zone Model and the LFM of a Gas-Fired Metal Reheating Furnace

Heating Time (hrs)		Temperature Difference (°C)		Fuel Consumption (GJ)	
2D	LFM	2D	LFM	2D	LFM
1.82	1.59	93.9	99.6	35.2	30.7

The full zone method allows an accurate treatment of radiation. The model is therefore very powerful and capable of providing detailed results in combustion chambers where the LFM may not be adequate. However, the greater number of dimensions increases the number of parameters which must be taken into account so that the input required from the user becomes considerable. For cylindrical furnaces simple models can be used to provide flow and combustion patterns but for more complex shapes these main features must be supplied from other sources, typically experimental results or less commonly CFD calculations. Unfortunately, the time and costs involved in obtaining the input information often discourages the widespread adoption of multi-dimensional zone models.

Recent Advances and Applications As originally formulated the zone method requires that surfaces and gas should be grey. However, it is well known that the radiative properties of the combustion products of hydrocarbon fuels are not grey. Instead, radiation is absorbed and emitted in specific regions of the spectrum and in between those regions it travels unattenuated through the medium. In most previous studies the non-grey behaviour of the gas was accounted for by using the mixed grey gas model which provides a method of allowing for the temperature variation of the gas total properties. In this model the non-grey atmosphere is replaced by a number of grey gases for which the heat transfer rates are independently computed. The overall heat transfer is then found from a weighted sum of those heat transfer rates. Although capable of accurately representing overall radiation properties, this representation does not model directly the spectral properties of the combustion products.

Early investigations on the effect of surface emissivity in furnace enclosures (see the section on zero dimensional models) have stressed the major effect of the spectral behaviour of the gas and surface linings on the heat transfer to the load. Ceramic fibre linings have been widely used in many furnaces. However, measurements by Jackson and Yen [98] showed that the radiative properties of these materials exhibit significant

spectral variation and, therefore, the grey assumption implicit in the zone method is crude and possibly not valid. Consequently, Khan *et al.* [99] have modified the original zone approach to include this spectral variation by successfully applying the zone analysis over a number of wavelength bands in each of which the properties are assumed to be constant. With the banded technique it is no longer possible to use the mixed grey gas model to represent the non-grey gas so that an exponential wide band model was used for determining the gas properties. When all zone temperatures are specified the calculation of the total heat fluxes can be performed directly by adding the individual contributions from each band. The solution procedure becomes, however, more complex and tedious if these temperatures are unknown since an iterative approach is required.

Calculations with the banded zone model have only been carried out on a simple box enclosure for steady-state conditions. In a comparison between the original and the banded zone model [100], only small improvements were reported with the heat transfer to the load changing by less than 7% whilst the heat transfer to the combustion products by approximately 15%. The banded technique was then successfully applied to investigate the effect on fuel consumption of different non-grey lining materials [101]. The improved model is therefore capable of a more accurate representation of the non-grey surface and gas behaviour. Although only simple calculations have been performed, the banded method can be used in principle to model complicated geometries comprising multiple volume and surface zones. Nevertheless, it is difficult to ascertain if the extra computational expense in using the banded technique would supply any valuable improvement when simulating a practical furnace with multi-dimensional zone models.

For many control applications the computational times associated with zone models are too great for on-line computation so that the use of artificial neural networks (ANNs) have been suggested as an alternative. These networks, with their short computing times, can be employed to represent the behaviour of the mathematical model over a range of conditions. ANNs are simplistic representations of the biological "brain" and have been used to represent complex non-linear functions and processes. The technique is relatively new to process monitoring and control of non-linear systems but recently a number of developments have spanned a wide range of disciplines. Thus, Chong *et al.* [102] have developed neural networks for the monitoring and control of a

chain grate coal fired stoker boiler. This work concentrated on operating the boiler at optimum efficiency while producing acceptable levels of pollutant emissions. The data was then used to train both the model and the controller of the plant and the neural model prediction agreed well with the actual plant response. This study has indicated that ANNs can be used with confidence to predict boiler output and are an effective tool for control and optimisation purposes. More recently, Carvalho and Azevedo [11] have successfully trained neural networks to reproduce emission levels of NO_x and CO at the exit of a conventional pulverised coal fired boiler. The neural model was part of an overall on-line expert system aimed at assisting and optimising the control of the boiler. Detailed experimental work was undertaken in the actual utility boiler and the neural model results were shown to be in good agreement with the measurements.

To control a furnace it is necessary to predict the thermal performance of the system. This can be achieved by training an ANN using data taken from an actual plant so that in this case the neural model acts as a black box simulation tool [103]. However, the difficulty and cost associated with this type of experimental work often limits the procedure and as an alternative ANNs can be trained with data obtained from a mathematical model (such as a zone model) which is capable of accurately representing the behaviour of a furnace.

In 1999, Ward *et al.* [104] developed an artificial neural network model to simulate the transient characteristics of a simple well-stirred zone model of a gas-fired batch furnace heating steel bars to a specified discharge surface temperature. The neural model was able to predict heating times, fuel consumptions and temperature differences within the load. A range of networks was tested and the predictions of the zone and neural models were in good agreement. This work demonstrated that ANNs are a promising technique in the prediction of furnace thermal behaviour for control purposes.

The use of parallel processing for the computations associated with radiative heat transfer has recently received attention. This involves networks of high performance workstations employing arrays of processing units operating in parallel to achieve high computational speed. Thus, Saltiel and Naraghi [105] and Saltiel and Kolibal [106] have looked at the parallelisation of the zone method for analysing radiative transfer in participating media. These computer architectures have the potential for speeding up the analysis of radiation transfer which can be computationally intensive. The method

involves representing the radiative exchange factors in matrix form to fully exploit the advantages of parallel computers. Noble [107] was the first to introduce explicit matrix relations for these factors for the zone method and this has led to a substantial reduction in the computational effort. Naraghi and Chung [108] in a later development have presented a single concise explicit matrix formulation (the so-called unified matrix formulation) and this requires much less computational effort when compared to the original zone method and the Noble formulation. This unified matrix approach was then employed by the authors to find the exchange factors and hence wall heat fluxes in two and three dimensional test problems.

2.5 Limitations of Previous Work

Following the above review a number of routes have been identified for improving zone applications. Although extensively reported for modelling high temperature systems, the zone approach has generally been limited to simplistic model representations of the furnace enclosure such as the LFM. This simplified model (in which the furnace chamber is split longitudinally into a number of zones) has successfully been employed to model systems where the flow of combustion products is essentially "plug-flow" along the furnace length. However, flow patterns are often considerably more complicated with, for example, substantial recirculation ensuing in the near burner regions. Transient simulations of furnace operation have also been restricted to either simplified calculation methods (IPM) or employed simplified zone arrangements. In most applications heat release patterns were neglected by assuming combustion to be complete within the burner. This simplification is, however, not appropriate to model diffusion flames where combustion progresses along the furnace chamber. Required input information on flow and heat release patterns has usually been assumed, sometimes derived from empirical formulae and less frequently obtained by means of experimental work. Seldom have the zone approach been couple to a CFD procedure to obtain more accurate flow field information. This is mainly because of the existing computer technology still lagging behind in terms of computational time when it comes to a complete and simultaneous zone/CFD analysis. Furthermore, little information has been given on the effect of the zone size on the overall model predictions.

The obvious scope for improvement has, therefore, prompted the present research programme in that:

(i) 2D zone models, in which both height and length of the furnace are subdivided, will be employed to simulate the transient behaviour of the system following a cold start-up from ambient conditions. This appears to be the first application of a 2D zone model to a non axi-symmetric furnace operating under non-idealised conditions.

(ii) "Equivalent" LFMs will be developed and predictions compared with those of the 2D models to illustrate differences from using simplified versions.

(iii) The effect of varying the number of zones will be investigated in both 2D and LFM models and the results compared for different operating conditions.

(iv) Information regarding the flow and combustion patterns, to be used as input in the zone models, will be derived by means of an isothermal ambient temperature CFD simulation. The coupling of CFD and zone models has again been rarely used in the past.

(v) The effect of combustion heat release will be assessed by including combustion patterns derived from an isothermal CFD model. A comparison of a 2D zone model with and without heat release will be made. This is the first time diffusion flames have been represented in a multi-zone transient model.

(vi) The 2D zone models will be used to investigate changes in furnace design and control including variations in burner geometry, furnace linings, roof set point temperature, etc.

(vii) 2D steady-state zone models will be developed to simulate continuous operation and the effect of changes in furnace design and operation will be investigated. Results from the 2D steady-state zone model will be compared with those from "equivalent" LFMs and transient simulations.

References

1. Hottel, H.C., Sarofim, A.F., *Radiative Transfer*, 1967, New York: McGraw-Hill.
2. Siegel, R., Howell, J.R., *Thermal Radiation Heat Transfer*. 3rd, 1992, Washington, USA: Hemisphere Pub. Corp.
3. Patankar, S.V., *Numerical Heat Transfer and Fluid Flow*, 1980, Washington, USA: Hemisphere Pub. Corp.
4. Carvalho, M.G., Farias, T.L., *Modelling of heat transfer in radiating and combusting systems*. Trans. IChemE, 1998. **76**(Part A, February): p. 175-184.

5. Crosbie, A.L., Dougherty, R.L., *Two-dimensional radiative transfer in a cylindrical geometry with anistropic scattering.* J. Quant. Spectrosc. Radiat. Transfer, 1981. **25**: p. 551-569.
6. Hottel, H.C., Cohen, E.S., *Radiant heat exchange in a gas-filled enclosure: allowance for non-uniformity of gas temperature.* J. AIChE, 1958. **4**(March): p. 3-13.
7. Patankar, S.V., Spalding, D.B., *Heat and Mass Transfer in Boundary Layers.* 2nd Ed., 1970, London, UK: Intertext.
8. Fitzgerald, F., Sheridan, A.T., *Prediction of temperature and heat transfer distribution in gas-fired pusher reheating furnaces.* J. Inst. Fuel, 1974. **47**(March): p. 21-27.
9. Anson, D., Godridge, A.M., Hammond, E.G., *Comparison of the calculated and measured heat transfer distribution in an oil-fired water-tube boiler.* J. Inst. Fuel, 1974. **47**(June): p. 83-90.
10. Whitman, D., *Combustion modelling*, in *MRS Report No. E527.* 1988, British Gas: Solihull.
11. Carvalho, M.G., Azevedo, J.L.T., *Heat transfer model-based control in industrial equipment.* in *3rd European Thermal Sciences Conf.,* Vol. 1: p. 35-39. 2000. Heidelberg, Germany.
12. Viskanta, R., Mengüç, M.P., *Radiation heat transfer in combustion systems.* Prog. Energy Combustion Sci., 1987. **13**: p. 97-160.
13. Howell, J.R., *Thermal radiation in participating media: the past, the present and some possible futures.* J. Heat Transfer, 1988. **110**(November): p. 1220-1229.
14. Rhine, J.M., Tucker, R.J., *Modelling of Gas-Fired Furnaces and Boilers and Other Industrial Heating Processes*, 1991, London, UK: McGraw-Hill.
15. Modest, M.F., *Radiative Heat Transfer*, 1993, New York: McGraw-Hill.
16. Charette, A., Erchiqui, F., Kocaefe, Y.S., *The imaginary planes method for the calculation of radiative heat transfer in industrial furnaces.* The Canadian J. Chem. Eng., 1989. **67**(June): p. 378-384.
17. Howell, J.R., Perlmutter, M., *Monte Carlo solution of thermal transfer through radiant media between grey walls.* Trans. of the ASME, J. Heat Transfer, 1964. **86**(February): p. 116-122.

18. Howell, J.R., *The Monte Carlo method in radiative heat transfer.* Trans. of the ASME, J. Heat Transfer, 1998. **120**(August): p. 547-560.
19. Schuster, A., *Radiation through a foggy atmosphere.* The Astrophysical Journal, 1905. **21**(1): p. 1-22.
20. Siddall, R.G., *Flux methods for the analysis of radiant heat transfer.* J. Inst. Fuel, 1974. **47**(June): p. 101-109.
21. Siddall, R.G., Selçuk, N., *The application of flux methods to prediction of the behaviour of a process gas heater*, in *Heat Transfer in Flames*,ed. N.H. Afgan, Beer, J.M. 1974, John Wiley & Sons: New York. p. 191-200.
22. Fiveland, W.A., *Three-dimensional radiative heat transfer solutions by the discrete-ordinates method.* J. Thermophysics and Heat Transfer, 1988. **2**(October): p. 309-316.
23. Mengüç, M.P., Viskanta, R., *Radiative transfer in three-dimensional rectangular enclosures containing inhomogeneous, anisotropically scattering media.* J. Quant. Spectrosc. Radiat. Transfer, 1985. **33**: p. 533-549.
24. Raithby, G.D., Chui, E.H., *A finite-volume method for predicting a radiant heat transfer in enclosures with participating media.* Trans. of the ASME, J. Heat Transfer, 1990. **112**(May): p. 415-423.
25. De Marco, A.G., Lockwood, F.C., *A new flux model for the calculation of radiation in furnaces.* La Rivista dei Combustibili, 1975. **29**(May-June): p. 184-196.
26. Vercammen, H.A.J., Froment, G.F., *An improved zone method using Monte Carlo techniques for the simulation of radiation in industrial furnaces.* Intl. J. Heat Mass Transfer, 1980. **23**: p. 329-337.
27. Haidekker, A., Charette, A., Kocaefe, Y.S., *Application of the hybrid zone/Monte Carlo method to 3-D curvilinear grids in radiative heat transfer.* Intl. J. Numerical Methods Eng., 1994. **37**: p. 203-216.
28. Sasse, C., Koenigsdorff, R., Frank, S., *Evaluation of an improved hybrid six-flux/zone model for radiative transfer in rectangular enclosures.* Intl. J. Heat Mass Transfer, 1995. **38**(18): p. 3423-3431.
29. Lockwood, F.C., Shah, N.G., *A new radiation solution method for incorporation in general combustion prediction procedures.* in *18th Symposium (Intl.) on Combust.*, p. 1405-1414. 1981. The Combustion Institute, Pittsburgh.

30. Carvalho, M.G., Oliveira, P., Semiao, V., *A three-dimensional modelling of an industrial glass furnace.* J. Inst. Energy, 1988. **61**(September): p. 143-156.

31. Carvalho, M.G., Lopes, J.B., Nogueira, M., *Mathematical modelling of fluid flow and heat transfer in a glass melting furnace.* in *2nd European Conference on Industrial Furnaces and Boilers,* Vol. 2: p. 42-51. 2 - 5 April 1991. Vilamoura , Portugal.

32. Gasdallah, M., Meunier, H., *Radiative heat transfer modelling in long continuous slab reheating furnaces. Improvements of the discrete transfer method.* in *2nd European Thermal Sciences and 14th UIT National Heat Transfer Conf.,* p. 1433-1439. 1996. Rome, Italy.

33. Coelho, P.J., Carvalho, M.G., *A conservative formulation of the discrete transfer method.* Trans. of the ASME, J. Heat Transfer, 1997. **119**(February): p. 118-128.

34. Whitacre, G.R., McCann, R.A., *Comparison of methods for the prediction of radiant heat flux distribution and temperature.* Trans. of the ASME, 1975. **75-HT-9**: p. 1-8.

35. Howell, J.R., *Radiative transfer in multi-dimensional enclosures with participating media.* Proc. of the ASME, 1983. **83-HT-32**: p. 1-7.

36. Chan, S.H., *Numerical methods for multi-dimensional radiative transfer analysis in participating media,* in *Annual Review of Numerical Fluid Mechanics and Heat Transfer.* 1987. p. 305-350.

37. Castellano, L., Pasini, S., Sani, E., *Comparison of numerical models for combined convection and radiation in three-dimensional complex enclosures containing participating gases.* in *28th National Heat Transfer and Exhibition,* Vol. HTD-203: p. 245-251. 1992. San Diego, USA.

38. Tong, T.W., Skocypec, R.D., *Summary on comparison of radiative heat transfer solutions for a specified problem.* in *28th National Heat Transfer and Exhibition,* Vol. HTD- 203: p. 253-264. 1992. ASME. San Diego, USA.

39. Charette, A., Haidekker, A., Kocaefe, Y.S., *3-D comparative behaviour of discrete transfer and imaginary planes methods for furnace modelling.* The Canadian J. Chem. Eng., 1992. **72**: p. 1198-1207.

40. Carvalho, M.G., Farias, T., Fontes, P., *Multi-dimensional modelling of radiative heat transfer in scattering media.* Trans. of the ASME, J. Heat Transfer, 1993. **115**(May): p. 486-489.

41. Coelho, P.J., Goncalves, J.M., Carvalho, M.G., *Modelling of radiative heat transfer in enclosures with obstacles.* Intl. J. Heat Mass Transfer, 1998. **41**: p. 745-756.

42. Beer, J.M., Chigier, N.A., *Combustion Aerodynamics*, 1972, London: Applied Science Pub.

43. Meunier, H., Cambier, M., *Application of thermal performance modelling to fuel consumption reduction and control of batch furnaces.* in *1st European Conference on Industrial Furnaces and Boilers,* 1988. Lisbon, Portugal.

44. Meunier, H., Cambier, M., *Modelling of batch furnaces for metal heat treatment and ceramic ware firing.* European J. Mech. Eng., 1989. **34**: p. 155-161.

45. Post, L., Hoogendoorn, C.J., *Modelling of gas-fired glass furnaces.* in *1st European Conference on Industrial Furnaces and Boilers,* 21 - 24 March 1988. Lisboa, Portugal.

46. Wieringa, J.A., Elich, J.J., Hoogendoorn, C.J., *Spectral effects of radiative heat transfer in high temperature furnaces burning natural gas.* J. Inst. Energy, 1990(September): p. 101-108.

47. Docherty, P., Tucker, R.J., *The influence of wall emisivity on furnace performance.* J. Inst. Energy, 1986. **59**: p. 35-37.

48. Elliston, D.G., Gray, W.A., Hibberd, D.F., Ho, Y.T., Williams, A., *The effect of surface emissivity on furnace performance.* J. Inst. Energy, 1987(December).

49. Alexander, I., Gray, W.A., Hampartsoumian, E., Taylor, J.M., *Surface emissivities of furnace linings and their effect on heat transfer in an enclosure.* in *1st European Conference on Industrial Furnaces and Boilers,* 21 - 24 March 1988. Lisboa, Portugal.

50. Guruz, H.K., *A simple method for predicting the overall performance of fuel-oil fired boilers.* Combustion Science and Technology, 1977. **17**: p. 163-168.

51. Palmer, M.R., *Modelling high temperature plant*, in *MRS Report No. E521.* 1988, British Gas: Solihull.

52. Fitzgerald, F., *Aspects of furnace design for hot working*, in *Publication 111.* 1968, I.S.I. p. 123-131.

53. Fitzgerald, F., Sheridan, A.T., *The heating of a slab in a furnace*, in *Publication 123.* 1969, I.S.I. p. 18-28.

54. Salter, F.M., Costick, J.A., *Mathematical model of the heat transfer within a reaheating furnace.* J. Inst. Fuel, 1974. **47**(March): p. 3-19.

55. Enemoto, H., Essenhigh, R.H., Tsai, Y.W., *Heat transfer in a continuous model furnace: comparison of theory and experiment.* in *Proc. of the ASME,* Vol. 75-HT-5: p. 1-11. 1975.

56. Hadvig, S., *Gas emissivity and absorptivity: a thermodynamic study.* J. Inst. Fuel, 1970. **43**(4): p. 129-135.

57. Chapman, K.S., Ramadhyani, S., Viskanta, R., *Modelling and analysis of heat transfer in a direct-fired continuous reheating furnace.* in *Winter Annual Meeting of the ASME,* Vol. 122: p. 35-43. 1989. San Francisco, USA.

58. Fontana, P., Boggiano, A., Furinghetti, A., *A two-dimensional mathematical model of slab reheating furnaces: theory and practical utilisation.* in *3rd Process Technical Conf. AIME,* p. 142-150. 1982. Pittsburgh, USA.

59. Faber, A., Michelfelder, S., *A one-dimensional mathematical model for the calculation of heat flux distributions in furnaces with substantial external recirculation*, in *Report No. G 04/a/8.* 1976, IFRF: IJmuiden.

60. Dugwell, D.R., Oakley, D.E., *A model of heat transfer in tunnel kilns used for firing refractories.* Intl. J. Heat Mass Transfer, 1988. **31**(11): p. 2381-2390.

61. Ribesse, S., Lybaert, P., Meunier, H., *A dynamic model of tunnel kilns for firing ceramics.* in *3rd European Thermal Sciences Conf.,* Vol. 2: p. 1235-1240. 2000. Heidelberg, Germany.

62. Lucas, D.M., Lockett, A.A., *Mathematical modelling of heat flux and temperature distribution in shell boilers.* in *4th Symp. on Flames and Industry, Paper 15,*1972. The Institute of Fuel. London, UK.

63. Lucas, D.M., Toth, H.E., *The calculation of heat transfer in the fire tubes of shell boilers.* J. Inst. Fuel, 1972. **45**(October): p. 521-528.

64. Niu, Z., Wong, K.F.V., *Adaptive simulation of boiler unit performance.* Energy Conversion and Measurement, 1998. **39**(13): p. 1383-1394.

65. Saimbi, M.S., Tucker, R.J., *Mathematical modelling of the thermal performance of furnaces operating under non-steady conditions*, in *MRS Report No. E407.* 1983, British Gas: Solihull.

66. Tucker, R.J., Lorton, R., *Mathematical modelling of load-recuperative gas-fired furnaces*, in *MRS Report No. E418.* 1984, British Gas: Solihull.

67. Tucker, R.J., Ward, J., *Use of a Monte Carlo technique for the determination of radiation exchange areas in long furnace models.* in *Proc. 8th Intl. Heat Transfer Conf.*, p. 391-396. 1986. San Francisco, USA.

68. Tucker, R.J., Ward, J., *Mathematical modelling of heat transfer in a gas-fired reheating furnace operating under non-steady state conditions.* in *Proc. 9th Intl. Heat Transfer Conf.*, Vol. 6: p. 221-226. 1990. Jerusalem, Israel.

69. Emery, A.F., Johnson, O., Lobo, M., Abrous, A., *A comparative study of methods for computing the diffuse radiation view factors for complex structures.* J. Heat Transfer, 1991. **113**(May): p. 413-422.

70. Larsen, M.E., Howell, J.R., *Least-squared smoothing direct exchange areas in zonal analysis.* Trans. of ASME, J. Heat Transfer, 1986. **108**: p. 239-242.

71. Lawson, D.A., Tucker, R.J., Sousa, J., Ward, J., *Advances in the zone method for furnace design.* in *BFRC Flame Days, Paper 1.3,*1994. Leeds, UK.

72. Lawson, D.A., Ziesler, C.D., *An accurate program for radiation modelling in the design of high-temperature furnaces.* IMA J. Math. Applied in Business and Industry, 1996. 7(2): p. 109-116.

73. Halliday, W., *Computer control model for continuous reheat furnaces.* in *1st European Conference on Industrial Furnaces and Boilers,*1988. Lisboa, Portugal.

74. Michotte, J., Bretton, V., *Incidence of thermal inertia on the thermal follow-up and operation of reheating furnaces.* Revue Generale de Thermique, 1990. **346**(October): p. 475-484.

75. Herapath, R.G., Peskett, S., *Excess oxygen and temperature control in furnaces - a dynamic modelling study.* J. Inst. Energy, 1987. **60**(December): p. 171-184.

76. Meunier, H., Cambier, M., *Simulation of a batch furnace for metal heat treatment: optimisation of setpoint schedule.* in *2nd European Conference on Industrial Furnaces and Boilers,* p. 48-57. 1991. Vilamoura, Portugal.

77. Yu, B., *Dynamic modelling of a tunnel kiln.* Heat Transfer Eng., 1994. **15**(2): p. 39-53.

78. Johnson, T.R., Beer, J.M., *The zone method analysis of radiant heat transfer: a model for luminous radiation.* in *4th Symp. on Flames and Industry, Paper 4,*1972. The Institute of Fuel. London, UK.

79. Johnson, T.R., Lowes,T.M., Beer, J.M., *Comparison of calculated temperatures and heat flux distributions with measurements in the IJmuiden furnace.* in *Fourth*

Symp. on Flames and Industry, Paper 11,1972. The Institute of Fuel. London, UK.

80. Steward, F.R., Tennankore, K.N., *Towards a finite difference solution coupled with the zone method for radiative transfer for a cylindrical combustion chamber.* J. Inst. Energy, 1979. **52**(September): p. 107-114.
81. Charette, A., Larouche, A., Kocaefe, Y.S., *Application of the imaginary planes method to three-dimensional systems.* Intl. J. Heat Mass Transfer, 1990. **33**: p. 2671-2681.
82. Charette, A., Larouche, A., Bui, R.T., Kocaefe, Y.S., *The imaginary planes method applied to the 3D simulation of the transient behaviour of metal processing furnaces.* in *Heat Transfer Conf.*, p. 425-430. 1990. Jerusalem, Israel.
83. Charette, A., Haidekker, A., Kocaefe, Y.S., *The imaginary planes method applied to three-dimensional cylindrical systems for modelling thermal radiation.* in *7th Intl. Conf. on Numerical Methods in Thermal Problems*, p. 776-785. 1991.
84. Charette, A., Kocaefe, Y.S., Larouche, A., Bui, R.T., *Modelling combustion systems using the imaginary planes method for radiation.* in *Spring Technical Meeting of the Combustion Institute*, p. 63-66. May 1990. Alberta, Canada.
85. Li, Z., Barr, P.V., Brimacombe, J.K., *Computer simulation of the slab reheating furnace.* Canadian Metallurgical Quarterly, 1988. **27**(3): p. 187-196.
86. Beltagui, S.A., Fuggle, R.N., Ralston, T., *Measurement and prediction of heat transfer in the NEL furnace.* in *2nd UK National Conf. Heat Transfer*, Vol. 2: p. 1219-1232. 1988. Glasgow, UK.
87. Jenkins, B.G., Moles, F.D., *Modelling of heat transfer from a large enclosed flame in a rotary kiln.* Trans. IChemE, 1981. **59**: p. 17-25.
88. Craya, A., Curtet, R., *On the spreading of a confined jet*, in *Comptes-rendus*. 1955, Academie des Sciences: Paris. p. 621-622.
89. Omori, T., *Monte Carlo simulation of indoor radiant environment.* Intl. J. Num. Meth. Eng., 1990. **30**: p. 615-627.
90. Omori, T., Nagata, T., Taniguchi, H., *Three-dimensional heat transfer analysis of a steel heating furnace.* in *7th Intl. Conf. on Numerical Methods in Thermal Problems*, Vol. 2: p. 1346-1356. 1991.

91. Olsommer, B., Von Spakovsky, M., Fravat, D., *Transfert de chaleur par rayonnement dans un four d'incineration industriel: application de la methods des zones.* Revue Generale de Thermique, 1997. **36**(2): p. 125-134.

92. Olsommer, B., Duperrex, Y., Von Spakovsky, M., Van Gilst, J., *Simulation numerique d'un four d'incineration d'ordures industrial couple a une chaudiere a circulation naturelle.* Rev. Gen. Therm., 1997. **36**(2): p. 135-148.

93. Steward, F.R., Guruz, H.K., *Mathematical simulation of an industrial boiler by the zone method of analysis*, in *Heat Transfer in Flames*,ed. N.H. Afgan, Beer,J.M. 1974, John Wiley & Sons: New York. p. 47-71.

94. Sousa, J.L.V.A., Ward, J., Wallis, R.A., Lawson, D.A., *Simulation and measurement of the transient performance of a gas-fired heat treatment furnace.* in *2nd European Thermal Sciences & 14th UIT National Heat Transfer Conf.,* May 29-30 1996. Rome, Italy.

95. Sousa, J.L.V.A., Ward, J., Wallis, R.A., *Development and validation of a multi-zone model of an intermittently operated gas-fired furnace.* in *4th European Conference on Industrial Furnaces and Boilers,*1997. Espinho, Portugal.

96. Ward, J., Correia, S.A.C., Sousa, J.L.V.A., *The application of multi-zone thermal radiation models to investigate the energy efficiency of a metal reheating furnace under start-up conditions.* in *Proc. of the ASME,* Vol. AES- 39: p. 621-626. 1999. Nashville, USA.

97. Lawson, D.A., *RADEX User Guide.* Coventry University, 1991.

98. Jackson, J.D., Yen, C.C., *Measurement of total and spectral emissivities of some ceramic fibre insulation materials.* in *Ceramics in Energy Applications Conf.,* p. 159-174. 1994. London, UK.

99. Khan, Y.U., Lawson, D. A., Tucker, R.J., *Radiative heat transfer calculations for non-grey surfaces.* in *Numerical Methods in Thermal Problems,* Vol. 9: p. 351-361. 1995.

100. Khan, Y.U., Lawson, D.A., Tucker, R.J., *Banded radiative heat transfer analysis.* Communications in Numerical Methods in Engineering, 1997. **13**: p. 803-813.

101. Khan, Y.U., Lawson, D.A., Tucker, R.J., *Analysis of radiative heat-transfer in ceramic-lined and ceramic-coated furnaces.* J. Inst. Energy, 1998. **71**(March): p. 21-26.

102. Chong, Z.S., *The Monitoring and Control of Stoker Fired Boiler Plant by Neural Networks.* University of Glamorgan, 1996.

103. Chong, Z.S., Wilcox, S.J., Ward, J., Butt, A., *The development of a neural network controller for a chain grate, stoker-fired boiler.* in *4th European Conf. on Industrial Furnaces and Boilers,* Vol. 1: p. 271-280. 1997. Espinho, Portugal.

104. Ward, J., Wilcox, S.J., Payne, R., *Prediction of the thermal performance of a high temperature furnace using neural networks.* in *6th UK National Heat Transfer Conf.,*1999. Edinburgh, UK.

105. Saltiel, C., Naraghi, M.H.N., *Parallel processing approach for radiative heat transfer prediction in participating media.* AIAA J. Thermophysics, 1993. **7**(4): p. 739-742.

106. Saltiel, C., Kolibal, J., *Parallel radiative transport using an unified matrix approach.* Applied Numerical Mathematics, 1997. **25**: p. 499-509.

107. Noble, J.J., *The zone method: explicit matrix relations for total exchange areas.* Intl. J. Heat Mass Transfer, 1975. **18**: p. 261-269.

108. Naraghi, M.H.N., Chung, B.T.F., *A unified matrix formulation for the zone method: a stochastic approach.* Intl. J. Heat Mass Transfer, 1985. **28**(1): p. 245-251.

CHAPTER THREE

PRINCIPLES OF THE ZONE METHOD

3.1 Introduction

The previous chapter examined the advantages and disadvantages of the different methods available for the solution of the radiative heat transfer in high temperature combustion systems. Based on these comparisons, the zone method was selected as the most appropriate modelling technique to be adopted in this research project since, in general, the method was capable not only of handling the transient behaviour of a metal reheating furnace but also of efficiently performing the computations. The principles of the zone model will now be presented along with a simplified generic formulation of the method. The method involves calculation of temperature dependent exchange factors which will also be defined in the next section. Non-steady state conditions can be easily implemented in the zone method for the simulation of transient processes and this will be briefly outlined in the last part. The principles laid out here form the basis of the mathematical models developed in the following chapters for the study of both intermittently and continuously operated high temperature metal reheating furnaces. Simulations were undertaken for both nozzle mix and diffusion flame burners.

3.2 Overall Principles

One of the most comprehensive methods available for calculating radiation heat transfer in combustion systems is the zone analysis originally introduced by Hottel and Cohen [1] and further developed by Hottel and Sarofim [2]. The method is essentially an energy balance technique which discretises the non-isothermal furnace bounding surfaces and combustion space into a series of isothermal zones with uniform radiative properties. Energy balances are then drawn up for each zone taking into account the complex nature of the radiation interchange between all zones in the system (both volume and surface) as well as convective heat transfer from appropriate hot gas zones to adjacent load or refractory surface zones. In addition, for each volume (gas) zone the energy balance includes energy release due to combustion within the zone together with the enthalpy transport into and out of the zone by the flow of combustion products. Providing that flow and combustion information are available, all terms in these equations may be specified and the resultant set of non-linear algebraic equations can be solved numerically for the unknown zone temperatures by means of rapidly converging methods such as the Newton-Raphson technique, see [3, 4]. Solution of these equations (one for each zone in the system) yields the sought temperature distribution and fluxes throughout the enclosure.

The calculation of the radiation interchange terms requires the knowledge of so-called exchange factors for each of the zone pairs in the furnace. These take into account the non-grey absorption and emission by the combustion products as well as multiple diffuse reflections and partial absorption of radiation at the load and refractory surfaces. These terms are computed in successive stages and can be found from knowledge of the geometry and radiation properties of the zones. There are three different types of radiation factors required, the formulation of which will be introduced later in the chapter. To begin with, the direct exchange areas between each pair of zones, that is, surface-surface, surface-gas and gas-gas are calculated and these factors express the effective area for direct radiative interchange between the two zones in the pair. This is followed by the total exchange areas, which are a measure of the radiation emitted by one zone that is absorbed by another, either directly or after multiple reflections from other surfaces. Finally, the directed flux areas are determined which account for the radiant energy transfer between zones, making allowance for the non-grey, temperature dependent character of the combustion products.

Although evaluation of the radiative exchange factors is an essential step in the application of the zone method, it is also the most time-consuming task in the overall process. This is because the complex expressions describing these factors, which depend upon the geometry and optical properties of the enclosure, are hardly ever possible to evaluate analytically. This is further aggravated in more elaborate zoning arrangements since a very fine subdivision will require the computation of numerous exchange factors and hence inevitably considerable computer storage. In order to ease the computational burden and arrive at tractable applications of the zone method, it is important to separate the calculation of the radiative exchange factors from the solution of the total energy balance equations for each zone and this is only possible when the direct and total exchange factors are independent of the temperatures in the furnace. However, this condition can only be realised when the gas and surfaces in the enclosure are considered to be grey, i.e. with radiant properties independent of temperature. With the grey gas restriction, the calculations of direct and total exchange areas need only be performed once for a given geometry and therefore are automatically excluded from the main solution of the radiative problem. The non-grey behaviour of combustion can, however, be represented by a so-called mixed grey gas model [2]. The exchange areas are then evaluated as weighted sums of the contribution of each of the grey gases.

3.3 Exchange Areas

The formulation of the three types of exchange factors which are required to describe the radiation term of the energy balance equation is now presented.

3.3.1 Direct Exchange Areas

The radiation exchange between two surfaces is illustrated in Figure 3.1. Because radiation is usually assumed to be emitted diffusively (as is the case in the present study) and travels in straight lines, not all the radiation leaving surface i reaches surface j. The fraction of the radiation leaving a body i and received directly by j without taking into account any reflections is commonly known as view factor, F_{ij} where i and j denote the emitting and receiving surfaces. The direct exchange area from surface i to j is then given by A_iF_{ij}.

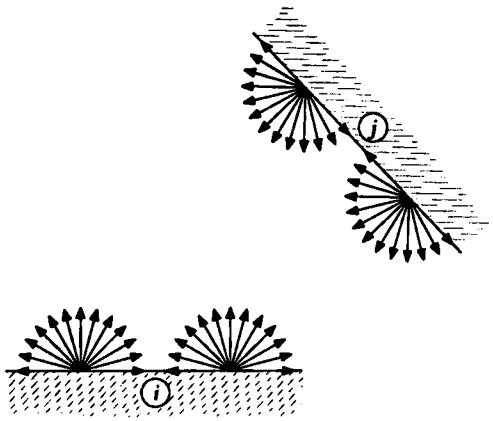

Figure 3.1 Radiation Exchange Between Two Diffuse Surfaces

Direct exchange areas are designated in this thesis by the symbols $\overline{s_i s_j}$, $\overline{s_i g_j}$ and $\overline{g_i g_j}$ for surface-surface, surface-gas and gas-gas respectively and are the constants of proportionality relating the radiation net exchange to the difference in the emissive powers ($E=\sigma T^4$) of the two zones:

$$Q_{ij} = \overline{s_i s_j}\ (E_i - E_j) \tag{3.1a}$$

$$Q_{ij} = \overline{s_i g_j}\ (E_i - E_{g,j}) \tag{3.1b}$$

$$Q_{ij} = \overline{g_i g_j}\ (E_{g,i} - E_{g,j}) \tag{3.1c}$$

Since the proportion of radiation leaving from a body which arrives directly at another body is dependent only on the shape and relative disposition of the zone pair, direct exchange areas are, therefore, a function of the geometry and do not depend on body and gas temperature. They have dimensions of area and may be expressed as:

$$\overline{s_i s_j} = \overline{s_i g_j} = A_i F_{ij} \tag{3.2a}$$

$$\overline{g_i s_j} = \overline{g_i g_j} = 4K_i V_i F_{ij} \tag{3.2b}$$

As mentioned previously the term F_{ij}, commonly referred to as view factor, is the fraction of radiant energy emitted by body i which is directly intercepted by body j. From Equations (3.2) it can be seen that all direct exchange areas are independent of surface emissivity but attenuation by any intervening grey gas can be allowed for by

including a term for the fraction of energy transmitted through the gas (known as the transmissivity):

$$\tau = \exp(-Kr) \tag{3.3}$$

K in this formula accounts for the radiative energy absorbed by the intervening gas per unit distance and is termed the attenuation or extinction coefficient and r is the path length.

The full mathematical derivation of these direct exchange areas is not included in this work but details can be found in Rhine and Tucker [4]. Nevertheless, the physical arrangement from which they can be derived is presented in Figure 3.2.

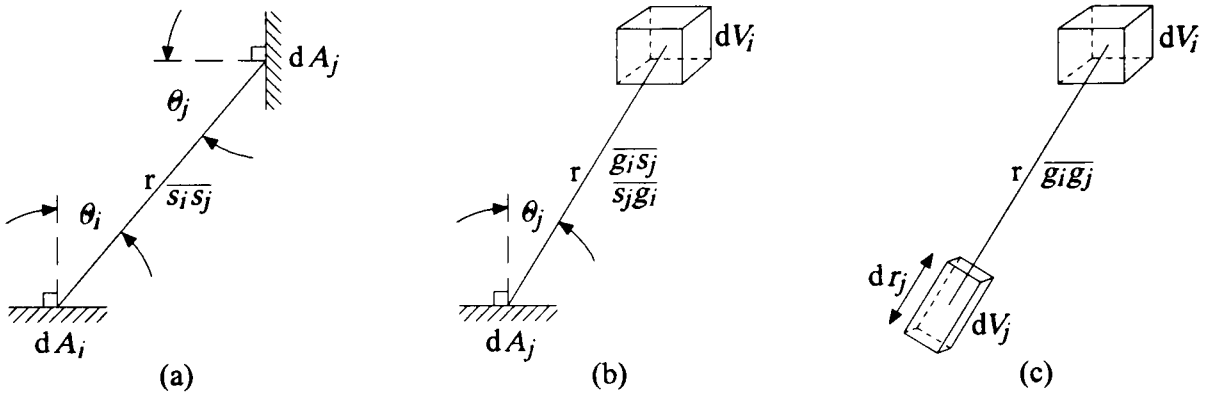

Figure 3.2 Direct Exchange Between Differential Surface and Volume Elements in a Radiating Enclosure

The direct exchange area between a surface i and surface j (Figure 3.2a) is defined by the following multiple integral:

$$\overline{s_i s_j} = \int_{Aj}\int_{Ai} \frac{\cos\theta_i \cos\theta_j \exp(-Kr)}{\pi r^2} \, dA_i \, dA_j \tag{3.4}$$

with the surface-gas $\overline{s_i g_j}$ and gas-gas $\overline{g_i g_j}$ areas having similar integral definitions.

In the case of surface to gas radiation interchange (Figure 3.2b), the integral is defined by:

$$\overline{s_i g_j} = \int_{Vj}\int_{Ai} \frac{K\cos\theta_i \exp(-Kr)}{\pi r^2} dA_i dV_j \tag{3.5}$$

and it describes the fraction of radiation emitted by surface i that is directly absorbed within volume j. If the interchange is between two volume zones (Figure 3.2c), the direct exchange area integral is given by:

$$\overline{g_i g_j} = \int_{Vj}\int_{Vi} \frac{K^2 \exp(-Kr)}{\pi r^2} dV_i dV_j \tag{3.6}$$

and it expresses the proportion of radiation emitted from all points within volume i that is directly absorbed within volume j.

The symmetry of the integrals allows the following relationships to be written:

$$\overline{s_i s_j} = \overline{s_j s_i} \tag{3.7a}$$

$$\overline{s_i g_j} = \overline{g_j s_i} \tag{3.7b}$$

$$\overline{g_i g_j} = \overline{g_j g_i} \tag{3.7c}$$

and these are known as the reciprocity relationships. For an enclosure comprising m surface elements and l volume elements conservation of energy also dictates that:

$$A_i = \sum_{j=1}^{m} \overline{s_i s_j} + \sum_{j=1}^{l} \overline{s_i g_j} \tag{3.8a}$$

$$4K_i V_i = \sum_{j=1}^{m} \overline{g_i s_j} + \sum_{j=1}^{l} \overline{g_i g_j} \tag{3.8b}$$

Equations 3.8 are obtained by performing an energy balance on a zone in thermal equilibrium with its surroundings.

Analytical evaluation of these multiple integral equations is extremely difficult if not impossible to perform in complicated geometries. Analytical, tabular and graphical values have, therefore, been compiled through experimental studies or mathematical

calculations but only for a few relatively simple geometric shapes. When the zone method is applied to real situations where the surface geometries are complex and no analytical expressions are available, entering the required exchange areas from these sources is tedious. Moreover, the inherent inaccuracies of values read from graphs can lead to errors in the calculation of the radiative fluxes and consequent failure of the overall radiative energy balance. In such cases, different approximate numerical techniques must be employed. It is important to note that for a grey gas with uniform radiative properties, the direct exchange areas are exclusively a function of the geometric configuration of the enclosure so that a single computation is sufficient.

Several numerical methods are available for the calculation of direct exchange areas [5]. However the present discussion is restricted to just two of these techniques, namely numerical integration and Monte Carlo. The numerical integration method involves subdividing the enclosure into small volumetric or surface elements and the direct exchange factor is found from the details on the centre-to-centre spacing, orientation of the elements and of the radiation properties of the participating gas. The computational effort involved can be great since in some cases high accuracy can only be obtained at the expense of adopting a small element size. They provide, however, useful results to check the accuracy of other approximate methods.

In the Monte Carlo method [6], the objective is to model the behaviour of photons by a smaller number of energy bundles emitted from the surface. Because emission can be considered to be diffuse, it is possible to represent this emitted radiation by large number of beams emitted in random directions from random points on the surface. Non-diffuse behaviour can be represented by biasing the direction of emission. The choice of the emitting location and direction is dictated by distributions based upon random numbers. Each ray is checked to see which surface or gas zone it strikes and the procedure is repeated until the total number of rays is used. For a gas zone a similar procedure is followed such that the emitting points from within the gas zone are uniformly distributed. Typically values for the total number of rays used are of the order of 10^4 to 10^6 with the accuracy increasing as this number increases. The exchange areas for $\overline{s_i s_j}$, $\overline{s_i g_j}$ and $\overline{g_i g_j}$ are then obtained by:

$$\overline{s_i s_j} = \frac{\text{Number of Rays Emitted by Surface } i \text{ Intercepted by Surface } j}{\text{Total Number of Rays Emitted by } i} A_i \qquad (3.9a)$$

$$\overline{s_i g_j} = \frac{\text{Number of Rays Emitted by Surface } i \text{ Absorbed by Volume } j}{\text{Total Number of Rays Emitted by } i} A_i \qquad (3.9b)$$

$$\overline{g_i g_j} = \frac{\text{Number of Rays Emitted by Volume } i \text{ Absorbed by Volume } j}{\text{Total Number of Rays Emitted by } i} 4K_i V_i \qquad (3.9c)$$

In contrast to the alternative methods in which a direct evaluation of the relevant integrals is attempted, the Monte Carlo approach simulates the actual physical process of radiative heat transfer. The method can be easily adapted to treat any complex geometry although the cost in terms of computational effort can be high. In a comparison study, Emery *et al.* [5] concluded that the method "*probably represents the best numerical method for computing view factors, F_{ij}*".

Although very flexible, the statistical nature of the method brings in some limitations in that the results are inherently subject to statistical errors. Because of this, the mean values of exchange factors found from the calculations do not necessarily meet the principle of reciprocity, see Equations 3.7. By the nature of the simulation, conservation of energy (i.e. Equations 3.8) is always ensured since all simulated beams are absorbed either by a surface or gas zone in the enclosure. However, averaging of the reciprocal exchange factors to satisfy reciprocity destroys this agreement so that it requires another step to re-establish the intrinsic energy conservation principle. To overcome this problem several techniques for adjusting exchange factors were proposed to ensure that the constraints are satisfied [7-10].

3.3.2 Total Exchange Areas

In enclosures containing grey surfaces, the exchange areas must also account for the additional exchange between zone pairs arising from multiple reflections from the surfaces, such as walls and load in a furnace. Total exchange areas can then be derived from direct exchange areas to include this mechanism and are designated by $\overline{S_i S_j}$, $\overline{S_i G_j}$ and $\overline{G_i G_j}$ in this thesis. The net radiative exchange between two grey and diffuse elements i and j with allowance for both direct and indirect radiation, the latter as a result of reflection from other surfaces in the enclosure, is proportional to their total exchange area, such that:

$$Q_{ij} = \overline{S_i S_j}\ (E_i - E_j) \qquad (3.10a)$$

$$Q_{ij} = \overline{S_i G_j}\ (E_i - E_{g,j}) \tag{3.10b}$$

$$Q_{ij} = \overline{G_i G_j}\ (E_{g,i} - E_{g,j}) \tag{3.10c}$$

This new set of exchange factors is, therefore dependent on the reflectivities of all surfaces and on the direct exchange areas and can be obtained by performing a radiative energy balance on each zone element and introducing the concept of radiative flux.

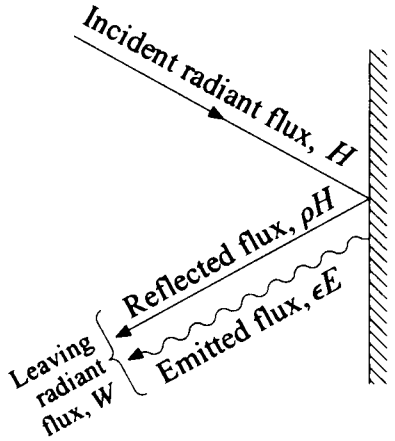

Figure 3.3 The Incident and Leaving Fluxes at a Surface Element

Considering a surface i of emissivity ε_i, and reflectivity ρ_i in the grey enclosure shown in Figure 3.3, we can write that the leaving radiative flux from the surface, W_i, is made up of the emitted flux $\varepsilon_i E_i$ due to emission from the surface, and the reflected flux $\rho_i H_i$ due to partial reflection of the incident flux, H_i, arriving from the surroundings:

$$W_i = \varepsilon_i E_i + \rho_i H_i \tag{3.11}$$

Now assuming that the same enclosure of arbitrary geometrical complexity is subdivided into m surfaces and l volume elements having diffusively reflecting walls and containing an uniform absorbing-emitting grey, non-scattering gas, the radiative energy balance equation at each surface element is given by:

$$A_i H_i = \sum_{j=1}^{m} \overline{s_i s_j} W_j + \sum_{j=1}^{l} \overline{s_i g_j} E_{g,j} \tag{3.12a}$$

And for each volume element:

$$4K_iV_iH_{gi} = \sum_{j=1}^{m} \overline{g_i s_j} W_j + \sum_{j=1}^{l} \overline{g_i g_j} E_{g,j} \tag{3.12b}$$

As originally formulated in Hottel and Sarofim [2], the procedure to calculate the total exchange areas was non-explicit and the scalar notation used to describe the above equations proved quite difficult to incorporate in an efficient computer code. In an attempt to simplify this calculation, Noble [11] proposed a method for calculating the total exchange areas explicitly from direct exchange areas and the method considered the above equations written in matrix form. Taking advantage of the matrix properties, Noble arrived at a general solution method for the calculation of the total exchange areas explicitly from knowledge of the direct exchange areas and this significantly improved the overall computational process. Tucker and Rhine [4] later introduced a further simplification to the derivation process proposed by Noble. Equations 3.11 and 3.12 can be arranged in matrix form as:

$$\mathbf{W} = \boldsymbol{\varepsilon}\mathbf{I}.\mathbf{E} + \boldsymbol{\rho}\mathbf{I}.\mathbf{H} \tag{3.13a}$$

$$\mathbf{AI}.\mathbf{H} = \overline{\mathbf{ss}}.\mathbf{W} + \overline{\mathbf{sg}}.\mathbf{E_g} \tag{3.13b}$$

$$\mathbf{4KVI}.\mathbf{H_g} = \overline{\mathbf{gs}}.\mathbf{W} + \overline{\mathbf{gg}}.\mathbf{E_g} \tag{3.13c}$$

where the last two expressions are the radiant energy flux incident either on a surface or on a gas zone as a result of radiation leaving all other zones. In these equations, the notation **AI**, $\boldsymbol{\varepsilon}\mathbf{I}$ and $\boldsymbol{\rho}\mathbf{I}$ is used to represent the diagonal matrices of A_i, ε_l and ρ_l, respectively.

An energy balance analysis at each of the m surface and l volume zones of the enclosure, yields:

$$\mathbf{Q} = \boldsymbol{\varepsilon}\mathbf{AI}.(\mathbf{E} - \mathbf{H}) \tag{3.14a}$$

$$\mathbf{Q_g} = \mathbf{4KVI}.(\mathbf{H_g} - \mathbf{E_g}) \tag{3.14b}$$

where **Q** equals the net radiation loss from surface zones and $\mathbf{Q_g}$ the net radiation absorbed by volume zones.

Using the concept of total exchange areas, it is possible to write the equations of the radiant energy balance on a zone as follows:

$$\mathbf{Q = \varepsilon AI.E - \overline{SS}.E - \overline{SG}.E_g} \tag{3.15a}$$

$$\mathbf{Q_g = \overline{GS}.E + \overline{GG}.E_g - 4KVI.E_g} \tag{3.15b}$$

Total exchange areas can then be obtained by mathematical manipulation of Equations 3.12, the results of which when compared with Equations 3.15 yield the desired expressions. Details of the elimination procedure adopted to arrive at the appropriate equations can be found in Rhine and Tucker [4]. Under matrix notation, the arrays defining the total exchange areas are as follows:

$$\mathbf{\overline{SS} = \varepsilon AI.R.\overline{ss}.\varepsilon I} \tag{3.16a}$$

$$\mathbf{\overline{SG} = \varepsilon AI.R.\overline{sg}} \tag{3.16b}$$

$$\mathbf{\overline{GG} = \overline{gs}.\rho I.R.\overline{sg} + \overline{gg}} \tag{3.16c}$$

where **R** is the inverse matrix defined as:

$$\mathbf{R = [AI - \overline{ss}.\rho I]^{-1}} \tag{3.17}$$

Thus, total exchange areas can be easily computed from direct exchange areas by simply applying a matrix inversion technique. They provide a complete description of the effects of system geometry, surface emissivities and gas absorptivities on the radiative transport between zones and in a sense can be considered to represent the effective area for black body radiation exchange between two zones. The method is however, restricted to systems with grey gases and grey surfaces. Nevertheless, for a particular geometry, total exchange factors need only be determined on a single occasion.

Consideration of thermodynamic equilibrium requires that the total exchange areas defined in Equations 3.15 satisfy reciprocity and the following conservation relations, commonly designated as summation rules:

$$\varepsilon AI = \overline{SS} + \overline{SG} \tag{3.18a}$$

$$4KVI = \overline{GG} + \overline{GS} \tag{3.18b}$$

which are similar to the relations found for direct exchange areas in Equations 3.8.

Both Equations 3.18 and 3.8 are useful for checking the accuracy of the calculation of the exchange factors. The expressions also allow estimation of some of the exchange areas to be performed by arithmetic difference. Failure to satisfy these energy conservation relationships results in errors arising in the solution of the system of energy balance Equations 3.15, since the emitted and receiving fluxes no longer correspond. This inconsistency can ultimately lead to the case where a solution is unattainable.

3.3.3 Directed Flux Areas

In computing the exchange of thermal radiation between any two zones, the equations are formulated assuming that the participating surfaces and gases in the system are grey. However, a real gas, in contrast to the hypothetical grey gas, exhibits a variation in absorption coefficient with both temperature and wavelength and is therefore non-grey. As a result, the total emissivity versus partial pressure-path length relation for a real gas does not conform to the familiar exponential law characterising grey gas radiation:

$$\varepsilon_g = 1 - \exp\left(-k_{g,n} pL\right) \tag{3.19}$$

where $k_{g,n}$ is the gas absorption coefficient, p is the partial pressure and L is the path length.

There is, nevertheless considerable advantage in retaining the grey gas formulation for gas emissivity and absorptivity, since the direct and total exchange areas can be determined without knowledge of the temperature field. This can be achieved by representing the real gas as a mixture of grey gases.

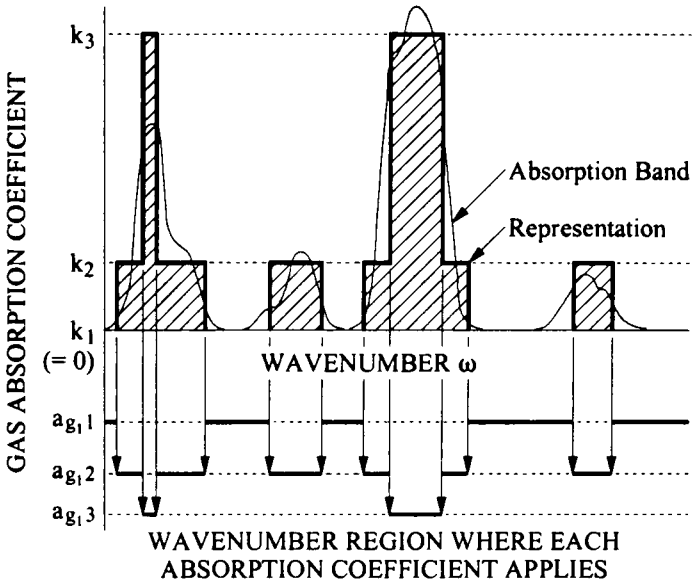

Figure 3.4 Representation of Real Gas Absorption Bands [2]

Hottel [1] demonstrated that the contribution of a real gas to the radiant flux in an enclosure can be represented as the weighted sum of the independent contributions of a number of grey gases (N_g) of different absorption coefficients $k_{g,n}$, see Figure 3.4, weighted in proportion to the coefficients $a_{g,n}$ in the function:

$$\varepsilon_g = \alpha_g = \sum_{n=1}^{N_g} a_{g,n}\left[1 - \exp\left(-k_{g,n} pL\right)\right] \tag{3.20}$$

where $$\sum_{n=1}^{N_g} a_{g,n} = 1$$

The weighting factors, $a_{g,n}$,may be interpreted as the fractional amount of blackbody energy in the spectral regions where the grey gas of absorption coefficient applies. In practice, the weighting factors are obtained by fitting Equation 3.20 to tabulated values of total emissivity and absorptivity and are generally represented by linear relationships with temperature. As shown in Equation 3.20, the grey gas emissivity is expressed in terms of temperature-independent absorption coefficients and the product of the partial pressure of the absorbing gas and path length. Total emissivity and absorptivity may then be evaluated once absorption and the polynomial coefficients for the weighting factors are available. Usually, the use of two or three grey gaseous components, one of

which is clear (i.e. it has a zero absorption coefficient) to account for the non-absorbing regions in the spectrum, is sufficient to accurately represent the total emissivity and absorptivity of a real gas over a wide range of temperatures and partial pressure-path length product. Figures 3.5 and 3.6 show the level of accuracy obtained with a three-term and four-term fit to the data for the non-luminous combustion products of natural gas as reported by Truelove [12].

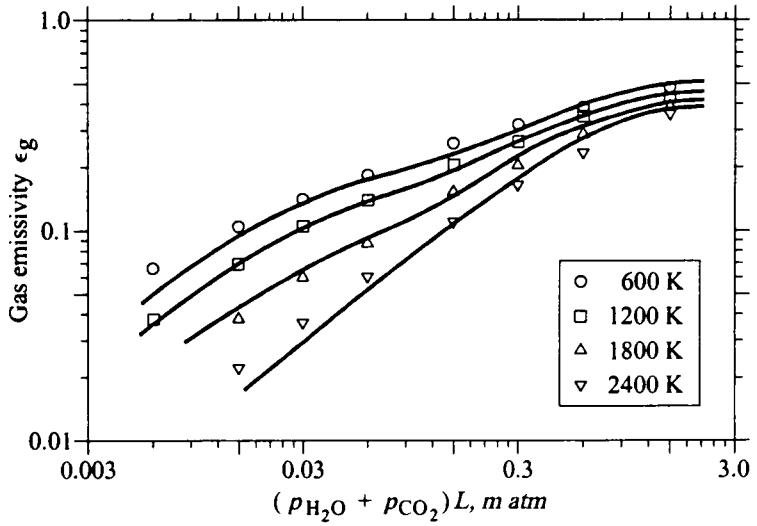

Figure 3.5 Three-Term (1 clear + 2 grey) Mixed Grey Gas Fit to Total Emissivity Data of Natural Gas Combustion Products [12]

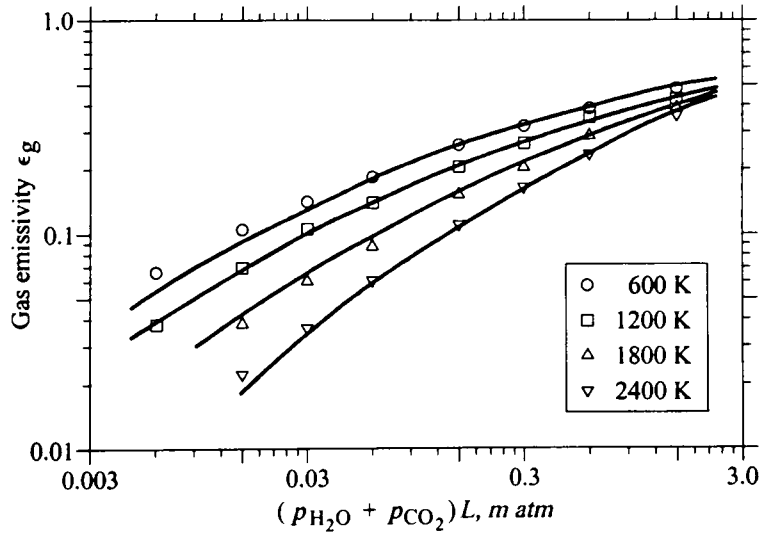

Figure 3.6 Four-Term (1 clear + 3 grey) Mixed Grey Gas Fit to Total Emissivity Data of Natural Gas Combustion Products [12]

The advantage of the mixed grey gas model is that it is possible to use a set of constant absorption coefficients and use the weighting factors to represent the temperature dependence of the gas emissivity and absorptivity. Under these conditions the total exchange areas can be evaluated for each of the grey gases with absorption coefficients $k_{g,n}$ and the net radiant flux between zones is then the weighted sum of the independent contributions of each grey gas using the weighting factors, $a_{g,n}$, evaluated at the temperature of the emitting source. The net radiative flux between a pair of zones then becomes:

$$\dot{Q}_{i\Leftrightarrow j} = \overrightarrow{S_iS_j}\, E_i - \overleftarrow{S_iS_j}\, E_j \tag{3.21a}$$

$$\dot{Q}_{i\Leftrightarrow j} = \overrightarrow{G_iS_j}\, E_{g,i} - \overleftarrow{G_iS_j}\, E_j \tag{3.21b}$$

$$\dot{Q}_{i\Leftrightarrow j} = \overrightarrow{G_iG_j}\, E_{g,i} - \overleftarrow{G_iG_j}\, E_{g,j} \tag{3.21c}$$

where $\overrightarrow{S_iS_j}$, $\overleftarrow{S_iS_j}$, $\overrightarrow{G_iS_j}$, $\overleftarrow{G_iS_j}$, $\overrightarrow{G_iG_j}$ and $\overleftarrow{G_iG_j}$ are the directed flux areas given by:

$$\overrightarrow{S_iS_j} = \sum_{n=1}^{N_g} a_{s,n}(\mathrm{T}_i)\left(\overline{S_iS_j}\right)_{K=K_n} \tag{3.22a}$$

$$\overleftarrow{S_iS_j} = \sum_{n=1}^{N_g} a_{s,n}(\mathrm{T}_j)\left(\overline{S_iS_j}\right)_{K=K_n} \tag{3.22b}$$

$$\overrightarrow{G_iS_j} = \sum_{n=1}^{N_g} a_{g,n}(\mathrm{T}_{g,i})\left(\overline{G_iS_j}\right)_{K=K_n} \tag{3.22c}$$

$$\overleftarrow{G_iS_j} = \sum_{n=1}^{N_g} a_{s,n}(\mathrm{T}_j)\left(\overline{G_iS_j}\right)_{K=K_n} \tag{3.22d}$$

$$\overrightarrow{G_iG_j} = \sum_{n=1}^{N_g} a_{g,n}(\mathrm{T}_{g,i})\left(\overline{G_iG_j}\right)_{K=K_n} \tag{3.22e}$$

$$\overleftarrow{G_iG_j} = \sum_{n=1}^{N_g} a_{g,n}(\mathrm{T}_{g,j})\left(\overline{G_iG_j}\right)_{K=K_n} \tag{3.22f}$$

with the weighting factors given by the simple linear expressions described in [12]:

$$a_{s,n}(T_i) = b_{1,n} + b_{2,n}T_i \tag{3.23a}$$

$$a_{g,n}(T_{g,i}) = b_{1,n} + b_{2,n}T_{g,,i} \tag{3.23b}$$

To reduce the computational effort associated with the zone method, the absorption coefficients for total emissivity and absorptivity are taken to be identical and so the fitting coefficients $b_{1,n}$ and $b_{2,n}$,which are obtained using a least square fitting procedure, are also the same. Values for the three-term and four-term mixed grey gas model parameters of Truelove for the combustion products of natural gas are reproduced in Table 3.1.

Table 3.1 Grey Gas Parameters Used in Mixed Grey Gas Correlations for Natural Gas Combustion Product Emissivity [4]

n	$b_{1,n}$	$b_{2,n}$x10^3 (K^{-1})	$k_{g,n}$ ($m^{-1}atm^{-1}$)
Three-term (two grey plus one clear) gas model:			
1	0.437	0.0713	0
2	0.39	-0.0052	1.88
3	0.173	-0.0661	68.8
Four-term (three grey plus one clear) gas model:			
1	0.423	0.0433	0
2	0.285	0.0513	0.89
3	0.227	-0.0676	15.5
4	0.065	-0.027	240.0

Directed flux areas express, therefore the energy issued by a surface or volume element i that is absorbed by a surface or volume element j. The formulation includes the effects of total enclosure geometry, multiple reflections and the non-grey absorption and emission of the combustion gases. They are a function of the temperature of the radiating emitter and can be computed from more fundamental sets of exchange areas which are themselves temperature independent. Thus, for a given geometry containing a gas which can be approximated by a mixture of grey gases, N_g sets of direct and total

exchange areas must be evaluated for all zone pairs prior to the evaluation of the radiative energy balance and consequently to the overall energy balance on each zone.

3.4 Total Energy Balances

To obtain the temperature distribution in a combustion system and consequently the heat transfer to the surrounding surfaces, the total energy balance equations, one for each zone of unknown temperature, must be solved. Directed flux areas enable the radiant energy balance to be drawn up for each surface and gas zone in the enclosure but for a total energy balance other forms of energy transport need to be considered. Figure 3.7 is a schematic representation of the radiant balance formulation for both surface and volume zones. It is obtained as the difference between the arriving radiation from all m surface and l volume zones in the enclosure and the leaving radiation of the zone which equals the emitted radiation by the zone.

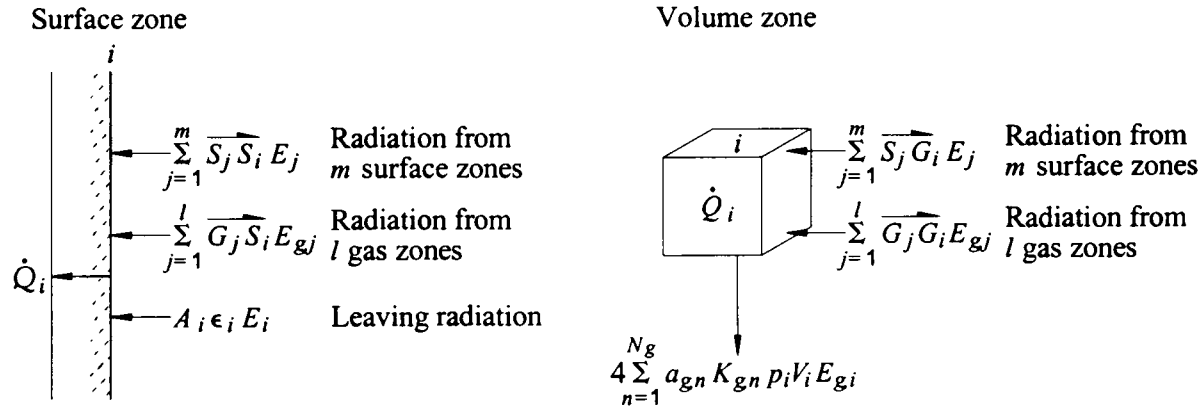

Figure 3.7 The Radiant Energy Balance at a Surface and Volume Zone *i*

For a surface zone the radiant balance becomes:

$$\sum_{j=1}^{m} \overrightarrow{S_j S_i} E_j + \sum_{j=1}^{l} \overrightarrow{G_j S_i} E_{g,j} - A_i \varepsilon_i E_i = \dot{Q}_{rad,i} \tag{3.24a}$$

and for a volume zone:

$$\sum_{j=1}^{l} \overrightarrow{G_j G_i} E_{g,j} + \sum_{j=1}^{m} \overrightarrow{S_j G_i} E_j - 4 \sum_{n=1}^{N_g} a_{g,n} k_{g,n} p_i V_i E_{g,i} = \dot{Q}_{rad,i} \tag{3.24b}$$

where $\dot{Q}_{rad,i}$ is the net radiant energy flow to zone i.

The only remaining terms to be evaluated for use in the total energy balance on each zone are the non-radiation terms, i.e. convection from the combustion products, energy transfer from neighbouring zones due to the flow of combustion products and if appropriate energy release by combustion in a particular volume zone.

For a gas zone i surrounded by a total number of surface elements N_s, the net heat transfer to the combustion products is:

$$\sum_{j=1}^{l} \overrightarrow{G_j G_i E_{g,j}} + \sum_{j=1}^{m} \overrightarrow{S_j G_i E_j} - 4 \sum_{n=1}^{N_g} a_{g,n} k_{g,n} p_i V_i E_{g,i} - \sum_{s=1}^{N_s} A_{N_s} h_{N_s} \left(T_{g,i} - T_{N_s} \right) + \\ + \dot{Q}_{enth,i} + \dot{Q}_{input,i} - \dot{Q}_{cp,i} = 0 \tag{3.25}$$

The first three terms of the equation correspond to the radiation transfer and this is followed by convection to all surfaces surrounding the volume zone. $\dot{Q}_{enth,i}$ is the net energy transferred across the boundaries of the volume zone due to enthalpy flows from adjacent volume zones. It can be obtained by knowledge of the properties of the combustion products, their mass flow rates and the direction of the flow. $\dot{Q}_{input,i}$ is the total energy input to a gas zone from fuel and combustion air and can be given as:

$$\dot{Q}_{input,i} = \left(\dot{Q}_{fuel,net} + \dot{Q}_{air} \right)$$

where

$$\dot{Q}_{fuel,net} = m_{fuel} * Cv_{fuel,net}$$

$$\dot{Q}_{air} = m_{fuel} * A/F * \left(1 + \frac{\%Excess\ Air}{100} \right) * H_{air}(T_{air}) \tag{3.26}$$

and m_{fuel} is the fuel mass flow rate, $Cv_{fuel,net}$ is the fuel net calorific value, A/F is the air/fuel ratio and $H_{air}(T_{air})$ is the specific enthalpy of the combustion air.

If combustion is assumed to occur outside of the furnace chamber such as when using nozzle mix burners, the above term is present only in the equations for gas zones where the burners are placed. However, when there is a gradual release of heat through the system (e.g. with a diffusion flame), only a fraction of the heat input in the fuel is

released at specific gas zones. In this case, it is important to find the zones confining the release of energy and get the appropriate fractional amount of fuel energy input (f) so that for those zones Equation 3.26 becomes:

Zone Immediately Adjacent to Burner

$$\dot{Q}_{input,i} = \left(f * \dot{Q}_{G,net} + \dot{Q}_{air} \right) \qquad (3.27a)$$

Other Heat Release Zones

$$\dot{Q}_{input,i} = f * \dot{Q}_{G,net} \quad \text{with } 0 \leq f \leq 1 \qquad (3.27b)$$

The last term of Equation 3.25, $\dot{Q}_{cp,i}$, represents the energy loss in the flue products and similarly to the preceding term it only appears in the equations for gas zones where the flue is placed.

In a similar fashion, an energy balance for a surface zone i adjacent to gas zone ad gives:

$$\sum_{j=1}^{m} \overrightarrow{S_j S_i} E_j + \sum_{j=1}^{l} \overrightarrow{G_j S_i} E_{g,j} - A_i \varepsilon_i E_i + A_i h_i (T_{g,ad} - T_i) = \dot{Q}_i \qquad (3.26)$$

where $\dot{Q}_i$ is the net heat transfer into surface i. For steady-state simulations, $\dot{Q}_i$ is specified as the steady-state wall conduction loss or the load enthalpy gain.

Energy balances are drawn for each zone of unknown temperature so that a system of simultaneous non-linear algebraic equations is obtained and these must be solved iteratively for the temperatures and hence heat fluxes by means of numerical techniques such as the Newton-Raphson method [3, 4].

The formulation of the zone method, as described above, allows estimation of only the steady-state conduction loss through surrounding walls and heat transfer to the load. However, the method can be easily modified to account for the time dependent temperatures within the system resulting from transient thermal conduction into the load and walls. This is done by solving the partial differential equation for the transient conduction for each surface zone (wall and load) within the system. The mathematical solution of these conduction equations can be obtained using standard finite-difference techniques as discussed in Croft and Lilley [13] or by finite-element methods.

The build up of the energy balance equations within the zone method is not always straightforward due to difficulties associated with the evaluation of some of the input information. This is, particularly, the case with multi-dimensional models where large quantities of input data are required. In addition to the computational effort involved in the calculation of exchange factors, rigorous treatment also depends on a detailed knowledge of the flow patterns of the combustion products and the distribution of heat release due to the progress of combustion. The zone method does not provide this type of information. Consequently, alternative methods such as published correlations, the use of physical models or CFD models must be employed. Detailed evaluation of these terms will be described in the next chapter which looks at the construction and implementation into a computer format of the multi-zone mathematical models employed in this study to assess the transient thermal performance of a high temperature metal reheating furnace.

References

1. Hottel, H.C., Cohen, E.S., *Radiant heat exchange in a gas-filled enclosure: allowance for non-uniformity of gas temperature.* J. AIChE, 1958. **4**(March): p. 3-13.
2. Hottel, H.C., Sarofim, A.F., *Radiative Transfer*, 1967, New York: McGraw-Hill.
3. Press, W.H., Teukolsky, S.A., Vetterling, W.T., Flannery, B.P., *Numerical Recipes in Fortran.* 2nd, Vol. 1, 1994, Cambridge: Cambridge University Press.
4. Rhine, J.M., Tucker, R.J., *Modelling of Gas-Fired Furnaces and Boilers and Other Industrial Heating Processes*, 1991, London: McGraw-Hill.
5. Emery, A.F., Johnson, O., Lobo, M., Abrous, A., *A comparative study of methods for computing the diffuse radiation view factors for complex structures.* J. Heat Transfer, 1991. **113**(May): p. 413-422.
6. Howell, J.R., Perlmutter, M., *Monte Carlo solution of thermal transfer through radiant media between grey walls.* Trans. of the ASME, J. Heat Transfer, 1964. **86**(February): p. 116-122.
7. Larsen, M.E., Howell, J.R., *Least-squared smoothing direct exchange areas in zonal analysis.* Trans. of ASME, J. Heat Transfer, 1986. **108**: p. 239-242.
8. Vercammen, H.A.J., Froment, G.F., *An improved zone method using Monte Carlo techniques for the simulation of radiation in industrial furnaces.* Intl. J. Heat Mass Transfer, 1980. **23**: p. 329-337.

9. Loehrke, R.I., Dolaghan, J.S., Burns, P.J., *Smoothing Monte Carlo exchange factors*. in *Trans. of the ASME, J. Heat Transfer,* Vol. 117: p. 524-526. May 1995.

10. Tucker, R.J., Ward, J., *Use of a Monte Carlo technique for the determination of radiation exchange areas in long furnace models*. in *Proc. 8th Intl. Heat Transfer Conf.,* p. 391-396. 1986. San Francisco, USA.

11. Noble, J.J., *The zone method: explicit matrix relations for total exchange areas.* Intl. J. Heat Mass Transfer, 1975. **18**: p. 261-269.

12. Truelove, J.S., *A mixed grey gas model for flame radiation*, 1976, Thermodynamics Division, AERE (Atomic Energy Authority): Harwell.

13. Croft, D.R., Lilley, D.G., *Heat Transfer Calculations Using Finite Difference Equations*. 1st ed., Vol. 1, 1977: Applied Science Pub.

CHAPTER FOUR

THE BASIC TRANSIENT MODEL OF THE GAS-FIRED FURNACE

4.1 Introduction

The zone method of radiation analysis is a widely used method for the prediction of the thermal radiation transfer in furnaces and other high temperature systems. Since it was first proposed [1], significant progress have been made and today the model is used extensively for the solution of the radiative heat transfer problem in multi-dimensional enclosures. Zone models vary greatly in complexity depending on the number and arrangement of zones that subdivide the furnace. Therefore, they may take various forms, from the simplest models of the well-stirred single gas zone type to the so-called long furnace models culminating in sophisticated multi-dimensional zone models. This chapter describes in detail the construction of a multi-dimensional model, based on the zone analysis. The sequence of calculations and the logic of the computer model are outlined. The chapter includes details on flow field and combustion data generation, estimation of exchange factors, zone calculations, transient conduction analysis in the load and furnace lining and also on the simulation of the mode of furnace control and operation. Transient and steady-state zone models were developed and then applied to investigate the thermal performance of a gas-fired metal reheating furnace. This chapter concentrates on the formulation of a transient zone model for the gas-fired furnace which was fitted with nozzle mix burners (i.e. combustion was assumed to be complete

within the burners). The modification of this initial model to incorporate diffusion flames (i.e. flames in which heat is released gradually within the furnace chamber) is described later in Chapter 9. In addition, the structure of the zone model which was employed to study continuous operation of the furnace is described in Chapter 8.

4.2 Furnace Details

The gas-fired furnace employed in this study was used to heat steel bars to a nominal discharge temperature of 1250°C. The overall dimensions and geometry are shown in Figure 4.1.

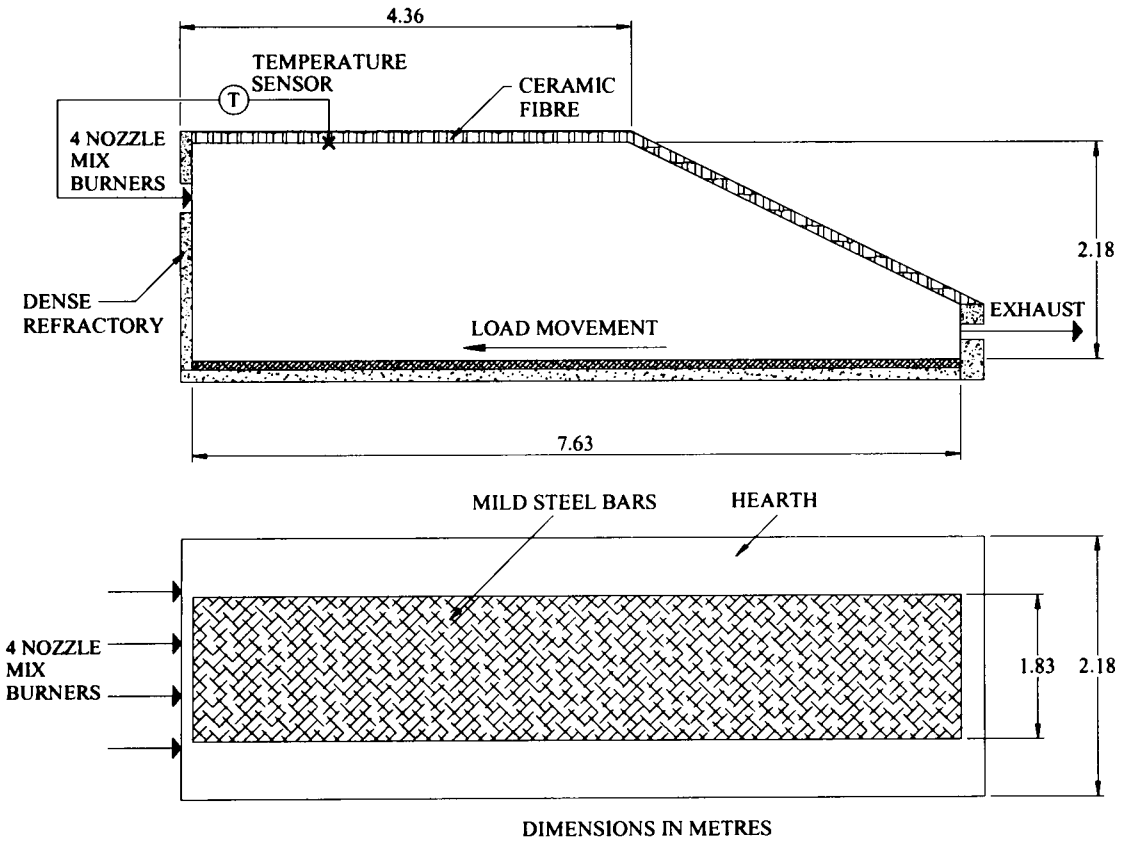

Figure 4.1 The Steel Reheating Furnace

The furnace was 7.63m long by 2.18m wide and had a maximum height of 2.18m with an inclined roof which sloped down to a height of 0.545m at the charge end with the exhaust combustion products also removed from this end of the furnace. It was normally fired by four nozzle mix cold air, gas burners each with a diameter of 0.19m mounted symmetrically at a pitch of 0.545m and at a height of 1.635m above the hearth in the end wall of the discharge end of the system. The overall maximum thermal input to the furnace (i.e. the maximum rating of the burners) was 5.4 MW based on the gross

calorific value of the natural gas, see Appendix A. The burners usually operated with an excess air level which was maintained constant at 5% and combustion was assumed to be complete within the burner nozzles. The furnace temperature was controlled by means of a control thermocouple mounted at the hot face of the roof near the discharge end. The natural gas and air input system were then controlled in response to changes in this sensor temperature relative to a specified set point. The walls and hearth of the chamber were constructed of dense refractory (density 2600 kg/m^3) whilst the roof was assumed to consist typically of lightweight (density 128 kg/m^3) ceramic fibre insulation. The thickness of the walls and roof were 300mm and 350mm respectively. The furnace load was a bed of mild steel bars 1.83m long and 64mm thick and these were positioned symmetrically on the hearth. The furnace was considered to be a "pusher" type so that as a new cold bar was introduced at the charge end a hot bar was discharged thereby maintaining a continuous bed of bars on the hearth.

4.3 Overall Structure of the Transient Model

As seen in the preceding chapter, the zone model starts by dividing the enclosure into a number of isothermal volume and surface zones. The degree of discretisation is strongly dependent on the particular problem and on the required accuracy. Energy balances are then performed for each zone taking into account all major forms of energy transfer and these balances require supplementary information about the flow field and combustion patterns. The resulting equations are non-linear in temperature but can be easily solved by rapidly converging numerical techniques. Transient behaviour can be included by successively solving the zone model at discrete time steps and using the new "most recent" estimated heat fluxes to update the walls and load temperatures. In this case the initial surface temperatures are specified at the start of the simulation so that only the heat balances on each gas zone need to be solved. The next section looks in detail at the fundamental steps required in the construction of a multi-dimensional transient zone model.

The overall solution procedure of a transient zone model can be represented schematically as shown in Figure 4.2:

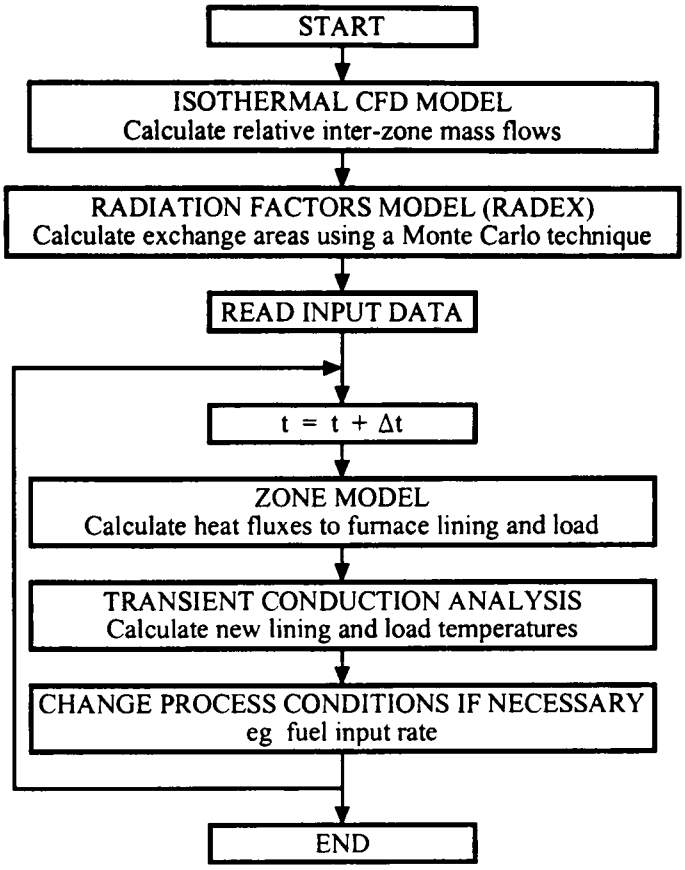

Figure 4.2 Simplified Flow Diagram for a Transient Zone Model

The first two modules are pre-processing routines for the zone model since they are run before the simulation itself to prepare the sets of data for flow and geometrical factors which will be used throughout the simulation. This prior calculation thus reduces the overall computational time for the transient zone model. The overall model incorporates the following main modules:

- the first module, *Isothermal CFD Model*, calculates the relative inter-zone mass flows for subsequent description of the enthalpy terms in the zone model. For a given geometrical configuration and burner arrangement, this block needs to be calculated just once since the flows are assumed to be independent of furnace temperature. Once the velocity data are generated by the CFD model, they must be reprocessed to provide the inter-zone mass flows which can, in turn, yield the enthalpy terms.
- the second module, *Radiation Factors*, evaluates the direct and total exchange areas between all zone pairs in the system. This block is again calculated just once for a given geometry and the results are then used to describe the radiation terms in the zonal energy balances.

- the third main module, *Zone Model*, solves the system of energy balance equations for each surface and volume zone in the enclosure to determine the gas temperatures and heat fluxes to the furnace lining and load.
- the final module, *Transient Calculations*, accounts for the transient behaviour of the furnace and is a combination of two sub-models one of which covers transient conduction within the "walls" and load and the other simulates the furnace temperature control system.

4.4 Isothermal CFD Model

Because the zone model analysis is limited to the solution of heat transfer, not all the terms in Equation 3.25 (i.e. the energy balance for a gas zone) are readily evaluated. One such term is the enthalpy, $\dot{Q}_{enth}$, which is calculated from the mass flow rates of the combustion gases across the zone boundaries and the specific enthalpies of these gases evaluated at the temperature of the zone from which the gas flows. These data must be supplied from other sources, as seen in section 1.6. For this particular investigation, data on the flow patterns inside the furnace were obtained from ambient isothermal CFD simulations as they can conveniently provide sufficiently reliable estimation of this flow information provided that similarity considerations between the CFD model and the furnace are taken into account.

Previous studies [2, 3] have demonstrated that cold flow models can provide adequate representation of flame systems as discussed in section 1.6. In these studies it was observed that the flow and combustion patterns were not substantially affected by the heat transfer but only by the geometry of the system and the burner characteristics. This means that the effects of temperature and combustion on the flow patterns can often be neglected and as a direct result the radiation and isothermal flow calculations in this present model can be carried out separately. To obtain sufficiently accurate information, allowance has to be made for non-isothermal conditions in the furnace and this is usually achieved by burner distortion in accordance with the Thring-Newby criterion, see Rhine and Tucker [3]. The setting up of a problem is complex in a CFD model and the subsequent selection, extraction and, if necessary, manipulation of the relevant data for input into the zone model is a further complication. The background to CFD modelling is therefore outlined in this chapter as well as the general procedure

employed to generate and extract the required flow information from the CFD models for subsequent input into the zone models.

4.4.1 Computational Fluid Dynamic Models

Computational fluid dynamics, usually abbreviated as CFD, has been used to describe the solution of fluid dynamics problems by means of a computer based simulation. The models consist mainly of a set of differential equations describing the important physics of the flow problem and these can be solved using numerical methods to obtain a description of the flow field of interest. These techniques date back to the early 1970's [4] and involve dividing the region of interest into a large number of cells or control volumes in each of which the partial differential equations (Navier-Stokes equations) are rewritten in algebraic form by relating the different variables to the values in the neighbouring cells.

In general, a CFD simulation requires a geometry model to describe the region of interest by a computational mesh which covers the flow field, a turbulence model to simulate high Reynolds number flows and numerical algorithms to solve the resultant discretised equations. Since the technique first appeared, rapid advances in computer technology combined with improvements in the solution algorithms have extended the range of applications of CFD to include more complex plant phenomena. This has led to the development of commercial CFD codes for the solution of complicated flow problems. A modern CFD code typically contains models for flows, combustion, heat transfer, NOx formation, multi-phase phenomena and particle transport. These commercial codes have now reached the point where there is considerable flexibility in the software due to development of sophisticated user interfaces to input the problem parameters and to examine the results.

The structure of a commercial CFD software consists mainly of three modules:

- the ***pre-processor*** module where the flow problem is initially defined. Here both the geometrical domain of the calculation and the finite difference grid are specified. This module is also used for the specification of solver, fluid properties and other additional input characteristics.
- the ***solver*** module solves the discretised representation of the problem. There are three distinct discretisation methods commonly used in CFD: finite difference, finite volume and finite element methods. The main differences between them are a consequence of the nature of the derivation process adopted

for the discretisation equations. The choice of a particular method depends on the level of accuracy, flexibility and efficiency required. Further details on discretisation methods are available in Patankar [4] and Versteeg and Malalasekera [5].

- the ***post-processor*** module houses the data visualisation tools which are used to produce the main graphics output.

4.4.2 The Governing Equations for a Fluid Flow Problem

The governing partial differential equations of fluid flow represent mathematical statements of the conservation laws for mass, momentum and energy and are usually expressed in the following form:

$$\underbrace{\frac{\partial(\rho\phi)}{\partial t}}_{transient} + \underbrace{div(\rho u\phi)}_{convective} = \underbrace{div(\Gamma_{eff}\, grad\phi)}_{diffusive} + \underbrace{S_\phi}_{source} \qquad (4.1)$$

where ϕ is the dependent conserved variable such as velocity, temperature, etc. Equation 4.1 describes the various transport processes with the rate of change and convective terms on the left hand side and the diffusive term (Γ is the diffusion coefficient) and the source term on the right hand side.

Most of the flows encountered in practical applications are turbulent, i.e. there is a state of chaotic and random behaviour changing continuously with time. Turbulent flows are more complex because of the appearance of rotational flow structures called eddies of a vast range of length and time scales. In these cases, complete solution could only be achieved by employing extremely fine grids and infinitesimal time steps, making the approach extremely expensive and demanding with current technology.

At present, the most commonly used CFD tool for solving the governing equations is the Reynolds Averaged Navier Stokes Solutions (RANS) technique. This method rather than attempting to model all the features of the turbulent motion by means of the Navier Stokes equations, opts for a simulation based on the time averaged behaviour. The RANS approach essentially expands the transport properties to account for the effects of turbulent eddy transport and this is done by replacing the variable ϕ in Equation 4.1 by the sum of mean and fluctuating components.

Thus,

$$\phi = \Phi + \phi' \tag{4.2}$$

The fundamental equations are averaged over a period of time, introducing additional terms called Reynolds' stresses and Reynolds' fluxes. Because the Navier Stokes equations are non-linear, averaging does not lead to a closed set of equations. Closure is then provided by means of a turbulence model which predicts these Reynolds stresses and fluxes. A number of turbulence models have been developed all of which vary in complexity and their suitability for specific flow problems. Classical models currently available in commercial CFD codes are the k-ε model, the Reynolds stress model (RSM) and the algebraic stress model (ASM). With these models the time-averaged equations for turbulent flow have the same appearance as the equations for laminar flow, however, the viscosity and diffusivity coefficients are replaced by effective (laminar + turbulent) coefficients.

$$\begin{aligned} \mu_{eff} &= \mu + \mu_t \\ \Gamma_{eff} &= \Gamma + \Gamma_t \end{aligned} \tag{4.3}$$

The problem of determining the Reynolds stresses and fluxes is then transformed into that of estimating these effective coefficients. In the k-ε model, the Reynolds stresses are approximated by a linear relationship to the turbulent viscosity, μ_t, and velocity gradients. The turbulent viscosity is assumed to be isotropic and is further related to the turbulence kinetic energy (k) and its rate of dissipation (ε) by:

$$\mu_t = C_\mu \rho \frac{k^2}{\varepsilon} \tag{4.4}$$

Approximate equations are then solved for k and ε, and this introduces additional constants. Because the velocity in turbulent flows has been found to vary logarithmically near the walls, a wall function of this type is used to avoid fully resolving the model equations in the near wall region. The approach has been shown to provide good representation of many industrially relevant flows and has been widely validated [5-7]. For more complex flows, where anisotropic turbulence plays an

important role, models such as the RSM and ASM can be used to produce more accurate results. However, the performance of these models has not always lived up to expectations with their success depending very much on the flow of interest [5, 8]. This together with the extra computational effort involved in these improved turbulence models has contributed to the widespread use of the k-ε turbulent treatment as employed in the present study.

4.4.3 Discretisation of the Equations and Solution Algorithms

This project uses a commercial flow solver, CFX 4.2, developed by AEA Technologies to perform the CFD calculations. The code is based on a finite volume method where all variables such as velocity, temperature, etc. are defined at the centre of the control volumes which represent the physical domain. Thus, the remainder of the discussion of the CFD analysis is solely concerned with this method.

The method uses a curvilinear coordinate transformation which transforms the complex boundary of the flow domain in physical space into one simple (rectangular) boundary flow domain in computational space. All equations are then solved in the transformed coordinate system. Equation 4.1 is integrated over each control volume to yield a discretised algebraic equation in ϕ at each cell centre. These equations, when supplemented by appropriate boundary and initial conditions can be solved to give the distribution of the variable at the cells. The inherent non-linearities in the governing equations impose the use of iterative solution techniques.

All the terms in Equation 4.1 are discretised in space using the second order central differencing scheme except for convective terms. To illustrate the diffusion term consider the one-dimensional geometry in Figure 4.3:

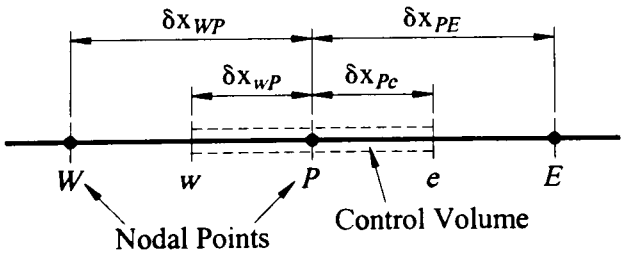

Figure 4.3 Control Volume Notation

The diffusion term at point P is discretised as:

$$\int_{\Delta V} \frac{d}{dx}\left(\Gamma \frac{d\phi}{dx}\right) dV = \left(\Gamma A \frac{d\phi}{dx}\right)_e - \left(\Gamma A \frac{d\phi}{dx}\right)_w = \Gamma_e A_e \left(\frac{\phi_E - \phi_P}{\delta x_{PE}}\right) - \Gamma_w A_w \left(\frac{\phi_P - \phi_W}{\delta x_{WP}}\right) \qquad (4.5)$$

This central differencing scheme involves using the values of node points E and W to evaluate the variable ϕ at the mid point P, whose value is thus always influenced by adjacent values in both directions. Details of the present central differencing scheme can be found in Appendix B. Convective terms on the other hand spread their influence only in the flow direction and therefore require a special treatment. CFX 4.2 provides a number of alternative discretisation techniques for the convective effects including central, upwind, hybrid and higher order differencing schemes. In the present study a hybrid scheme was used for the convection term. The accuracy of the solutions of the model equations is a function of the discretisation approach chosen for the convective terms since the more accurate schemes are also computationally more demanding.

A number of iterative methods are available for the solution of the coupled non-linear algebraic transport equations. These equations describe the influence on a particular variable in a particular cell of: other variables in the same cell; values of the same variable in the neighbouring cells and values of other variables in the neighbouring cells. The iterative procedure is therefore taken at two levels: an inner iteration solves the spatial coupling for each variable and an outer iteration solves the linkage between variables. Popular solvers for the algebraic equations are the line-by-line solver and more recently Stone's algorithm [9]. To avoid difficulties caused by instability in the iterative solution of the algebraic equations of non-linear problems, under-relaxation is often used to slow down the changes from iteration to iteration in the values of a particular variable. Further details on solvers and the under-relaxation process are available in Patankar [4] and Anderson [10].

The treatment of the non-linearity of the momentum equations introduces, however, a further complication since there is no obvious equation for obtaining the pressure term. This can be resolved by adapting an iterative technique such as the SIMPLE algorithm to ensure correct coupling of pressure and velocity. In this algorithm an assumed pressure field is used to solve the momentum equations and pressure correction equations are then solved to update the pressures and correct the velocity

field. Further details of SIMPLE and other variants of this method may be found in Patankar [4]. To avoid unrealistic behaviour of the discretised momentum equation for spatially oscillating pressure fields, the grid for the velocity field is usually staggered. An algorithm developed by Rhie and Chow [11] has, however, removed the need for staggered grids and this approach is particularly suitable for non-orthogonal grids since staggered grids demand additional storage allocations. The non-staggered approach requires, nevertheless, special procedures to ensure proper velocity and pressure coupling and to suppress the pressure oscillations. Details of some of these special procedures can be found in Rhie and Chow [11].

4.4.4 The Present Model Set Up

To obtain the relative inter-zone mass flow rates in the zone models it is necessary to know the velocity fields in the furnace. Given that the flow within a furnace normally exhibits considerable variation in all three coordinate directions, particularly near the burners, it was decided to treat the problem as three-dimensional. The velocity data was provided by the commercial finite-volume code which was used to obtain an ambient temperature, isothermal, 3D flow field in the furnace chamber. The steps taken to adapt the general program to the present furnace problem are now outlined.

In any modelling exercise it is important to maintain equivalent conditions between the model and the actual plant. Beer and Chigier [2] have listed a large number of dimensionless groups which must be held constant in the model and in the furnace to ensure similarity. With a cold isothermal model it is impossible to simulate all the complex processes that occur in a hot combustion system and at best the model can only partially represent the full-scale conditions. Beer and Chigier [2] examined several methodologies of partial scaling and presented some general guidelines which are taken into consideration in this study. The Reynolds number is an established index of the character of the flow so that equality of this number in the model and in the furnace is usually the main consideration in combustion systems. This condition corresponds to:

$$\left(\frac{\rho_{air} u_{air} D_{model}}{\mu_{air}}\right)_{model} = \left(\frac{\rho_{cp} u_{cp} D_{furnace}}{\mu_{cp}}\right)_{furnace} \tag{4.6}$$

where ρ is the density, u the mean velocity, D is the characteristic length and μ the viscosity.

Rearranging the equation we obtain:

$$u_{air} = u_{cp} * \frac{\rho_{cp}}{\rho_{air}} * \frac{D_{furnace}}{D_{\text{model}}} * \frac{\mu_{air}}{\mu_{cp}} \tag{4.7}$$

From this assembly of ratios, the relationship between the model velocity and the furnace velocity may be obtained for the furnace conditions and the properties of air. The ratio $\frac{D_{furnace}}{D_{\text{model}}}$ is the overall geometric scaling factor which in our case is equal to 1 as the actual furnace and the computer model have the same dimensions. Because air and combustion products have approximately the same composition, the ratio of densities can be written in terms of temperatures and Equation 4.7 becomes:

$$u_{\text{model}} = u_{furnace} * \frac{T_{air}}{T_{cp}} * \frac{\mu_{air}}{\mu_{cp}} \tag{4.8}$$

This equation requires an estimate of the temperature and viscosity of the combustion products to properly scale the velocities. However, in the present study Reynolds number similarity was not necessary and only one burner throughput condition was simulated. This is appropriate since the relative inter-zone mass flow rates were insensitive to any changes in burner throughput (although the magnitudes of the actual velocities change) provided that the flows remain turbulent. This implies that the flow patterns are similar provided that turbulent conditions are retained and this has been observed previously, see Rhine and Tucker [3]. A series of simulations were, however, carried out to verify that the inlet burner velocity could be lowered for a given burner geometry and it was confirmed that the flow patterns and hence relative inter-zone mass flow rates did remain unchanged down to a burner Reynolds number of 5000. For convenience an inlet velocity of 1.0m/s was assumed and all the CFD calculations were carried out at this value. These inter-zone flows were related to the burner throughputs and were then scaled in the final zone model to provide actual mass flows and hence enthalpy flow rates.

In order to achieve the correct mixing and flow patterns within the isothermal model, the actual nozzle diameter of the burners has to be distorted to account for the density changes in the hot nozzle fluid as it expands in the real furnace, see Rhine and Tucker [3], etc. This burner attempts to achieve momentum similarity between the hot and the cold systems. The equivalent distorted model burner diameter is then obtained from consideration of the entrainment capacities of the hot burner and cold isothermal model jets so that:

$$d_{eq(\text{model})} = d_{furnace}\left(\frac{\rho_{flame\,jet}}{\rho_{cp}}\right)^{0.5} \tag{4.9}$$

This density correction equation is commonly known as the Thring-Newby scaling criterion [12]. To calculate the equivalent nozzle diameter the following was assumed:

1. Combustion products in the furnace are well-mixed and are at a mean temperature of 1400K.
2. The jet issuing from the nozzle mix burners were at the adiabatic flame temperature i.e. approximately 2198K for natural gas burning with 5% excess air.

Since in this case the burner jet and entraining hot gases have approximately the same composition, albeit different temperatures, equation 4.9 can be rewritten in terms of temperatures to give:

$$d_{eq(\text{model})} = d_{furnace}\left(\frac{T_{cp}}{T_{flame\,jet}}\right)^{0.5} \tag{4.10}$$

where $\left(\frac{T_{cp}}{T_{flame\,jet}}\right)^{0.5}$ is the distortion correction factor and in this nozzle mix model was equal to 0.798.

The commercial RANS solver was used to obtain the velocity field in the isothermal, ambient temperature furnace model. As previously mentioned, CFX 4.2, is a structured multi-block, finite volume code developed by AEA Technologies. Initially, the furnace geometry was created and meshed using the pre-processor CFX-

MESHBUILD, a structured multi-block grid sub-program in CFX 4.2. This means that the geometry is built in blocks of cells which must be topologically cuboidal. The basic building blocks defined by the coordinates of the grid system are the control volumes where the transport equations are to be solved. In general, each control volume has a regular/irregular hexahedron shape. Most of the flows encountered in many practical combustion systems are three-dimensional and recirculating in nature so that a three-dimensional model of the furnace is necessary. However, it was possible to take advantage of the symmetry of furnace about the central vertical plane to increase grid resolution and reduce computational convergence times. For the symmetrical 3D isothermal simulation of the furnace, the physical domain was subdivided into 50 sub-domains, each of which had an associated H-type sub-grid, see Figure 4.4. Due to the geometric symmetry only two nozzle mix burners were modelled.

Figure 4.4 The H-type Grid

Once the geometry is defined the next stage is to set the boundary conditions to the flow solvers by using the concept of patches i.e. sub-arrays of control cells or control cell faces internal to the blocks where boundary conditions are to be imposed. The correct specification of the boundary conditions for a given problem is of paramount importance in obtaining accurate solutions since inappropriate selection of these conditions can lead to unrealistic results and possible rapid divergence in the solver. In CFX 4.2 the real information on boundary surfaces is set up using patches which can take the form of inlets, outlets, walls, etc. Some of these patches are used to model inflow and outflow boundaries such as at the burner inlets and the exhaust exit of the furnace while others are used to model surface boundaries such as walls and symmetry planes. More details on patch types can be found in CFX 4.2 Solver Manual [13]. Four different patch types were identified for the present furnace geometry: 2 circular inlets corresponding to the nozzle mix burners, 1 rectangular outlet pressure boundary for the exhaust, 1 symmetry plane and finally "walls" for the remaining external surfaces which represent the furnace lining and load.

At the inlets, all the flow variables (velocity components, turbulent quantities) were specified (i.e. so-called Dirichlet condition) except for the pressure which was

extrapolated from downstream. The inlet velocity profiles issuing from the burners were assumed uniform. At the outlet exhaust pressure boundary, the pressure was set constant at the atmospheric value and zero normal gradients were imposed on all other variables (i.e. the Neumann condition). The "walls" were assumed, by default, to have zero velocity conditions (i.e. the no-slip condition) and there was no flow across the vertical central symmetry plane. The specification of the patches was generally easy to perform, except in the case of the circular burner inlets where it involved setting a mesh constraint since the inlets did not extend over the whole block face so that only part of the grid of this face was occupied. A mesh constraint is a method of forcing the grid over the inlet (child object) to be identical with that of the block face (parent object).

The final step of CFX-MESHBUILD is the generation of a mesh based on the block structure and subsequent production of the geometry file to be used by the flow solver. The total number of subdivisions or cells to be employed in the problem is controlled by the number and relative position of any mesh constraints. Consequently, in the present case this was always dictated by the dimensions of the circular burner inlets. The process involved estimating the minimum number of cells required to match the burner nozzle. When the grid was generated an elliptic smoothing technique was used to provide a smooth representation of the burner geometry. Although the method is much slower then an alternative algebraic interpolation technique, it produces a more orthogonal grid in the interior of a block or face.

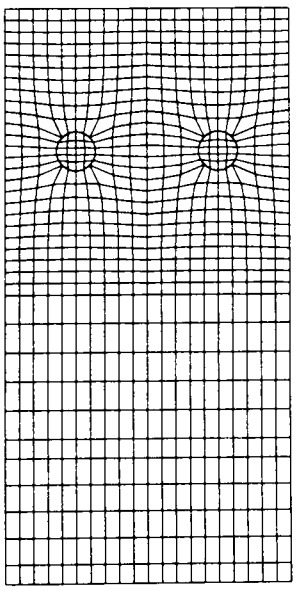

Figure 4.5 CFD Grid Representation of the Burner Inlets

Near orthogonality is one of three properties to look for in the generation of a satisfactory grid. The other two are the smoothness which is a measure of how rapidly the cell sizes change, and sufficient grid resolution to adequately model the flow. Figure 4.5 is an example of the grid generated in the plane where the circular inlet was placed. CFX-MESHBUILD provides a number of features which allow detailed assessment of the quality of the generated grid.

The determination of an appropriate grid for modelling a specific problem is dependent on the available computer technology and the degree of accuracy required in the final solution. The requirement of achieving reasonable computing times drives the user to adopt relatively coarse meshes although this may decrease the quality of the mesh and increase the difficulty in obtaining a converged solution. However, to minimise errors due to the coarseness of a grid, it is necessary to demonstrate that the solution is insensitive to the number of grid points employed. This usually dictates the minimum number of cells which can be employed in any simulation. A grid independence study involves carrying out solutions of the CFD model with successively refined grids until certain key results do not significantly change. Therefore, for practical reasons the grid design should balance the conflicting requirements of increasing the accuracy whilst minimising the solution cost. With this in mind a grid independence study was performed for the present calculation and the results were balanced against the computational time involved. Details of this are presented in Chapter 5. This study indicated that a grid with a total of 36000 cells would be appropriate to provide adequate modelling of the current furnace. This mesh system is illustrated in Figure 4.6 and it is clear that a finer structure was employed near the burners where the more severe velocity gradients are encountered.

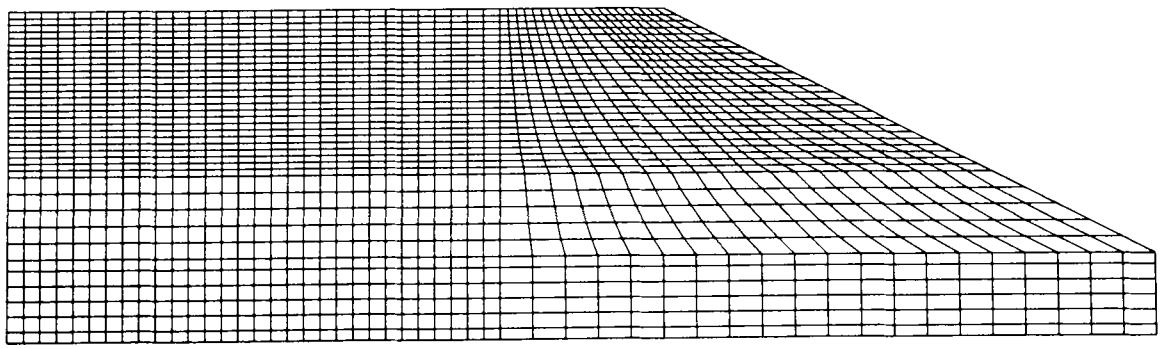

Figure 4.6 CFD Grid Arrangement

Grid generation is a very time consuming step in the overall CFD model. The subsequent step is the input specification where the global features of the problem under consideration are set including the flow modelling options, the fluid properties, the solution strategy and the boundary conditions. This is done using CFX-SETUP, a module program within CFX 4.2 which produces a single file containing the above information to be accessed by the solver module.

The flow field within the furnace chamber is predicted by solving the governing partial differential equations set in its time-averaged steady-state form in order to account for the turbulent nature of the flow. They were solved for the three-dimensional space and under ambient isothermal conditions using air at a temperature of 20°C as the working fluid. The fluid properties were read from a database within CFX-BUILD. A standard k-ε turbulence model was employed to describe the turbulent viscosity and this requires the solution of two additional equations, one for the turbulent kinetic energy k and other for its rate of dissipation ε, as previously described. This turbulence model has been widely applied and performs particularly well in confined flows as in the present application. At inlets the velocity components were specified together with estimated values for the turbulent kinetic energy k and turbulence dissipation length D. The value for k was obtained using the relationship [13]:

$$k_{inl} = 0.002 u_{inl}^{\,2} \tag{4.11}$$

The dissipation length scale is geometry dependent and was taken as equal to the distorted burner diameter. This value was then used to calculate the value of the turbulent dissipation rate ε using [13]:

$$\varepsilon_{inl} = \frac{k_{inl}^{1.5}}{0.3D} \tag{4.12}$$

The convection terms were discretised using the hybrid scheme and SIMPLEC, a variant of the SIMPLE algorithm, was used to handle the pressure-velocity coupling. The final set of linearised equations for a particular variable was fed into a linear solver which uses an iterative solution method. Because of the iterative process adopted it is necessary to specify a convergence criterion after which the solution calculation is

stopped. In the present study the residual of the continuity equation was used to monitor the progress of convergence. Residuals close to 10^{-3} were found to be adequate and for most cases these were achieved within 500 iterations and this in turn required an average convergence time of approximately one hour on a SUN ULTRA-1, SPARC workstation.

The file containing the final solution values can also be read by the CFX graphic modules to produce graphical plots for analysis and presentation of the results. Figure 4.7 shows a typical velocity-vector field plot on the burner centre plane. The strong recirculation near the burners is apparent and the CFD results are discussed in detail in the next chapter.

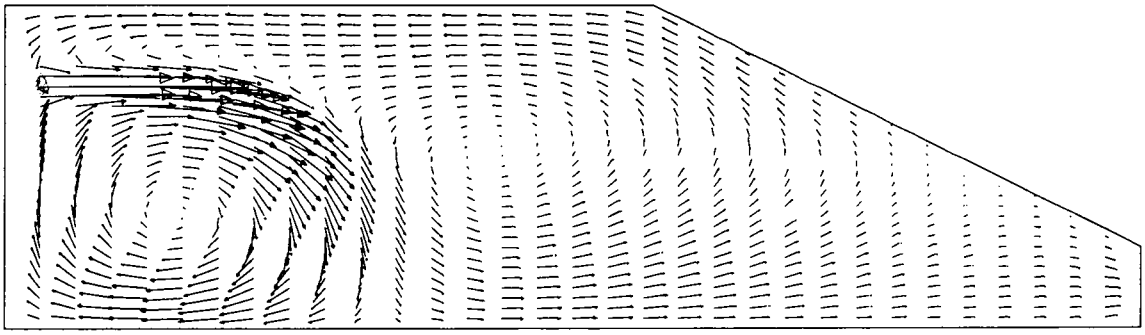

Figure 4.7 Example of a Velocity Pattern Obtain in the CFD Model

CFX 4.2 allows the user to control the contents of the output file and this feature was employed to generate the inter-zone mass flow rates which are required in the zone model. Thus the values of the velocity components u and v were extracted for the cells which correspond to the boundaries of the zones in the zone model. With this information, the inter-zone mass flow rates were estimated by integrating the individual cell mass flow rates normal to the boundaries of the gas volumes in the zone model. These mass flow rates were then subsequently normalised relative to the total input mass flow rate. The CFD cells did not necessarily coincide with the boundaries of the volume zones. In these cases the inter-zone velocities were interpolated from values for the adjacent cells either side of the zone boundaries. The whole procedure for determining these relative mass flow rates was carried out prior to running the zone model. The inter-zone mass flows corresponding to the flow pattern in Figure 4.7 are illustrated in Figure 4.8.

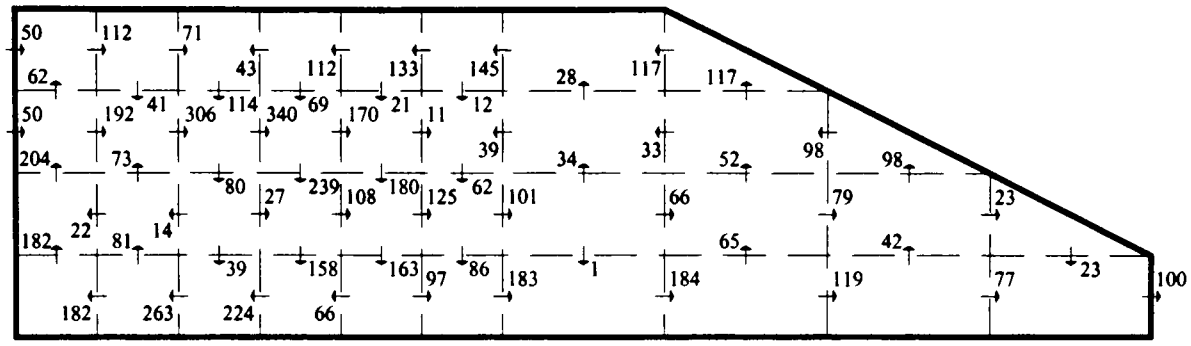

Figure 4.8 Inter-Zone Relative Mass Flows for Figure 4.7

4.5 Radiation Factors

As mentioned in Chapter 3, the zone method of radiation analysis requires knowledge of the so-called exchange factors between all zone pairs in the enclosure to be able to write the radiation transfer term of the energy balance equations. These factors are complex functions of the geometry and optical properties of the zones and hence, evaluation of all surface-surface, surface-gas and gas-gas radiation factors requires considerable computing time and storage space. Because of these restrictions many previous investigations were limited to geometrically simple configurations or involved some form of geometrical simplification. However, the latter was shown by Tucker and Ward [14] to significantly misrepresent the heat flux profile to the load and this could result in erroneous predictions in applications where assessment of the quality of the heated product was essential.

The restriction on geometry can, however, be overcome by adopting a method such as the Monte Carlo method which allows for the effects of complicated shapes. In the present work a Monte Carlo based computer program, RADEX [15], was used to evaluate the radiation exchange areas and it was possible to obtain an accurate representation of the furnace geometry including the sloping roof. RADEX has the ability to deal with complex geometries with relative ease whilst maintaining acceptable computational times. This is achieved by employing two sets of grids: a fine mesh to allow accurate detailed representation of the geometry and a coarse mesh to define the heat transfer zoning arrangement.

Underlying the zone method formulation is the assumption of uniform absorptivity and emissivity of each volume and surface zone in the enclosure. These can, however, differ from zone to zone so that in RADEX a range of options is presented to the user in

defining these parameters. In this study the emission and absorption characteristics of the furnace atmosphere were set using a mixed grey gases model (1 clear and two grey) with the appropriate absorption coefficients and temperature sensitive weighting factors derived from Rhine and Tucker [3], see section 3.3.3. In this option, the type of fuel used for combustion and the excess air level are required and these were specified as natural gas and 5%, respectively.

Calculation of the radiation factors for all three gases was performed simultaneously. The simultaneous processing of the different atmospheres by the code means that for one set of rays fired and traced all the various exchange factors (view factors, direct and total exchange areas) can be generated and this reduces significantly the execution time. Emissivities were assigned to the walls, floor, roof and load and these were assumed to be 0.6, 0.6, 0.5 and 0.7, respectively. One final parameter requiring special attention was the total number of rays fired from a zone. In principle, as the number of rays traced increases, the Monte Carlo method is expected to converge to the exact solution. In a similar study, Tucker and Ward [14] have found that large samples of rays generally produced more accurate results so that in this present study the radiation exchange factors were calculated using a sample of just over 420000 rays corresponding approximately to 6000 rays fired per unit area which is considerably in excess of the ray density employed successfully by the previous authors.

The Monte Carlo method is a purely statistical method in which the history of a large number of rays is traced. Due to its stochastic nature, the results achieved are always subject to statistical scatter and this means that the exchange factors computed by RADEX do not necessarily meet the summation rules or the reciprocity principle (see Chapter 3). To ensure conformity to both rules a technique for smoothing the radiation factors was employed. Smoothing was carried out in two steps: firstly reciprocity was satisfied by the arithmetic averaging of the reciprocal exchange factors and then secondly energy conservation, which was undermined by the reciprocity operation, was re-established. This second step used the method described by Larsen and Howell [16] to satisfy the summation rules. It was only necessary to calculate the radiation factors once since they are independent functions of the temperature. They were evaluated prior to the zone model simulation and accessed in this model in a form of a single file.

4.6 The Zone Model

At this point all the necessary input information was organised in a consistent way to produce the set of energy balance equations (one for each zone) which were solved to provide the gas temperatures and surface heat fluxes. The main assumptions for the transient model developed in this project as well as the structure of the FORTRAN computer code will now be presented.

Model Assumptions The transient zone models for the nozzle mix burner case were constructed with the following assumptions:

- The gas zones were assumed to be well-stirred i.e. they have uniform temperature and composition.

- The surface zones were assumed to be isothermal, radiatively grey and diffusely reflecting.

- Inter-zone radiation exchange was included by incorporating exchange factors for every zone pair in the furnace chamber.

- The furnace enclosure was assumed to contain non-luminous, non-grey combustion products and these were represented by an imaginary mixture of 1 clear and 2 grey gaseous components.

- Convection between gas zones and adjacent surface zones was taken into account. At the furnace operating temperatures (>1000°C), this mode of heat transfer is likely to account for less than 5% of the total heat transferred, so that a constant heat transfer coefficient of $25 W/m^2K$ [17] was considered to be sufficiently accurate for all surface zones.

- Combustion was assumed to be virtually complete within the burner nozzles so that heat release was confined to the "input" gas zones.

- Conduction within the load and furnace lining was assumed to be one-dimensional. A fully implicit finite-difference technique, Croft and Lilley [18] was employed to ensure stability in the conduction models.

- Variation of the thermal properties with temperature for the lining and load materials was included by using polynomial expressions (see Appendix A).

- The contact thermal resistance between the bottom of the load and the hearth was taken as $0.002 m^2K/W$ based on data provided by [19].

- The thermal input to the furnace was controlled to maintain the furnace temperature at a stipulated set point although the air/fuel ratio was kept constant throughout the simulations.

The models were used to simulate the transient thermal performance of the furnace during a start-up from cold and also during a period of continuous operation at a constant production rate. The models were capable of predicting heating rates, load temperatures and fuel consumptions over the specified period of operation.

Structure of the Code The set of energy balances for each zone takes into account radiation, convection and in the case of a gas element it is also necessary to include the enthalpy flow term. Implementation of these expressions in the form of a computer code requires a sequence of operations or sub-routines, the details of which are now described:

I. *Parameters* Essential parameters relevant to a particular furnace and model were defined e.g. the number of: gas zones, surface zones, the furnace atmosphere, the number of nodes in the walls and load, etc. Specification of these values provide flexibility in the model.

II. *Input Data* This assigns initial values to a range of parameters e.g. geometric information such as the areas and volumes of the zones, the length of the time increments, the fuel and air properties, surface emissivities, initial surface temperatures, grey gas parameters, etc.

III. *Gas Properties* This provides the partial pressures of the radiating constituents in the combustion products, the grey gas attenuation coefficients and any other information for the computation of the directed flux areas.

IV. *Radiation Factors* This routine reads the temperature independent total exchange areas generated by RADEX.

V. *Combustion Air Preheat* This is an optional module which simulates combustion air preheating by an external recuperator. The combustion air temperature is related to the furnace exhaust temperature, T_{cp}, and the thermal effectiveness of the device, η_{eff}, by:

$$T_{air} = \eta_{eff}(T_{cp} - T_{air,in}) + T_{air,in} \tag{4.13}$$

VI. *Calculation of Gas Temperatures* This routine provides the solution to the energy balance equations and contains sub-routines to provide the terms for convection, radiation and enthalpy transport:

Convection Sub-Routine – This specifies the heat transfer coefficients from the outside of the lining to the ambient surroundings. They were estimated using polynomial equations for turbulent free convection from either horizontal or vertical surfaces. The convection heat transfer term, $\dot{Q}_{conv}$, from each relevant gas zone i to the adjacent surface was also calculated.

Radiation Sub-Routine – This transformed the corrected total exchange areas into directed flux areas using equations (3.22) and the radiation transfer term, $\dot{Q}_{rad}$, from each gas zone i was then obtained.

Flow Sub-Routine – The purpose of this was to specify the terms for the energy loss in the flue gases, $\dot{Q}_{cp}$, and the energy input in the fuel and combustion air, $\dot{Q}_{input}$. It also calculated the enthalpy flows, $\dot{Q}_{enth}$ (calculated from the product of mass flow rate and specific enthalpy of the combustion products and air) into or out of each zone. The isothermal CFD simulation provided the flow data and the specific enthalpy data for the combustion products and any preheated air were represented by polynomial relationships from Rhine and Tucker [3].

Once all the necessary terms were computed, the system of heat balances, one for each gas zone, was set up in the form of Equation 3.25. Because these

equations are non-linear in temperature, they were solved using a Newton-Raphson iterative method. Starting from an initial estimate of the gas temperature, the algorithm iteratively refined these temperatures until a predetermined convergence criterion was satisfied. The criterion used in this study was that successive residuals of the heat balance equations were within a limit of 0.001. The method converges rapidly if sufficiently good initial estimates are made. Further details of the method can be found in [20].

VII. *Surface Heat Fluxes* The energy converged balances for each surface, Equation 3.26, yielded the heat fluxes at each surface zone. These heat fluxes were subsequently employed as boundary conditions in the one-dimensional finite-difference calculations of conduction in the walls and load to predict the transient temperature profiles in these materials.

VIII. *Transient Conduction Model* This routine provided the temperature sensitive thermal properties (thermal conductivity, k, and specific heat, Cp) for the walls and load which were used in the conduction calculations. Implicit finite-difference nodal equations were defined for each node within these surfaces and solved for the unknown nodal temperatures using an iterative technique. This aspect will be discussed in the next section.

IX. *Furnace Control* This module allows simulation of the furnace control mechanism. It varied the fuel input as a result of deviations from a specified set point temperature. Further details are given in the next section.

X. *End of the Simulation* The whole calculation procedure was repeated sequentially at time intervals of 10 seconds over the entire heating period. In the start-up case the simulation was stopped when the top surface of the load achieved a pre-determined value (usually 1250°C). For continuous operation of the furnace a load movement routine (i.e. a push rate) was included and the overall operation period was defined. Further details on this module will be given in the next section.

4.7 Transient Calculations

In most metal reheating furnaces the operational procedure is characterised by an unsteady or transient behaviour as a result of changes arising due to interruptions in production, furnace controlling parameters or even due to other time-dependent events such as the discharge of the load. Modelling of the transient thermal performance, therefore, requires a model capable of incorporating all these time dependent effects. In this study, the zone analysis includes a transient conduction routine which uses a one-dimensional implicit finite-difference method with a time step equal to that used in the zone model to simulate the effects of conduction and hence of heat storage in the furnace structure and load. Under transient conditions and with no internal heat generation, the governing one-dimensional partial differential equation of conduction takes the form of:

$$\frac{\partial}{\partial x}\left(k\frac{\partial T}{\partial x}\right) = \rho C_p \frac{\partial T}{\partial t} \tag{4.14}$$

In order to solve equation 4.14 it was necessary to specify initial and boundary conditions. For each wall and load surface two boundary conditions were required, one for each face of the surface. For the sidewalls and roof of the furnace, a constant heat flux (as calculated by the zone model) was applied at each time step to the internal surface exposed to the combustion products with a convection boundary condition on the outside external surface. A constant heat flux (as calculated in the zone model) was applied at the top surface of the load and the underside of the hearth lost heat by convection to the surroundings. The node at the interface of the load and hearth was formulated in terms of the thermal contact resistance, C_r, between the two surfaces. This resistance was assumed to be $0.002 m^2K/W$ based on data in Howells *et al.* [19].

The finite-difference conduction models used eleven, eight and seven equally spaced nodes in the load, ceramic fibre roof and dense refractory walls respectively. Equation 4.14 was discretised at each node by applying conservation of energy to a control volume about the node. This reduced the differential form of equation 4.14 to a series of algebraic expressions. Central differencing was employed as the discretisation scheme to approximate the spatial derivatives, see Appendix B. However, in addition to

the spatial discretisation, the problem must also be discretised in time and the finite-difference approximation will have the form:

$$\left(\frac{\partial T}{\partial t}\right)_n \approx \frac{T_n^1 - T_n^0}{\Delta t} \tag{4.15}$$

where the superscripts 1 and 0 are associated with the times at the end and start of the time step. The nature of the finite-difference solution depends on the time allocated to the temperatures in the approximate expressions for the spatial derivatives.

In an explicit scheme, these temperatures are evaluated at the time, T_n^0, so that the temperature at the node n is obtained explicitly in terms of the known temperatures at the beginning of the time step. The solution scheme, although simple does, however, limit the size of the time step to ensure stability [21].

An alternative is the Crank-Nicolson approach [22] which uses the arithmetic mean value of the temperatures, T_n^0, and, T_n^1, to define the spatial derivatives. This results in a set of simultaneous equations which must be solved at each time step. Although computationally more demanding than the explicit method, the Crank-Nicolson approximation is more accurate and larger time steps can be employed, thereby reducing the total number of steps in the calculation. The scheme is, however, still subject to numerical oscillations which if large enough can lead to instability in the solution [21].

A fully implicit method, as used in the present study, is unconditionally stable for all time steps [21]. The size of the time interval was, however, limited by the need to avoid too large a change in the temperature of the surface node of the ceramic fibre. The fully implicit method was adopted in this study because of its robustness and unconditional stability.

The resulting set of linear algebraic expressions in the conduction models were cast in matrix form $\mathbf{A.T^1=B}$ and solved simultaneously for the temperatures at each node using the LU decomposition and back-substitution routines [20]. This iterative technique was similar to the one used to solve the linearised system of energy balances in the main zone model so that no additional routines were necessary in the computer code. Variation of the thermal properties with temperature, and hence position, were taken into account and these were evaluated from polynomial expressions from Rhine

and Tucker [3], see Appendix A. The thermal conductivity over the path between the adjacent nodes i and j was assumed to be:

$$k_{ij} = \frac{k(T_i) + k(T_j)}{2} \tag{4.16}$$

A summary of the implicit finite-difference nodal equations used in this study is presented in Table 4.1, including the interface nodes between the dissimilar materials of the load and hearth and the nodes at the boundaries of the surfaces [23].

Table 4.1 Summary of Nodal Implicit Finite-Difference Equations

Node 1	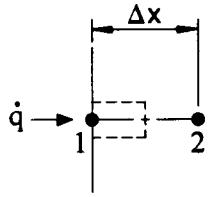	$\dot{q}_{surf} + \left(\frac{k_1 + k_2}{2}\right)\left(\frac{T_2^1 - T_1^1}{\Delta x}\right) = \rho_1 Cp_1 \Delta x/2\left(\frac{T_1^1 - T_1^0}{\Delta t}\right)$
Interior Nodes	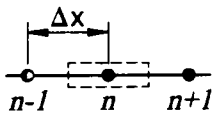	$\left(\frac{k_{n-1} + k_n}{2}\right)\left(\frac{T_{n-1}^1 - T_n^1}{\Delta x}\right) + \left(\frac{k_n + k_{n+1}}{2}\right)\left(\frac{T_{n+1}^1 - T_n^1}{\Delta x}\right) =$ $= \rho_n Cp_n \Delta x\left(\frac{T_n^1 - T_n^0}{\Delta t}\right)$
Node N	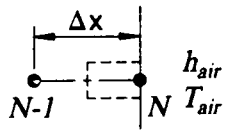	$\left(\frac{k_N + k_{N-1}}{2}\right)\left(\frac{T_{N-1}^1 - T_N^1}{\Delta x}\right) + h\left(T_\infty - T_N^1\right) = \rho_N Cp_N \Delta x/2\left(\frac{T_N^1 - T_N^0}{\Delta t}\right)$
Interface Node at Load	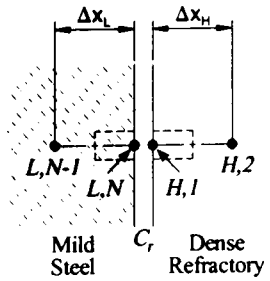	$\left(\frac{k_{load,N} + k_{load,N-1}}{2}\right)\left(\frac{T_{load,N-1}^1 - T_{load,N}^1}{\Delta x}\right) + \frac{\left(T_{hearth,1}^0 - T_{load,N}^1\right)}{C_r} =$ $= \rho_{load} Cp_{load} \Delta x/2\left(\frac{T_{load,N}^1 - T_{load,N}^0}{\Delta t}\right)$
Interface Node at Hearth		$\left(\frac{k_{hearth,1} + k_{hearth,2}}{2}\right)\left(\frac{T_{hearth,2}^1 - T_{hearth,1}^1}{\Delta x}\right) + \frac{\left(T_{load,N}^0 - T_{hearth,1}^1\right)}{C_r} =$ $= \rho_{hearth} Cp_{hearth} \Delta x/2\left(\frac{T_{hearth,1}^1 - T_{hearth,1}^0}{\Delta t}\right)$

At the end of each time step it was necessary to check if changes in operating conditions such as the burner throughput or movement of the load were required. Thus, the fuel input was adjusted based on the deviation of the "furnace temperature" from a specified set point. In this study, the furnace temperature corresponds to the temperature measured by a thermocouple mounted at the hot face of the roof near the discharge end of the system.

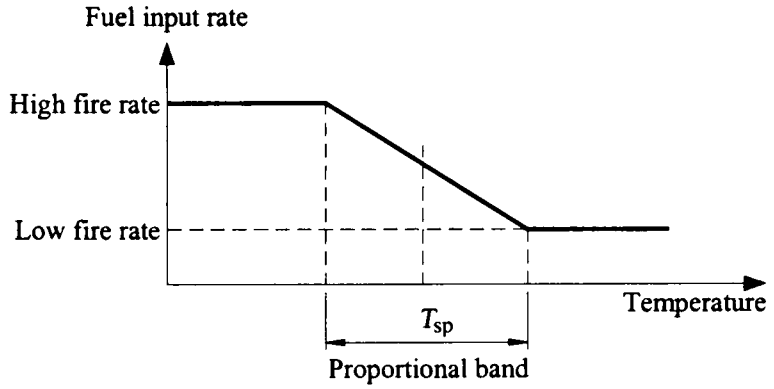

Figure 4.9 The Proportional Gas Input Control Strategy

A simple proportional gas input/temperature control band, see Figure 4.9, was employed to vary the natural gas supply to the burners so that the thermal input was varied over a 5:1 range in response to deviations of the sensor temperature over an error band of ± 7.5°C from the specified set point. The variation of the burner thermal input with temperature was expressed as a proportion, F, of the maximum firing rate value. Below the lower temperature of the proportional band, P_b, F=1 which means that the burners fire at their maximum thermal input. Within the band, F was related to the temperature, T, by the following linear expression:

$$F = aT + b \tag{4.17}$$

where

$$a = \frac{(t_d - 1)}{P_b} \text{ and } b = \frac{(t_d - 1)}{2} - \frac{(t_d - 1)T_{sp}}{P_b}$$

where t_d is the turndown ratio (i.e. ratio of the minimum fuel input to the maximum firing rate) and T_{sp} is the temperature of the set point. Above the upper temperature of

the band, the control system modulates the burners to operate at the minimum thermal input so that $F=t_d$. By simulating furnace control, prediction of the actual energy required to achieve a specific discharge condition was possible.

With continuous operation of the system it was necessary to specify the overall operating period and the load push rate i.e. the rate of production of steel bars. Following the initial start-up and whenever discharge of load from zone 1 was due, the load transfer zone-by-zone was handled by assigning the load nodal temperatures to the next adjacent zone whilst in the last gas zone a cold load was entered. These push intervals were arranged to be a multiple of the time step. The simulation was complete when the maximum number of bars were discharged and this was calculated from knowledge of the mass of the load, M_{load}, in each zone, push rate, P_{rate}, and remaining simulation time after the start-up period ($Stime_{after\ start\text{-}up}$):

$$Push\ Interval = \text{int}\left(\frac{M_{load}}{P_{rate}}\right) \tag{4.18}$$

$$Max\ Number\ of\ Drops = \text{int}\left(\frac{STime_{after\ start-up} * 3600}{Push\ Interval} + 1\right) \tag{4.19}$$

It was relatively easy to simulate conditions such as production delays, set point temperature changes and variations in the load throughput.

4.8 Summary

The overall structure of the multi-zone transient mathematical model used in the present study is described in this chapter. A knowledge of velocity and hence inter-zone mass flows was required. Consequently, isothermal CFD models were used to provide this information. This method solves the governing equations of continuity and momentum at each cell of the computational grid which subdivides the geometry. The resultant flow field was then supplied to the zone model in the form of relative inter-zone mass flows to allow for the enthalpy transport by the flow of combustion products between zones.

In the zone method the furnace enclosure is subdivided into a number of volume and surface zones each of which is assumed isothermal and with constant radiative

properties. Energy balances were then formulated for each zone taking into account the complex nature of the radiation interchange in the furnace by using so-called total exchange areas, as well as convective heat transport from appropriate hot gas zones to adjacent load and surfaces. These energy balances yielded a set of non-linear simultaneous equations which can be solved iteratively to provide the temperature of the gas zones and the corresponding heat fluxes at the surfaces. The zone calculations were undertaken at a series of time steps over the operating period. The temperatures of the load and furnace lining were updated at each time step using finite-difference conduction models.

References

1. Hottel, H.C., Cohen, E.S., *Radiant heat exchange in a gas-filled enclosure: allowance for non-uniformity of gas temperature.* J. AIChE, 1958. **4**(March): p. 3-13.
2. Beer, J.M., Chigier, N.A., *Combustion Aerodynamics*, 1972, London: Applied Science Pub.
3. Rhine, J.M., Tucker, R.J., *Modelling of Gas-Fired Furnaces and Boilers and Other Industrial Heating Processes*, 1991, London: McGraw-Hill.
4. Patankar, S.V., *Numerical Heat Transfer and Fluid Flow*, 1980, Washington, USA: Hemisphere Pub. Corp.
5. Versteeg, H.K., Malalasekera. W., *An Introduction to Computational Fluid Dynamics, The Finite Volume Method.* 3rd, 1995: Longman.
6. Patankar, S.V., Spalding, D.B., *Simultaneous predictions of flow patterns and radiation for three-dimensional flames*, in *Heat Transfer in Flames,* Ed. N.H. Afgan, Beer,J.M. 1974, John Wiley & Sons. p. 74-94.
7. Launder, B.E., Spalding, D.B., *The numerical computation of turbulent flows*, in *Computer Methods in Applied Mechanics and Engineering,* 1974, North-Holland Pub. Co. p. 269-289.
8. Ferziger, J.H., Peric, M., *Computational Methods for Fluid Dynamics.* 2nd ed., 1999: Springer.
9. Stone, H., *Iterative solution of implicit approximations of multidimensional partial differential equations.* SIAM J. Numer. Anal., 1968. **5**(September): p. 530-559.

10. Anderson, J.D., *Computational Fluid Dynamics, The Basics with Applications.* Mechanical Engineering, 1995, New York: McGraw-Hill.
11. Rhie, C.M., Chow, W.L., *Numerical study of the turbulent flow past an aerofoil with trailing edge separation.* AIAA Journal, 1983. **21**(November): p. 1525-1532.
12. Thring, M.W., Newby, M.P., *Combustion length of enclosed turbulent jet flames.* in *Fourth Symp. (Intl) on Combust.*, p. 789-796. 1953. Baltimore, USA.
13. *CFX-4.2: Solver Manual*, 1997, CFX International, AEA Technology.
14. Tucker, R.J., Ward, J., *Use of a Monte Carlo technique for the determination of radiation exchange areas in long furnace models.* in *Proc. 8th Intl. Heat Transfer Conf.*, p. 391-396. 1986. San Francisco, USA.
15. Lawson, D.A., *RADEX User Guide.* Coventry University, 1991.
16. Larsen, M.E., Howell, J.R., *Least-squared smoothing direct exchange areas in zonal analysis.* Trans. of ASME, J. Heat Transfer, 1986. **108**: p. 239-242.
17. Sousa, J.L.V.A., *Application of the Zone Method of Radiation Analysis to Simulation of the Non-Steady State Operation of Metal Reheating Furnaces.* PhD Thesis, University of Glamorgan, 1995.
18. Croft, D.R., Lilley, D.G., *Heat Transfer Calculations Using Finite Difference Equations.* 1st ed., Vol. 1, 1977: Applied Science Pub.
19. Howells, R.I.L., Ward, J., Probert, S.D., *Thermal conductances of contacts at high temperatures.* J. Iron Steel Inst., 1973. **211**(March): p. 193-196.
20. Press, W.H., Teukolsky, S.A., Vetterling, W.T., Flannery, B.P., *Numerical Recipes in Fortran.* 2nd, Vol. 1, 1994, Cambridge: Cambridge University Press.
21. Myers, G.E., *Analytical methods in conduction heat transfer.* 1st ed., Vol. 1, 1987, Madison, USA: Genium Pub. Corp.
22. Crank, J., Nicolson, P.A., *A practical method for numerical evaluation of solutions of partial differential equations of the heat conduction type.* Proc. Camb. Phil. Soc., 1947. **43**(17): p. 50-67.
23. Incropera, F.P., De Witt, D.P., *Introduction to Heat Transfer.* 2nd ed., 1985, New York: John Wiley & Sons.

DETERMINATION OF FURNACE FLOW PATTERNS

5.1 Introduction

The zone method requires a knowledge of the flow distributions within the furnace chamber in order to evaluate the inter-zone enthalpy flows. The CFD models were checked for grid independence and the adopted grid was a compromise between accuracy and the model running time. Since no experimental data were available, a limited validation was attempted based on comparisons with data from closely related problems reported in the open literature.

5.2 Flow Calculations

In principle, three-dimensional models can provide improved results when compared to other more simplistic models. This advantage can, however, be offset by the increased computational effort so that these complicated models are often impractical for design purposes. The task of improving existing combustion systems or developing new concepts requires detailed information of the distribution of key variables such as the gas temperature, velocity and concentration of unburnt fuel at various sections. Only then is it rigorously possible to estimate the heat transfer to the furnace walls and load and hence predict the furnace performance. The zone method of radiation analysis is a modelling tool which provides accurate estimates of the heat

transfer particularly in high temperature systems where radiation predominates. In constructing a zone model, it is important to select an appropriate number of zones to produce a model which is at the same time reasonably accurate and computationally efficient.

Most previous investigations of zone models have often not taken the fluid dynamics of the furnace atmosphere into account. They have frequently assumed simplified plug-flow patterns [1-3] although in some cases allowance was made for recirculation of the combustion products [4, 5]. This approximation is, however, over-simplified in cases where the flow patterns are significantly different from those produced in a long tunnel furnace. The flow of combustion products can influence the thermal behaviour of an industrial furnace and this may need to be determined using either physical models or computational fluid dynamics. With the advent of faster computers, CFD models have found widespread application in predicting fluid flows.

Consequently, in order to determine the flow patterns within the present furnace arrangement described in section 4.2, an isothermal, ambient temperature, CFD simulation was used to determine the 3D velocity field. This simplified approach of using an isothermal model to predict non-isothermal flows was considered to yield reasonable estimates of the flow patterns since the use of small-scale, experimental, near ambient temperature models have been successfully employed in the past to investigate flow related behaviour of combustion systems, as mentioned in the previous chapter [5, 6]. Since the furnace geometry was symmetrical about the central vertical plane, it was sufficient to make the computations for only one longitudinal half of the furnace enclosure. This allowed the grid resolution to be increased, thereby improving the accuracy and reducing the calculation time. The symmetrical 3D representation of the furnace included 2 inlet burners and the flue.

The need to ensure that a CFD solution is accurate and valid, requires investigation of grid dependence effects on the final solution. The fact that the governing equations are approximated by the use of a finite number of grid cells means that the real fluid processes are not solved. Only by reducing the mesh size to near zero can the algebraic approximations approach the real expressions and then provide a more accurate solution. It is, therefore, essential when performing a CFD study to demonstrate that grid independence has been achieved. A grid independence study involves continuously increasing the number of grid points until a solution is reached which is substantially

insensitive to changes in the number of points. The degree of refinement is, however, related to the level of accuracy required in the final solution. Grid independence studies are useful means to test the reliability of the calculated results in cases where experimental data is not available.

5.2.1 Grid Independence Study

Preliminary solutions with coarse grids were used to find the initial velocity patterns within the furnace geometry. With this information it was possible to construct a more suitable non-uniform grid with smaller size cells employed in regions where the variation of velocity was likely to be steepest. Initially, a non-uniform coarse grid of 15x36x10 control volumes yielding a total of 10800 cells was employed to determine the inter-zone mass flow rates between the boundaries of gas zones 1-3 and 2-4, as these results were chosen to indicate the variation of the solution with grid arrangement.

The 3D CFD computation was performed under ambient, isothermal conditions using a commercial code, CFX 4.2, with air as the working fluid. The k-ε model was used to model turbulence effects and suitable boundary conditions were specified at the burner inlets and flue outlet, see Chapter 4 for more details. Table 5.1 provides a summary of the model conditions used for the grid independence study. All this information was then supplied to the CFD programme in the form of a command file. A typical CFX command file for the nozzle mix simulations is presented in Appendix C.

Table 5.1 CFD Model Operating Conditions for Grid Study

Working Fluid	Air
Temperature (°C)	20.0
Burner Inlets u velocity (m/s)	1.0
Burner Inlets v velocity (m/s)	0.0
k-ε turbulence model	
k (m^2/s^2)	0.002
Dissipation Length Scale (m)	0.33
Total Air Flow per Burner (kg/h)	370
Reynolds Number	2.8×10^4
Excess Air (%)	5
Burner Distorted Diameter (m)	0.33
Burner Angle to Horizontal	0°

The predictions were then repeated for finer grid arrangements. In these predictions the calculations were terminated when the sum of the mass source residuals, normalised to the total input mass flow, was found to be less than a certain amount. In this case the stopping convergence criterion was set equal to 10^{-2} to save computing time. As an indication of how well the process converged, Figure 5.1 presents the variation of the error in the continuity equation with the number of iterations. It is seen that after the initial sudden increase, successive changes between iterations decrease substantially and the solution rapidly converges.

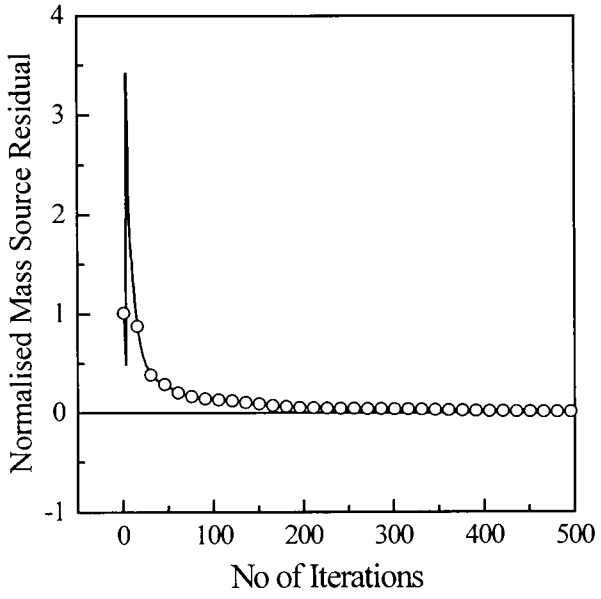

Figure 5.1 Convergence of the Solution Process

Table 5.2 compares the results for the relative inter-zone mass flow at the boundaries of gas zones 1-3 and 2-4 for all six grids analysed. Three cases with finer grid layouts were tested in which grid points where added in the *X* direction (i.e. along the length of the furnace), see Figure 5.2.

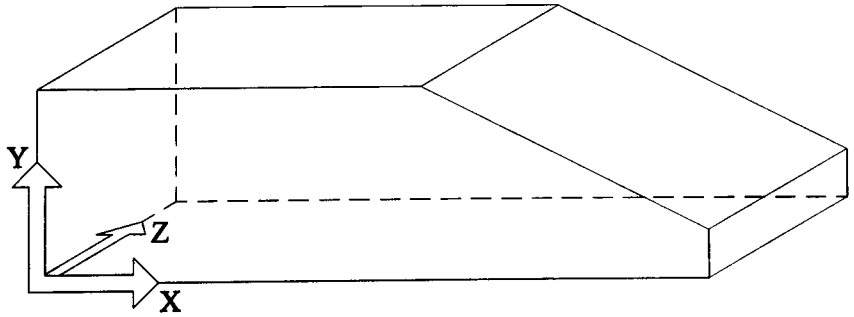

Figure 5.2 The *X*, *Y* and *Z* Coordinate Directions

Table 5.2 Demonstration of Grid Independence

	Relative Inter-Zone Mass Flow Rate		*Mass Residual*	*Computational Time (hrs)*
	Gas Zones 1-3	**Gas Zones 2-4**		
Grid 1 (15x36x20): 10800 cells	74	174	10^{-2}	0.5
Grid 2 (25x36x20): 18000 cells	106	206	10^{-2}	0.7
Grid 3 (50x36x20): 36000 cells	115	215	10^{-2}	1.2
Grid 4 (60x36x20): 43200 cells	116	216	10^{-2}	1.3
Grid 5 (50x39x20): 39000 cells	113	213	10^{-3}	2.5
Grid 6 (60x39x20): 46800 cells	115	215	10^{-3}	2.9

As it can be seen the relative inter-zone mass flow rate values varied substantially between grids 1 and 3. However, a further increase in the number of nodes, grid 4, only marginally improved the solution obtained for grid 3. Having established that solutions from grid 3 and 4 are acceptably stable, it was decided to investigate these two grid layouts for variations in the results when the number of nodes is increased in the Y direction (i.e. the height of the furnace), grids 5 and 6. In addition, a stricter stopping criterion, 10^{-3}, was employed with the dual aim of generating more accurate solutions and checking the appropriateness of the original convergence criterion.

The results of these simulations show only minor improvements when compared with the corresponding results from grids 3 and 4. However, the computational time for grid 3 was less than half of that required for grids 5 and 6. The nearly identical values obtained mean that the initial choice of grid in the Y direction was adequate. Further refinements in the *Z* direction (i.e. the width of the furnace) were found impractical to perform with the available computer resources. The reason for the poor performance of grids 1 and 2 can be attributed to the failure to represent the substantial variations of the flow variables in the *X* direction. Thus, as a compromise between accuracy and computing costs, grid 3 with a total of 36000 cells, see Figure 5.3, was selected since it appears to provide adequate representation of the flow behaviour of the metal reheating furnace under consideration. The numerical solutions were thus essentially grid independent, were obtained with reasonable convergence times and were sufficiently accurate for the purposes of this study.

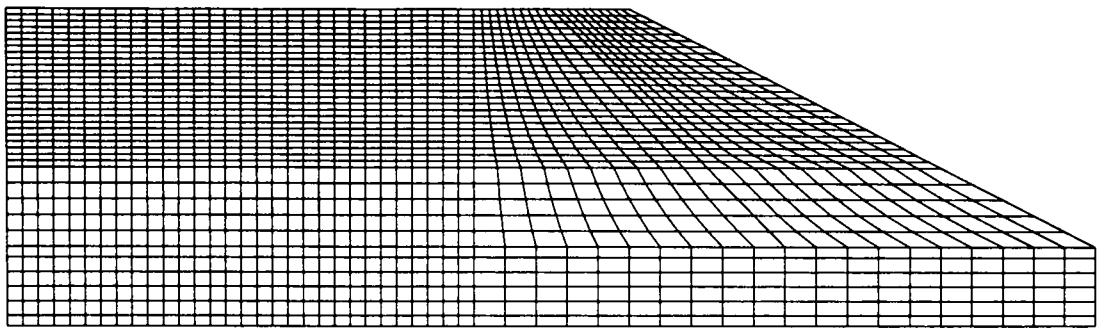

Figure 5.3 Grid Adopted in the CFD Model for Nozzle Mix Burners

5.2.2 Flow Patterns

Following the grid independence study, flow calculations were undertaken for the furnace to investigate the influence of burner geometry including change in diameter, orientation and location, on the velocity field inside the furnace.

Variations in the nozzle diameter and hence in the momentum of the natural gas burners has a significant effect on the flow patterns. Consequently, four different burner diameters namely 0.14m, 0.19m, 0.28m and 0.42m (all firing horizontally) were simulated and the resultant flow patterns (1-4) in the central vertical plane of the burner are displayed in Figure 5.4. The velocity vectors represent both the magnitude and direction of the component of the velocity on the plane of projection and show clearly the path of the jet, the recirculation regions and the position of any vortices inside the furnace.

The patterns reveal a central jet region surrounded by recirculation zones. In general, there is a strong recirculation in the lower part of the furnace close to the discharge end with much weaker circulation in the upper part. The velocity plots also illustrate the effect of the burner diameter on the size and intensity of the recirculation region. It can be seen that the size of the recirculation zone in the lower part of the jet decreases as the burner diameter is reduced although the intensity i.e. the velocities in the region are increased. At the same time the size and strength of the upper recirculation region increases as the diameter is reduced.

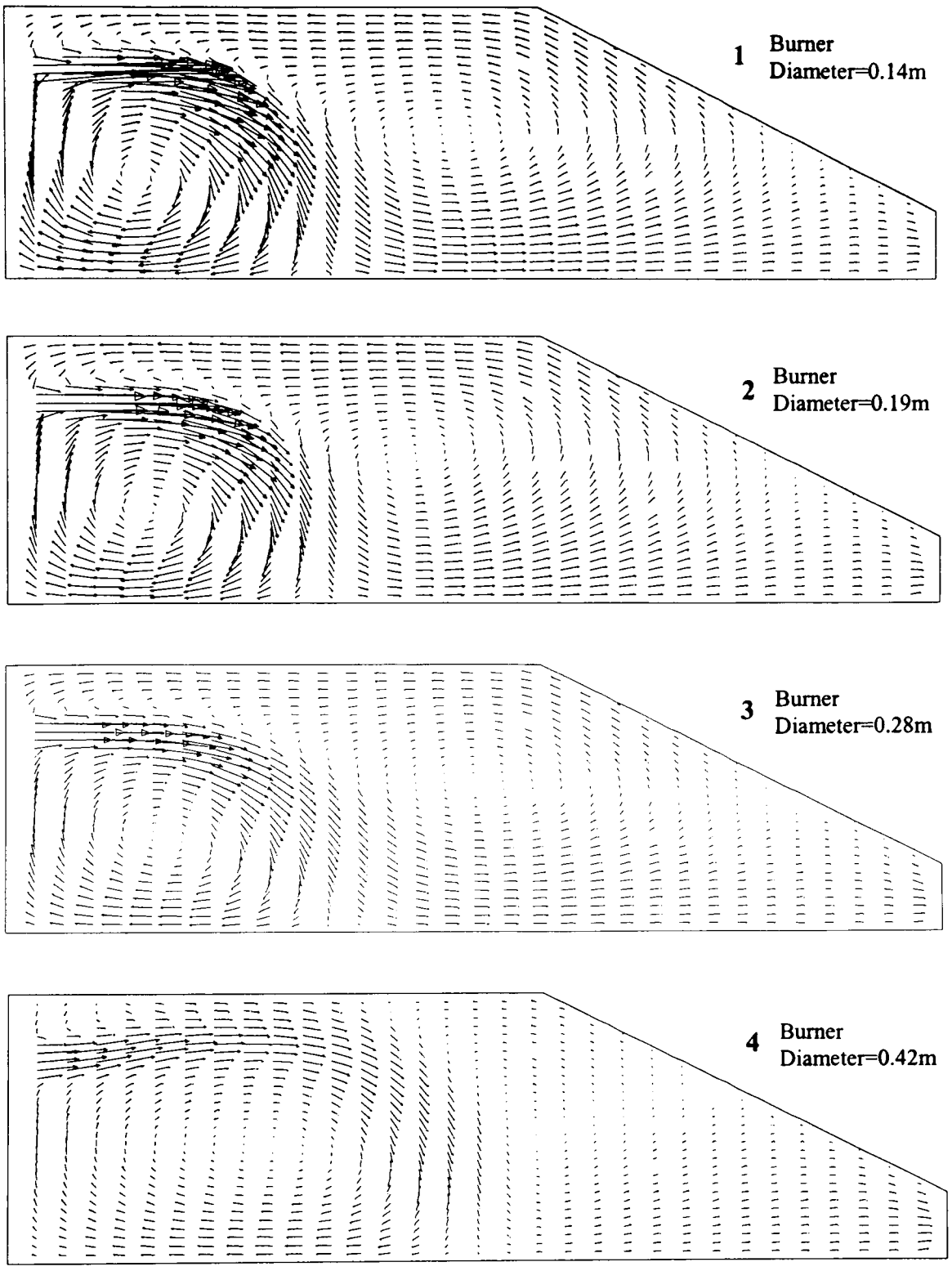

Figure 5.4 Predicted Velocity Patterns for Different Burner Diameters at z=0.275m

Further general aspects of the flow predictions are given in Figure 5.5. Because the flow results for the different burner diameters exhibit qualitatively similar features only predictions for a burner diameter of 0.19m are presented here.

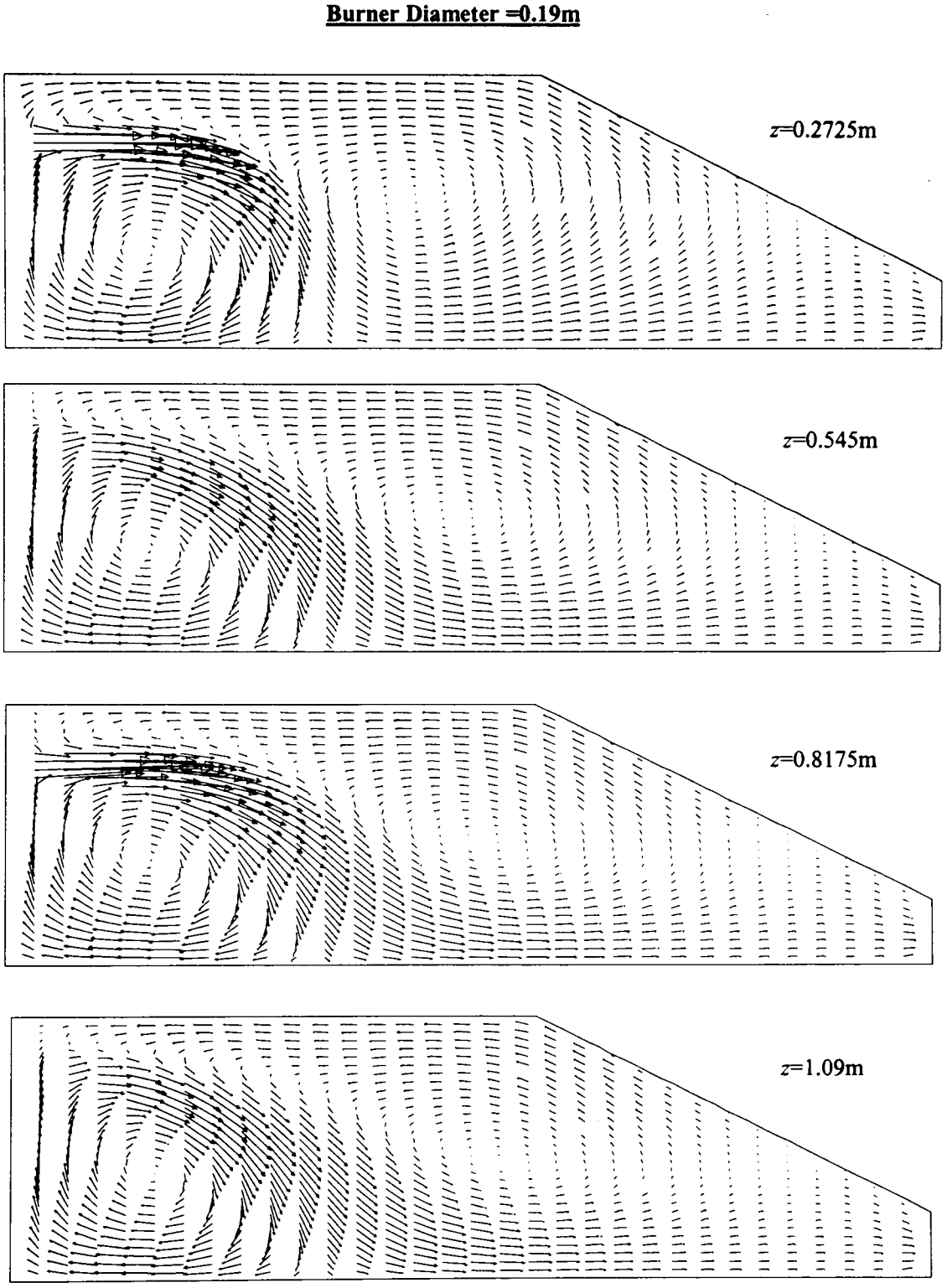

Figure 5.5 Predicted Velocity Patterns at Different Positions along the Furnace Width (*Z* direction)

Figure 5.5 shows the predicted velocity vector field for selected vertical planes normal to the wall containing the burners. Planes z=0.2725m and z=0.8175m are positioned on the axis of the two burners while the remaining two planes, z=0.545m and z=1.09m, are located middle way between the burners and at the symmetry plane of the

furnace. From Figure 5.5 it can be seen that the flows are essentially symmetrical about the burner axis.

Figure 5.6 shows the sectional profiles of velocity at different heights and lengths along the furnace. Near the burner exits the presence of two distinct jets can be observed. Outside this near burner region the velocity profiles are found to be reasonably uniform across the width of the furnace. These profiles are seen to flatten out quite rapidly with increasing distance from the burners. At y=1.635m the velocity profile is asymmetric with the burner near the side-wall having much smaller velocities. This is probably due to the influence of the side-wall of the furnace on the flow patterns. Overall, however, the flow can be considered to be essentially uniform across the furnace width except near the burners so that the use of two-dimensional zone models would appear to be appropriate.

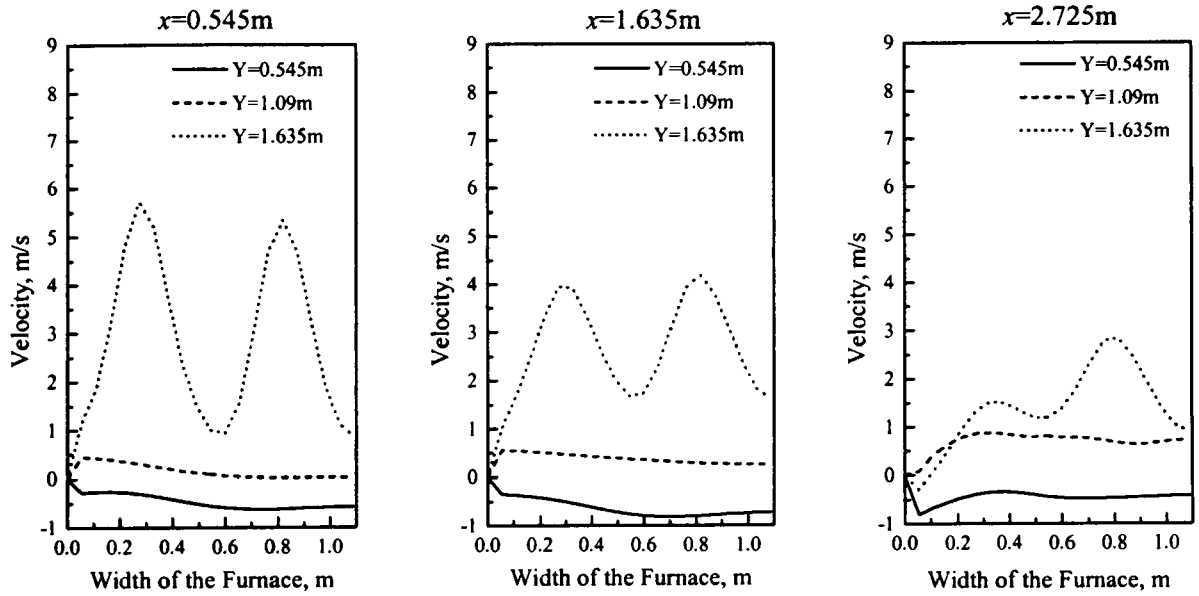

Figure 5.6 Profiles of Velocity for the Nozzle Mix Burner Jets

The effect of ***burner inclination*** on the overall flow patterns was also studied for a 0.19m diameter burner inclined downwards at an angle of 20°. The resultant flow pattern for the vertical plane on the burner axis is presented in Figure 5.7. Again two distinct recirculation zones can be identified, a large anti-clockwise recirculation region above the jet and a smaller clockwise recirculation zone near the hearth. Figure 5.7 clearly shows that the jet flow is initially directed towards the bottom of the furnace before the upper recirculation zone gradually directs the flow towards the roof. This figure also shows that the air flows along the sloping roof towards the flue. This flow

pattern is very different from the one associated with a horizontal burner in that the main recirculation occurs in the upper part of the enclosure whereas with the horizontal burners it occurs in the lower part.

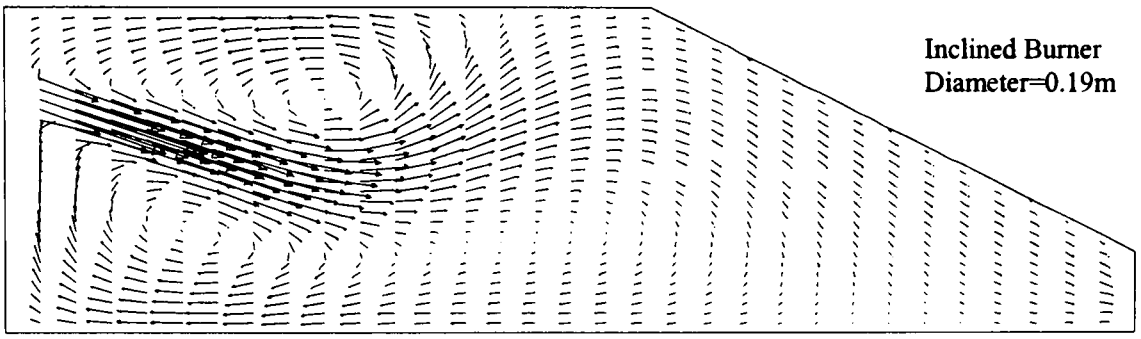

Figure 5.7 Predicted Velocity Pattern for Inclined Burners

The effect of changing the ***position of the burners*** was also investigated. In this case the 0.19m diameter burners were positioned in the lower half of the furnace. The velocity vector plot shown in Figure 5.8 for a plane passing through the burner axis again shows the presence of recirculation zones above and below the jet.

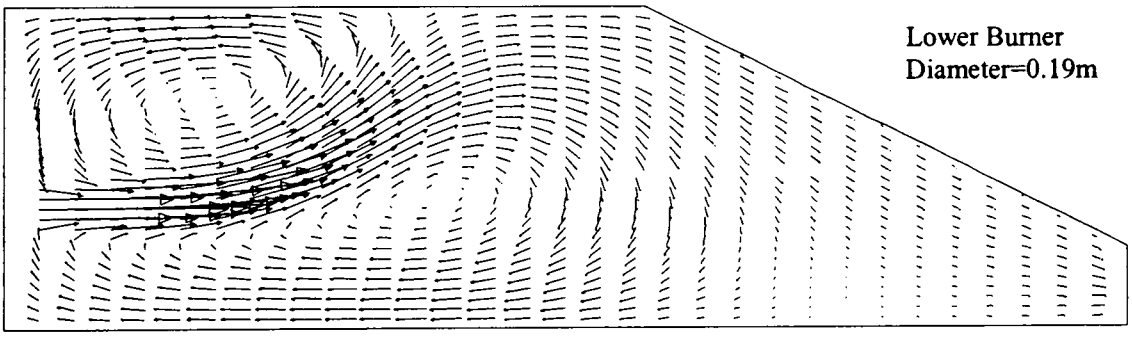

Figure 5.8 Predicted Velocity Pattern for Burners Positioned at the Lower Half of the Furnace

5.2.3 General Findings

The aim of a metal reheating furnace is to heat up slabs to a suitable uniform temperature for subsequent hot forming operation. This is best achieved when the combustion gases are uniformly distributed across the width of the furnace. The momentum of the inlet jet is the most important variable to control uniformity within the furnace. The 3D CFD model studies investigated here have clearly shown that the inlet jets entrain the surrounding fluid and because of confinement recirculating flow occurs. The flow patterns were shown to depend on the burner diameter as well as the

position and inclination of the burners. The magnitude of the recirculated mass flow and the location and size of the recirculation eddies varied considerably for the different burner geometries. However the flows were found to be substantially uniform across the width of the furnace suggesting that a two-dimensional zone model will suffice.

It is not possible to validate the velocity predictions by direct measurements of velocities on full-scale furnaces since data are extremely difficult to obtain due to the harsh operating environment. Consequently, limited comparisons were made with predictions from similar studies.

Thus, Chen and Ho [7] examined the flow field inside a steel reheating furnace using an isothermal ambient 3D CFD model. Their furnace geometry in many aspects resembled a scaled-down version of the metal reheating furnace analysed in this project. It incorporated an inclined roof near the charge end of the furnace and the horizontal burners were located in the top half of the discharge end wall. Their computed velocity field at the plane of the burners was in good qualitative agreement with the general patterns described in section 5.2.2 for the current horizontal burners. The overall effects on the flow of the sloping roof were also similar.

Despite the lack of experimental validation for the current flow predictions, these limited qualitative comparisons have confirmed that the overall flow features produced by the CFD model are reliable. This suggests that the present isothermal CFD models can be used with reasonable confidence to obtain the flow patterns in the reheating furnace and hence the enthalpy data required by the zone models.

5.3 Summary

Initially grid dependence tests were performed on the CFD model and a final non-uniform grid with 36,000 cells was selected since it provided relatively good representation of the flow characteristics while still computationally efficient. The final grid is denser in the near burner region where steep variations are likely to occur and gets coarser downstream of the furnace towards the exhaust. The main features of the flow were displayed and discussed and it was found that changes in burner geometry, orientation and position substantially affect the flow of combustion products. It is therefore important to realistically represent flow patterns since these are likely to affect the temperature distribution and hence the overall furnace predictions. Comparisons of flow predictions in the current investigation with previously published studies suggest that the CFD calculations can provide reliable estimates of the flow patterns.

References

1. Tucker, R.J., Lorton, R., *Mathematical modelling of load-recuperative gas-fired furnaces*, in *MRS Report No. E418.* 1984, British Gas: Solihull.
2. Palmer, M.R., *A practical computer package for the thermal design of high temperature industrial plant*, in *MRS Report No. E567.* 1989, British Gas: Solihull.
3. Wieringa, J.A., Elich, J.J., Hoogendoorn, C.J., *Spectral effects of radiative heat transfer in high temperature furnaces burning natural gas.* J. Inst. Energy, 1990(September): p. 101-108.
4. Tucker, R.J., Ward, J., *Application of a long furnace model to a continuous, gas-fired, steel reheating furnace.* in *1st European Conference on Industrial Furnaces and Boilers,* 1988. Lisboa, Portugal.
5. Rhine, J.M., Tucker, R.J., *Modelling of Gas-Fired Furnaces and Boilers and Other Industrial Heating Processes*, 1991, London: McGraw-Hill.
6. Beer, J.M., Chigier, N.A., *Combustion Aerodynamics*, 1972, London: Applied Science Pub.
7. Chen, J.D., Ho, T.Y., *Numerical analysis of isothermal flow fields in modelled reheating furnace.* in *Intl. Symp. Steel Reheat Furnace Technology,* p. 199-210. 1990. Ontario, Canada.

CHAPTER SIX

COMPARISON OF DIFFERENT ZONE MODELS

6.1 Introduction

Following the isothermal CFD simulations, several different zone models were developed to simulate the behaviour of the metal reheating furnace operating under transient conditions. In most previous investigations, transient zone models have featured simplified multi-zone models such as the so-called long furnace model where the enclosure is subdivided longitudinally [1]. In these cases the flow of combustion products is assumed to be "plug-flow" since the simplified furnace geometry resemble that of a long tunnel. In practice, however, furnaces are often of non-uniform cross section and flow patterns are more complicated so that in these cases a two-dimensional transient zone model can provide improved predictions. In order to determine the influence of the number of zones on the overall furnace predictions, different zone arrangements were investigated ranging from simple one-dimensional to more sophisticated multi-dimensional models.

6.2 The Need for a Two-Dimensional Zone Model

Initially for comparison purposes a one-dimensional long furnace model (LFM) comprising 7 divisions along the furnace length was constructed to simulate the system,

see Figure 6.1 with a thermal input to gas zone 1 near the burners and the exhaust at gas zone 7.

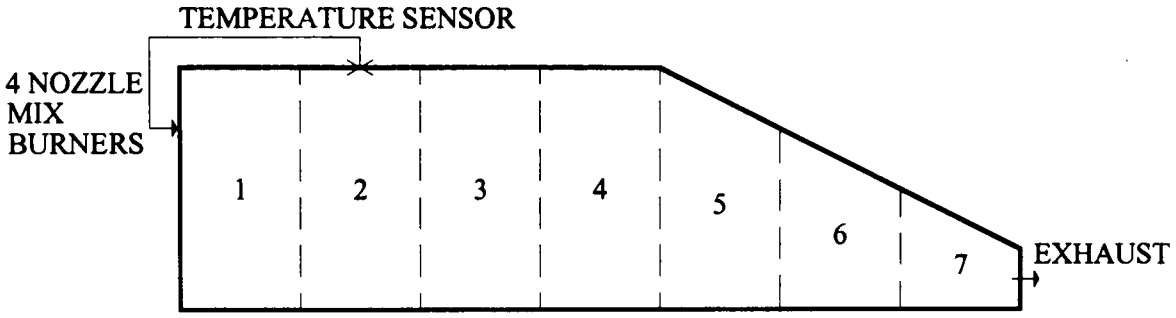

Figure 6.1 The LFM Zoning Arrangement

The subdivision resulted in 7 volume zones, 30 zones on the refractory surfaces and 7 for the load. The temperature distribution and hence the rate of heat transfer was assumed uniform both across the width and height of the furnace chamber so that only longitudinal variations were considered. For comparison purposes a second two-dimensional model, see Figure 6.2, was also employed in which both the height and length of the furnace were split.

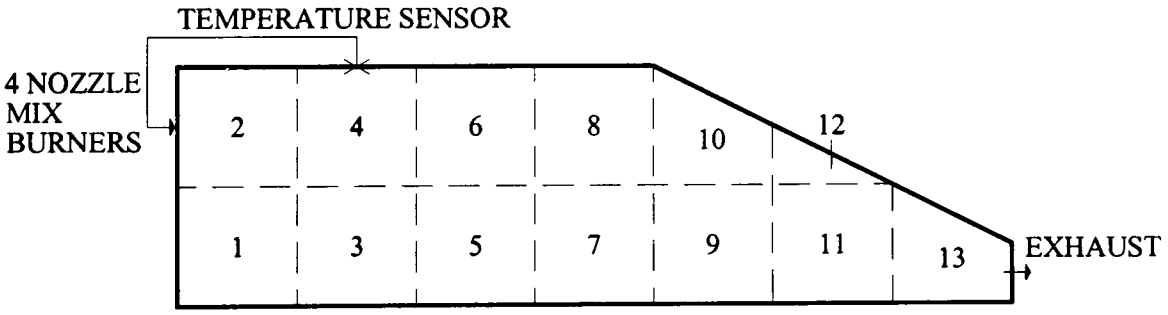

Figure 6.2 The 13 Gas Zone Model Arrangement

This involved 13 gas zones, 43 refractory surface zones and 7 load surface zones. The natural gas was supplied and fully combusted in zone 2 and the combustion products exited from zone 13. In this case the temperature profile and hence rate of heat transfer were considered to be substantially uniform across the width of the furnace so that this dimension was not subdivided.

The models were employed to simulate the performance of the furnace starting from cold ambient conditions so that the initial refractory and load temperatures were specified at ambient temperature. Appropriate radiation exchange areas were evaluated

by RADEX [2], as described in the previous chapter. The furnace atmosphere was represented by a mixture of three grey gases including one clear component to account for the non-absorbing wavelengths in the spectrum. All load, ceramic fibre roof and refractory walls and hearth were assumed grey and diffuse.

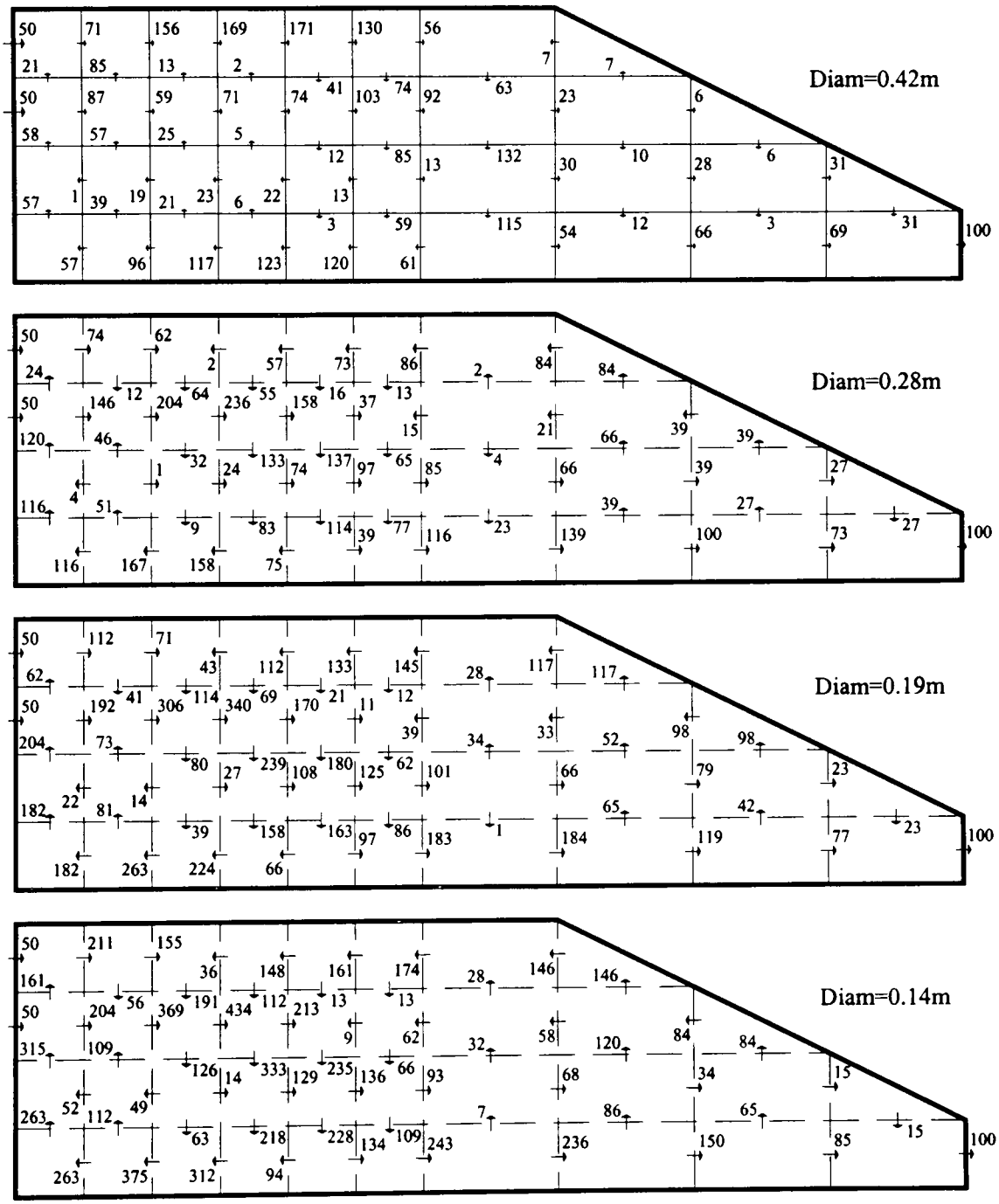

Figure 6.3 Inter-Zone Relative Mass Flows for Different Burner Diameters

A value of 25W/m^{2}K was specified for the convective heat transfer coefficient at each of the surface zones in accordance with the experimental work of Sousa [3] and

this approach was found to be adequate due the minor contribution of this mode of heat transfer in high temperature systems. Energy release as a result of combustion in any of the volume zones was neglected since it was assumed that the natural gas was completely burnt within the nozzle mix burners. The enthalpy flows were estimated using ambient, isothermal CFD computations as described previously. Figures 6.3 and 6.4 illustrate the flow patterns obtained by the CFD calculations for the models with 37 gas zones which are used later in this chapter and for each burner condition considered in section 5.2.2. These are given in terms of the relative mass flow rate issuing through the nozzle-mix burners. The inter-zone mass flows in cases with coarser zonings can be obtained by combining the appropriate volume zones.

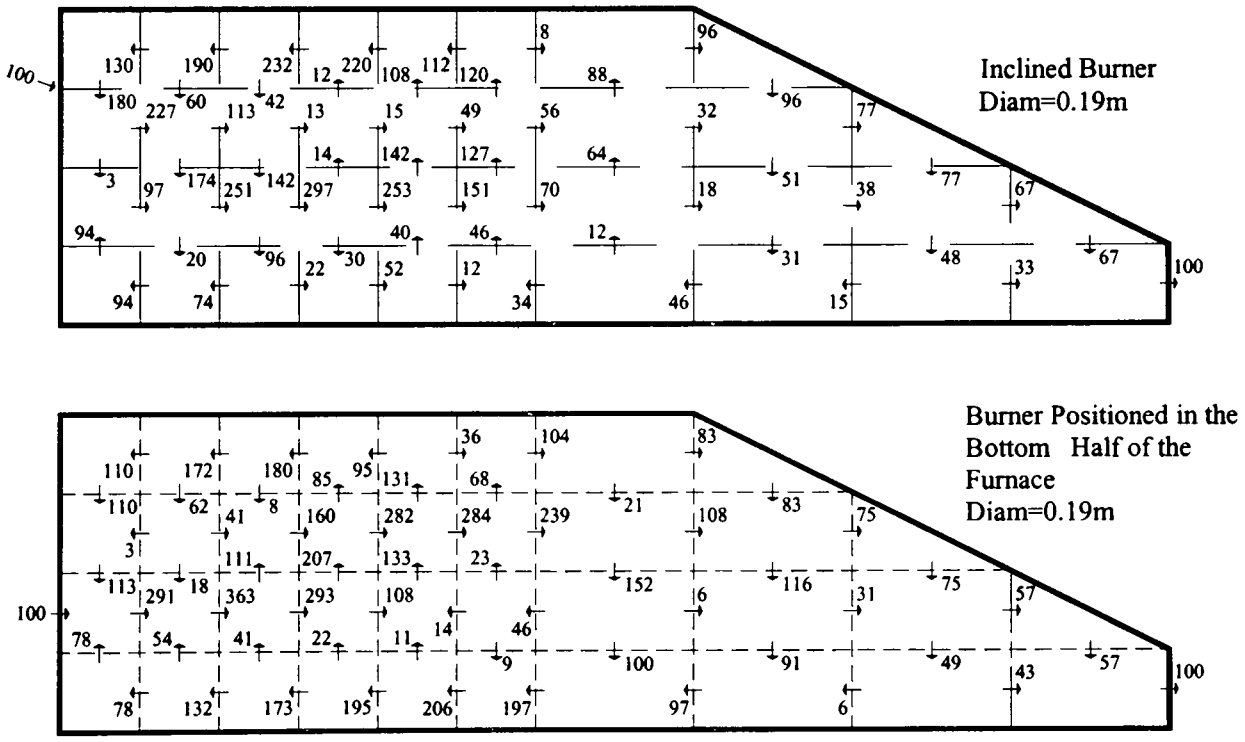

Figure 6.4 Inter-Zone Relative Mass Flows for Inclined and Horizontal Lower Burners

The predicted refractory roof temperature in the zone containing the control thermocouple was used to control the thermal input to the furnace and the set point value was varied from 1300 to 1380°C during the simulations. A simple linear proportional control adjusted the input of natural gas in response to deviations from the set point temperature with the air/fuel ratio kept constant throughout the calculations so that an excess air level of 5% was employed.

Conduction into the load and refractories was assumed to be one-dimensional. The temperature of the hot face of the ceramic fibre lining responds rapidly to changes in

fuel input and this can lead to instabilities in the calculations. Consequently, to ensure stability of the conduction models a fully implicit finite-difference formulation [4] was used with a time step of 10 seconds. The models take into account variations with temperature of the thermal properties of the load and furnace lining. The bottom of the billets was allowed to lose heat into the hearth and the thermal contact resistance between these surfaces was assumed to be $0.002 m^2K/W$ as described previously.

The main interest at this stage was to study the initial start-up of the furnace from cold so that the numerical simulations were concluded when the upper surface of the load adjacent to the first gas zone achieved a temperature of 1250°C.

Table 6.1 summarises the furnace zoning, operating conditions and other parameters used in the simulations. Conditions marked with the symbol * correspond to the baseline specifications against which other parameters will be compared.

Table 6.1 Zone Model Conditions

Zoning Characteristics	**1D LFM**	**2D Model**
Number of Volume Zones and hence Simultaneous Equations which are Solved	7	13
Total Number of Surface Zones	37	50
of which		
Walls	16	29
Hearth	7	7
Roof	7	7
Load	7	7
Volume Zone Dimensions (m)		
Length	1.09	1.09
Height	2.18	1.09
Width	2.18	2.18
Model Conditions		
Load Dimensions (m)		
Length	1.089	
Thickness	0.0635	
Width	1.83	
Lining Thickness (m)		
Walls and Hearth	0.3	
Roof	0.35	
Burners		
Number	4	
Type	Nozzle Mix	
Fuel	Natural Gas	
Max Thermal Input (MW gross)	5.4	
Excess Air (%)	5	
Diameter (m)	0.14, 0.19*, 0.28, 0.42	
Location	Top*, Bottom (Side Wall, Discharge End)	
Inclination	0°*, 20° to horizontal	

Combustion Products Representation	Weighted Sum of Grey Gases (1 clear + 2 grey)
Emissivities of the Materials	Steel Bars = 0.7; Ceramic Fibre Roof = 0.5; Refractory Walls and Hearth = 0.6
Radiation Exchange Areas	RADEX (Monte Carlo based code)
Enthalpy Flows	3D Ambient, Isothermal CFD Calculation
Convective Heat Transfer Coefficient (W/m^2K)	25
Initial Surface Temperatures (°C)	Ambient = 20
Conduction Through Surfaces	
Model	1D, Finite Difference, Fully Implicit
Number of Nodes Through the Thickness	
Load	11
Roof	8
Walls and Hearth	7
Thermal Contact Resistance Load-Hearth (m^2K/W)	0.002
Load Top Surface Discharge Temperature (°C)	1250
Set Point Temperature (°C)	1300, 1320, 1340, 1360, 1380*
Sensor Location	2nd roof, hot face
Control System	
Type	Proportional
Error Band (°C)	±7.5
Turndown	0.2
Calculation Time Step (sec)	10

6.2.1 Effect of Burner Diameter

The momentum or so-called thrust of the natural gas burners can influence the recirculation pattern of the hot combustion products within the furnace chamber and hence the rate of heat transfer to the load. Consequently, the two zone models were used to assess the influence of the burner characteristics on the behaviour of the furnace following a cold start-up.

The temperature–time histories for the top and bottom surface of the load in zone 1 are shown in Figure 6.5 for the two different zone models using the flow pattern of the 0.19m diameter burners firing horizontally into the top half of the furnace, i.e. the so-called baseline conditions. The furnace set point was maintained at 1380°C in these simulations. Due to the similarity between the different burner diameter cases, no further heating curves are presented.

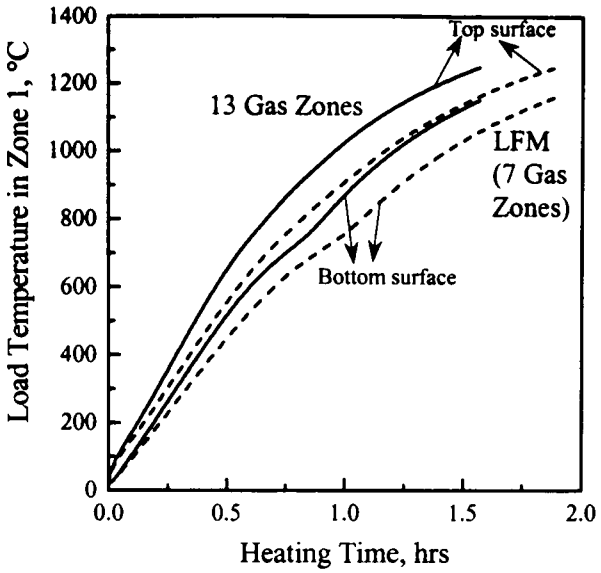

Figure 6.5 Temperature-Time Histories for Different Models (SPT=1380°C)

Tucker [5] and Sousa [3] found similar heating curves when investigating the performance of gas fired metal reheating furnaces. Because the degree of near burner recirculation in their studies differed substantially from any of the cases presented here no direct comparisons could be made. The predicted heating period necessary to attain a top surface temperature of 1250°C varied from 1.88 hours for the simple LFM to 1.57 for the two-dimensional model i.e. a difference of 16%.

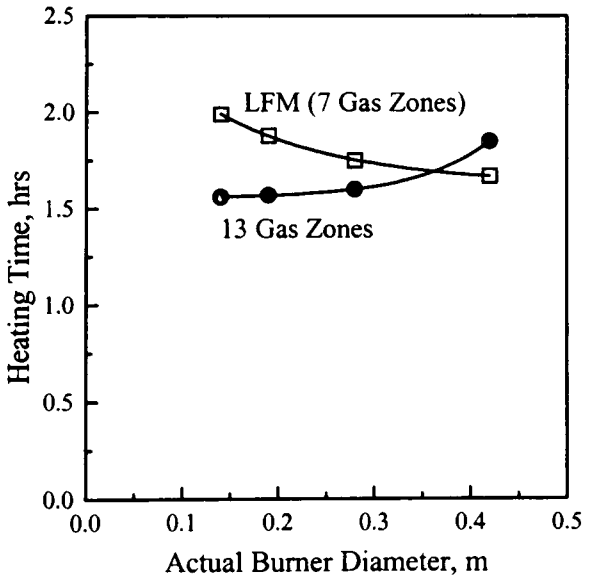

Figure 6.6 Variation of the Initial Heating Period with Burner Diameter (SPT=1380°C)

However, the predicted durations of this initial start-up period depends on the burner diameter and hence momentum, as shown in Figure 6.6 and Table D.1 (see Appendix D), which presents predicted initial start-up times for both the LFM and 13 gas zone

models for the horizontal burners mounted in the top half of the furnace. It is clear that the two zone models behave very differently. This is probably due to differences in the predicted temperature distribution between the two zone models.

As seen in Figure 6.3, the degree of recirculation near the burners in the lower half of the furnace increased as the diameter was reduced i.e. the velocity of the combustion products leaving the nozzle was increased. For example, in the 13 gas zone model from a total of 100 units of mass flow input by the burners only 115 units flow from gas zone 3 to 1 with the biggest burner diameter compared with 424 units with the smallest diameter. For the smallest burner diameter the recirculation region was tightly confined to the bottom zones near the load at the discharge end. The large degree of recirculation results in relatively cold flow from downstream regions of the furnace to recirculate back along the roof towards the burners resulting in the dilution of the high peak temperature in these zones. Thus, the "overall" temperature of the flame was reduced with a consequent reduction in heat transfer to the load. In addition, the recirculation near the roof close to the control sensor induces a drop in these temperatures so that modulation does not occur throughout the entire heating period. The use of burners with 0.19m diameter resulted in similar but less marked temperature reductions due to the lower degree of recirculation generated. The temperatures of the control roof and volume gas adjacent to the first load were, therefore, slightly higher than in the previous case and this can lead to shorter heating times as predicted by the 2D model.

As the burner diameter is increased to 0.28m the size of the recirculation vortex in the lower half of the furnace increased and the flow of cool combustion products from downstream regions of the furnace results in lower temperatures and hence a longer heating time. This effect is even more pronounced when the burner diameter is increased to 0.42m so that even longer times were predicted for the load to reach its final discharge condition. The long furnace model, however, predicts an opposite trend with the initial start-up heating period increasing as the burner diameter is reduced.

The differences in behaviour between the two models are probably due to detailed differences in the predicted zone temperatures. To illustrate this Figure 6.7 shows a comparison of the temperatures-time histories for the roof and gas zones immediately adjacent to the burners and also for the volume zone above the load at the discharge end for the smallest and largest burner diameters. The remaining two burner geometries provided results in between those reported here so that they are not presented.

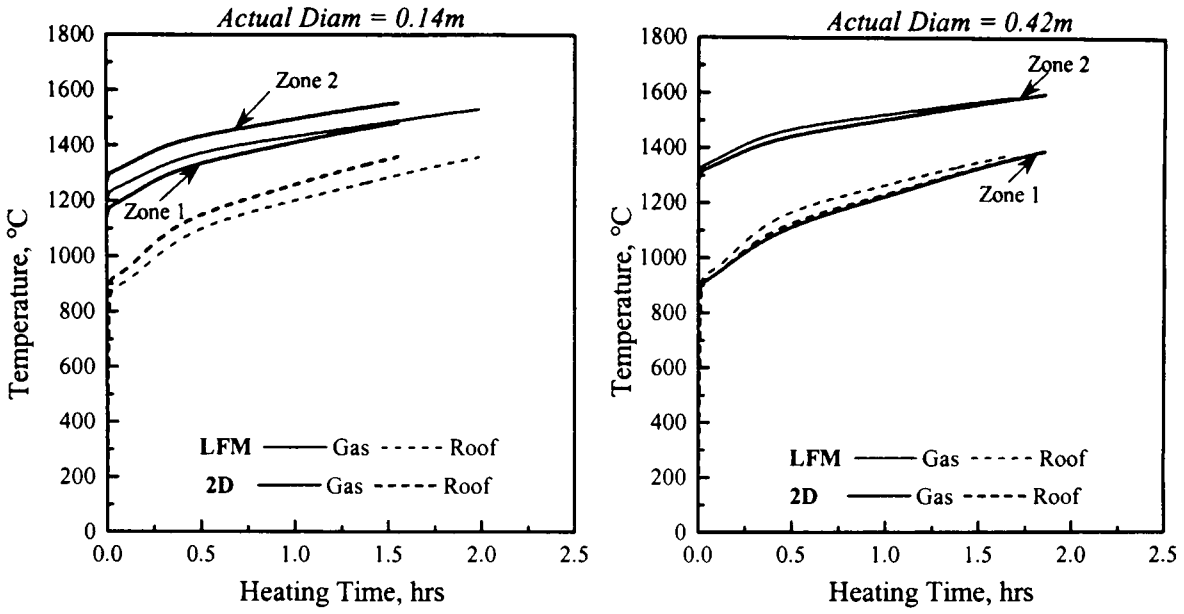

Figure 6.7 Comparison of the Predicted Gas and Roof Temperatures in the Near Burner Region for the LFM and 2D 13 Gas Zone Model (SPT=1380°C)

The distributions indicate the temperature dilution effect in the near burner volume zones with the smallest diameter burners. With the largest diameters, it is clear that lower temperatures occur in the bottom zones in the 2D model as a consequence of the flow of cool recirculated combustion products from downstream regions of the furnace. Comparing the temperature-time histories obtained with the LFM and the 13 gas zone model, it is clear that the temperature of the gas zone containing the load is not the only variable affecting the heating rate of the load. Near gas zone and roof temperatures are also important.

From this figure it can be observed that during the entire start-up period the bottom gas zone temperatures in the 2D model are generally lower than the temperatures predicted by the LFM. This does not necessarily, however, lead to corresponding longer heating periods with the smallest diameter burners. In this case the top gas zone and roof temperature in the 2D model are significantly higher than the equivalent LFM gas and roof temperatures. Consequently, the shorter heating times predicted by the 2D model, see Figure 6.6, suggest that the effect of radiation from the roof and upper gas zones exert a substantial influence on the heat transfer to the steel bars and this effect outweighs the lower temperatures in gas zone 1.

On the other hand, with the largest diameter burners the 2D model predicts lower temperatures than the simpler LFM. In addition, because of the recirculation of cool combustion products into the bottom zones of the furnace near the burners the

difference in temperature between top and bottom gas zones is much greater. These effects lead to the 2D model predicting a longer initial start-up period. The 2D 13 gas zone model, therefore, predicts a continuous increase in heating period as the burner diameter was increased whilst in contrast the LFM predicts a continuous reduction in the initial start-up heating period so that the two models behave very differently in this simulation.

The above results have clearly demonstrated the importance of employing more sophisticated 2D zone models in furnaces where the flows cannot be adequately represented by a simple plug-flow. The results also highlight the need to correctly specify the flow patterns. The different burner diameters produced different flow patterns with respect to recirculation and consequently were found to have a significant influence on the rate of heat transfer to the load and hence heating time. Further comparisons between the two zone models for the different burner diameters are presented in Table 6.2.

Table 6.2 Comparison of Predicted Transient Furnace Performance Between the LFM and 2D 13 Gas Zone Model (Horizontal Burners, SPT=1380°C)

Flow Pattern	*Actual Burner Diameter (m)*	Start-Up Heating Time (hrs)		Temperature Difference (°C)		Total Fuel Consumed (GJ)	
		LFM (7Gas Zones)	13 Gas Zones	LFM (7 Gas Zones)	13 Gas Zones	LFM (7 Gas Zones)	13 Gas Zones
1	*0.14*	1.99	1.56	84.5	97.6	38.5	30.1
2	*0.19*	1.88	1.57	87.3	97.5	36.5	30.3
3	*0.28*	1.75	1.60	91.8	98.0	33.9	31.0
4	*0.42*	1.67	1.85	95.6	93.6	32.3	35.9

In all cases the predicted fuel consumptions are directly related to the duration of heating times since the burners fire at their maximum thermal input throughout the simulations. The top-to-bottom temperature differences within the load are also related to the initial start-up periods.

6.2.2 The Effects of Burner Location and Inclination

These effects were investigated for the 0.19m diameters by firstly inclining the burners in the top of the furnace so that they fire downwards at an angle of 20° to the horizontal and secondly by placing "horizontal" burners in the lower half of the furnace. The resultant inter-zone mass flows are presented in Figure 6.4.

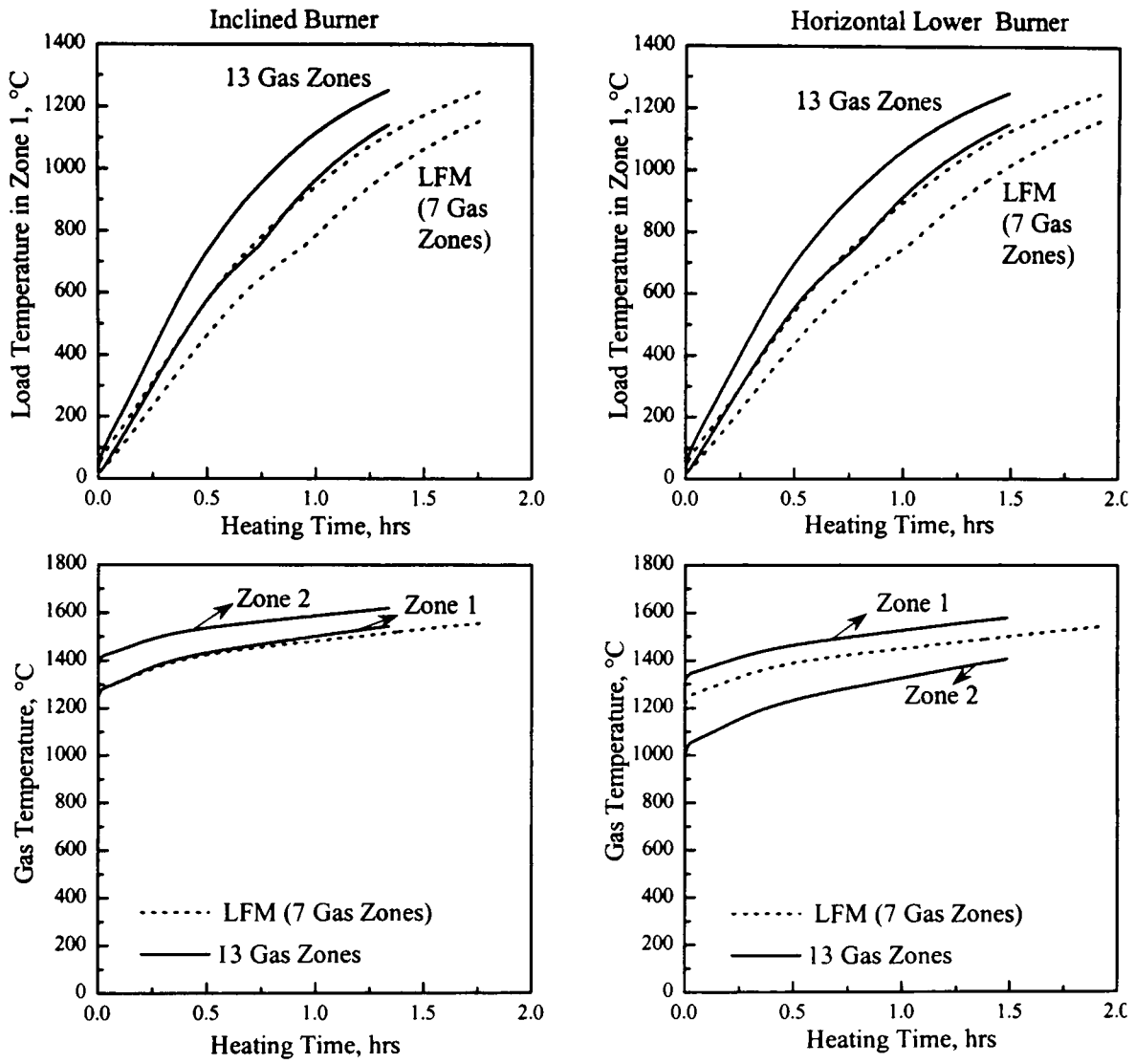

Figure 6.8 Effect of Burner Location and Inclination on the Predicted Near Burner Gas Temperatures for the LFM and 13 Gas Zone Model (SPT=1380°C)

Comparisons between the predictions of the 2D (13 zones) model and the LFM (7 zones) are shown in Figure 6.8 to illustrate the effect of burner location and inclination on the period necessary to attain a load top surface temperature of 1250°C.

For this burner diameter, the 2D model again predicts shorter heating times than the LFM. The flows from the inclined burner result in hot combustion products near the load due to the relatively small recirculation vortex formed in this region while in the upper part relatively cool recirculated gases flow near the roof. For the volume zone adjacent to the burners the predicted temperature given by the LFM is lower than the corresponding top and bottom temperature in the 2D model. Thus, relatively high rates of heat transfer to the load from these hot zones result in significantly shorter heating times so that the duration of the initial heating period is 1.34 hours with the 2D model compared with that of 1.78 hours in the LFM.

Displacement of the burners to the lower half of the furnace resulted in substantially different flow patterns, see Figure 6.4. The predicted gas temperature profiles were generally lower than those with the inclined burner due to the substantial amount of downstream cooler recirculation products brought towards the load. This reduced the overall temperature of the flame. This together with the relatively lower temperatures near the roof led to a significant decrease in heat transfer to the load in this case. The burners were not modulated so that they operated at maximum thermal input over the whole heating period in both cases. The fuel consumptions during start-up and the top-to-bottom surface temperature differentials were related to the heating periods in each case, see Table 6.3. These results indicate the need to represent the flow patterns for accurate simulation of a metal reheating furnace.

Table 6.3 Comparison of Fuel Consumption for Different Burner Configurations

	Total Fuel Consumption (GJ)	
	LFM (7 Gas Zones)	13 Gas Zones
Inclined Burner	34.4	25.9
Horizontal Lower Burner	37.2	28.8

6.2.3 The Effect of Varying the Set Point Temperature

Control of metal reheating furnaces is usually achieved by measurements of the roof temperature which act as the control set point. This control temperature is then varied depending on the load characteristics and throughput. Therefore, the 2D and long furnace models were also used to investigate the effect of varying the set point temperature on the furnace performance, see Figure 6.9 and Table D.2, for a burner diameter of 0.19m.

As the control temperature is reduced the heating time to achieve a discharge surface temperature of 1250°C is increased. This is because at the lower set point temperatures the control system modulates the thermal input so that the burners operated under low fire conditions for longer periods. This effect is more pronounced in the 13 gas zone model since the subdivision of the height was able to more accurately represent the higher temperatures in the gas zones adjacent to the burners and control thermocouple as well as the recirculation of cooler combustion products in the bottom zones near the load. In the LFM, only average estimates along the height were provided

so that any temperature gradient effects in this dimension could not be properly represented.

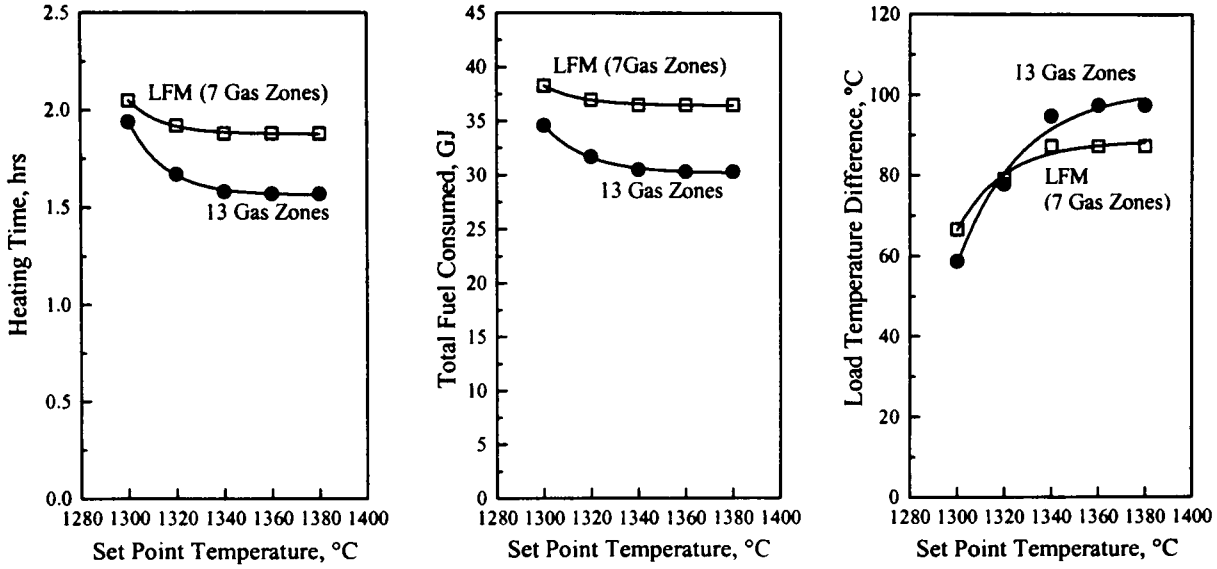

Figure 6.9 Effect of Set Point Temperature on the Transient Furnace Performance for the 2D Model and LFM

The difference in predicted heating times between the two models, however, decreases as the set point temperature is reduced with the LFM always over-predicting the length of the start-up. Thus, at a set point value of 1300°C the LFM predicted heating time is only 6% higher than that for the more sophisticated 2D model compared with the 20% increase at 1380°C.

The 2D zoning arrangement also gave hotter gas zones near the roof with consequent higher adjacent roof and wall temperatures which increased the rate of heat transfer to the load. This also contributed to the reduction in heating times. At lower set points the high temperatures registered by the control thermocouple in the roof results in early modulation of the thermal input to the system so that a relatively long heating time was predicted with the 2D model. In contrast less reduction in thermal input occurs with the simpler LFM so that the difference between the models was substantially reduced.

As expected, the longer heating times at low set point temperatures result in an increase in fuel consumption with the LFM always overpredicting in comparison with the 2D model. The variation of fuel consumption in the two models with set point temperature is, however, less marked than the equivalent increases in heating time since these two parameters are now no longer directly related due to burner modulation over part of the heating process. Thus, at the lowest set point the predicted difference in

natural gas consumption between the two models is about 10% whereas the start-up heating periods differ by 6%.

As would be expected the top-to-bottom temperature differences in the load were reduced as the control temperature was reduced with the LFM generally predicting lower differentials than the 2D models except at the two lower set points. At these set points, the combined effects of the degree of burner modulation and high load heating rate in the more sophisticated model result in substantially lower temperature gradients. The 2D model, therefore, predicted a stepper reduction in temperature gradients as the set point was reduced. Again these results indicate that over-simplification of the zoning can have a marked effect on the predicted initial start-up from cold. It is also clear from the predictions that it is important to accurately represent the behaviour of the furnace control system.

6.2.4 Simulation of Continuous Operation

Continuous operation of the metal reheating furnace was also investigated where a period of constant production rate was simulated following the initial start-up from cold. Overall this covered a total of 8 hours operation (including start-up). The purpose was to compare the predictions given by the LFM and 2D model under this mode of operation. The production rate was maintained at 6.5t/hr of steel bars and this corresponds to discharge of the load adjacent to gas zone 1 and associated movement of the rest of the load zone-by-zone through the furnace at intervals of 550 seconds. The simulations were performed using the baseline conditions, see Table 6.1, i.e. horizontal burners with a diameter of 0.19m and a set point temperature of 1380°C.

The predicted load discharge surface temperatures are shown in Figure 6.10. The higher load discharge temperatures in the 2D model are a consequence of the higher rates of radiative heat transfer from the hotter near burner gas and surface zones while only average zone values are obtained with the LFM. The trends in discharge temperature are, however, similar for both models. Initially the surface temperature is increased and this is probably due to overheating of the load near gas zones 1 and 2 during start-up. The temperatures of the load upper surface then fall as new cooler bars pass through the system. The substantially lower load discharge temperature in the LFM are a result of the lower gas temperatures and hence rates of heat transfer to the load. The subsequent increase in discharge surface temperatures towards the end of the

overall operating period may well be due to a gradual heating up of the dense refractory walls and hearth within the furnace.

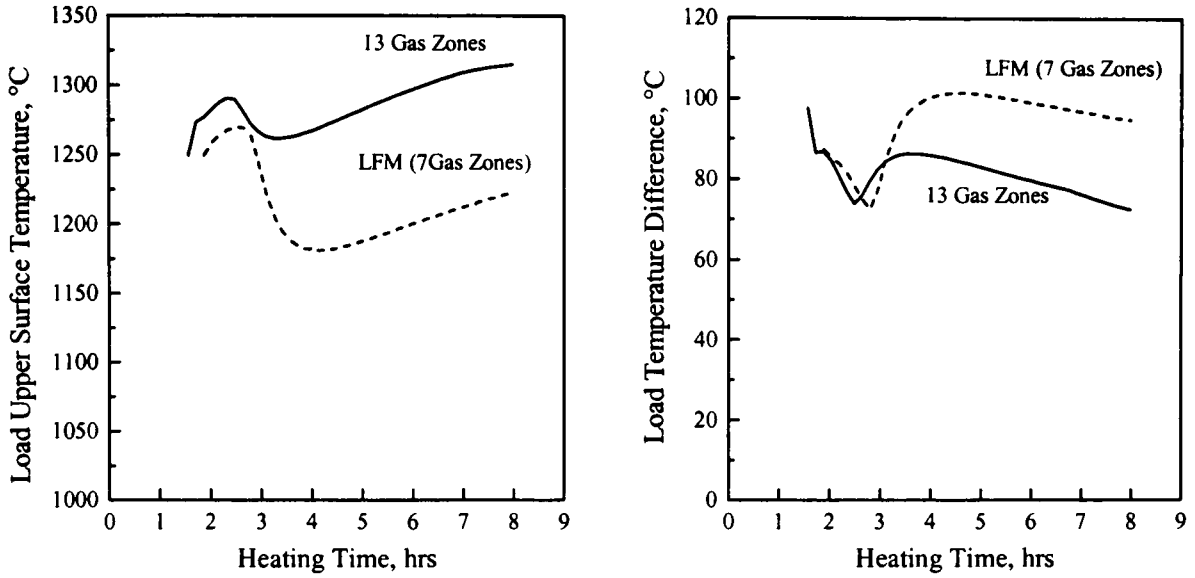

Figure 6.10 Comparison of the Predicted Load Hot Surface Temperature and Temperature Difference for the LFM and 2D 13 Gas Zone Model for Continuous Operation (SPT=1380°C)

Inspection of the discharge temperatures reveals in the 2D case values exceeding 1280°C over much of the operating period while in the LFM this value is only about 1180°C. Overheating of slabs can in practice lead to problems of excessive oxidation and scaling of the steel surface and consequently to a deterioration in quality of the final product. It is apparent from the predictions that the simpler LFM was incapable of detecting this important effect. Predicted top-to-bottom load temperatures at discharge are also presented with the LFM predicting higher differentials. The differences in predicted overall gas usage during the operating period were negligible despite modulation of the burners in the 2D model.

6.2.5 Conclusions

This study has indicated that there are considerable differences in the predictions from the two models. The use of simpler models such as the LFM, where variations are allowed only along the length of the system, can lead to significant misrepresentation of heat fluxes and hence load temperature profile in this type of furnace. This is particularly significant in cases where the quality of the final product is of utmost importance since less accurate models can fail to predict the likely occurrence of undesirable phenomena such as scaling and oxidation of load surface. Moreover, the

two-dimensional zoning of the furnace enclosure can better account for the individual characteristics of the flow and control system since these were found to strongly affect the heat distribution within the enclosure. Consequently, in order to achieve an accurate simulation of the transient behaviour of a gas-fired metal reheating furnace when the flow patterns are two-dimensional, it is necessary to adopt a more complex zoning system than the simple LFM.

6.3 The Effect of Varying the Zonal Arrangement in a 2D Model

In any model (such as CFD or zone models) where the governing equations are approximated over discrete regions, it is important to reduce the errors due to the coarseness of the zoning system. To investigate this effect the number of zones in the 2D model was varied. In addition, to the 13 gas zone model already described three additional zone arrangements, see Figure 6.11, were tested to determine the effect of the zoning system on the predicted furnace performance and computer running time.

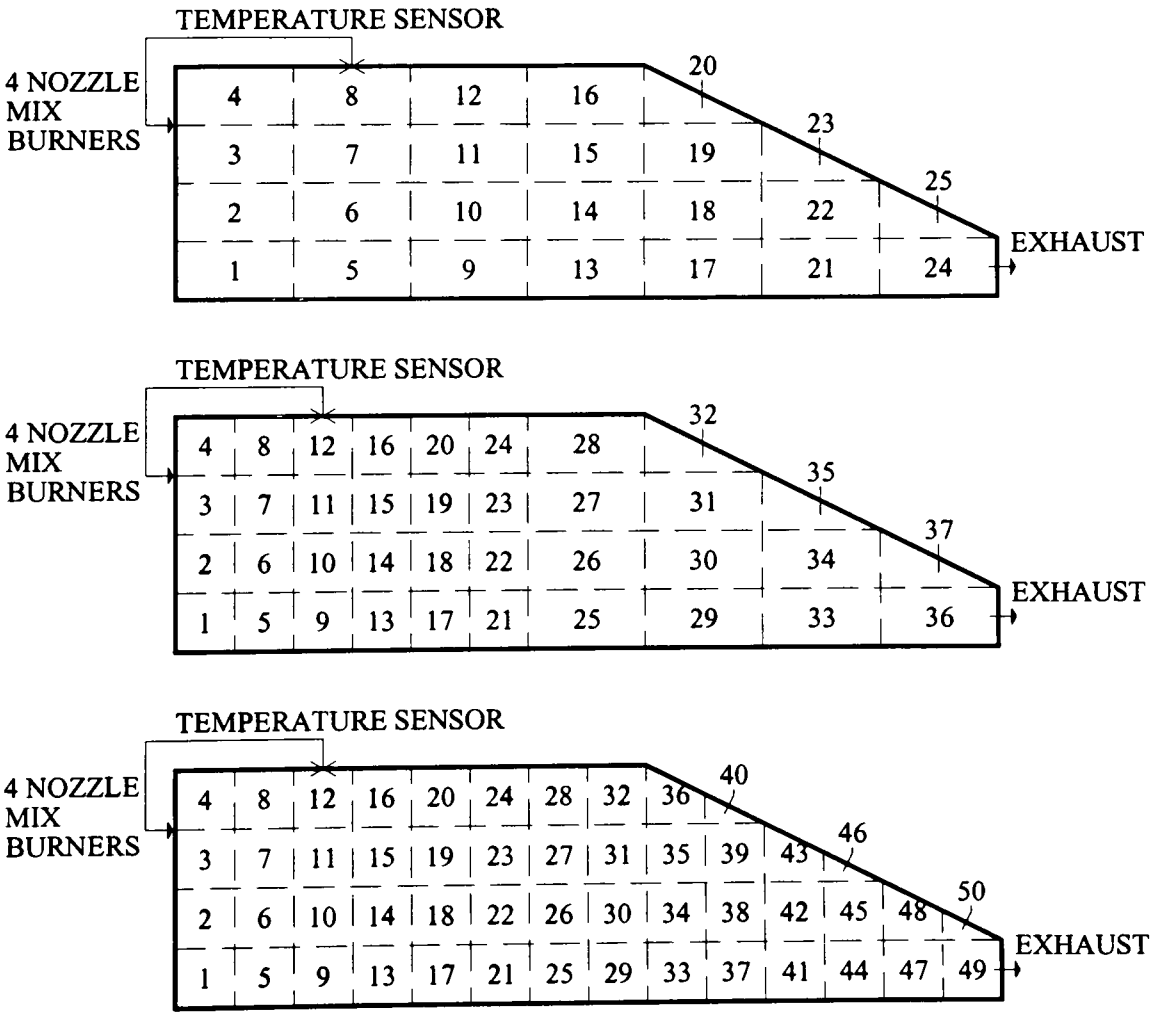

Figure 6.11 Additional Zoning Arrangements for the Steel Reheating Furnace

Initially, the furnace enclosure was subdivided into 25 gas zones with the height split into four equally spaced elements. This model was then modified by using a finer subdivision along the length near the burners because of the likely steeper temperature gradient in this region. This resulted in a system with 37 gas zones. Finally a zoning system combining 50 gas zones was also tested where the finer subdivision was extended over the whole system.

The details of the different zoning arrangements are shown in Table 6.4. All the simulations of the initial furnace start-up from cold were performed with 0.19m diameter burners firing horizontally into the top of the furnace and two set point temperatures of 1380°C and 1300°C were also used.

Table 6.4 Characteristics of the Different Zoning Systems

Model Characteristics	**Case 1**	**Case 2**	**Case 3**
Number of Volume Zones and hence Simultaneous Equations which are Solved	25	37	50
Total Number of Surface Zones of which	76	109	147
Walls	55	79	105
Hearth	7	10	14
Roof	7	10	14
Load	7	10	14
Volume Zone Dimensions (m)			
Length	1.09	0.545/1.09	0.545
Height	0.545	0.545	0.545
Width	2.18	2.18	2.18
Load Dimensions (m)			
Length	1.089	0.5445/1.089	0.5445
Thickness	0.0635	0.0635	0.0635
Width	1.83	1.83	1.83
Sensor Location	2nd roof, hot face	3rd roof, hot face	3rd roof, hot face

Results for the different zone arrangements are presented in Table 6.5. It can be seen that predictions of heating period, fuel consumption and load temperature differentials are all sensitive to the number of zones employed in the calculation. For the relatively simple 13 gas zone model, the time necessary to heat up the load to the stipulated discharge temperature varied substantially from the more consistent values obtained with the more complex models.

This is particularly the case at the lower set point. Similar variations were also observed for the largest diameter burner case with the 37 and 50 gas zone models

predicting near identical heating times. This variation with the number of zones illustrates that simple models are not able to take into consideration all features likely to affect the furnace performance predictions such as the position of the burners, control system and flow patterns.

Table 6.5 Effect of Varying the Zone Arrangement in the 2D Model of the Furnace Start-Up

Number of Zones	Heating Time (hrs)		Total Fuel Consumed (GJ)		Load Temperature Difference (°C)		Computational Time (min)	
	1380°C	1300°C	1380°C	1300°C	1380°C	1300°C	1380°C	1300°C
7 (LFM)	1.88	2.05	36.5	38.3	87.3	66.6	0.35	0.63
13	1.57	1.94	30.3	34.6	97.5	58.7	3	5
25	1.97	2.23	38.1	41.1	86.6	58.8	6	12
37	1.94	2.76	37.6	45.5	87.6	44.6	22	60
50	1.91	2.78	37	45.2	89.1	44.2	63	330

For these cases, the assumption of well-stirred conditions in each gas zone does not provide an adequate representation. Therefore, a higher zone density is required to ensure that differences arising from over-simplification of the zoning are small. The results also indicate that the control system has a significant effect on the predictions in the different zoning cases. At the lower set point of 1300°C where the temperature control modulates the burners over most of the heating period, variations between the simple and more complex zoning arrangements are more pronounced. Thus, at this set point the differences in heating times between the simple 13 zone and the 50 gas zone models was about 26% as opposed to less than 18% at a set point of 1380°C. This indicates that significant "errors" may arise if coarser near burner zoning representations are adopted.

The computational effort depends strongly on the number of zones. Consequently, the choice of an appropriate zoning system is a trade off between the accuracy of the solution and the computational requirements. Thus, the improvement in the solution obtained with the 50 gas zone model was less than 2% when compared with the 37 gas zone version, see Table 6.5. This is not unexpected since further subdivision of the enclosure at the exhaust end where temperature gradients are low is likely to provide only small improvements in the solution. In terms of computation, the 50 gas zone

model required much longer running times, see Table 6.5. Thus, at a set point of 1380°C approximately 1 hour was necessary to perform the calculations on a standard PC against the 22 minutes needed with 37 gas zone model. At 1300°C, the computational time for the 50 gas zone model increased significantly to 5.5 hours in contrast with 1 hour needed by the 37 gas zone model. Consequently, there is little advantage in using 50 gas zones so that further comparisons are restricted to the 25 and 37 zone cases.

The predicted results for these two models are presented in Figure 6.12 and Table D.3 and compare heating times, fuel consumptions and temperature variations in the load at discharge. At the higher set point temperatures (>1340°C) the use of finer zoning was found to have little effect. Under these conditions relatively little modulation of the burners occurred so that they fired at maximum thermal input throughout almost the whole start-up heating period with consequent little variation in furnace behaviour.

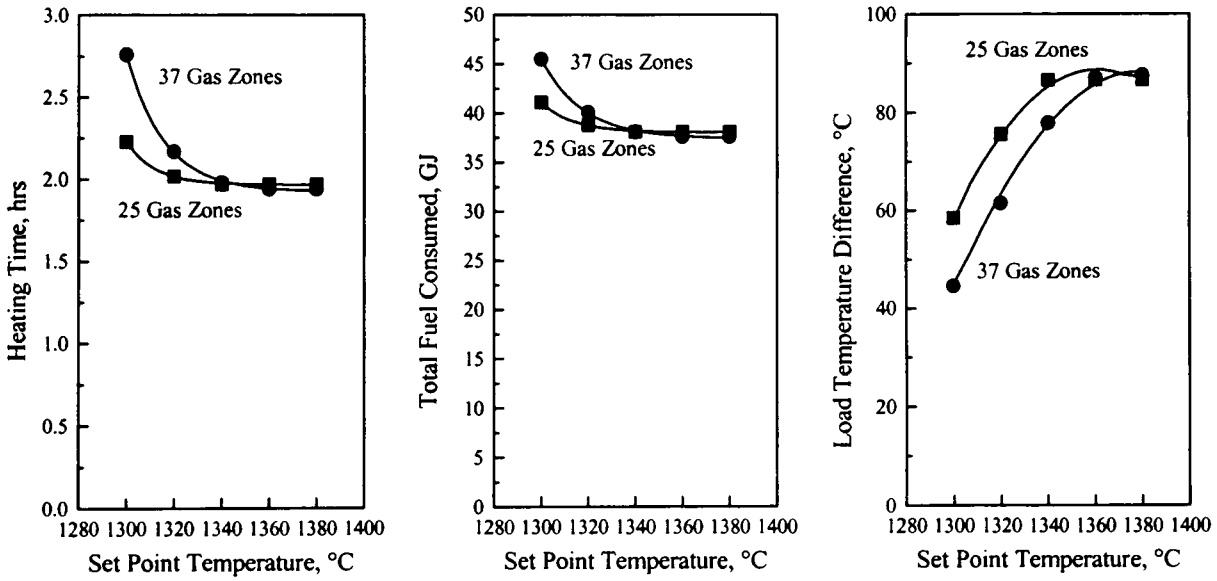

Figure 6.12 Effect of Set Point Temperature on the Transient Furnace Performance for the 25 and 37 Gas Zone Model

Different behaviour was predicted at lower set points where discrepancies between the two models were more marked. For both models there was a marked increase in the heating time necessary to achieve the discharge condition. This is because at these conditions the control system modulated the thermal input so that the burners operated under low fire conditions for longer periods. This effect was particularly intense with the 37 zone model since the finer zoning arrangement resulted in higher temperatures in the gas volumes near the control sensor and this triggered the control system to operate

earlier in this process. Consequently, longer heating times were predicted for the 37 zone model at the lower set point values (<1340°C).

Similar, but less marked, trends in fuel usage were predicted for the two zone models as the control temperature was varied. These variations in gas consumption were as previously discussed a function of both the duration of the initial heating period and burner modulation during the process. Top-to-bottom temperature differences in the load followed expected trends with smaller differentials at the lower set points. The 25 gas zone model predicting higher gradients than the more sophisticated 37 gas zone simulation.

These results indicate that the number of zones can significantly affect the predicted initial start-up performance of the furnace. The comparisons between the different models with different zoning geometries have demonstrated that relatively simple zone models with 7 (LFM) or 13 zones can result in substantial "errors". The differences between the models are reduced when the number of zones is increased to 25 or more. In particular, an increase in the number of subdivisions along the height resulting in a total of 25 gas zones provided results which significantly differed from those obtained with the 13 gas zone model without major penalty in the calculation time.

A further refinement of the zones near the burners where steeper temperatures gradients were expected proved to be important. The computational time increased by about a factor of four but this value is still acceptable. With the faster grow in computer technology these running times are likely to be substantially reduced so that the 37 gas zone model will become more affordable. The use of a finer zoning to describe the entire furnace enclosure has resulted only in small improvements. The time to perform the calculations was, however, 28 times greater than with the 25 zone model at a set point temperature of 1300°C so that any improvement on accuracy was totally undermined by the excessive calculation time. Consequently, a 37 gas zone model was selected to investigate the design and control of the furnace in the next chapter. It was considered that the model was capable of providing solutions within acceptable accuracy and computational time.

6.4 Validation of the Zone Models

The importance of testing the predictions by comparison with experimental results, whenever possible, cannot be underestimated. In any modelling exercise it is important

to ensure that the outcomes constitute a realistic representation of the actual physical system. In practice, it is extremely difficult and expensive to obtain reliable measurements on industrial furnaces. To undertake a suitable series of tests is outside the scope of this thesis. Consequently, an alternative approach was then used to provide some insight about the performance of the zone mathematical models developed in the course of this investigation.

Although the mathematical models were particularly geared to simulate the metal reheating furnace described in Chapter 4, only minor modifications were required to adapt the models to other furnace configurations. Consequently, the simple LFM was therefore adapted to simulate the continuous reheating furnace studied by Tucker [1] so that a 10 zone long furnace model was developed as illustrated in Figure 6.13.

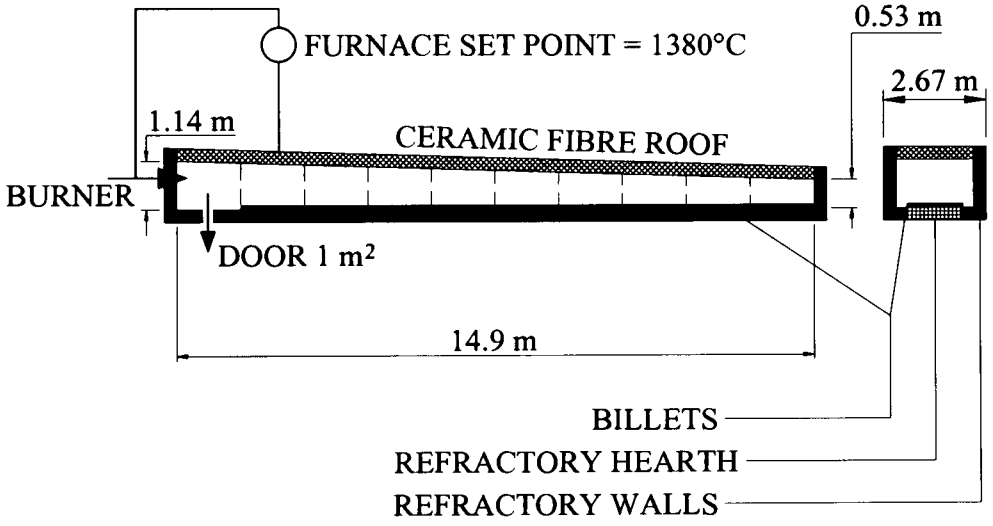

Figure 6.13 The 10 Zone Long Furnace Model [1]

Tucker compared results from a transient LFM with data acquired in a real continuous steel reheating furnace so that it was possible to mimic his model and analyse the results against his findings. The purpose of this study was to establish if the structure of the current models were valid. Table 6.6 shows the input data to the zone model to replicate the furnace conditions of Tucker [1].

Figure 6.14 compares the results obtained with the present LFM with Tucker's predictions and his measurements obtained for the furnace during the initial start-up period from cold.

Table 6.6 Transient LFM Specification [1]

Model Conditions	**1D LFM**
Number of Volume Zones hence Simultaneous Equations which are Solved	10
Zone Length (m)	1.5113
Furnace Width (m)	2.667
Load Width (m)	2.0883
Lining Thickness (m)	
Walls and Hearth	0.35
Roof	0.3
Load	0.0603
Burners	
Number	4
Type	Nozzle Mix
Fuel	Natural Gas
Max Thermal Input (MW gross)	5.8
Excess Air (%)	2.5
Diameter (m)	0.241
Location	Side Wall, Discharge End
Combustion Products Representation	Weighted Sum of Grey Gases (1 clear + 2 grey)
Emissivities of the Materials	Steel Bars = 0.8; Ceramic Fibre Roof = 0.5; Refractory Walls and Hearth = 0.9
Radiation Exchange Areas	Monte Carlo Technique
Enthalpy Flows	Craya-Curtet Formula
Initial Surface Temperatures (°C)	Ambient = 20
Conduction Through Surfaces	
Model	1D, Finite Difference, Implicit
Number of Nodes Through the Thickness	
Load	11
Roof	6
Walls and Hearth	6
Contact Conductance Between Load-Hearth (W/m^2K)	$T < 350°C$, $Cc = 5000 W/m^2K$ $T > 350°C$, $Cc = 500 W/m^2K$
Load Top Surface Discharge Temperature (°C)	1200
Set Point Temperature (°C)	1380
Sensor Location	2^{nd} roof, hot face
Control System	
Type	Proportional
Error Band (°C)	±10
Turndown	0.5
Calculation Time Step (sec)	5

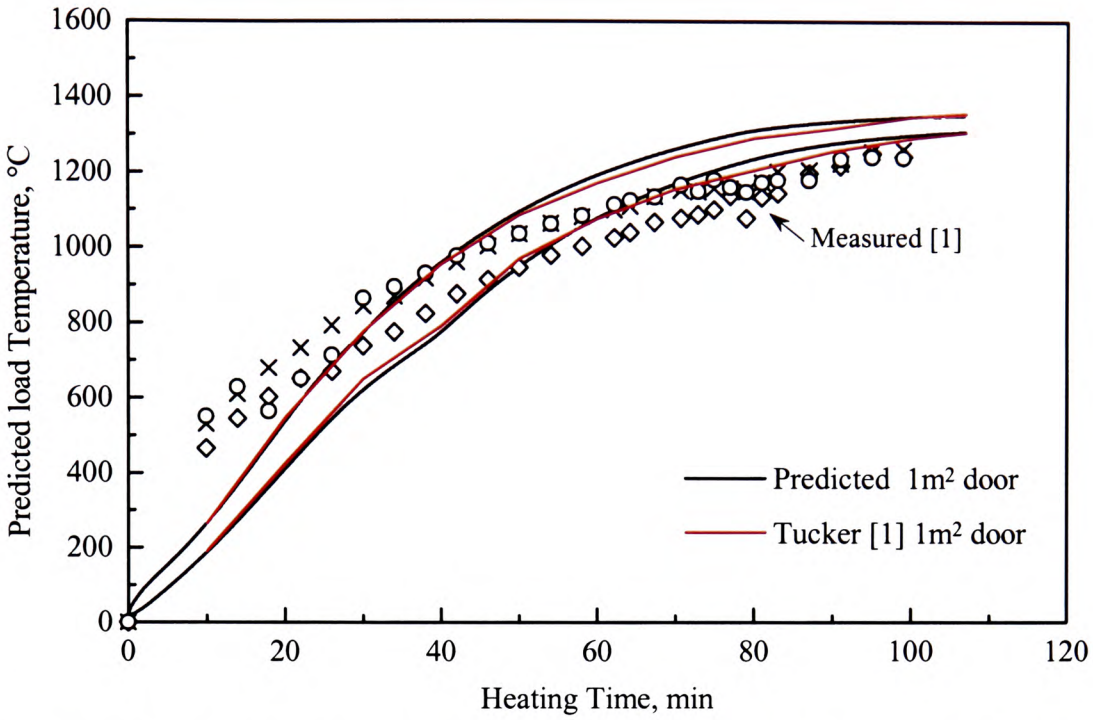

Figure 6.14 Comparison of Predicted and Measured Load Temperature During Start-Up

The initial heating curves follow the trends observed by Tucker for a bar positioned near the discharge door during a start-up from cold. The predicted billet temperatures are slightly higher than the measured values. This may result from overheating of the thermocouple leads and hence errors in the measurements. Acceptable agreement in fuel consumption is also obtained, see Table 6.7.

Table 6.7 Comparison of Predicted and Measured Fuel Consumption

	Measured	Predicted	Tucker's Model
Fuel Consumption (GJ)	31.8	35.5	33.3

Comparisons of the load temperature profiles obtained by the present LFM with Tucker's predictions are in good agreement. Overall the close agreement with both Tucker's measurements and predictions suggests that the current structure of the mathematical models is adequate. Because the LFM provided the base for the more complex zone models developed in this project, it is likely that these latter models also perform satisfactorily in their task of predicting the transient performance of the present metal reheating furnace.

6.5 Summary

A range of zone models were developed to simulate the transient operation of a gas-fired metal reheating furnace. The required flow information was provided by isothermal, ambient temperature CFD simulations of the 3D velocity vector field inside the furnace chamber. Predictions from a LFM and a 13 gas zone two-dimensional model showed that there are substantial differences between the models and indicated the need for more accurate representation of the control system and flow behaviour than can be obtained with the relatively simple LFM. The effect of varying the number of zones used to subdivide the enclosure was further investigated by testing three other zoning arrangements. The overall differences in the predictions between these various multi-zone models suggested that a relatively fine subdivision near the burner region may provide improved representation when simulating the transient behaviour of a gas-fired furnace. Consequently, a 37 gas zone model was selected to investigate the performance of the metal reheating furnace. The next chapter examines the application of this model to investigate a range of practical design and control options for the furnace. These include the effects of burner characteristics, changes to the control system, alternative furnace constructions, heat recovery and variation in the excess air on the furnace thermal performance during start-up as well as over continuous periods of production.

References

1. Tucker, R.J., Ward, J., *Mathematical modelling of heat transfer in a gas-fired reheating furnace operating under non-steady state conditions.* in *Proc. 9th Intl. Heat Transfer Conf.*, Vol. 6: p. 221-226. 1990. Jerusalem, Israel.
2. Lawson, D.A., *RADEX User Guide.* Coventry University, 1991.
3. Sousa, J.L.V.A., *Application of the Zone Method of Radiation Analysis to Simulation of the Non-Steady State Operation of Metal Reheating Furnaces.* PhD Thesis, University of Glamorgan, 1995.
4. Croft, D.R., Lilley, D.G., *Heat Transfer Calculations Using Finite Difference Equations.* 1st ed., Vol. 1, 1977: Applied Science Pub.
5. Tucker, R.J., *Evaluation and Development of the Zone Method for Modelling Metal Heating Furnaces.* PhD Thesis, The Open University, 1990.

APPLICATION OF THE 37 GAS ZONE MODEL TO INVESTIGATE FURNACE PERFORMANCE

7.1 Introduction

Having established the "optimum" zone arrangement to adequately model the gas-fired reheating furnace, it was decided to apply this two-dimensional transient model with 37 gas zones and 109 surface zones to examine the influence of a range of parameters on the thermal behaviour of the furnace. The influences of burner geometry (including location and firing direction) as well as the effects of changes to the value of the roof set point temperature were studied. The effects of varying the position of the roof temperature control sensor relative to the burners and of using alternative roof constructions were also investigated. In addition, studies were conducted to assess the effect of preheating the combustion air and of varying the amount of excess air used for combustion. The simulations were performed for two different operating conditions. Initially the study concentrated on the initial period when starting up from cold so that the mathematical simulations were concluded when the upper surface of the load adjacent to the first gas zone achieved a temperature of 1250°C. In addition, the model was used to simulate a period of constant production rate so that an overall operating period of 8 hours (including the start-up from cold) was investigated. In this latter mode of operation the production rate was maintained fixed at a value of 6.5t/hr.

7.2 Details of the 2D Zone Model

Although details of the model have been outlined previously for reasons of clarity this section outlines the particular features of the two-dimensional zone model selected for this part of the study. The model divided the furnace enclosure into 37 volume zones, 99 refractory surface zones and 10 zones on the upper surface of the bed of mild steel bars as shown in Figure 7.1. A finer zonal subdivision was employed near the burners because of steeper temperature gradients in this region. The use of four burners across the width of the furnace resulted, as previously seen, in flow patterns which were essentially two-dimensional except close to the burner nozzles. Consequently, the furnace width was not subdivided since the combustion product temperatures and consequent heat transfer rates were assumed to be substantially uniform in this direction so that a two-dimensional representation was sufficiently accurate.

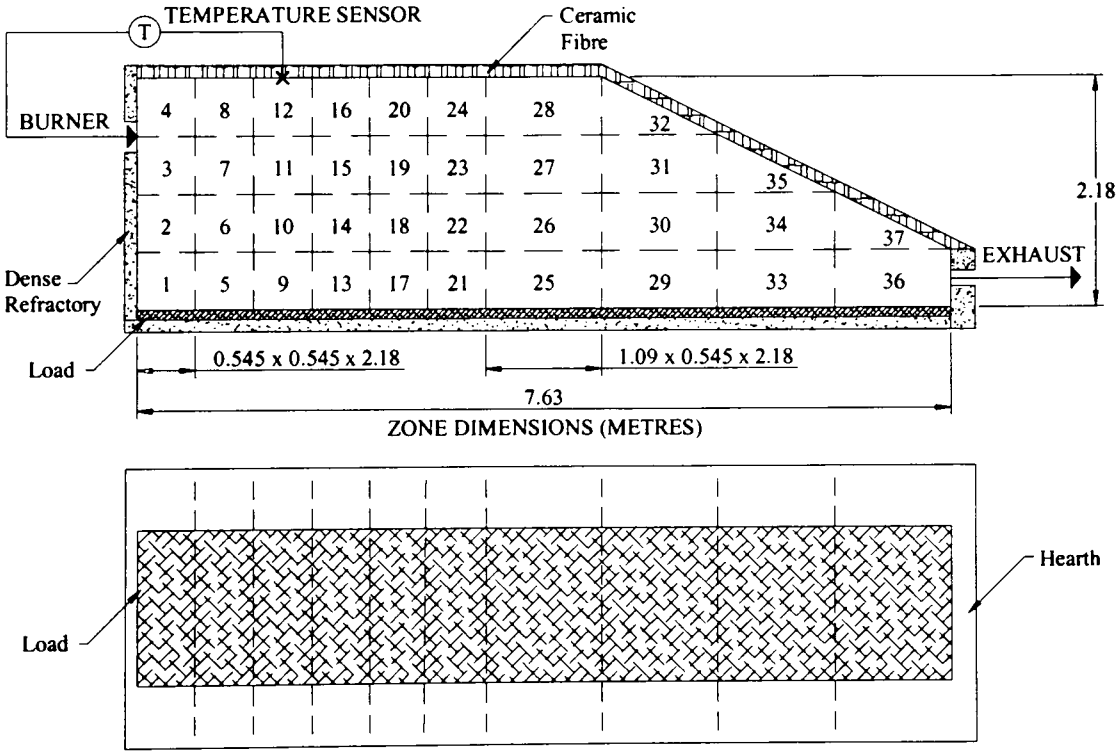

Figure 7.1 Zoning of the Steel Reheating Furnace

The necessary total exchange areas between every pair of zones were calculated by means of a Monte Carlo technique using a minimum of 6000 rays per unit surface area which was considerably in excess of the ray density employed successfully by Tucker and Ward [1]. All surfaces were assumed to be grey and diffuse for radiation purposes and the emissivities of the load, ceramic fibre lining and dense refractory were specified

as 0.7, 0.5 and 0.6 respectively. In general the roof was considered to be of ceramic fibre whilst the walls and hearth were constructed of dense refractory although alternative refractory linings were investigated. A constant value of 25W/m^{2}K was specified for the convective heat transfer coefficient at each of the surface zones since a more accurate representation was not necessary because of the relatively minor contribution of convection (usually <5%) to the overall heat transfer. The non-grey emission and absorption characteristics of the combustion products were represented by an imaginary mixture of 1 clear and 2 grey gaseous components. Heat release by combustion was confined to the volume zones immediately adjacent to the burners as this closely simulated the combustion characteristics of the nozzle mix burners.

Conduction into the refractories and load was assumed to be one-dimensional and the number of nodes used in the finite-difference models for the load, roof and walls were 11, 8 and 7 respectively. A fully implicit finite-difference technique [2] was employed with a time step of 10 seconds to ensure stability in the calculations particularly at the hot face of the ceramic fibre linings where rapid changes in surface temperature can occur. The temperature sensitive thermal properties of the mild steel, ceramic fibre and dense refractory were represented by appropriate polynomials [3], see Appendix A. Heat transfer across the interface between the underside of the steel and the refractory hearth was simulated using a thermal contact resistance between the surfaces of 0.002m^{2}K/W [4].

The so-called set point temperature was maintained at a specified value ranging from 1300 to 1380°C during the simulations. The refractory roof temperature adjacent to gas zone 12, see Figure 7.1, was normally employed as this control value although in some cases the roof zones adjacent to gas zones 8 and 16 were used. The natural gas input to the burners was varied over a 5:1 turndown range in response to deviations in roof temperature from the stipulated set point using a simple linear proportional control system over an error band of ±7.5°C. This was considered to provide a reasonable representation of the method of control employed to control the thermal input on this type of furnace. Throughout the simulations the air/fuel ratio was usually maintained constant with an excess air level of 5% although other values were also investigated as part of the study. The burners were usually supplied with air at cold, ambient temperature although the effect of preheating the combustion air was also simulated. In

this latter case a heat exchanger with an effectiveness of 30% was employed to preheat the air using the hot exhaust from the furnace.

The mathematical model was initially used to predict heating times, fuel consumptions and load temperatures in this gas-fired furnace when starting-up from cold. In addition, after the initial start-up a typical transient operating period of 8 hours was simulated in which the passage of hot steel bars through the furnace was allowed for by transferring the load through the system zone-by-zone. The movement of the load occurred at discrete time intervals which depended on the rate of discharge of the bars and was arranged to be a multiple of the time step in the transient zone model.

7.3 Simulation of an Initial Start-Up from Cold

Metal reheating furnaces are known to consume large amounts of energy of which only a small fraction is transferred to the load with the remaining lost through various sources. Furnace efficiency and fuel consumption can thus be improved by reducing these energy losses from the system. In addition, operating the installation so that the rate of heat transfer to the load is enhanced may also increase the furnace output and efficiency. In order to understand the effect that operating conditions can have on the performance of the reheating furnace described above, a number of applications were studied to show how these models can be employed for furnace design and control purposes.

7.3.1 The Effect of Burner Geometry

As seen in the previous chapter variation of the ***burner nozzle diameter*** and hence the momentum of the natural gas burners can affect the recirculation pattern of the combustion products inside the furnace and hence the heat distribution to the load. Therefore, the 37 gas zone model was employed to assess the influence of this parameter on the thermal behaviour of the reheating furnace. The flow patterns obtained for the four different burner diameters considered in this study (0.42m, 0.28m, 0.19m and 0.14m) firing horizontally into the chamber were presented in Figure 6.3 in terms of the relative mass flows across the zone boundaries.

The use of different burners diameters was found previously to generate different flow behaviour so that the temperature distribution within the furnace can also be affected. Figure 7.2 and Table D.4 (see Appendix D) show the predicted initial start-up times and corresponding fuel consumptions and temperature gradients in the load.

For the largest burner diameter the recirculation region extended along the furnace so that cooler combustion products from the charge end of the furnace were brought towards the bottom zones near the load at the discharge end. This led to a decrease in the temperatures of these zones so that longer times were required for the load to reach its final discharge condition of 1250°C. In addition, the flow near the roof resulted in relatively high refractory temperatures so that burner modulation occurred over a significant proportion of the start-up period and this also contributed to the relatively long heating time. These effects become particular important as the set point value is reduced where an increase of 63% in heating time is predicted for the lowest set point comparing with that obtained at 1380°C.

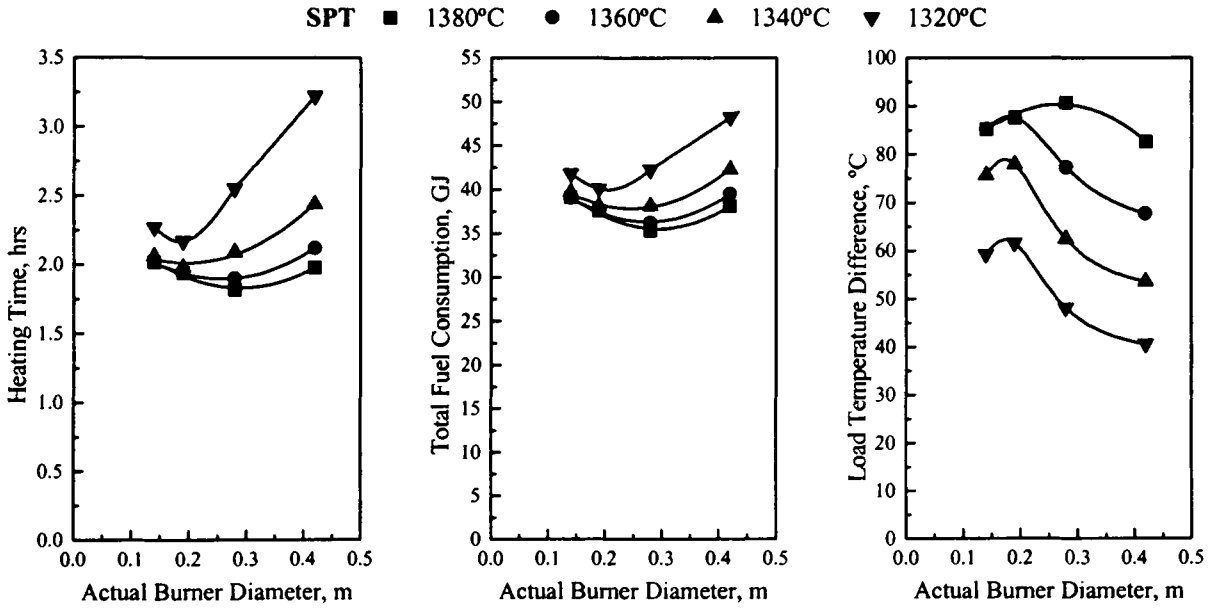

Figure 7.2 Variation of the Furnace Thermal Behaviour with Burner Diameter

When the burner diameter was reduced to 0.28m the degree of recirculation increased and the recirculation vortex in the lower half of the furnace was more tightly confined so that the temperature of these lower gas zones were generally increased with a consequent enhancement in radiative transfer to the load. At the top half of the furnace the gas temperatures close to the control sensor were kept reasonably high despite recirculation of relatively cold combustion products along the roof back towards the burners. At the highest set point temperature modulation of the burners did not occur so that the furnace operated at full thermal input over virtually the whole of the heating period. This led to a shorter initial start-up period in this case. However, as the set point

is reduced the control system operates to maintain the furnace temperature at a specific condition resulting in an increase in the time required to initially heat up the load. This effect is particularly pronounced at lower set points where an increase of 40% in time is predicted when varying the set point from 1380 to 1320°C.

Further reductions in burner diameter, which were seen previously to increase the degree of recirculation in the lower half of the furnace, resulted in dilution of the high peak temperatures in the zones close to the burners. Thus, the overall "flame" temperature was reduced with a consequent reduction in heat transfer to the load and hence longer heating times. Slightly larger reductions are achieved with a burner diameter of 0.14m where a higher degree of recirculation is obtained when compared with that of the 0.19m burner diameter. In both cases relatively cold combustion products recirculate from downstream back towards the burners resulting in lower temperatures in these zones so that modulation of the burner occurs only at lower set point temperatures. The resultant increase in time is, however, not as marked as with the two largest burner diameters so for these cases only a 12% increase time is predicted when reducing the set point from 1380°C to 1320°C.

The above effects are illustrated in Figure 7.3 which plots the temperature variation for the "flame" region, control sensor roof surface and gas zone 1 during the heating period with a set point temperature of 1380°C.

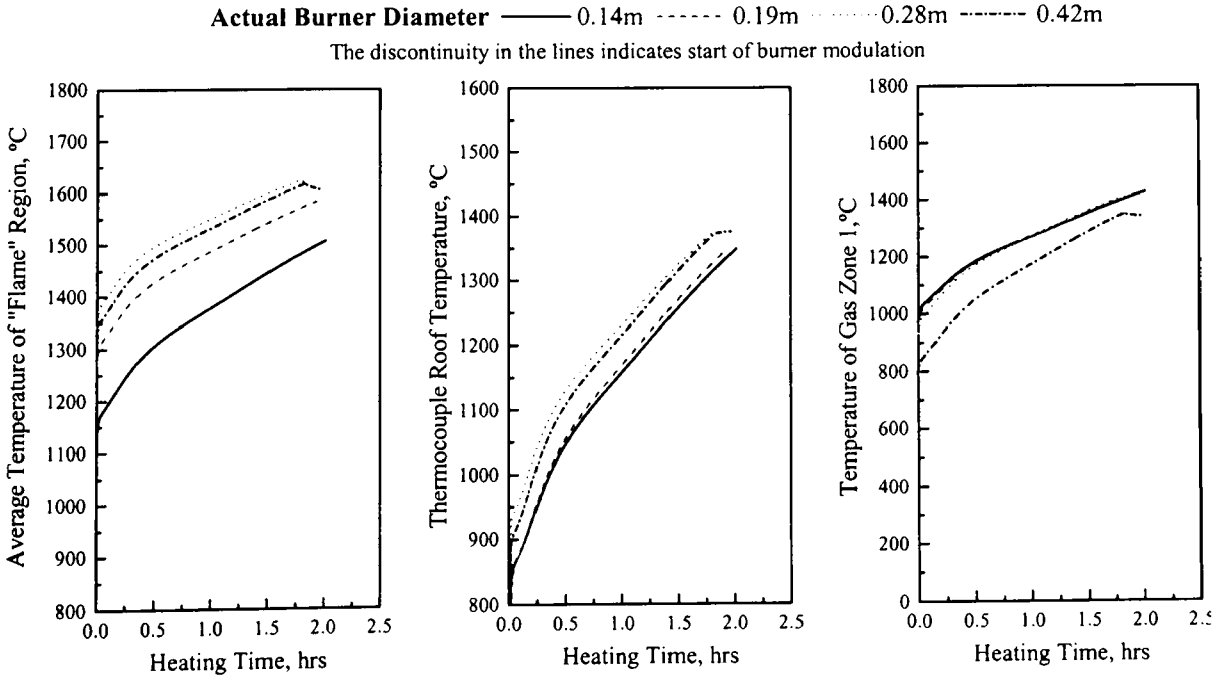

Figure 7.3 Temperature-Time Variation for the Different Burner Diameters at a Control Set Point Temperature of 1380°C

The "flame" region was assumed to be contained in gas zones 3, 4, 7 and 8 and only the average temperature from these zones is presented. From the graphs it is clear the cooling effect produced by the recirculation of combustion products from cooler downstream zones on the thermocouple roof surface when small diameters were employed. Under these conditions there was no need for the control system to modulate the burners. It is also visible in the reduction in flame temperature for the small burners in particular the 0.14m burner diameter which led to a reduction in heat transfer to the load and hence longer heating periods.

In contrast, with the larger diameter burners high temperatures ensue at the roof thermocouple surface particularly with a burner diameter of 0.28m. However, with this burner diameter a much more rapid rise in the load upper surface temperature is predicted while the increase in temperature for the "sensor zone" is much smaller so that modulation of the burner did not occur. A similar behaviour is predicted for the largest burner diameter, however the lower temperature registered near the load at discharge means more time was required for the load to reach a top surface of 1250°C and hence modulation of the burner occurred at the end of the heating period as can be seen in the graphs. Further reductions in the set point temperature produce similar trends but modulation occurs over a much greater proportion of the heating period particular in those cases where higher temperatures are registered near the control sensor such as with the larger burner diameters.

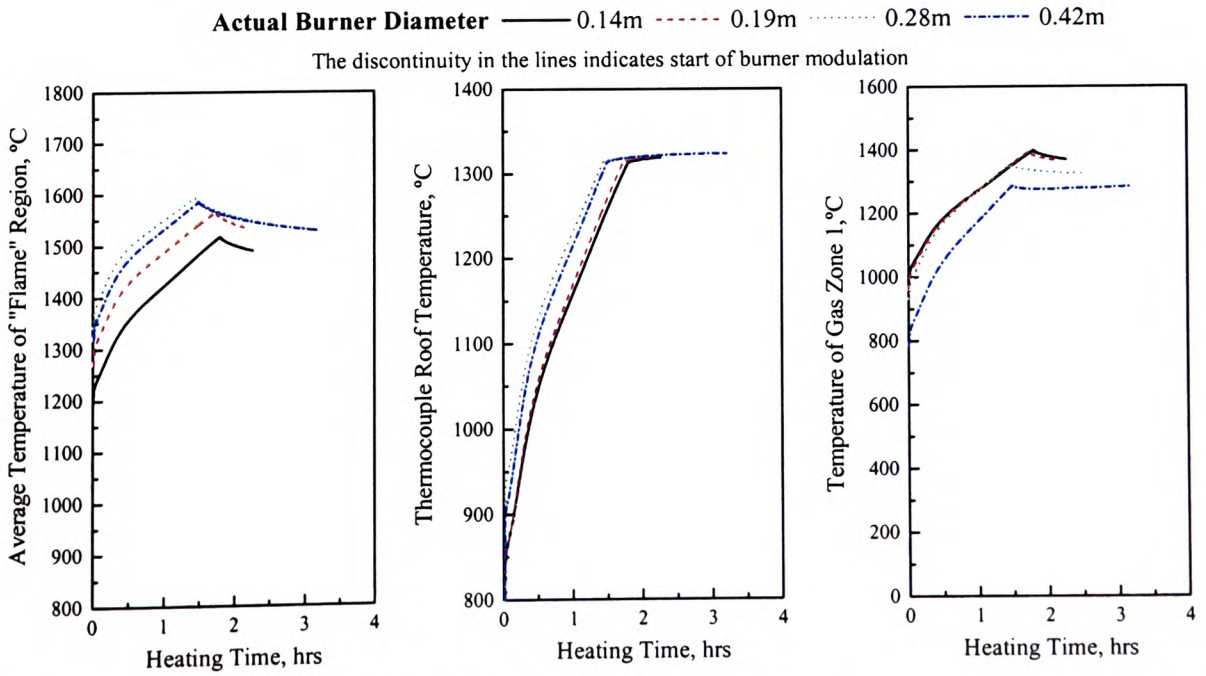

Figure 7.4 Temperature-Time Variation for the Different Burner Diameters at a Control Set Point Temperature of 1320°C

Thus, burners operate at lower thermal inputs over a substantial part of the process and this leads to longer heating cycles as can be seen in Figure 7.4 which presents temperature-time histories for the "flame" region, thermocouple roof surface and gas zone 1 for a set point of 1320°C.

The resultant profiles of heat flux to the load during the start-up period is plotted in Figure 7.5 for the two extreme set point conditions of 1380 and 1320°C clearly showing the behaviour produced by the different burner diameters.

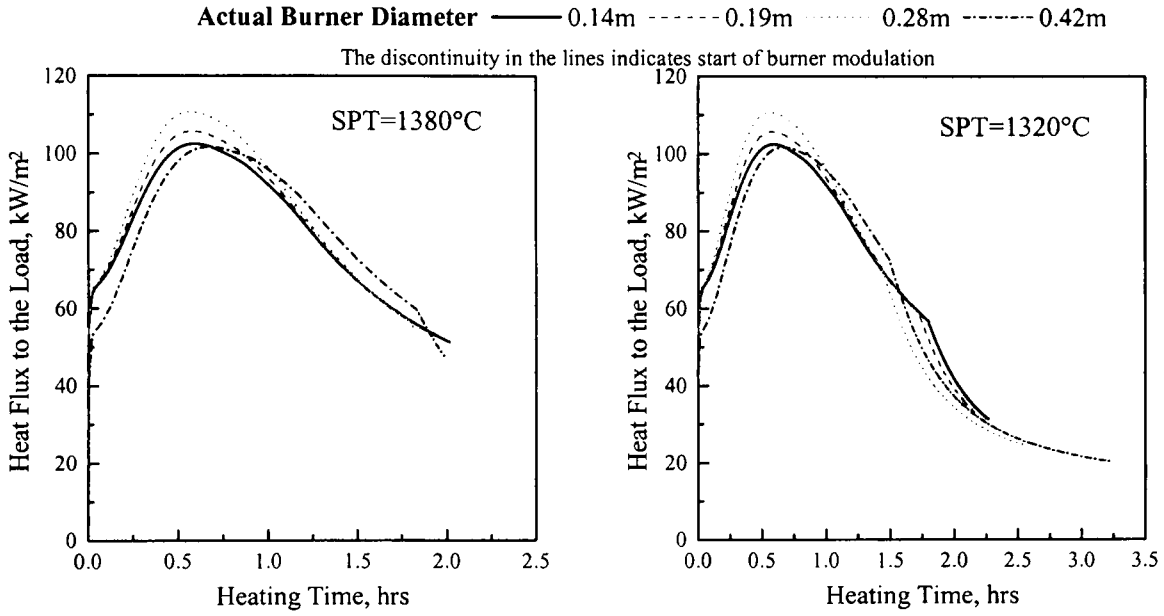

Figure 7.5 The Effect of Burner Diameter on the Load Heat Flux Profile During Start-Up for a Set Point Temperature of 1380°C and 1320°C

In all cases the variations in fuel consumption follow the same trends as the initial heating time curves but the effects are less marked since they are also a function of the burner modulation during the heating process. Greater load temperature differences are, as expected, found for the smaller diameters except at a set point of 1380°C where the rapid increase in temperature of the load at discharge in comparison with that of the sensor roof surface resulted in shorter heating times and hence greater temperature gradients for the load when a 0.28m burner diameter is employed. As expected the load temperature differences were generally reduced as the set point was reduced due to the increase in heating time. The reductions in temperature difference are more marked at larger burner diameters due to the correspondingly longer heating times in this case. Thus, at a set point of 1320°C the difference in temperature for the largest diameter is approximately 51% lower than that at the highest set point whereas at the smallest diameter this difference is about 31%. Overall the predictions indicate that the burner

diameter and hence momentum can have a very marked effect on the start-up performance.

The ***position and inclination*** of the burners were found previously to affect the flow behaviour of the combustion products within the furnace chamber so they can also have an important influence on the performance of the reheating furnace. The resultant relative inter-zone flow patterns for these conditions when employing a burner diameter of 0.19m were shown in Figure 6.4. As shown in Figure 7.6 and Table D.5, the duration of the start-up period depends on the set point temperature and the inclination and position of the burners.

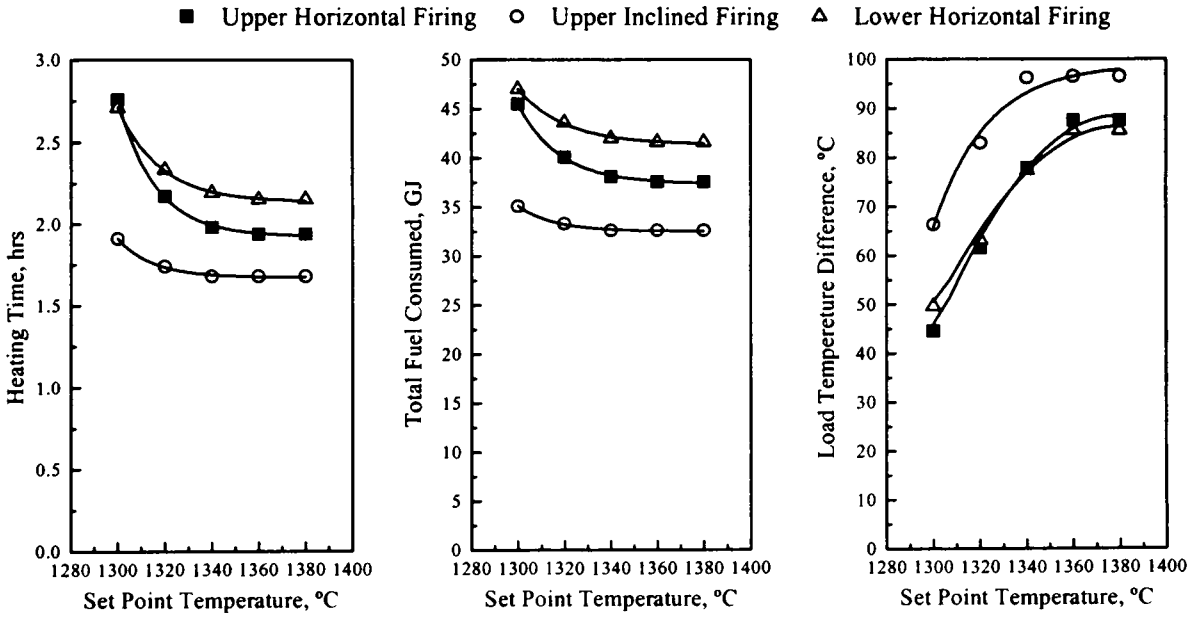

Figure 7.6 Effect of Burner Firing Position on the Furnace Thermal Performance

The flows from the upper horizontal burners result in relatively hot combustion products near the roof and cooler recirculated gases near the load zones at the discharge end of the chamber. Thus relatively high rates of heat transfer and correspondingly high temperatures were predicted for the roof zones near the burners. The control system then modulates the burners so that they operate at reduced thermal inputs which in turn results in even lower combustion product temperatures close to the load at the discharge end of the system. These effects are somewhat exacerbated at lower set point temperatures, see Figure 7.6, so that the duration of the initial heating period is 2.76 hours with a set point temperature of 1300°C compared with that of 1.94 hours at 1380°C.

Burner inclination results in substantially different flow patterns, as seen in the previous chapter, with hot combustion products near the load and relatively cool recirculated gases near the roof. The resultant relatively high rates of heat transfer to the steel bars from the adjacent hot combustion products result in significantly shorter heating times. Moreover, the length of the initial start-up period is almost independent of the set point temperature which indicates that the roof temperature barely achieves he set point except at the lowest value of 1300°C where modulation of the burners only just occurs. Thus, the burners operated at full thermal input over most of the heating period and this again contributes to the reduction in heating times so that at the lowest set point a reduction in the start-up period of approximately 30% was predicted when compared with the upper horizontal burner case.

Positioning the burners in the lower half of the furnace closer to the load at the discharge end has resulted in higher heating times than the previous cases and this is a consequence of the relatively cold flow of combustion products over the steel bars at discharge. This induces a drop in the temperature of these zones and less heat is transferred to the load so that it requires more time for the load to achieve the discharge condition. The difference in predicted heating times for the two positions considered is, however, reduced at lower set point values since with the upper burner position hotter gas temperatures are predicted for the zones near the roof close to the burners and therefore modulation of the burners occurs much earlier in the simulation.

Longer heating times during start-up result in higher fuel consumptions, see Figure 7.6 although the savings due to the installation of inclined burners are slightly less marked than the corresponding reductions in heating time. Thus, for the inclined burners the predicted saving is about 23% at a set point of 1300°C since the upper horizontal burners operate with reduced thermal input over part of the heating process due to modulation by the control system.

As expected, the inclined burners result in greater temperature gradients at any particular set point while the other cases predict somewhat lower temperature differences. Although displacement of the burner to the lower half of the furnace results in slightly longer heating times, it takes more time for the control system to operate in this case due to the relatively cool temperatures of the gas zones near the control sensor. In contrast, the use of upper horizontal burners results in hotter gas zones in this region so that the burners modulate much earlier in the heating process and consequently the

rate of heat transfer to the load is reduced. In particularly, at the lowest set point where the predicted heating times are nearly identical, it is clear that the control system can also have an effect. From these results it can be seen that the thermal furnace behaviour is dependent on the burner geometry and location. For example, to produce bars with a top-to-bottom difference of 60°C, the use of inclined burners results in heating times of approximately 1.8hrs compared with 2.3hrs for the other two burner conditions and corresponding fuel savings of up to 20%.

Variation of the maximum ***thermal input*** to the burners i.e. their thermal rating was also simulated in that four different values were tried, namely 4.6, 5, 5.4 and 5.8MW, in order to assess the effect on the furnace behaviour. Only the upper burners firing horizontally into the chamber were simulated. Figure 7.7 and Table D.6 shows an increase in the initial start-up heating period as the burner thermal rating is decreased but any variations are reduced at the lower control values. This is because at these lower control values burner modulation occurs and therefore the furnace operates at lower thermal rates over substantial part of the heating cycle. The modulation effect is, however, more marked at high thermal inputs since under these conditions higher gas temperatures are predicted for zones close to the control sensor. Thus, at a set point temperature of 1380°C, a reduction in the maximum burner thermal input from 5.8MW to 4.6MW results in a difference in start-up time of about 23% whereas at 1300°C the difference is of only 13%.

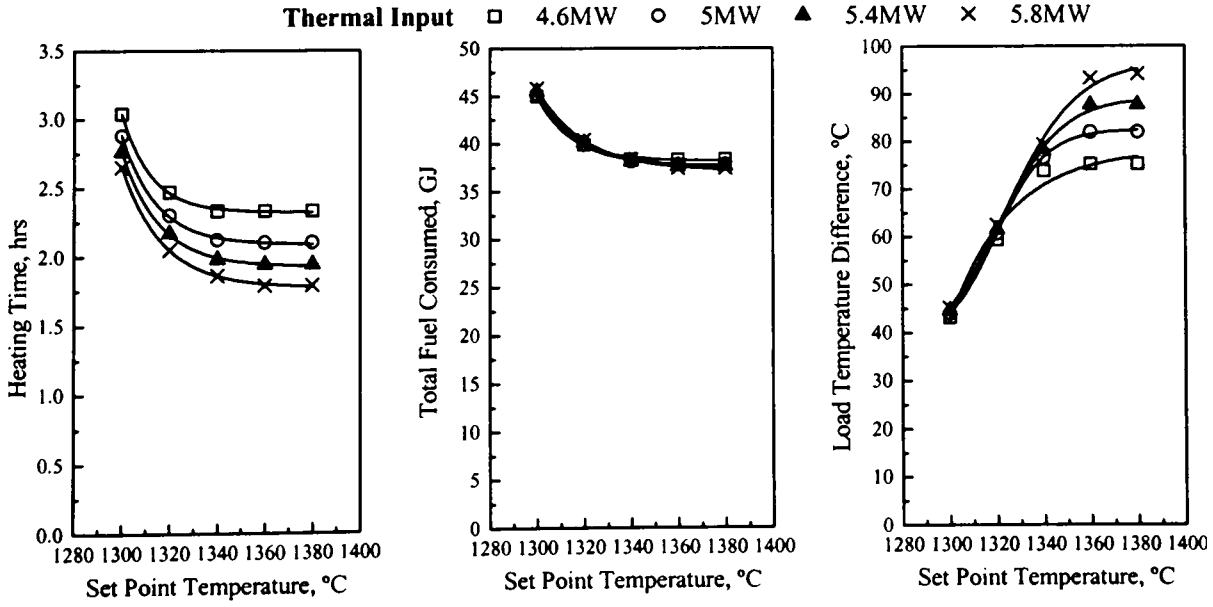

Figure 7.7 Effect of Burner Thermal Input on the Furnace Thermal Performance

Unlike the start-up times, the variations in fuel consumption between the four thermal inputs investigated are insignificant under all set point conditions. For the reheating furnace the pattern of energy usage is a function of both the heating time and burner input rate so that any change in the maximum thermal input to the burners is reflected in the time required to heat up the load to the discharge condition of 1250°C. This in turn results in similar amounts of fuel being used for the different burner firing rates simulated. The profile of temperature difference in the load shows greater gradients at high set point values as a consequence of the shorter heating times predicted. However, the differentials are substantially reduced at lower set points due to modulation of the burners so that more time is available for conduction heat transfer within the load. The results showed here indicate the importance of representing both the furnace control system and the combustion product flow patterns when simulation the transient operation of the system.

7.3.2 Changes in Furnace Control

Most metal reheating furnaces are controlled by means of a set point thermocouple mounted in the roof. Deviations from this control temperature result in modulation of the thermal input to the burners so that the furnace temperature is maintained at the desired conditions. Control temperatures are varied according to the type of load, production rate and heating requirements of the process. Figure 7.6 has already shown the effect of varying the set point temperature on the overall furnace performance. Consequently, results are now presented on the influence of changing the position of the control. Two burner firing arrangements were considered namely horizontal and inclined burners both positioned in the top half of the furnace. Simulations were undertaken with the control sensor mounted in turn in the 2^{nd}, 3^{rd} and 4^{th} roof zones downstream from the burner end of the furnace. Data is presented on the resultant fuel consumptions and the times required for the initial discharge of the load as well as the temperature differentials in the load at discharge.

As Figure 7.8 and Table D.7 indicate the predicted initial start-up heating times for the horizontal firing arrangement depend significantly on the control sensor position. At higher set point temperatures there is little effect on the duration of the initial start-up since all of these roof zones barely achieve the control temperature under these conditions. Relatively little modulation of the burners is, therefore, necessary and the thermal input to the system is virtually independent of the sensor position. Different

behaviour was predicted at the lower set points and the initial heating period was lengthened when the control sensor was displaced along the roof towards the burners.

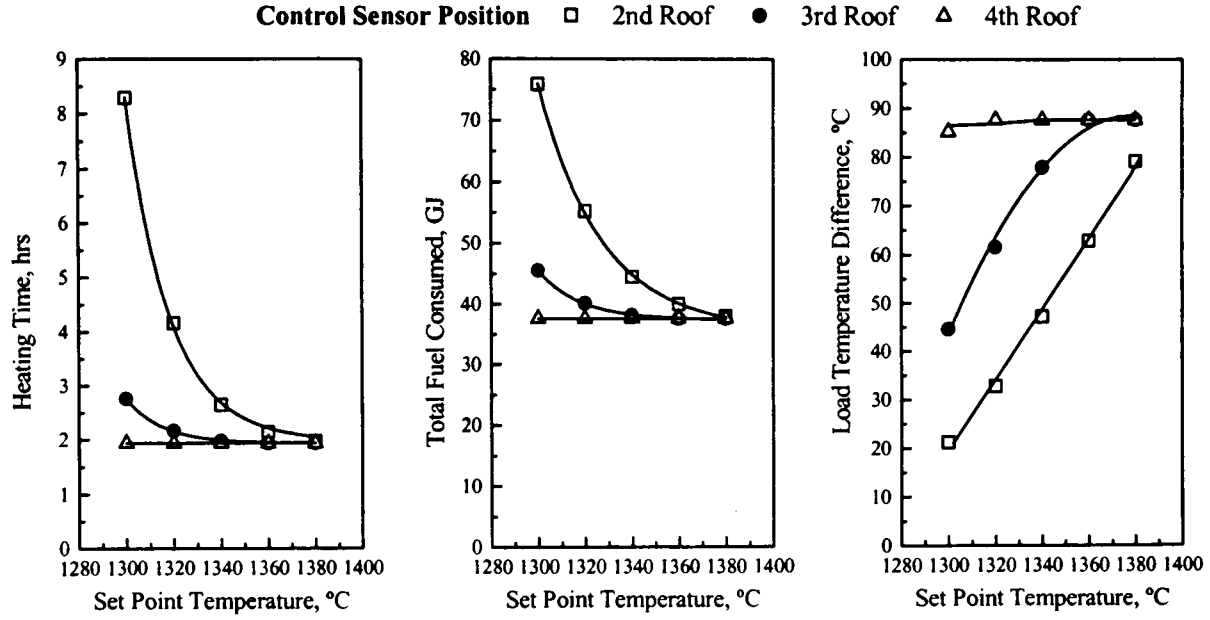

Figure 7.8 Effect of Set Point Position on the Furnace Thermal Performance for the Horizontal Burners

This effect is due to the higher temperatures registered by the control thermocouple causing modulation of the thermal input over a significant part of the heating period. The burner modulation effect was intensified when the control set point was placed in the 2nd roof zone since this surface was closer to the burners and therefore adjacent to a hotter gas zone.

Movement of the control sensor also influenced the start-up fuel consumption and temperature gradients within the load. The fuel consumptions depend on both the heating time and the degree of burner modulation so that the differences due to repositioning of the control sensor are less pronounced than the corresponding variation in heating time. Greater temperature gradients are, as expected, found when the control thermocouple was placed further away from the burners. Furnace operators aim to discharge the steel bars with both the surface temperature and the top-to-bottom temperature difference meeting specified values. The simulations indicate that the set point which would be necessary to meet a particular specification depends upon the position of the control sensor. As an example, a set point temperature of approximately 1340°C would be required to initially produce bars with a surface temperature of

1250°C and a temperature difference of 50°C with the sensor in roof 2 whilst the corresponding control value is about 1310°C with the sensor in roof zone 3. To achieve these conditions when the control sensor is placed in roof zone 4, a much lower set point would be required since for the range of set points investigated the resultant temperature differentials always exceeded 80°C.

The use of inclined burners produces results quite different from the above case. As illustrated in Figure 7.9 and Table D.8, the variations of start-up, fuel consumption and temperature gradients in the load are substantially less marked than the ones obtained with the horizontal firing.

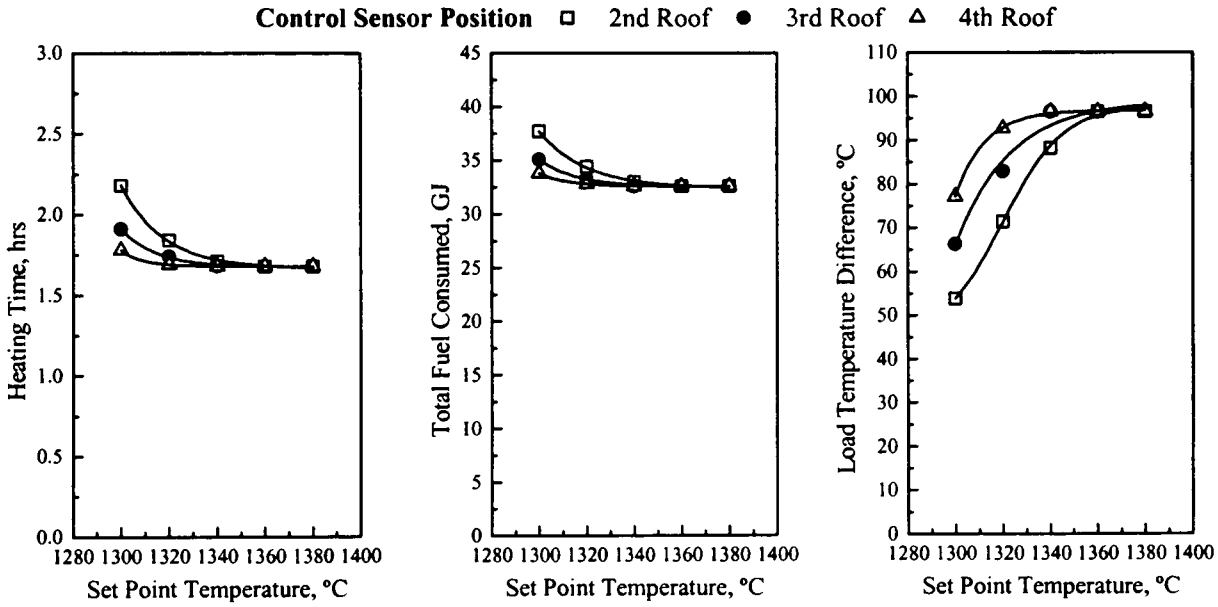

Figure 7.9 Effect of Set Point Position on the Furnace Thermal Performance for the Inclined Burners

The inclined burners always result in shorter heating up periods. Thus, for example, when the control set point is placed in the "2nd roof" changing from a horizontal to an inclined burner configuration results in a reduction of 15% in start-up time at the highest set point value whilst at the lowest value a reduction of 74% is predicted. This trend is a consequence of the high temperatures registered close to the load at discharge in the inclined simulation so that higher rates of heat transfer ensue to the load and this leads to shorter start-up times. Furthermore, recirculation of cool combustion products near the roof induces a drop in temperature of the gas zones close to the temperature sensor so that the control system operates at full thermal rating for most of the heating period. At lower set point temperatures there is a slight increase in the initial time as the

sensor is displaced towards the burners due to proximity to a hotter gas zone. This leads to a more rapid heating of the control roof with consequent early modulation of the thermal input. Consequently, reducing the set point value from 1380 to 1300°C results in an increase in the initial heating time of 30% when the control sensor is place in the 2nd roof and hence closer to the burners.

The longer heating times predicted as the sensor is placed close to the burners result in higher fuel consumptions. The variations are, however, less pronounced than the corresponding changes in heating times due to burner modulation over part of the heating process so that reducing the set point from 1380 to 1300°C with the control sensor in the 2nd roof results in an increase of 16%. Savings of up to 50% are, however predicted when changing from horizontal to inclined burners so that increases in thermal performance may be possible.

Variation of the temperature within the load shows greater differentials at high set points and these are independent of the sensor position since at those conditions the burners operate at their maximum thermal rating. As the set point temperature is reduced the magnitude of the temperature gradients is also decreased with larger reductions found as the control sensor is moved towards the burners. These reductions are, however, not as noticeable as for the horizontal burners simulation since the corresponding variations in heating times are small. It is clear that the complex interaction between the hot combustion products and the set point control sensor can markedly affect the transient performance of this type of furnace. As an example, to discharge bars with a top-to-bottom temperature difference of 70°C, displacement of the control sensor to the zone closest to the burners (2nd roof) requires a higher control set point although the fuel consumptions are virtually independent of the position of the sensor.

7.3.3 The Effect of Changes to the Furnace Lining

Furnace walls and roofs are usually constructed from refractory materials to reduce the heat losses from the flame and combustion products. In intermittently operated systems these refractory structures are alternatively heated and cooled. As a consequence the thermal energy stored during the heating cycle is lost during the cooling period. The total heat losses from the furnace refractories, therefore, contain the storage thermal energy in the linings as well as the conduction loss through the linings. In many cases storage losses can be larger than conduction losses so that lightweight

materials such as ceramic fibres can be used to reduce the heat storage effect. These materials possess a low thermal capacity and high thermal shock resistance and when used to replace the conventional brick lining can result in shorter warm up and cool down periods for furnaces operating under transient conditions with a consequent reduction in energy requirements.

The effect of employing different lining materials for the furnace structure is shown in Figure 7.10 and Table D.9 for start-up durations, overall gas usage and temperature differences in the load during the initial start-up from cold for the baseline case.

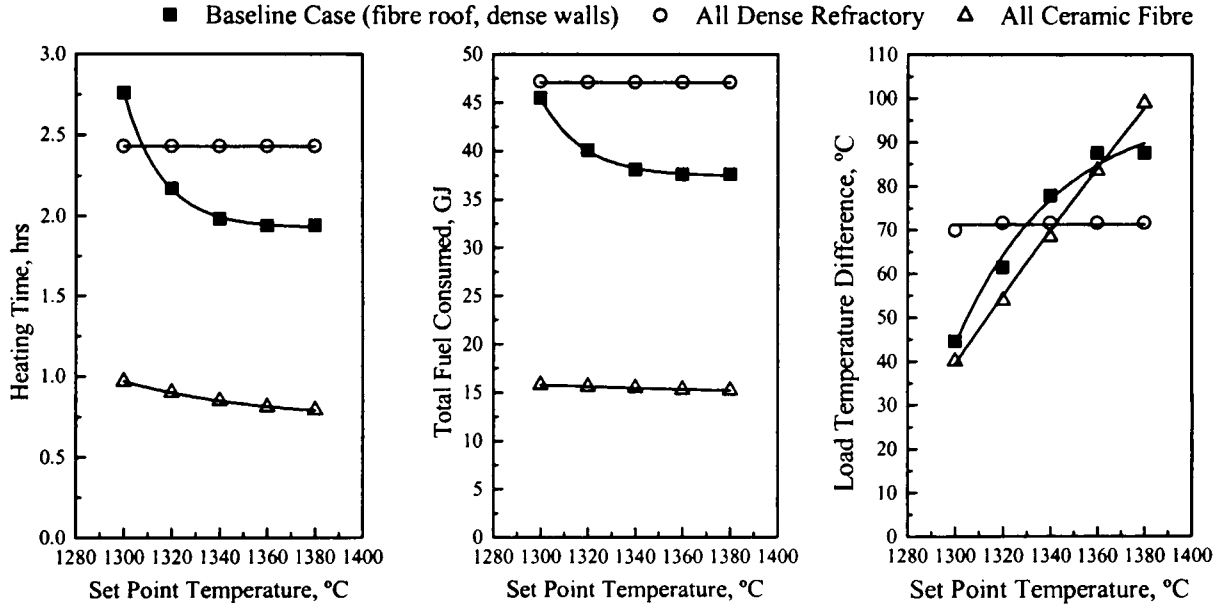

Figure 7.10 The Effect of Different Furnace Linings

As expected at the higher set points the use of a lightweight ceramic fibre resulted in a considerable reduction in the time required to heat the bars to an initial discharge surface temperature of 1250°C. This is due to the more rapid rise in temperatures of the ceramic fibre and hence enhanced radiation interchange between the lightweight roof and the load. These effects are particularly marked in the case where the whole of the walls and roof are constructed from lightweight materials. Under these conditions reductions in the operating cycles of up to 65% are predicted. As the set point temperature is reduced, the predicted heating times for the so-called basecase increases sharply and at the lowest set point longer heating times are predicted when a ceramic fibre roof is used in comparison with a dense refractory lining including the roof. This is probably associated with the ceramic fibre roof achieving the low set point value much

earlier in the transient simulation so that the thermal input is modulated over substantial proportion of the process whereas less reduction in thermal input occurs with the dense refractory roof.

The combined effects of the length of the initial heating period and burner modulation are reflected in the predicted overall natural gas usage during the initial start-up from cold. The installation of a ceramic fibre roof whilst retaining dense refractory walls provides energy savings at all control settings. However, greater benefits are obtained when both walls and roof are lined with low thermal mass materials where the shorter operating periods coupled with the lower heat storage losses have produced significant fuel economies of up to 67% at the lowest set point. Top-to-bottom temperature differences in the load are reduced as the control value is reduced except for the case of a furnace lined with dense refractory where a constant gradient is found at all control values tested. This is because under these conditions no modulation of the burners occurs so that they operate at their maximum thermal input throughout the whole heating period. On the contrary, results for the ceramic fibre walls and roof simulation show the control system operates at all set point values investigated so that as this control value is reduced a sharp decrease in temperature gradients is found. The greater temperatures achieved at the hot face of the linings result in an early modulation of the burners so that they operate at reduced fuel inputs for most of the start-up time. However due to the rapid rise in the temperatures of the lining surfaces, re-radiation from the surrounding walls to the load becomes important and therefore higher rates of heat transfer to the load are achieved.

As expected similar but less marked trends are obtained with the inclined burners employing different lining constructions, see Figure 7.11 and Table D.10. Shorter heating times and lower fuel consumptions are predicted with load temperature differences generally higher with in the horizontal burners. Again this is a consequence of the flow pattern produced by this burner arrangement where hot combustion products flow over the steel bars at discharge and cooler gases recirculate near the roof close to the burners. This combined effect results in high rates of heat transfer to the load so that the final discharge temperature is reached faster as well as with less modulation of the burners. The modulation effect is particularly noticeable at the lowest set point. Thus with the baseline lining arrangement, a reduction in the set point from 1380 to 1300°C

results in a increase in heating time of 14% for the inclined burners whilst an increase of 42% is predicted for the horizontal burners.

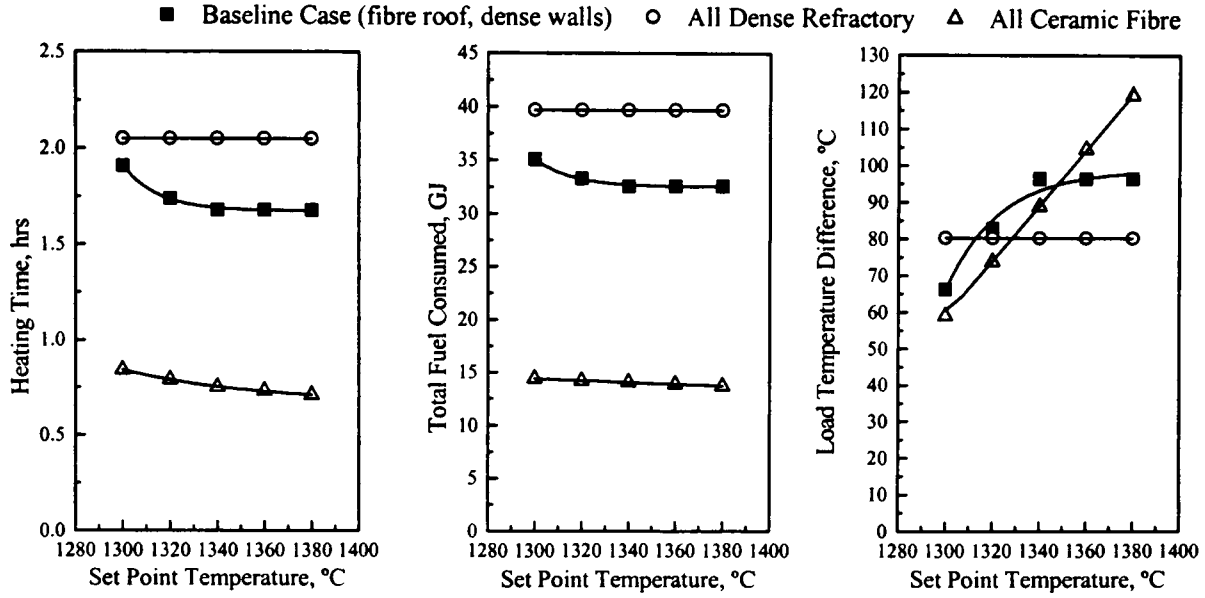

Figure 7.11 Variation of Thermal Performance of Inclined Burners with Set Point Temperature for Different Roof Constructions

7.3.4 The Effect of Combustion Air Preheating

One of the major sources of inefficiency in high temperature systems is the energy lost in the waste gases. Improving energy utilisation in a furnace can, thus, be accomplished by recovering part of the energy contained in the hot combustion gases leaving the system. This is often achieved by installing a suitable heat exchanger for preheating the combustion air and this can lead to considerable energy savings, see Figure 7.12 and Table D.11.

Preheating the combustion air by means of a heat exchanger with an effectiveness of 30% mounted in the exhaust reduces start-up periods by up to 26% and the corresponding fuel consumptions are also reduced. The value of the effectiveness used in the simulations was chosen as typical for a large recuperator mounted in the exhaust. Considerably high rates of heat transfer to the load are obtained since under preheating conditions flame temperatures are also increased. As the control temperature is reduced the heating time required to achieve the final discharge temperature of 1250°C is considerably increased particularly at the lower set point. This is because under these conditions higher temperatures are registered by the control thermocouple causing

modulation of the thermal input so that the burners operate under low firing conditions for a significant proportion of the heating period.

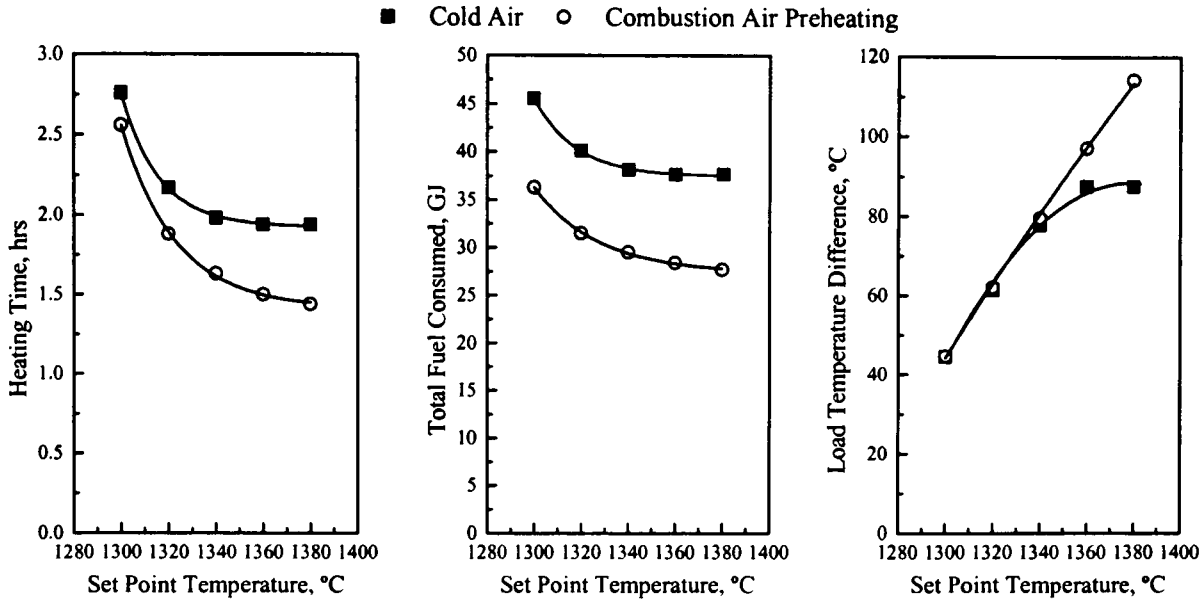

Figure 7.12 The Effect of Combustion Air Preheating on the Furnace Thermal Performance

A closer look at the variation of the temperatures for the "flame" region, sensor roof and gas zone 1 with time for a set point of 1380°C, Figure 7.13, clearly shows that preheating combustion air increases the flame temperature and this consequently enhances the heat transfer to the load and leads to shorter heating times.

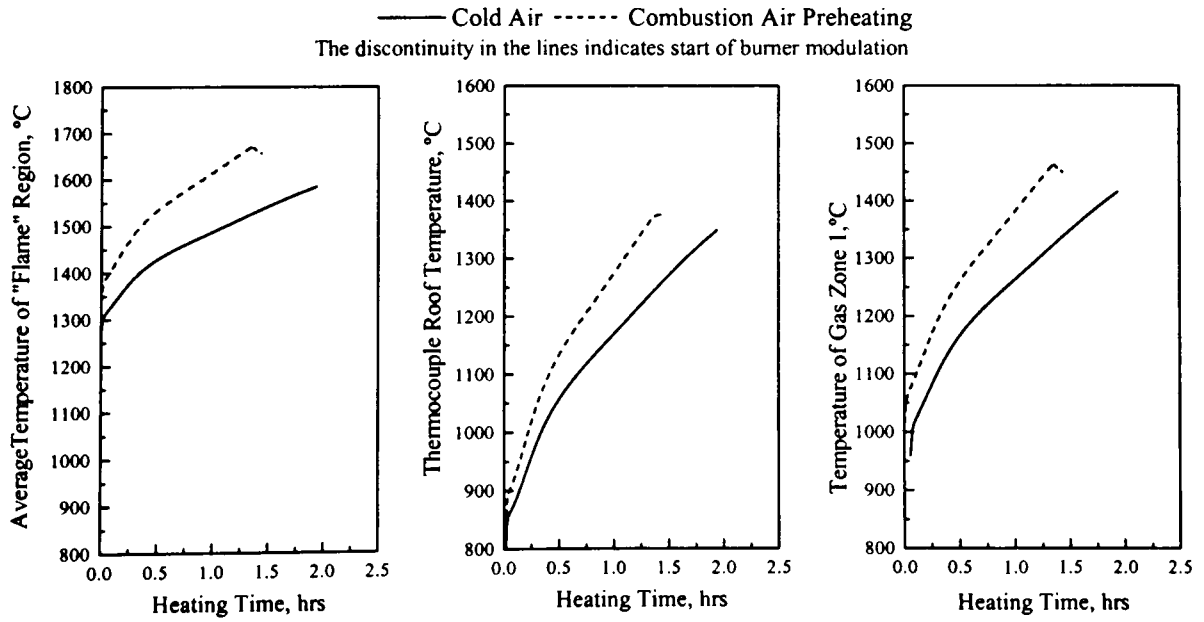

Figure 7.13 The Effect of Combustion Air Preheating on the Furnace Temperature

The enhancement is particularly significant towards the end of the heating cycle since at these conditions the temperature head between the flame and load is larger than with cold air burners. The difference in predicted start-up time between the two simulations is, however, less as the set point is reduced. Thus at a set point of 1300°C, only 7% reduction in the start-up time is predicted when employing preheated air. With lower set point values the control temperature is reached much earlier in time so that modulation of the burners occurs over a large part of the heating process whereas less modulation of the burners occurs with a cold combustion air supply.

The longer heating times at low set point values result in an increase of fuel usage. This variation is, however, less marked than the corresponding increases in heating time due to burner modulation over a substantial part of the process. Thus the difference in predicted natural gas utilisation between the two simulations is 20% at the lowest set point temperature. Again results show a top-to-bottom temperature reduction as the control temperature is reduced. Different temperature differentials are predicted at high set point values but further reductions of this control parameter results in temperature gradients of similar magnitude. Although the use of air preheating leads to shorter heating periods over the range of control temperatures investigated, the enhanced heat transfer in the furnace as a result of the increased flame temperatures means that more heat is available for conduction in the steel bars. This is particularly significant at lower set point temperatures where burner modulation occurs early in the simulation and this prolongs both the load discharge time and the time for minimising temperature gradients. There is thus under preheating conditions a nearly linear decrease of the temperature differentials within the load as the set point is reduced.

7.3.5 The Effect of Changes in Excess Air

It is common practice in most combustion systems to operate burners with air in excess of the theoretical required amount to ensure that combustion of the fuel is complete. However, adding more air than necessary to complete combustion can result in lower flame temperatures and subsequently a drop in the rate of heat transfer. Furthermore, it increases the flue gas losses and reduces non-luminous flame emissivity so that further reductions in radiative heat transfer can occur. To assess the effect of excess air on the efficiency of the gas-fired reheating furnace, four different levels of this parameter were used which tested the range of values typically employed for

burning natural gas. The model simulated excess air conditions of 5, 10, 15 and 20% and the results obtained are presented in Figure 7.14 and Table D.12.

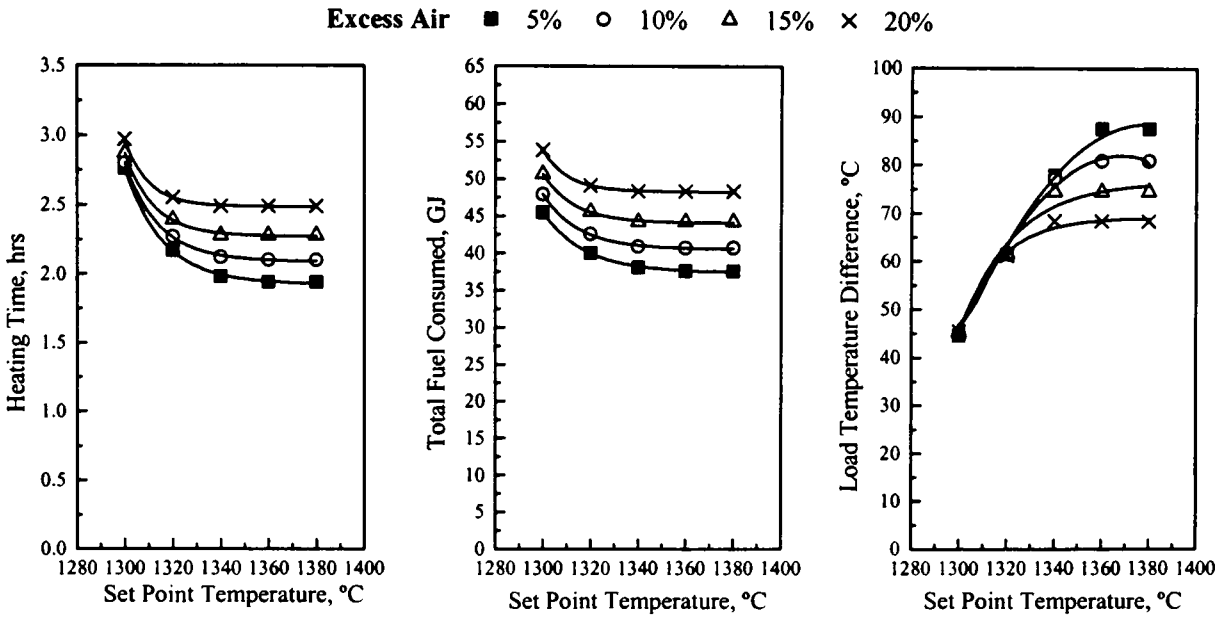

Figure 7.14 Variation of Furnace Thermal Performance with Set Point Temperature for Different Levels of Excess Air

In terms of heating times there are obvious differences between the cases at high set point temperatures but these are gradually reduced as the set point value is lowered. As expected the greater the amount of excess air used, the longer the time required to initially heat up the load surface to 1250°C. This effect is due to the cooling of the "flame" as more excess air is used which in turn results in a reduction of the heat transfer to the load. Figure 7.15 shows the effect of this parameter on the temperature of gas zones 3 and 4 immediately adjacent to the burners and on the rate of heat transfer to the load near the discharge end. The graph on the left is plotted in terms of the mean temperature of gas zones 3, 4, 7 and 8 to provide an estimate of the average temperature in the "flame region". The set point temperature was maintained at 1380°C in all cases. Thus, for example an increase in excess air level from 5 to 20% can result in reductions of about 100°C in flame temperature with consequent drops in the heat transfer to the load up to 12%.

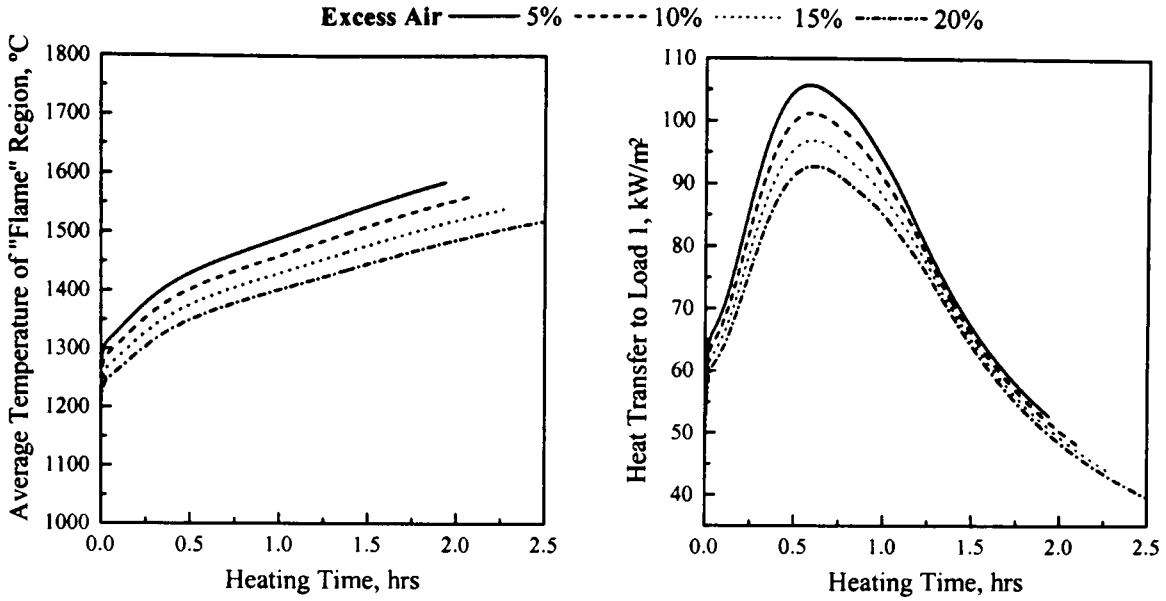

Figure 7.15 Effect of Excess Air on the Furnace Temperature and Heat Transfer to the Load

As the set point is reduced the start-up times are increased since at these lower values modulation of the thermal input occurs so that the burners operate under low-fire conditions for most of the heating period. The modulation effect is particularly intense at low excess air levels since the higher "flame" temperatures predicted under these conditions result in higher temperatures for the control set point roof zone which results in early operation of the control system. In terms of fuel consumption longer heating times means more fuel used. This variation of fuel consumption is, however, not as significant as the corresponding start-up times due to burner modulation over part of the process. For the range of set points investigated it can be seen that temperature gradients decrease as the level of excess air is increased particularly at high control values. Differences of up to 22% are predicted at the highest set point of 1380°C whereas the differences at the lower set point values are much less. This results from the longer heating times predicted when higher levels of excess air are used since more time is available for conducting heat through the load.

7.4 Simulation of Continuous Operation

Following the initial start-up from cold the model was used to simulate a period of constant production so that an overall 8 hour period was covered. The furnace throughput was maintained at 6.5t/hr of steel bars so that the discharge of load and associated movement through the furnace occurred every 280 seconds. The objective was again to study the effect of different operating parameters on the load discharge

temperature and temperature difference as a measure of the quality of the heated product as well as the overall thermal efficiency. The effects of varying the control set point, burner inclination as well as different lining constructions were investigated. In these simulations it was intended to produce steel with a nominal discharge surface temperature of 1250°C and with temperature differences of approximately 50°C as they represent typical output specifications for heating metal bars prior to hot forming.

7.4.1 The Effect of Varying the Control Set Point

Variations of the set point temperature can markedly affect the load upper surface temperature as well as the temperature gradients within the load at discharge, see Figure 7.16, which provides data for the horizontal burner case.

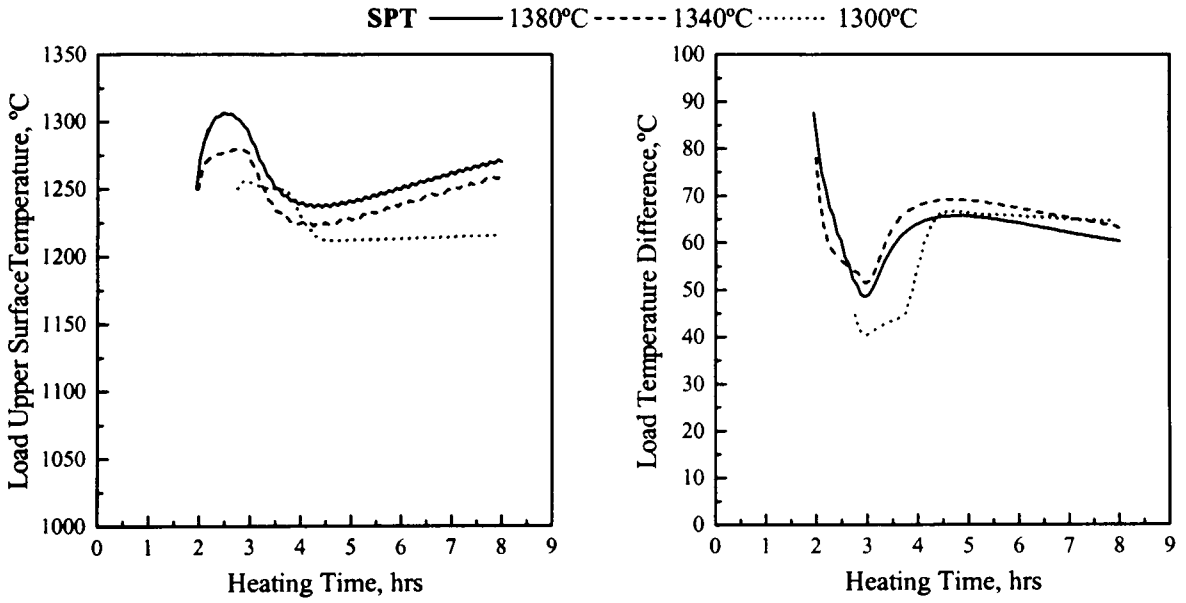

Figure 7.16 Load Upper Surface Temperature and Temperature Difference at Discharge for Different Set Point Temperatures

Initially the surface temperature is increased and this can be attributed to "overheating" of the load near gas zones 5, 9 and 13 during start-up. This also results in lower temperature gradients in the load, as more heat is available for conduction at this stage. The overheating effect is more pronounced at higher set points since under these conditions little modulation of the burners occurs so that they operate at maximum thermal input. The load temperatures then fall as new cooler bars pass through the system with a consequent increase in the load temperature difference. There is a subsequent increase in discharge surface temperatures at higher set points over the

remainder of the overall operating period and this may well be a result of the slow heating up of the refractory walls and hearth within the furnace. The temperature gradient in the load is, however relatively similar for all three cases near the end of the production period. Furnace operators usually aim to discharge the load with both surface temperature and temperature difference meeting specified values. As an example, the simulations indicate that controlling the set point temperature at 1340°C would produce bars with a surface temperature reaching the 1250°C and top-to-bottom temperature differentials of approximately 65°C. It is, however, not clear at this point if the effect of the gradual increase in load surface temperature would continue if production was extended for periods longer than the 8 hour interval investigated.

Table 7.1 presents predicted data for the overall performance of the furnace for the three set point conditions investigated. The overall throughput was reduced from 40t at a set point of 1380°C to 34t at 1300°C due to the longer start-up period at lower set points. A reduction in the total fuel consumption of about 15% was also predicted and this is a consequence of the higher degree of burner modulation at lower control temperatures so that the burners operated at reduced thermal inputs throughout most of the time. However, the overall thermal efficiency is virtually independent of the specified set point. Again the predictions indicate the need to represent the furnace control system for accurate simulation of a pusher-type furnace.

Table 7.1 Predicted Efficiency Data for the Baseline Furnace Arrangement at Different Temperature Controls

SPT (°C)	Overall Efficiency (%)	Cumulative Production of Bars (tonne)	Total Fuel Consumed (GJ)
1380	30	40	158.1
1340	31	39.5	152.8
1300	31	34	134.9

7.4.2 The Effect of Burner Inclination

The complex interaction between the control system and the flow patterns is further illustrated in Figure 7.17, which examines the effect of burner inclination. As would be expected the use of inclined burners produced higher discharge surface temperatures at

both set point temperatures investigated. The trends in discharge temperatures are, however, similar for both burner arrangements.

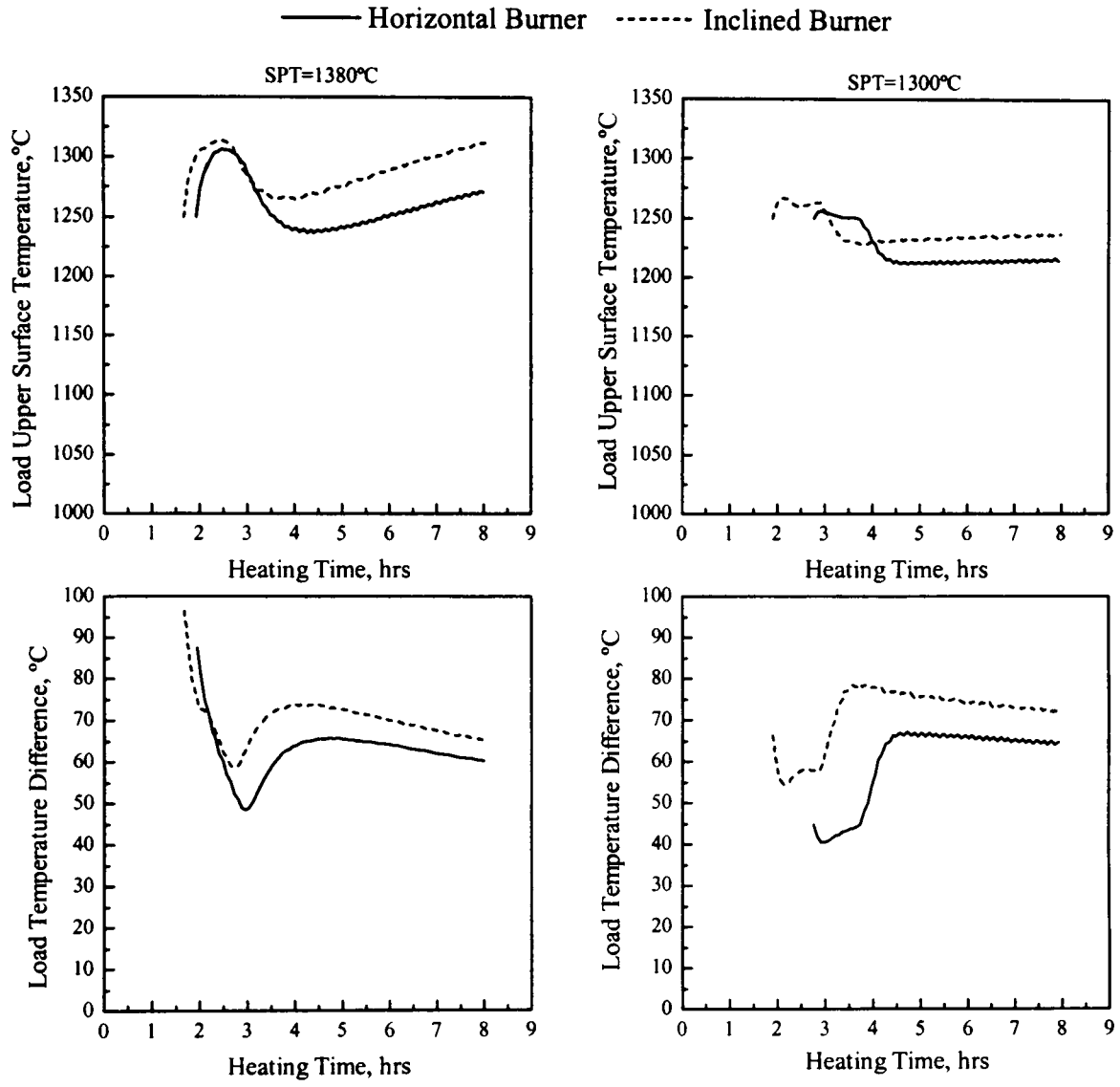

Figure 7.17 Predicted Discharge Load Temperature Profiles for Different Burner Geometries

At the highest set point value the burners operate at maximum thermal input over the whole simulation period in both cases so that the higher discharge temperatures and temperature differences can be attributed to the higher rates of radiative heat transfer from the hotter combustion products in the lower half of the enclosure. Under these conditions the discharge surface temperatures exceeded 1280°C over much of the operating period with corresponding temperature gradients of approximately 70°C when inclined burners were simulated. In practice this "overheating" could lead to problems of excessive oxidation and scaling of the steel surface which together with the high top-

to-bottom temperature differentials could result in poor product quality. In general heating of the load, to temperatures higher than strictly necessary for subsequent processing, results in reduced furnace efficiency. However, there is considerable scope to reduce these high temperatures by increasing the throughput of steel bars or by substantially lowering the control set point temperature, both of which would result in lower specific natural gas consumptions and hence improved energy utilisation.

At lower set points it can be seen that the load "overheating" period immediately after start-up is not as significant as at higher values due to the higher degree of burner modulation in this case. Over the rest of the operating period the upper load surface temperatures are considerably reduced to more uniform values with the inclined burners always predicting slightly higher temperatures. For the inclined burners the load surface temperatures approximate to 1235°C whereas in the horizontal case they are down to around 1215°C. Predicted temperature differences within the load at discharge are slightly higher at lower set points since under these conditions less heat is transferred to the load due to modulation of the burners. Thus, as an example controlling the set point to 1300°C with inclined burners produces steel bars with average top-to-bottom temperature differences of less than 80°C whereas at 1380°C the difference drops to less than 70°C.

Table 7.2 Predicted Efficiency Data for the Incline Burners at Different Temperature Controls

SPT (°C)	Overall Efficiency (%)	Cumulative Production of Bars (tonne)	Total Fuel Consumed (GJ)
1380	32	41.5	157.6
1300	33	40	140.7

The overall efficiency and furnace output at the higher set point case is similar for the both horizontal and inclined burners, see Tables 7.1 and 7.2. However, at the lowest set point temperature inclined burners are predicted to produce 17% more steel than the horizontal burners with slightly improved energy utilisation.

Figure 7.18 shows the effect of higher steel production rates on the load surface temperatures at discharge when employing inclined burners. In all cases the set point was controlled at 1380°C.

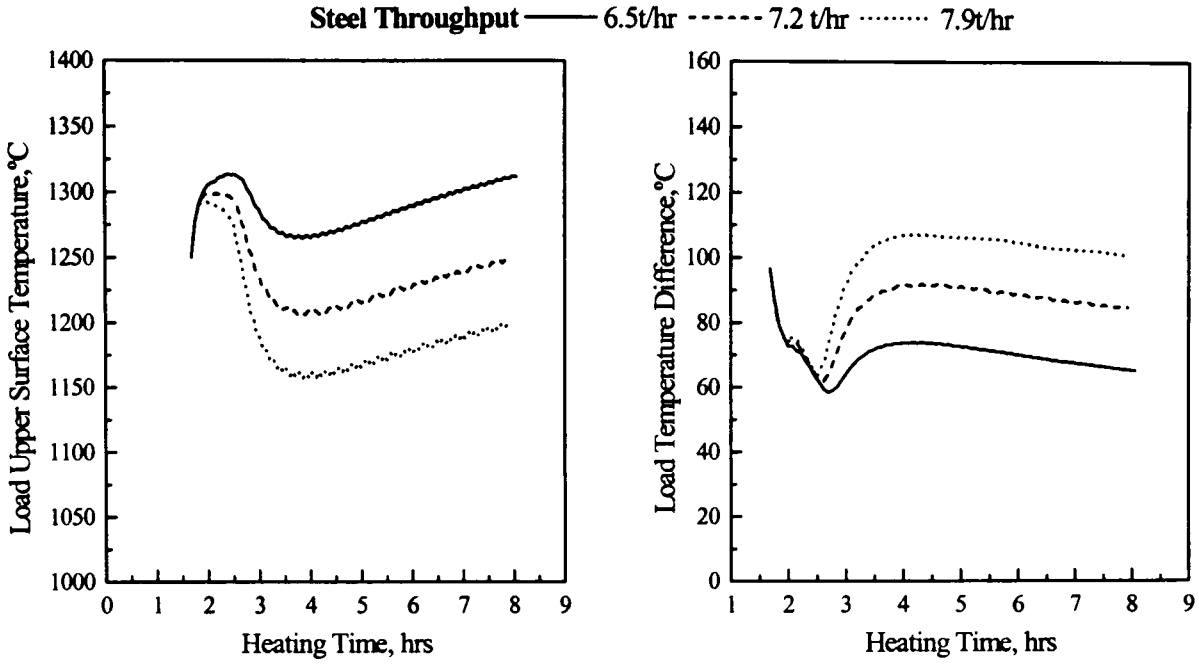

Figure 7.18 The Effect of Production Rate on the Temperature of the Discharged Load for the Inclined Burners

As the production rate is increased the discharge load surface temperatures decrease quite substantially particularly after the initial "overheating" period. Thus, for example, at a throughput of 7.2t/hr the overall reduction in load temperatures is about 6% whereas at 7.9t/hr a 10% reduction is predicted. The initial "overheating" peak also decreases with increasing throughput since the time between pushes is substantially reduced so that the load stores less energy. The increase in production rate leads, however, to higher temperature gradients in the load at discharge so that for a throughput of 7.9t/hr predicted temperature differentials are well over 100°C.

In terms of the overall efficiency it can be seen from Table 7.3 that only slight improvements are obtained at higher throughputs despite the lower load output surface temperatures. Any advantage is also offset by the substantial increase in load temperature difference. The simulations suggested that in order to produce material meeting the initial load surface temperature of 1250°C, the use of inclined burners at a set point of 1300°C would be appropriate, however, the high temperature differentials in the load may cause problems in the subsequent rolling operation.

Table 7.3 Predicted Efficiency Data for the Inclined Burners at Different Production Rates

Production Rate (t/hr)	Cumulative Production of Bars (tonne)	Overall Efficiency (%)	Total Fuel Consumed (GJ)	Final Load Surface Temperature (°C)
6.5	41.5	32	157.7	> 1300
7.2	44.9	33	155	< 1250
7.9	48.9	34	155	<1200

7.4.3 The Effect of Varying the Furnace Lining

The model was also employed to investigate the replacement of the lightweight ceramic fibre roof by a dense refractory construction, see Figure 7.19 which presents the temperature variation of the load surface at discharge for the horizontal burner case. The simulations were also repeated for a case where the roof and walls were lined with lightweight ceramic fibre.

As expected at the higher set point the use of a ceramic fibre lining resulted in substantially higher load temperatures at discharge. This is a consequence of the reduced capacity of these alumino-silicate fibres to store and conduct heat so that a much more rapid rise in the temperature of the lining occurs which enhances the radiation exchange between the load and surrounding surfaces. High surface temperatures can result, as previously seen, in deterioration of the product. In the case where all the lining is constructed from dense refractory the heat up of the lining is more gradual and this considerably reduces the rate of radiative energy transfer from the walls to the load. The dense refractory constructions also take substantially longer to reach thermal equilibrium so that an increase in load surface temperature is still predicted towards the end of the 8 hour simulation whereas for a ceramic fibre lining alone more steady output temperatures are obtained. As the set point is reduced, a substantial decrease in the load output surface temperature is predicted for the case of a ceramic fibre lining. Thus at a set point of 1380°C, a load surface temperature of 1335°C is predicted compared to 1235°C at the lowest set point.

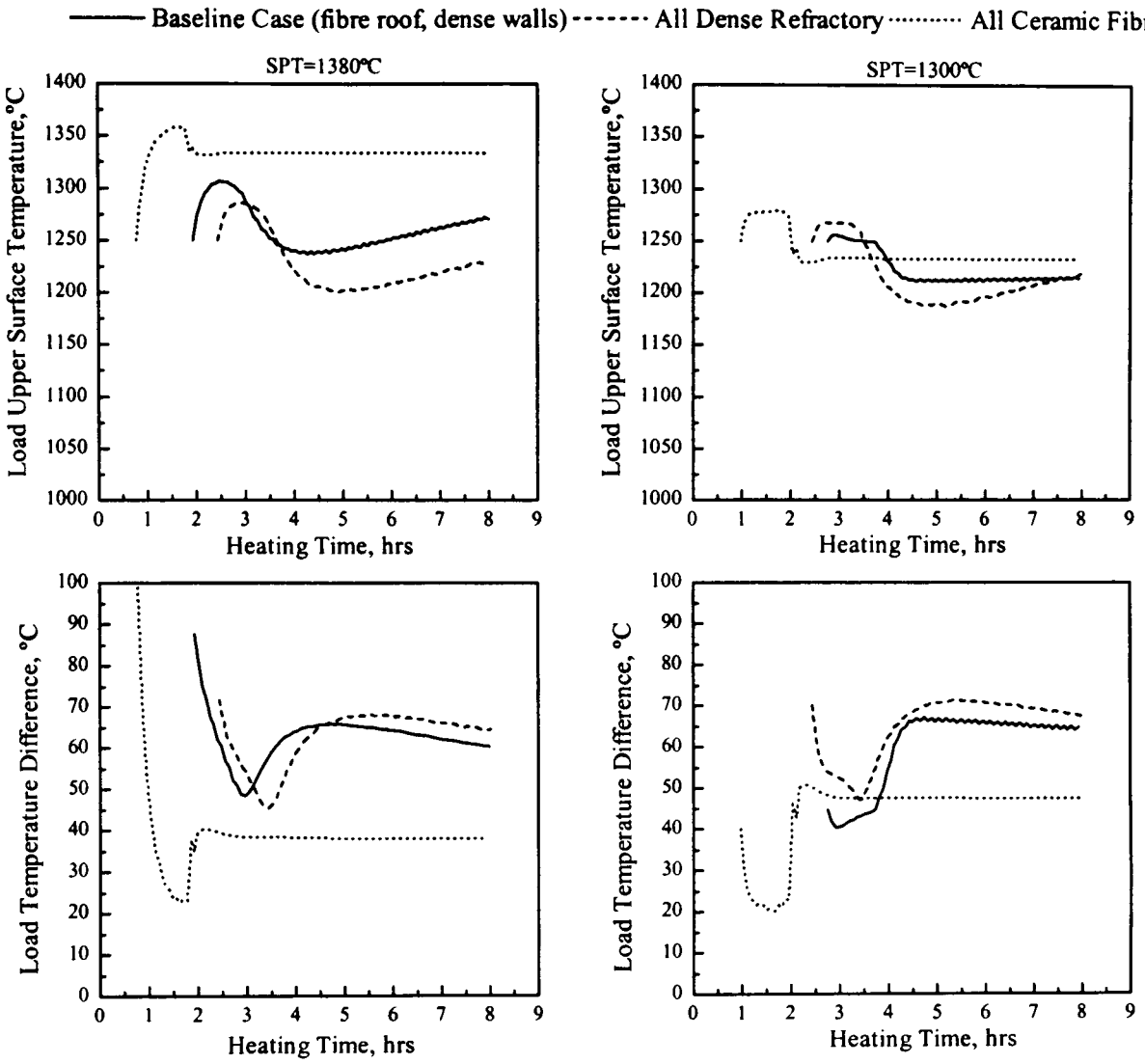

Figure 7.19 Predicted Discharge Load Temperature Profiles for Different Surface Lining Constructions

The use of a dense refractory lining generally results in lower load surface temperatures. The incorporation of a ceramic fibre roof (whilst retaining refractory walls) results in substantial burner modulation during a great deal of the heating process particularly at lower set point temperatures. In contrast with a dense refractory roof, relatively little modulation is required due to a much more gradual heating up of these materials. Consequently, the burners operate at their maximum thermal rating over much longer intervals even at the lower control temperatures. The ceramic fibre linings generally result in improved temperature uniformity at higher set points. As previously discussed, slightly higher temperatures gradients were found at lower set points for most

cases as a result of the effects of burner modulation so that less heat is transferred to the load during each push interval.

The use of an all-lightweight ceramic fibre lining resulted in improved overall efficiency when compared to the other constructions investigated with the dense refractory lining always predicting lower efficiencies, see Table 7.4. In addition, the furnace output is increased by using the lightweight refractory material as a result of the shorter start-up period. Also significantly less fuel is consumed so that energy utilisation is improved with this lining at both set point conditions. The predictions indicate that replacing the baseline furnace lining of dense refractory walls and a ceramic fibre roof by one with all these surfaces constructed with ceramic fibre materials would result in an increase of 18% in the steel production rate at a set point temperature of 1380°C while at 1300°C the increase would be approximately 35%. Corresponding fuel savings are 12% and 16% respectively. The models thus indicate that replacement of the so-called base lining with lightweight ceramic fibre provides energy savings and increased steel output at both set points. However, it is only at the lower control set points that the required load output specifications are met and therefore greater benefits obtained.

Table 7.4 Predicted Efficiency Data for Different Furnace Lining Constructions

Furnace Construction	Overall Efficiency (%)		Cumulative Production of Bars (tonne)		Total Fuel Consumed (GJ)	
	1380°C	1300°C	1380°C	1300°C	1380°C	1300°C
Baseline	30	31	40	34	158.1	134.9
All Refractory	28	28	37	37	157.1	153.9
All Ceramic	39	43	47	46	139.5	113.6

7.4.4 The Effect of Combustion Air Preheating

The use of preheated air was also found to influence the load output characteristics as shown in Figure 7.20. High surface temperatures are obtained at the higher set point when employing preheated air due to the high rates of heat transfer in this case. These load temperatures are substantially reduced as the set point temperature is reduced so that at a set point of 1300°C the upper surface temperatures approach 1200°C compared with 1300°C at the higher set point. Load temperature differences for both cases follow

similar trends with slightly higher values at the lower set points. This is because under these conditions the burners operate at reduced fuel inputs over most of the process with consequent reductions in the heat transfer to the load. If preheated combustion air is used the simulations suggest that a set point temperature of approximately 1340°C would be required to produce steel bars with a surface temperature of 1250°C but temperature differences in this case would likely approach 70°C.

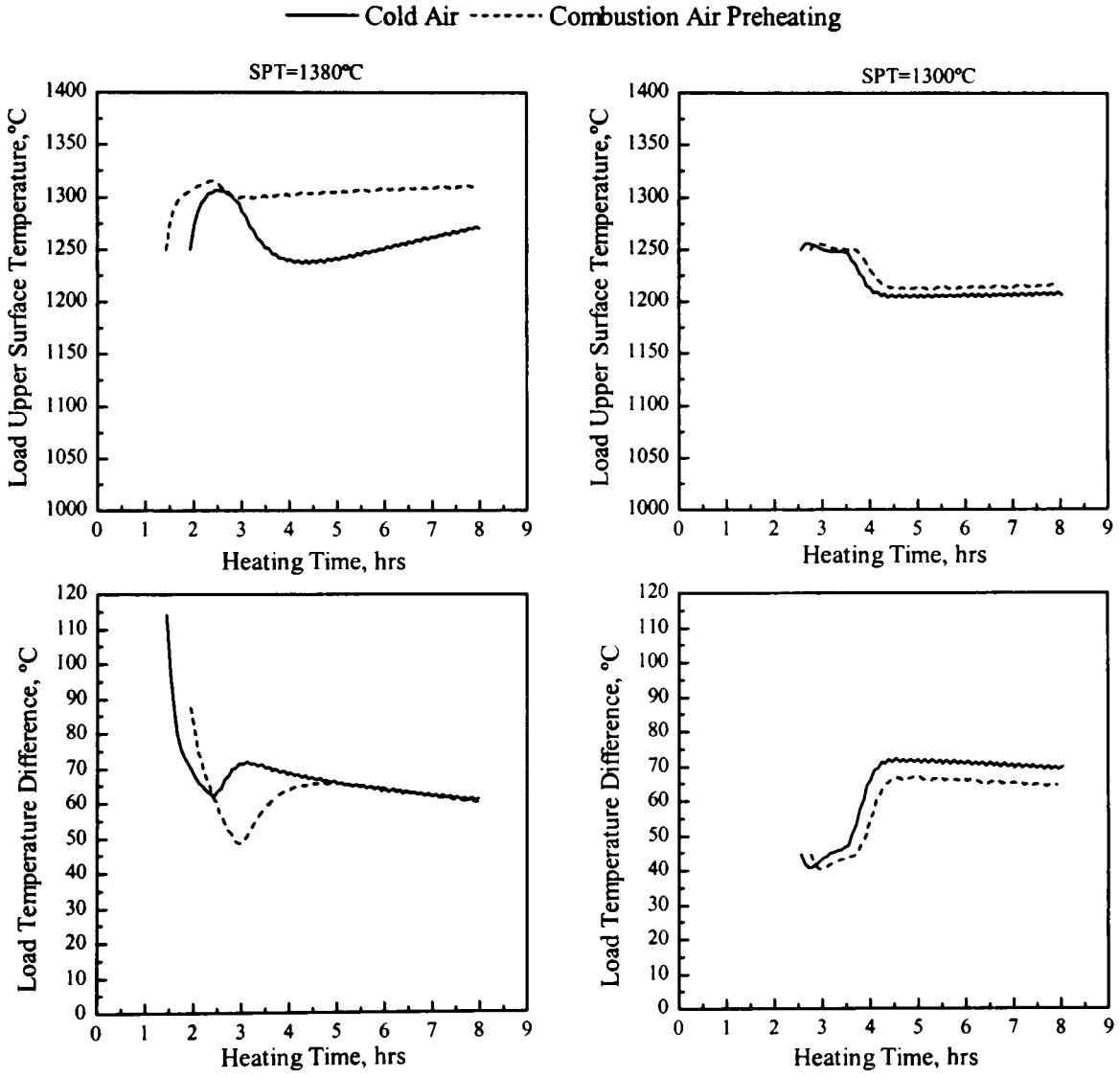

Figure 7.20 The Effect of Combustion Air Preheating on the Predicted Discharge Load Surface Temperature

In terms of the overall performance, Table 7.5 provides data for the preheated air simulation. The overall efficiency is the same for both set point conditions with less tonnage produced at the lower set points as a consequence of the longer start-up time in this case. Increases of about 30% are, however, predicted for the overall efficiency

when compared with that of the baseline simulations for a set point temperature of 1380°C. Energy savings of up to 20% are also predicted at the lower set points with corresponding increases in steel output of about 7%.

Table 7.5 Predicted Efficiency Data for the Preheated Air Simulation at Different Temperature Controls

SPT (°C)	Overall Efficiency (%)	Cumulative Production of Bars (tonne)	Total Fuel Consumed (GJ)
1380	39	42.9	136
1300	39	36	108.1

7.5 Simulation of an Extended Period of Operation

The baseline conditions were subsequently employed to simulate an extended period of 20 hrs of production, in order to predict the quasi-steady state thermal performance of the reheating furnace. The throughput was maintained at 6.5t/hr and the variations of load temperature and temperature difference for two control set point temperatures were analysed, see Figure 7.21.

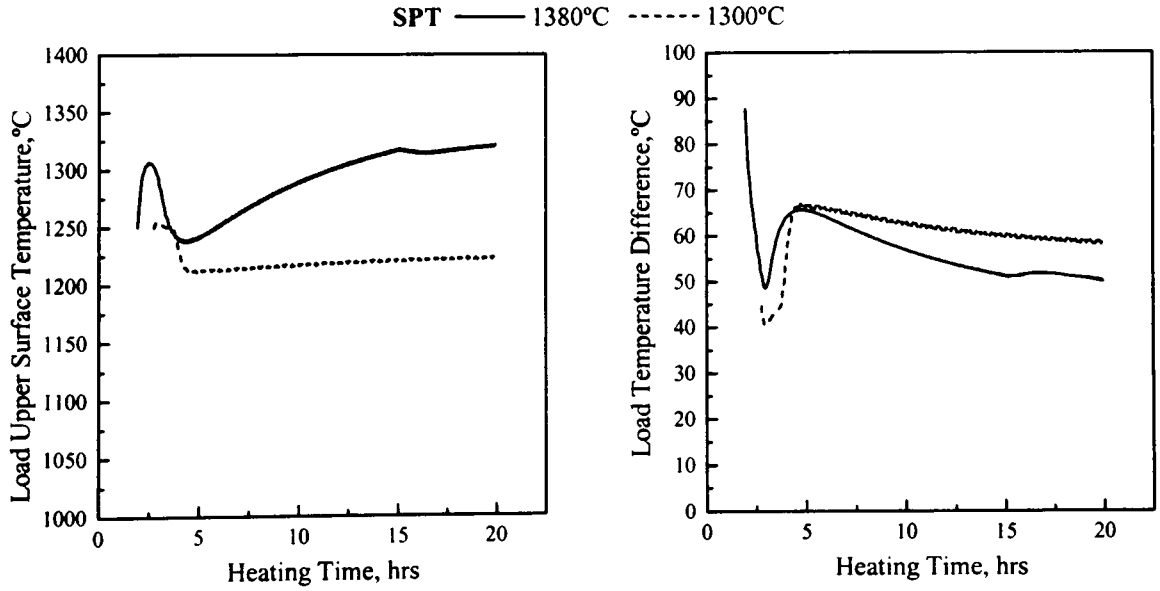

Figure 7.21 Predicted Discharge Load Temperature Profiles for an Extended Period of 20 hours

It can be seen that after approximately 15 hrs the load top surface temperatures at a control set point value of 1380°C reaches a virtually stable value of about 1315°C

whereas with the lower set point this value is about 1210°C. Relatively acceptable temperature uniformity within the bars is also apparent towards the end of the process. The reasons for this comparatively long period to reach quasi-steady state conditions can be deduced from the plot of the predicted heat distribution within the furnace chamber for a set point of 1380°C, see Figure 7.22.

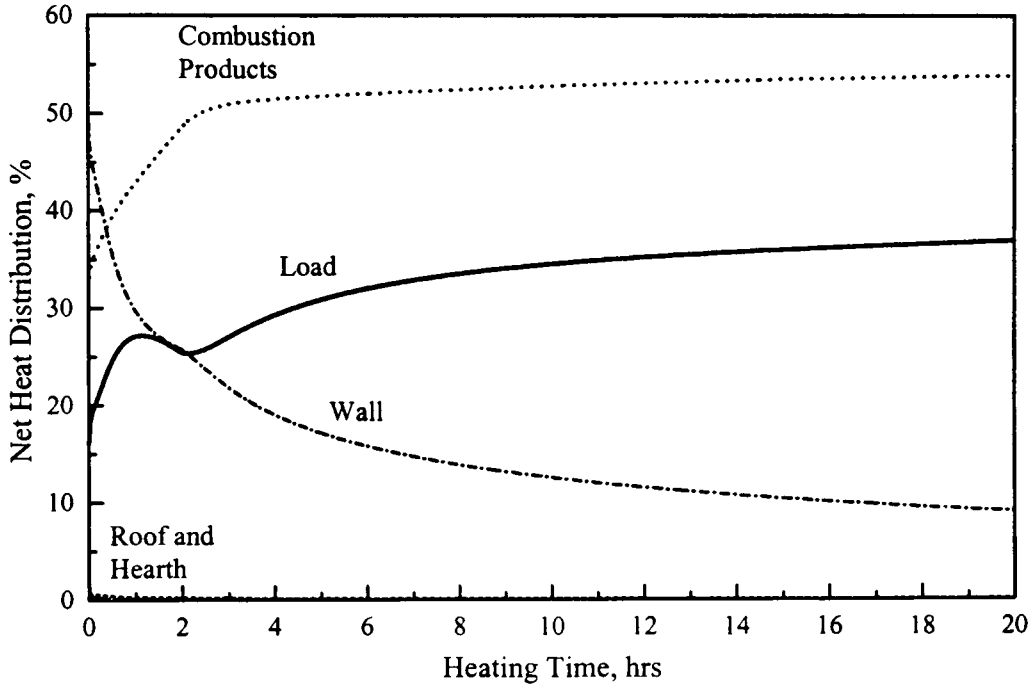

Figure 7.22 Predicted Heat Distribution for an Overall Period of 20 hours

The picture shows the importance of the wall losses during the initial part of the heating process where the furnace is first switched on from cold. The flat profiles of the curves towards the end of the simulation also indicate that steady-state thermal equilibrium has been virtually achieved.

7.6 The Effect of Increasing the Furnace Length

The models were also used to illustrate the effect of changing the furnace configuration so that it includes two more zones at the exhaust end as shown in Figure 7.23. A total number of 39 gas zones are now employed and the flow patterns remained the same as the baseline case. This is because extending the length at the exhaust end of the furnace will not significantly influence the upstream flow and plug-flow conditions can be assumed over the furnace extension.

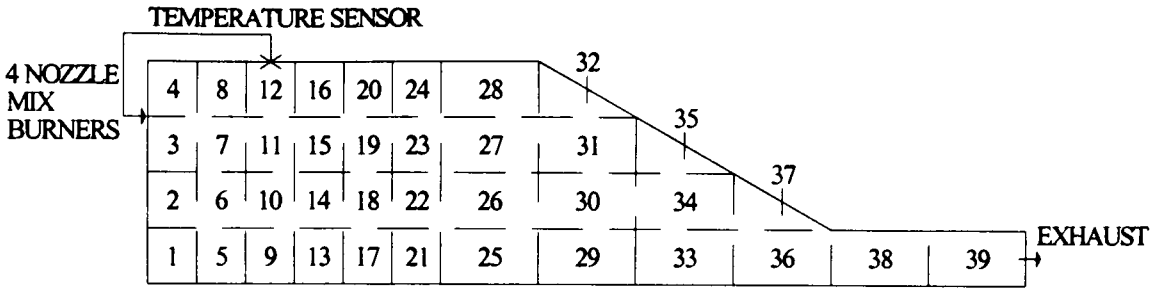

Figure 7.23 The 39 Gas Zone Arrangement

The influence on the load surface temperature and temperature difference can be seen in Figure 7.24 for two control set points, namely 1380°C and 1300°C.

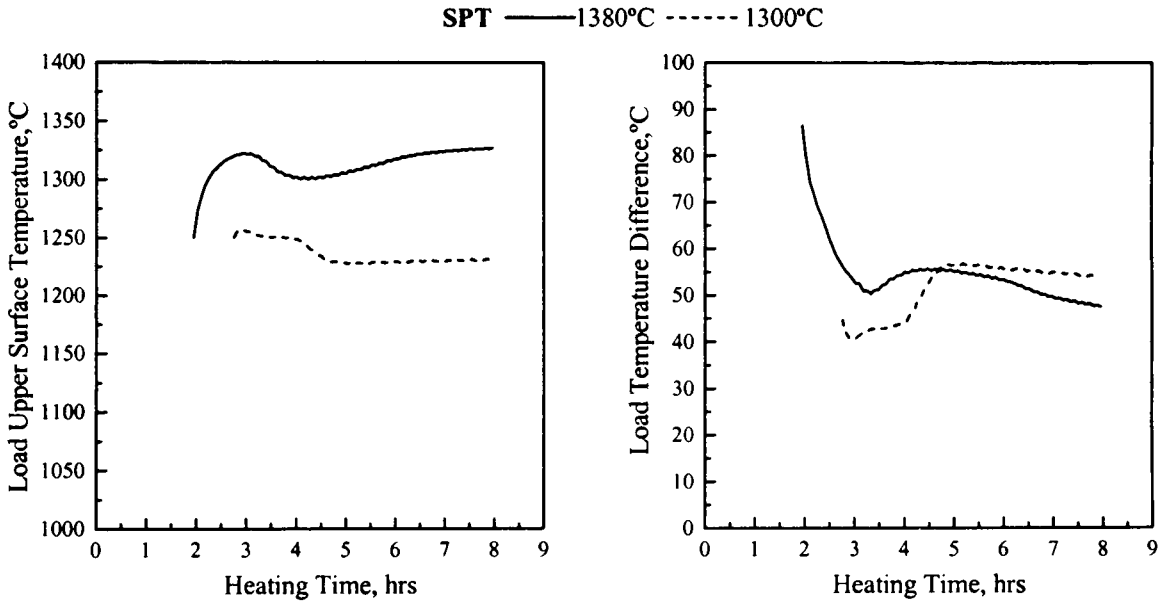

Figure 7.24 Predicted Discharge Load Temperature Profiles for the Extended Furnace

As expected the longer furnace configuration leads to higher load surface temperatures and lower temperature gradients when compared with the baseline simulation, see Figure 7.16. This is a result of increased heat transfer during the longer period that the bars spend in the system. In addition, the initial "overheating" peak is also slightly higher. At the highest set point the steel at discharge exceeds the target temperature of 1250°C and this can affect the quality of the final heated product. In most metal reheating furnaces tight temperature control is important if the final products are to meet specific metallurgical properties. Reduction of the control temperature can, however provide an option to decrease load output surface temperatures. Thus at a set point of 1300°C, the load output temperatures are approximately 1230°C compared with

1330°C at the highest control temperature. The predicted energy distribution over this period is shown in Figure 7.25 for a set point of 1380°C. From this picture it can be seen that the longer furnace makes better used of the heat in the combustion products so that less energy is wasted in the exhaust.

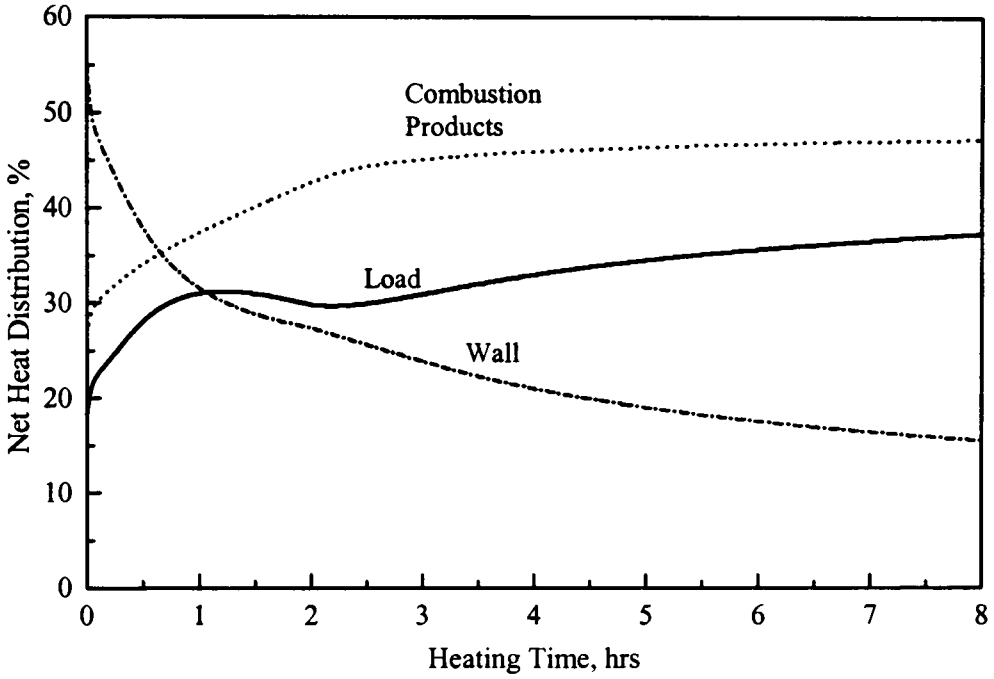

Figure 7.25 Predicted Heat Distribution for a Total Production Period of 8 hours

Thus at the end of the heating period, the total heat lost in the flue gas is about 45% of the total input energy for the longer furnace compared to 55% in the baseline configuration. Again the predictions indicate the importance of the wall losses in the initial start-up period. The predicted efficiencies for the two furnace arrangements are presented in Table 7.6. As expected for the longer furnace exhibits improved energy utilisation due to an increase in the "stock preheating" effect.

Table 7.6 Predicted Efficiency Data for Two Different Furnace Configurations

Furnace Configuration	SPT (°C)	Overall Efficiency (%)	Cumulative Production of Bars (tonne)	Total Fuel Consumed (GJ)
Baseline	*1380*	30	40	158.1
(37 Zones)	*1300*	31	34	134.9
39 Zones	*1380*	34	40	153.6
	1300	35	34	124.2

7.7 Summary

Overall the current work demonstrates that the zone models were capable of predicting the effect of changes in the operating conditions. The numerical predictions have highlighted the importance of adequately representing the interaction between the heat transfer characteristics of the furnace and those of the control system, which modulates the thermal input to the burners. Changes in burner characteristics can markedly affect the thermal performance of the system during both initial start-up from cold as well as over prolonged production periods. The thermal behaviour was also influenced by the magnitude of the furnace set point and position of the roof mounted thermocouple which acted as the control sensor. The use of low thermal mass ceramic fibre materials in the furnace provided benefits particularly when the whole of the furnace lining was constructed from these lightweight materials. The study has shown that potential energy savings can be made when employing heat recovery systems to preheat incoming combustion air. The models also demonstrated the effect of adding more air than necessary to complete combustion.

References

1. Tucker, R.J., Ward, J., *Use of a Monte Carlo technique for the determination of radiation exchange areas in long furnace models.* in *Proc. 8th Intl. Heat Transfer Conf.*, p. 391-396. 1986. San Francisco, USA.
2. Croft, D.R., Lilley, D.G., *Heat Transfer Calculations Using Finite Difference Equations.* 1st ed., Vol. 1, 1977: Applied Science Pub.
3. Rhine, J.M., Tucker, R.J., *Modelling of Gas-Fired Furnaces and Boilers and Other Industrial Heating Processes*, 1991, London: McGraw-Hill.
4. Howells, R.I.L., Ward, J., Probert, S.D., *Thermal conductances of contacts at high temperatures.* J. Iron Steel Inst., 1973. **211**(March): p. 193-196.

CHAPTER EIGHT

STEADY-STATE MODELS

8.1 Introduction

In the previous chapter mathematical models were developed to provide predictions of a gas-fired metal reheating furnace operating in a transient manner. Whilst these models are able to describe realistic operating conditions such as unscheduled delays or changes to the fuel input they can only represent quasi-steady operation by simulating long periods of operation. For systems which are operated continuously at a steady firing and production rate much simpler steady-state models can be employed which require less input data and shorter computing times. These conditions can simulate a real furnace operating over a prolonged period of continuous production, as is the case in some reheating applications. Thus, steady-state models were used to investigate the thermal performance of a continuously operated gas-fired metal reheating furnace. The influence of changes in furnace design and control were studied and the effect of varying the number of zones was also investigated in a two-dimensional arrangement. The predicted results are again compared with equivalent long furnace models to assess the differences arising from the use of simpler models.

8.2 Steady-State Calculations

The steady-state models developed in this chapter are again based on the zone method of radiation analysis where energy balances (incorporating radiation and other heat transfer modes) are written for each zone. These models were used to assess the continuous operation of the gas-fired reheating furnace described earlier in this thesis. In contrast to the transient models where only the energy balance for each gas volume zone needs to be solved, steady-state models require simultaneous solution of both gas and surface energy equations. An initial linear load surface temperature is thus assumed at the start of the simulation and the zone models employed to calculate the heat flux distribution to the load surface, see Figure 8.1.

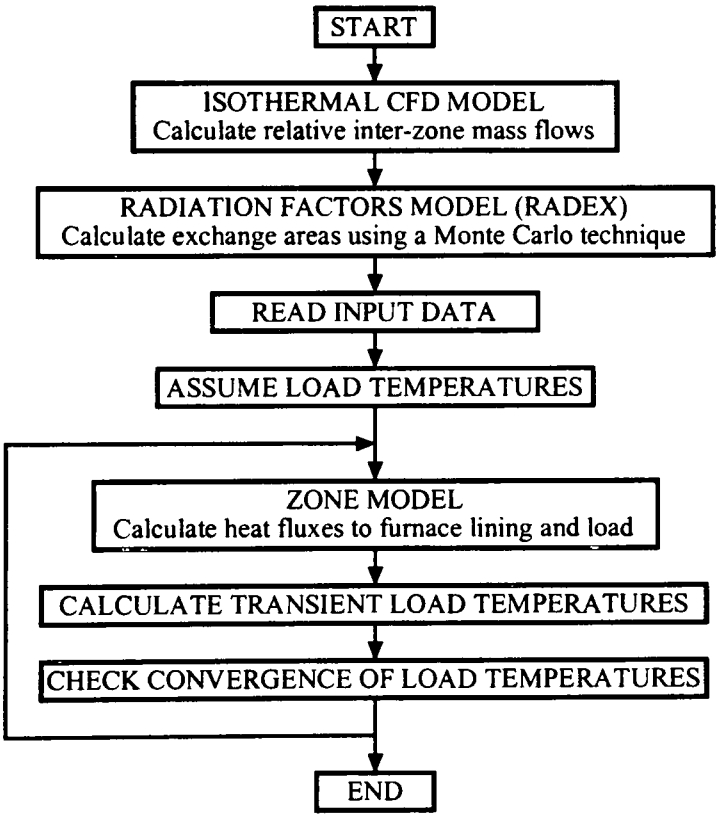

Figure 8.1 Simplified Flow Diagram for a Steady-State Zone Model

A new set of load temperatures is then calculated by a one-dimensional finite-difference conduction model using the calculated load heat fluxes as a time-dependent boundary condition at the surfaces. The overall calculation is repeated using the latest load temperature profile until the differences between two consecutive sets of load surface temperatures are within a predefined tolerance. With this approach it is possible to represent the passage of steel bars through the furnace and follow the evolution of the

temperature. Figure 8.2 shows an example of the progress of the load surface temperature with the number of iterations. In this particular case a maximum of 10 iterations were required to achieve convergence. More generally convergence was obtained over a range of 6 to 30 iterations depending on the fuel thermal input and production rate and this corresponds approximately to 1 to 8 minutes of computing time.

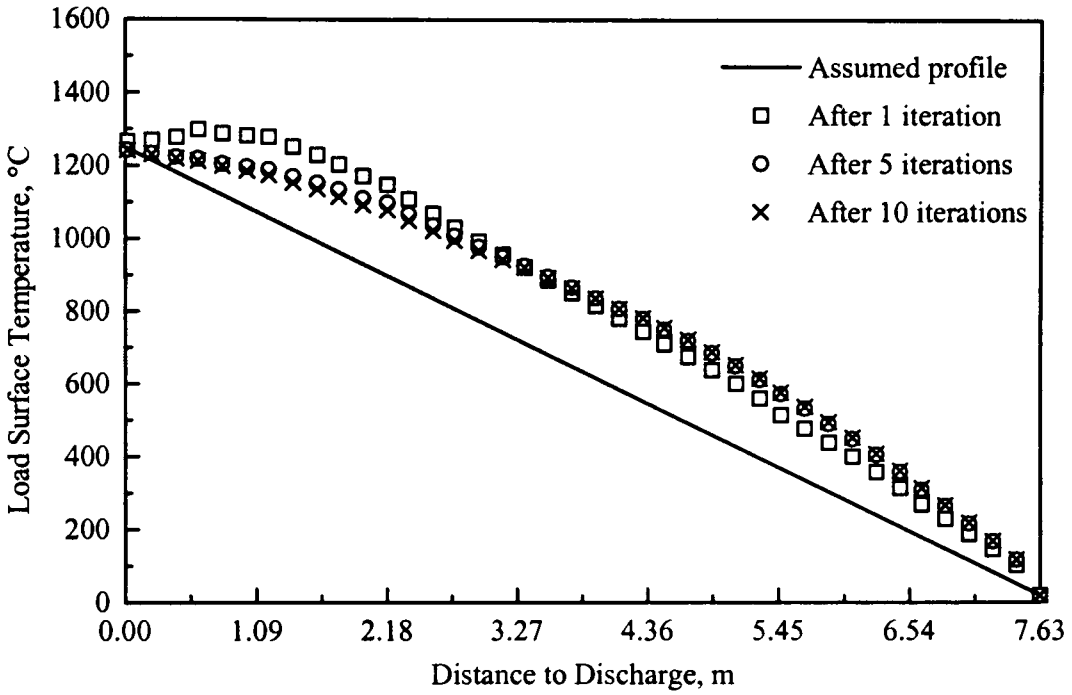

Figure 8.2 Load Surface Temperature Evolution with Number of Iterations

For the steady-state models the initial calculation stages are identical to those described in the transient models with the enthalpy flows, necessary to describe the distribution of thermal and mass inputs to the gas zones, obtained from an isothermal CFD simulation. The radiation factors required to define the radiation term in the energy balance equations were again calculated by a Monte Carlo technique due to the furnace complex shape. The furnace atmosphere was assumed to be a mixture of one clear and two grey gases and the load and surface walls properties were as specified in the transient model. Convection was determined by using a constant convection heat transfer coefficient of $25 W/m^2K$ since in high temperatures applications this mode of heat transfer normally accounts for only 5% of the overall energy transfer. The cold steel bars enter the furnace at the exhaust end and are discharged at the firing end when the top surface reaches 1250°C. Since load temperature uniformity is important an

independent transient conduction analysis into the load was carried out. This model considers temperature variations only along the load thickness so that the horizontal temperature gradients are neglected. A fully implicit finite-difference technique with 11 nodes was used to calculate the temperature distribution through the load and the bottom surface of the steel bars was assumed completely insulated so that the temperature gradient at this surface is zero. In this study the furnace walls and roof were assumed adiabatic for simplicity reasons although in general wall conduction heat losses from continuous operated systems can represent about 5-10% of the overall energy input. The simulations were stopped when differences between consecutive values of both the top and bottom temperatures of the load at discharge were less than 1°C.

The models were used to predict the discharge temperature within the steel bars, as well as the furnace thermal efficiencies, for a range of production rates and thermal inputs. In the steady-state models simulation of furnace control is not possible because this is a time dependent variable. However, for a given throughput and thermal input, it possible to obtain the temperature for the roof surfaces normally associated with the control system to indicate the corresponding furnace operating set point. With this approach the effect of different operating conditions on the magnitude of the control set point and the influence of varying the position of the control sensor can be assessed. To demonstrate the effect of zone size, a number of zoning arrangements were used in a 2D simulation of the furnace. These varied from 13 to 50 gas zones as in the transient case, see Chapter 6. The influence of varying the position of the roof temperature control sensor relative to the burners as well as changes to the roof set point temperature were studied. Burner orientation was varied and the furnace length modified to examine the effects of changes in furnace-burner geometry. Comparisons were also drawn with predictions from equivalent long furnace models to demonstrate the differences arising through the use of these simplified versions of the furnace geometry.

During the simulations the load throughput was varied from 6 to 8t/hr and the thermal input to the burners from 3.2 to 4MW. The models predict the load surface temperature profile along the furnace length, the temperature difference at discharge, the wall and roof temperatures and the steady-state efficiency. The purpose of this continuous reheating furnace was again to heat up the steel bars to a nominal discharge temperature of 1250°C.

8.3 Comparison of Steady-State LFM with 2D Models

The steady-state models were developed for a range of multi-dimensional zone arrangements which split up the furnace enclosure not only along the length but also across the height. The importance of a two-dimensional representation of the furnace has previously been demonstrated for transient operation. Initially, therefore comparisons were made between the 2D models and simpler models such as the LFM for this continuously operated case. In this study four 2D models were employed with 13, 25, 37 and 50 volume zones, see Chapter 6 for the overall zone arrangement. The equivalent LFMs employed 7, 7, 10 and 14 gas volume zones respectively and were obtained by grouping zones together vertically so that variations are only allowed in the longitudinal direction. The steady-state simulations took minutes to perform on a PII 450 with the time increasing as the number of zones subdividing the furnace enclosure was increased.

A comparison of predicted steady-state load surface temperature profiles for the different 2D models and their corresponding LFMs indicates generally reasonable agreement, see Figure 8.3. These comparisons were carried out for a load throughput of 6.5t/hr and a thermal input of 3.6MW but similar agreement was also found with other sets of operating conditions.

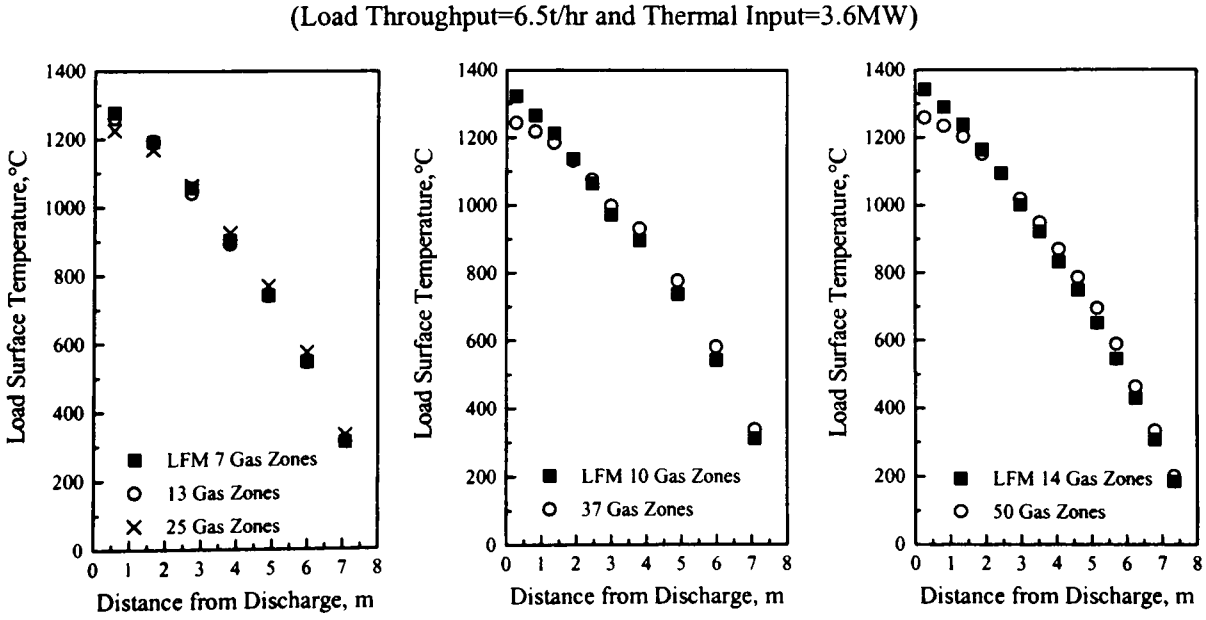

Figure 8.3 Comparison of Predicted Steady-State Load Temperature Profiles for the Different 2D Models and the Corresponding LFMs

The LFMs slightly underpredict the load surface temperature in the first stages of heating near the charge end when compared with results from equivalent 2D models. This difference is however reduced as the load moves along the furnace until near the discharge (burner end) the simulations show the LFMs overpredicting the load surface temperature. This is probably due to the LFMs assuming a single gas temperature value at each zone along the enclosure so that near the burners and close to the discharge end the LFMs predict temperatures which are higher than the temperature of the recirculating combustion products and this leads to higher load heating rates. In addition the LFM does not account properly for the effect of flows bringing hot gases from the zones near the roof to the load and this can also lead to the LFMs underpredicting slightly the rate of heat transfer to the load at the charge end. This is illustrated in Figure 8.4 which compares the predicted load heat flux distributions for the different models and corresponding LFMs. It can be seen that the differences in the predicted heat flux between the 2D models and corresponding LFMs are more marked near discharge and these increase with model refinement. The finer subdivision adopted in the near burner region results in equivalent LFMs of the 37 and 50 gas zone models (i.e. those with 10 and 14 zones) predicting even higher heat fluxes to the load at discharge than those obtained in the 7 gas zone LFM. As a consequence differences in surface temperature profile are more distinct in these cases. Generally, the 2D models result in a greater variation in heat flux over the length of the furnace with higher peak heat fluxes.

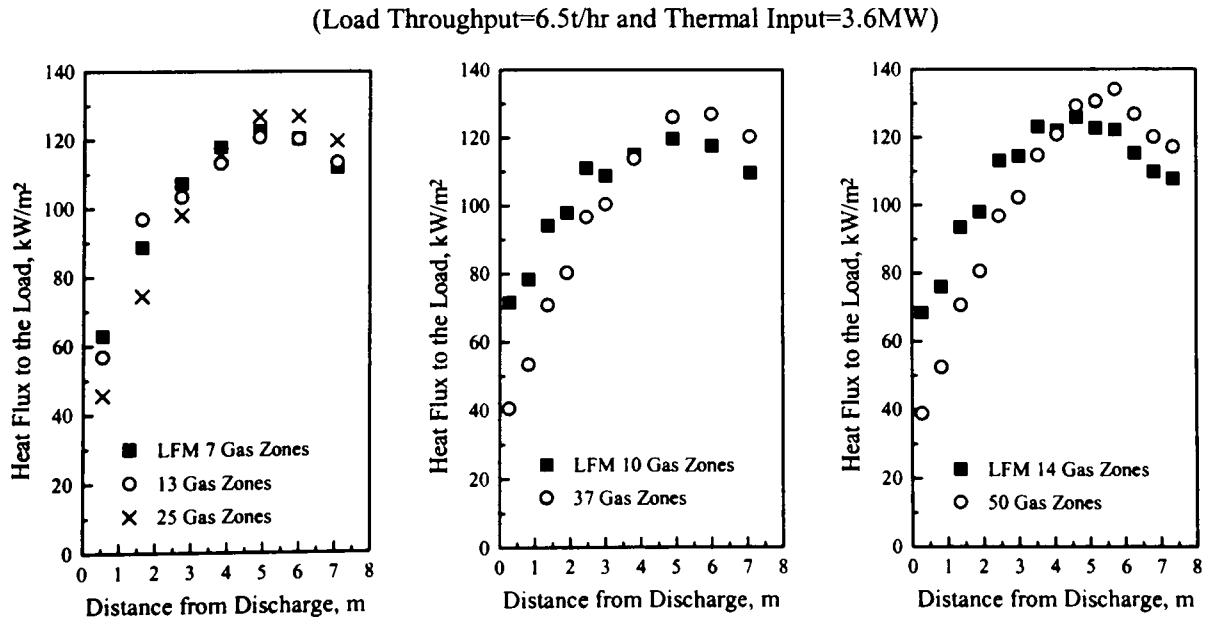

Figure 8.4 Comparison of the Load Heat Flux Distribution for the Different Models

The load temperature differences, roof set point temperatures and steady-state efficiencies were also investigated. This study was carried out for different production rates and for a range of thermal inputs.

Figure 8.5 and Table D.13 (see Appendix D) show the variation of the top-to-bottom load temperature with load throughput when producing steel bars with a top surface temperature of 1250°C. It can be seen that for a given rate of load throughput the simpler LFMs always overpredict these temperature variations when compared with the corresponding 2D models.

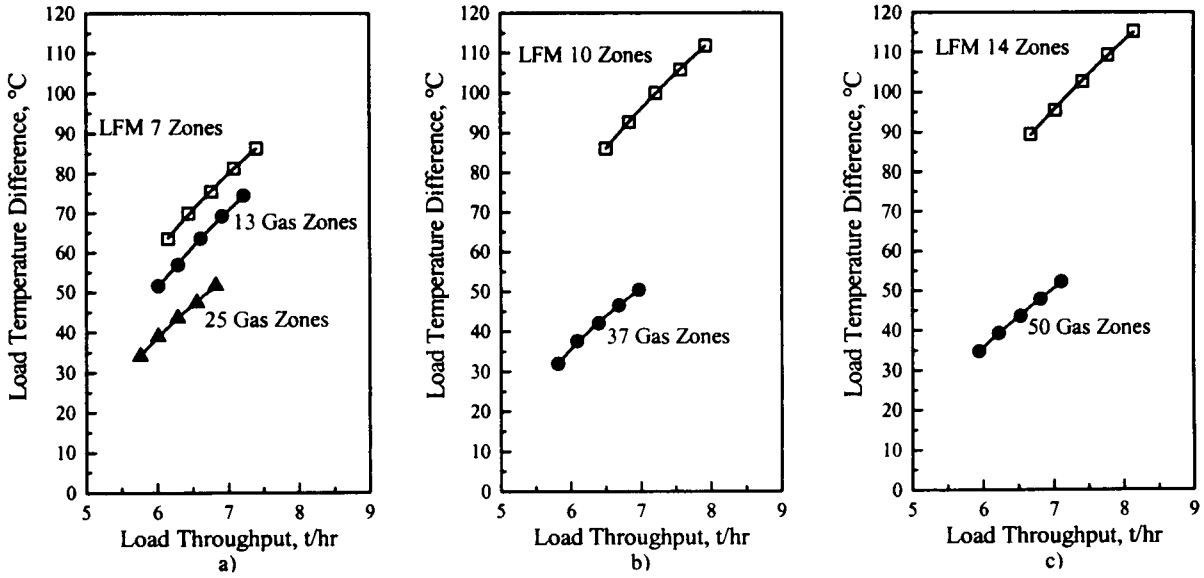

Figure 8.5 Comparison of the Predicted Load Temperature Difference at the Discharge Condition for the 2D Models and Corresponding LFMs

A closer look at the behaviour of the discharge temperatures predicted by the LFM with 7 zones and the equivalent 2D models, see Figure 8.6, shows that the LFM simulations for a range of load throughputs and thermal inputs always result in higher load discharge temperatures. This means that for the same load throughput, the LFM predicts that a lower heat input is required to meet the discharge output condition.

The difference between the LFM and 2D model predictions, see Figure 8.5a, increases with the number of zones taken to subdivide the enclosure. This is because increasing the number zones along the furnace height results in lower temperatures near the load so that for the same load throughput a higher thermal input is required to achieve a top temperature of 1250°C. As a result a reduction of the temperature differences in the load is achieved particularly in the 25 gas zone simulation where even

lower temperatures are predicted close to the load. Thus, the difference between the LFM and the 13 gas zone model at all throughputs is about 13% while with the 25 gas zone model a larger difference of approximately 33% is predicted.

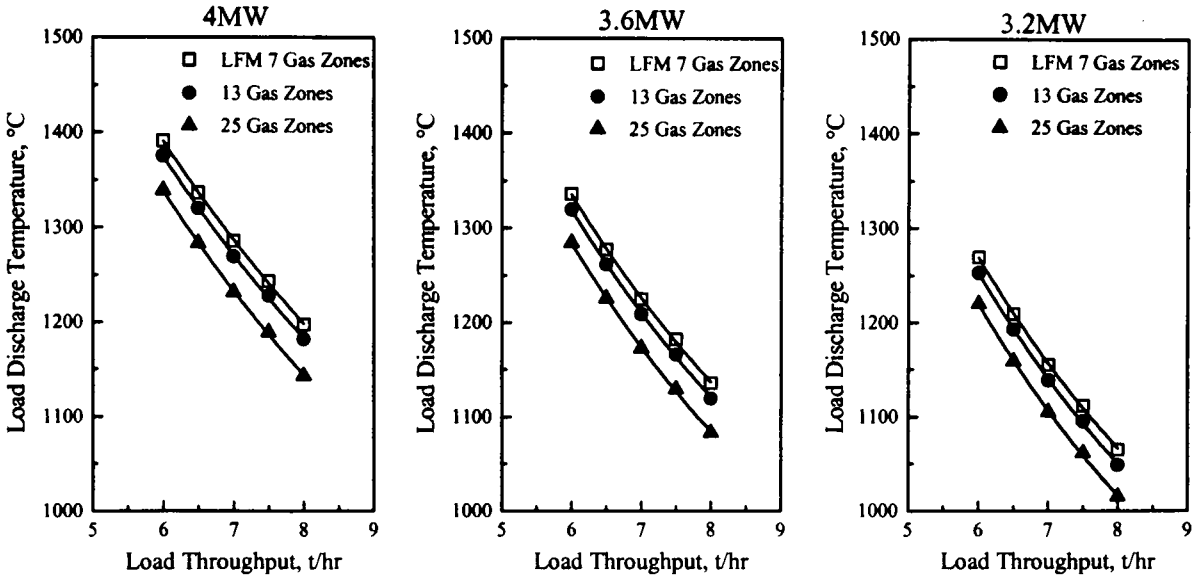

Figure 8.6 Comparison of Predicted Load Discharge Temperature for a LFM with 7 Gas Zones and Equivalent 2D Models at Different Thermal Inputs

A similar situation is found in Figures 8.5b and 8.5c where the more complex two-dimensional models predict much lower load temperature differentials when compared with the equivalent LFMs. A difference of approximately 53% is however predicted between the models in both 37 and 50 gas zone simulations. In these cases the corresponding LFM yield discharge temperatures which are much higher than those predicted by the LFM with 7 gas zones, see Figure 8.7.

In the LFMs pairs of volume zones are grouped vertically to form a zoning arrangement which only varies along the length of the furnace. With the 37 gas zone arrangement, the equivalent LFM has a non-uniform longitudinal zone distribution which is finer close to the burners at the discharge end. In the 50 gas zone model a finer uniform zone size is employed throughout the whole furnace length. Under the same operating conditions both 10 and 14 gas zone LFMs predict gas temperatures which close to the burners are higher than the equivalent gas temperature predicted by the LFM with 7 zones. A higher heat flux is, therefore, obtained for the load close to the burners end and this leads to an increase in load surface temperature at discharge in the 10 and 14 gas zone models. Thus with the 10 and 14 LFMs, to obtain steel bars at the desired output specification and throughput, a lower input to the burners must be

employed and this consequently leads to lower heat flux to the load and hence larger temperature gradients at discharge.

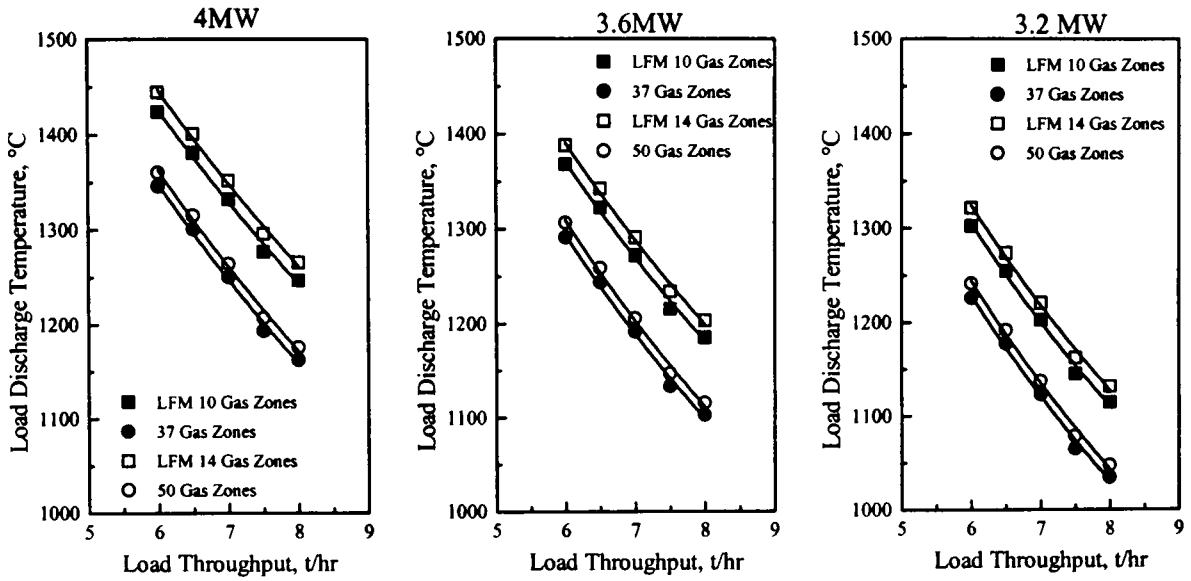

Figure 8.7 Comparison of Predicted Load Discharge Temperature for LFMs with 10 and 14 Gas Zones and Equivalent 2D Models at Different Thermal Inputs

These results have shown that the use of LFMs has a significant effect on the performance predictions of a continuously operated furnace when compared with the 2D simulations. Increasing the number of subdivisions in the LFMs results in larger differences in the predictions when compared with the corresponding 2D model predictions.

As previously mentioned simulation of the control system is not possible using a steady-state model. However it is possible to obtain the temperature of the roof where the control sensor is placed to find the operating set point of the system. Figure 8.8 and Table D.14 show the differences in predicted set point temperature for the LFMs and corresponding 2D models when the load is discharged at 1250°C. In this case all the LFM simulations predict that lower set points are necessary when compared with the equivalent 2D models. As a consequence of neglecting temperature variations along the furnace height, simulations employing LFMs result, see Figures 8.6 and 8.7, in increased load discharge temperatures at specific throughputs and thermal inputs. Thus to obtain steel bars at the desired surface temperature lower thermal inputs must be employed and therefore lower gas, wall and roof temperatures are predicted. The difference between the LFM and the 2D models is seen in Figure 8.8a to decrease with the 25 gas zone arrangement because the finer subdivision close to the roof leads to

lower temperatures in the zone immediately adjacent to the control sensor whilst in the 13 gas zone case the overall temperature in that zone is higher. The results presented in 8.8b) and 8.8c) correspond to the same roof surface position.

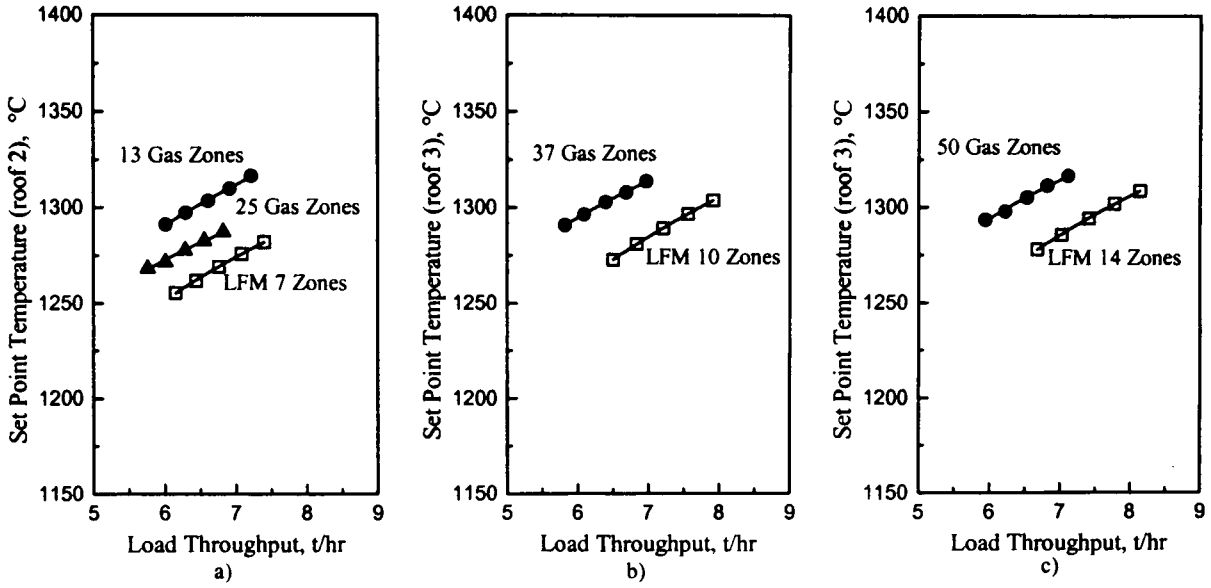

Figure 8.8 Comparison of the Predicted Set Point Temperature for 2D Models and Corresponding LFMs at a Load Top Discharge Temperature of 1250°C

The comparisons above were made for one specific load output temperature of 1250°C which is appropriate in cases where accurate temperature control is required. However, in many cases an acceptable range of temperatures may be considered for the load at discharge and therefore simulations were carried out to predict the set point temperature band which will provide a suitable range of load discharge temperatures. An output temperature range of 1230 to 1250°C was considered as appropriate in this study.

It is, however, clear that even taking into account variations in the load temperature at discharge there are still substantial differences in the predicted set points for the different 2D models and corresponding LFMs as illustrated in Figure 8.9 and Table 8.1. These results are for a load throughput of 7t/hr but overall they demonstrate that even when a band of discharge temperatures are specified the LFMs models predict that a significantly lower range of set points are required i.e. the LFMs provide substantially different predictions than the 2D simulations.

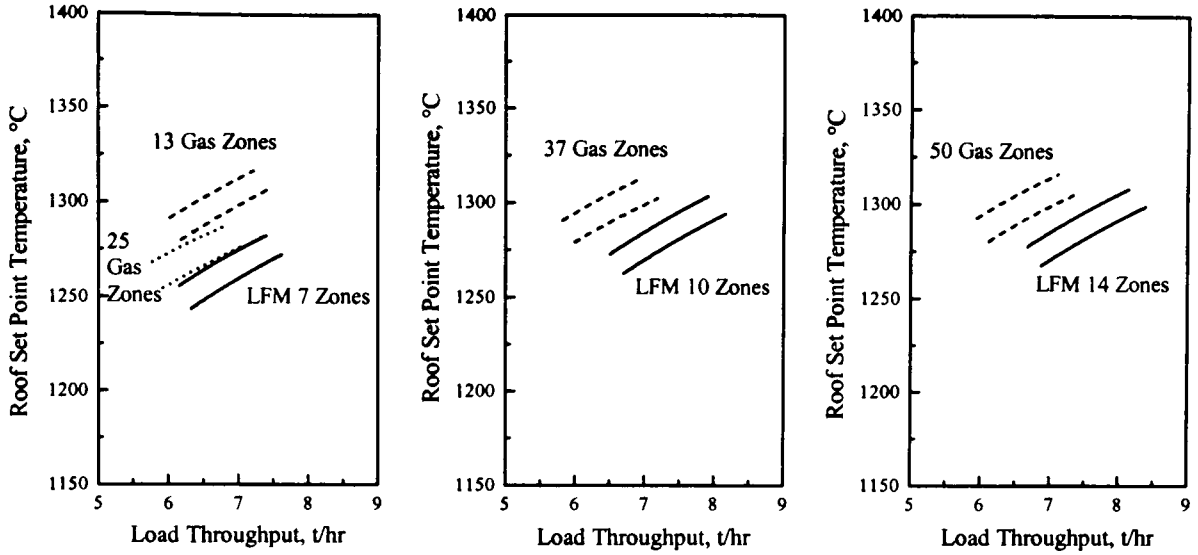

Figure 8.9 Comparison of the Predicted Set Point Temperature Band for the 2D Models and Corresponding LFMs for Two Load Discharge Conditions

Table 8.1 Comparison of the Predicted Set Point Temperature for the 2D Models and Corresponding LFMs for Two Load Discharge Conditions (Load Throughput=7t/hr)

Zone Model	Set Point Temperature (°C)	
	Discharge Temperature=1250°C	Discharge Temperature=1230°C
LFM 7 Gas Zones	1275	1260
13 Gas Zones	1310	1300
25 Gas Zones	1290	1275
LFM 10 Gas Zones	1280	1270
37 Gas Zones	1310	1295
LFM 14 Gas Zones	1280	1270
50 Gas Zones	1315	1300

A comparison of the steady-state efficiencies shows that the LFMs predict substantially higher efficiencies than the corresponding 2D models, see Figure 8.10 and Table D.15. This is because of the lower thermal inputs required by the LFMs to produce steel bars at a nominal discharge temperature of 1250°C. Less fuel is, therefore, used to heat up the bars to the discharge condition and hence a higher efficiency is achieved. These results also agree with early findings where LFMs were found to predict lower exhaust temperatures so that less energy is lost in the waste gases.

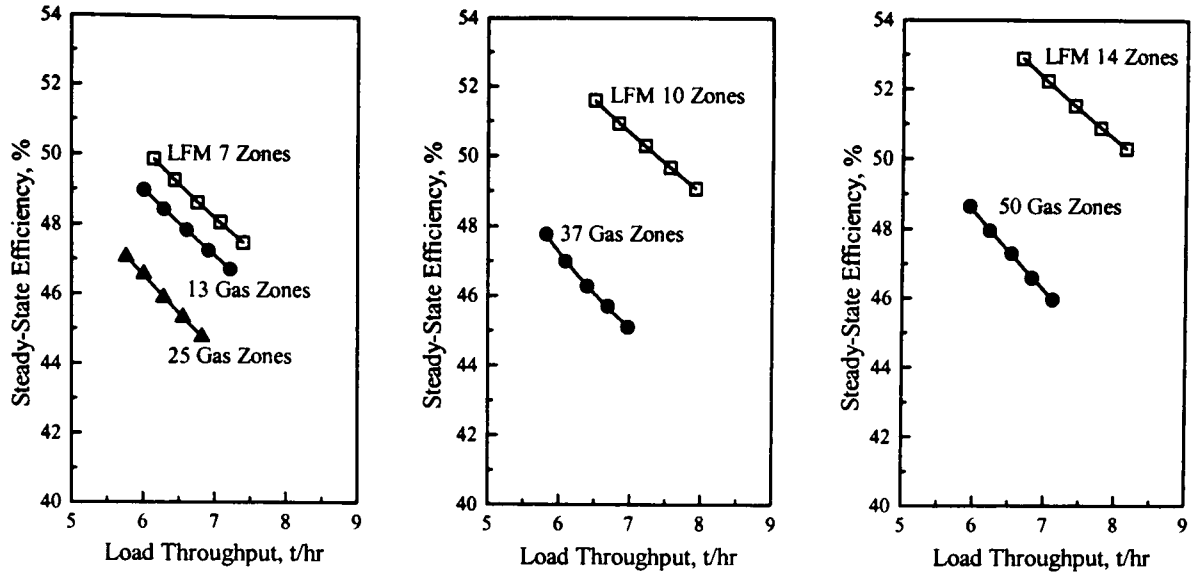

Figure 8.10 Comparison of the Predicted Steady-State Efficiency for the 2D Models and Corresponding LFMs at a Top Discharge Temperature of 1250°C

Overall the results confirm that substantial differences are obtained with simpler LFMs when compared with more sophisticated 2D versions for this continuously operated furnace. Failure to represent variations along the height of the furnace resulted in higher temperatures close to the load and lower temperatures near the roof close to the burners when compared with those from the more sophisticated 2D models. In general the LFM simulations indicate that to produce bars at a nominal discharge temperature of 1250°C lower thermal inputs must be employed at all throughputs and as a result higher temperature gradients are obtained within the load. In addition lower temperatures are predicted for the entire enclosure including walls and roof surfaces. As a consequence a lower temperature is predicted for the roof surface acting as the set point and this indicates that a much lower control temperature would be required in a LFM simulation. The lower thermal inputs predicted by the LFM result in higher efficiencies since for the same output of steel bars less fuel is necessary. The simulations have, therefore, demonstrated that in this furnace where the flows are two-dimensional, more sophisticated 2D models are necessary since the LFM representation appears to underestimate the necessary thermal input. The results indicate that LFMs should not be applied to furnaces with a large height to length ratio since they can lead to substantial differences particularly as the number of zones is increased.

8.4 The Performance of the 2D Models

The previous section has demonstrated the need for a two-dimensional representation of the gas-fired metal reheating furnace operating continuously to produce bars with a top surface temperature of 1250°C. However it is now important to establish any differences in the 2D models since predictions are known to be dependent on the number of zones used to describe the furnace. The various steady-state 2D models were thus employed to provide predictions on the top-to-bottom temperature differences in the load, the required roof set point temperatures as well as the thermal efficiencies when heating the steel bars to a top surface temperature of 1250°C.

The variations of the load surface temperature as the bars move through the furnace are shown in Figure 8.11 and generally there is good agreement between the different 2D models.

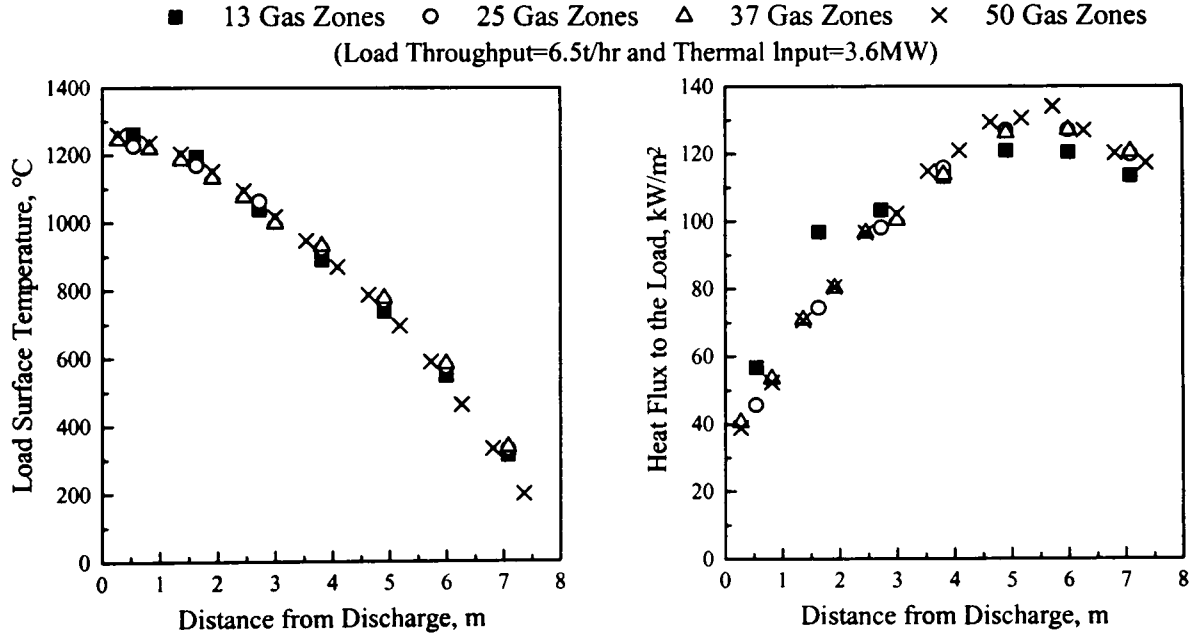

Figure 8.11 Comparison of the Load Surface Temperature and Heat Flux Profile for the 2D Models

The presented results are for a load production rate of 6.5t/hr and a thermal input of 3.6MW but the relatively close agreement of the load temperature profile between the different models was maintained at other production rates and thermal inputs. The values for the predicted heat flux to the load are also generally in good agreement although the 13 gas zone model tends to underpredict the heat transfer to the load at entry to the furnace and overpredict the heat transfer towards the discharge end. This is because with a coarser subdivision along the height, temperatures near the load at the

firing end are higher than those of the other 2D models and correspondingly lower near the exhaust. The results emphasise the need for finer subdivisions along the height to improve predictions in furnaces with a large height-to-length ratio. In these cases significant variations in gas temperature and heat flux can occur and must be appropriately accounted for.

Comparisons of the furnace performance are shown in Figure 8.12 and Table D.16 for the different 2D zoning arrangements. This figure plots the predicted temperature differential in the load, the required roof set point temperature to achieve the efficiency for a range of production rates and thermal inputs. As the rate of load throughput is increased, the temperature differences in the load at discharge are significantly increased. This is because at higher production rates, the load spends less time in the furnace so that less time is available for heat conduction within the steel bars. Higher differentials are predicted with the 13 gas zone model since the crude subdivision adopted in the firing zones near discharge leads, as previously mentioned, to higher heat fluxes at the load surface than when employing more refined zone arrangements, see Figure 8.10. As a result for the same load production rate, less heat is necessary in the simplest zone arrangement to bring the load to an output surface temperature of 1250°C. The lower thermal inputs lead as expected to lower heating rates and large temperature gradients in the load at discharge.

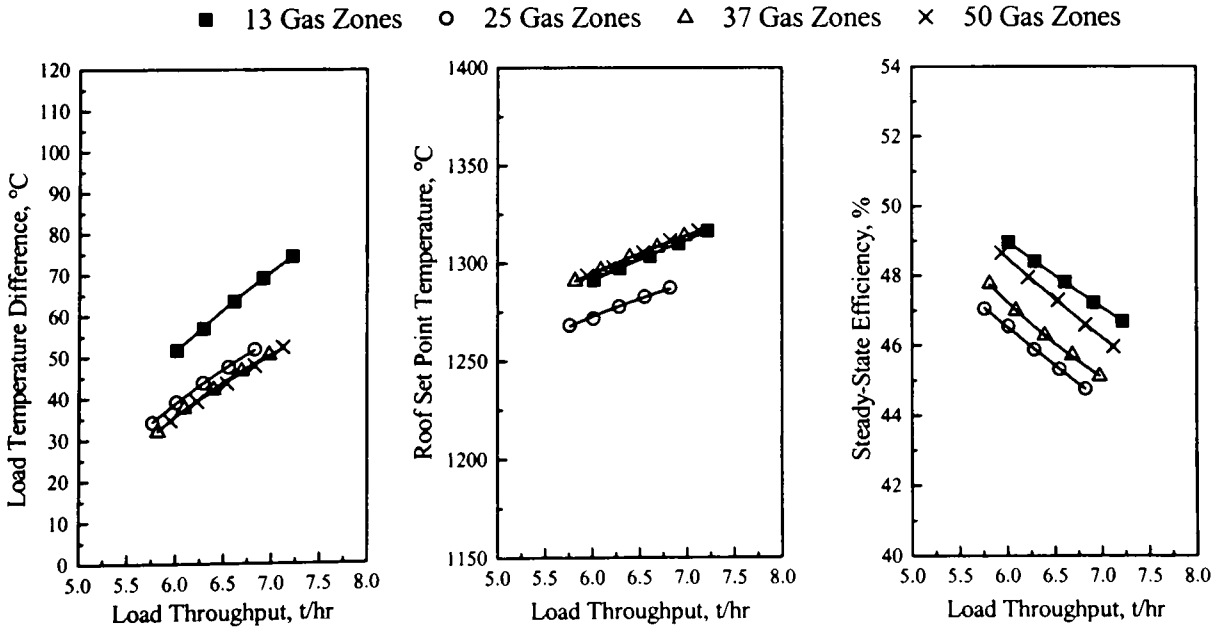

Figure 8.12 Comparison of Performance for the 2D Models

As the number of zones taken to subdivide the enclosure is increased, better estimates are found for the heat fluxes at the load so that differences between the models are reduced. For example the differences in predicted load gradients for the 13 gas zone model and the 37 gas zone model are in the order of 30% whilst an increase to 25 gas zones results in maximum differences of about 10%. Further increases result in nearly identical predictions for the 37 and 50 gas zone model. This indicates that subdivision of the enclosure height has a major effect in the predictions from the different models.

Predicted roof temperatures are, as expected, increased with increasing load throughputs since under these conditions a higher thermal input to the system is necessary to produce the steel bars at the required top temperature. It is, however, difficult to establish a direct comparison between all the models because the different zone arrangements result in the control sensor being positioned differently. Nevertheless, it is possible to compare the models which share the same control sensor position such as the 13 with the 25 gas zone models and the 37 with the 50 gas zone models. Increasing the number of zones from 13 to 25 is seen to have an effect on the temperature of the control set point with the 25 gas zone model predicting always lower values in comparison with the 13 gas zone model. This is mainly due to the furnace subdivision along the height so that the 25 gas zone simulation results in temperatures of the gas zone immediately adjacent to the control which are lower than that predicted by the 13 gas zone model. As we move away from the burners the decrease in gas temperature near the roof is more abrupt in the 25 gas zone model than in the 13 gas zone model due to the finer zoning. The roof surface acting as the control set point is thus subject to lower levels of heat transfer and consequently lower temperatures are obtained with the 25 zone arrangement. The crude zoning in the 13 gas zone model leads in this case to higher average temperatures for the gas immediately adjacent to the control sensor. Very good agreement is, however, obtained in the more refined two-dimensional models of 37 and 50 gas zones so that in this case the solution is practically zone independent.

Comparison of the predicted steady-state efficiencies for the different models shows relatively close agreement between all models with efficiency decreasing with increasing load throughput. This is expected as the thermal input to the furnace increases with throughput i.e. the furnace is "driven harder". The differences in predicted efficiency for the models are of the order of 2 to 4%. It should also be noted

that the predicted load discharge temperature also varies to some extent with the number of zones, see Figure 8.13. The results of these comparisons indicate that the predictions for the simulation of continuous operation of a gas-fired metal reheating furnace depend upon the number of zones. In particular the furnace predictions clearly depend on the number of subdivisions used for the region close to the burners where large variations in temperature are likely to occur. Thus, a coarse zoning arrangement (i.e. the 13 gas zone model) tends to underpredict load heat fluxes at the charge end and overpredict them at discharge which consequently affects the final load temperature predictions and furnace performance.

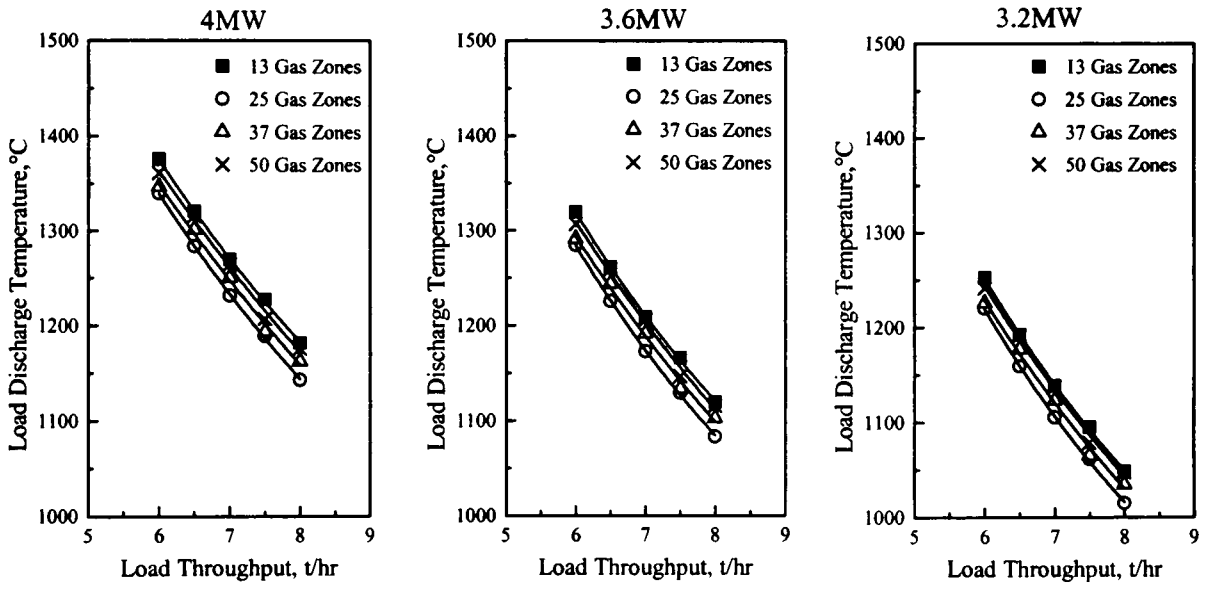

Figure 8.13 Comparison of Predicted Load Discharge Temperature for the 2D Models at Different Thermal Inputs

Increasing the number of subdivisions along the height so that a total of 25 gas zones is achieved leads to better heat flux predictions at the load surface. However at the roof surfaces near the burners large longitudinal temperature variations can still occur and finer subdivisions along the length of the furnace are therefore required to obtain reliable estimates of the heat flux at these surfaces. With the 37 gas zone model where a finer mesh is employed at the firing end, consistent estimations of heat fluxes and temperatures variations are obtained. Further increases aimed at extending the finer mesh to the whole furnace enclosure and were shown to have little effect on the predicted results. It thus appears that the performance of the models is improved with a relatively fine zoning particularly in the near burner region. Since the final zone

arrangement is a function of the furnace geometry and heating application no general guidelines can be drawn for zoning. Because little improvement has resulted from increasing the number of zones from 37 to 50 it was decided to use the 37 gas zone model in the remainder part of this chapter.

This 37 gas zone model was initially used to assess the effect of neglecting the heat losses through the refractory walls and roof by including one-dimensional steady-state conduction losses through the refractory structure in the calculation. This involves specifying an outside ambient temperature and a convective heat transfer coefficient at the external surface of the lining as well as the conductive thermal resistance for the roof and walls. The overall impact on the model results is shown is Figure 8.14 and Table D.17 which present data for slabs discharged with a top surface temperature of 1250°C.

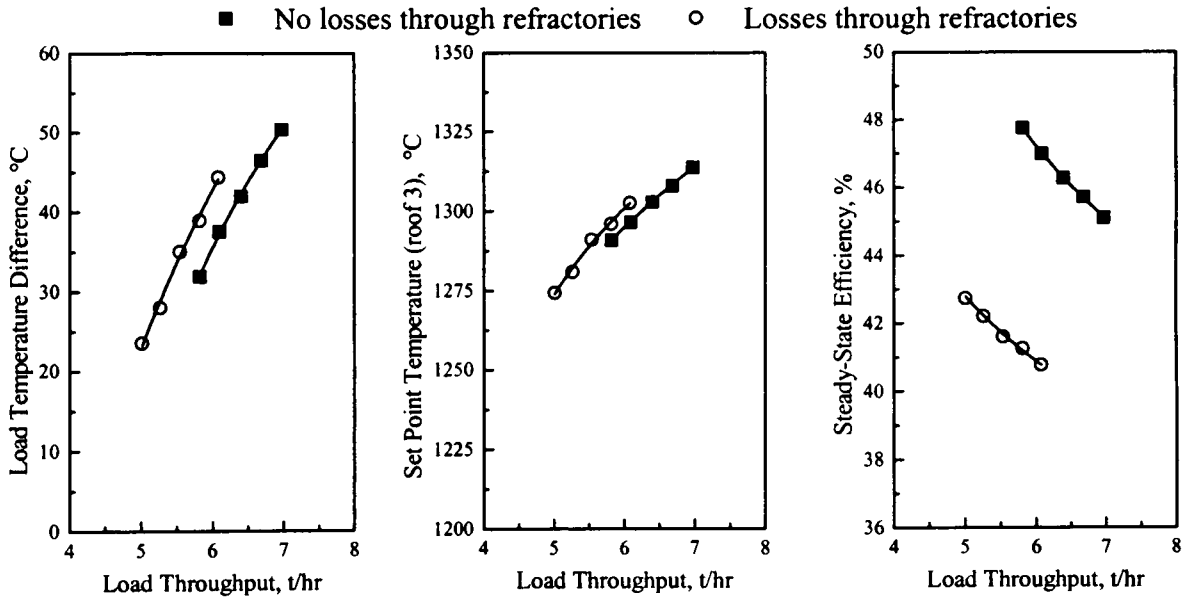

Figure 8.14 The Effect of Wall and Roof Heat Losses in the Overall Model Performance

Allowing for heat losses through the refractories results in approximately 7°C higher top-to-bottom temperature differences in the load at discharge for the same production rates. Lower throughputs and/or higher thermal inputs are therefore required to achieve a specific temperature gradient when compared with the adiabatic lining case. Slightly higher set point temperatures are also required when accounting for the losses through the walls and roof and this is probably a consequence of the increase in thermal input which results in hotter zones close to the burners near the control system. Allowing for wall heat losses has a more significant effect on the furnace thermal

efficiency, see Figure 8.14. Thus at a throughput of 6t/hr, the efficiency is reduced from approximately 48% to 41%. This follows because higher thermal inputs are required to produce the steel bars at the desired discharge conditions as a result of overcoming the losses through the refractory surfaces. This exercise illustrates that the trends in the data are similar for the adiabatic and non-adiabatic cases. Due to the relatively small differences in the predictions the remaining simulations were carried out considering adiabatic wall and roof surfaces.

8.5 Application of the Steady-State Model

The steady-state model can be applied to identify and evaluate opportunities for improving the overall furnace performance. This model enables the effect of changes in furnace design and operation to be quickly assessed. The model was thus used to predict the temperatures within the steel bars at discharge, as well as the furnace thermal efficiencies, for a range of production rates. The inclination of the burners was varied and the furnace lengthened to examine the effects of changes in furnace-burner geometry. The effect of varying the position of the roof temperature control sensor (which is used to control the thermal input to the burners) relative to the burners was studied. The burners were usually supplied with cold, ambient temperature air but in one case preheated combustion air was employed to assess the benefits from recovering energy from the hot exhaust gases. Since crude assumptions were made with regard to the convection heat transfer estimations the model was applied to investigate the importance of changes in the convective heat transfer coefficient on the performance of the furnace.

8.5.1 Burner Orientation

Figure 8.15 shows the evolution of the load surface temperature along the length of the furnace for two different burner orientations and fixed throughput and burner thermal input. In the first case horizontal firing of the burner was maintained but in a second simulation a downward inclination of 20° was considered so that the burners fired towards the surface of the steel bars near the discharge end of the system. As expected, higher temperatures are predicted for the load at discharge when employing inclined burners. This behaviour, which has already been observed in the transient simulations, is a consequence of the flow pattern generated by this type of burner. In this case relatively hot combustion products flow near the load in comparison with the

relatively cooler flows predicted with the horizontal burners. Thus under the same operating conditions, the rates of heat transfer to the load are increased with inclined burners.

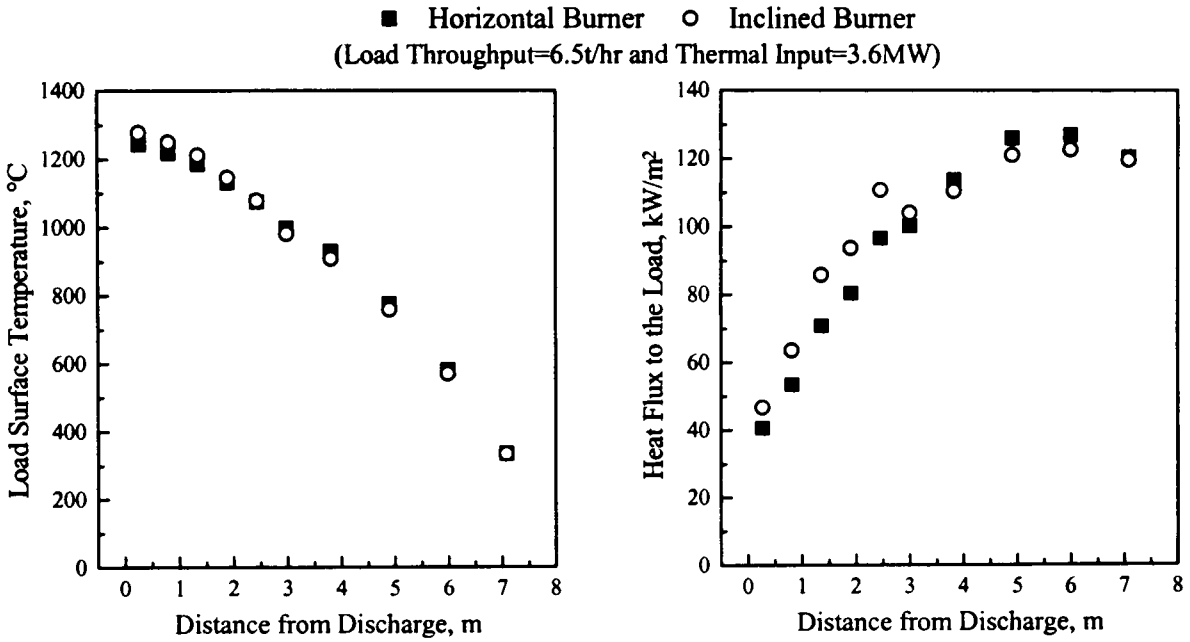

Figure 8.15 The Effect of Burner Orientation on the Load Surface Temperature and Heat Flux Profile

The effect of burner orientation on the overall furnace performance when operated to discharge bars at 1250°C is displayed in Figure 8.16 and listed in Table D.18.

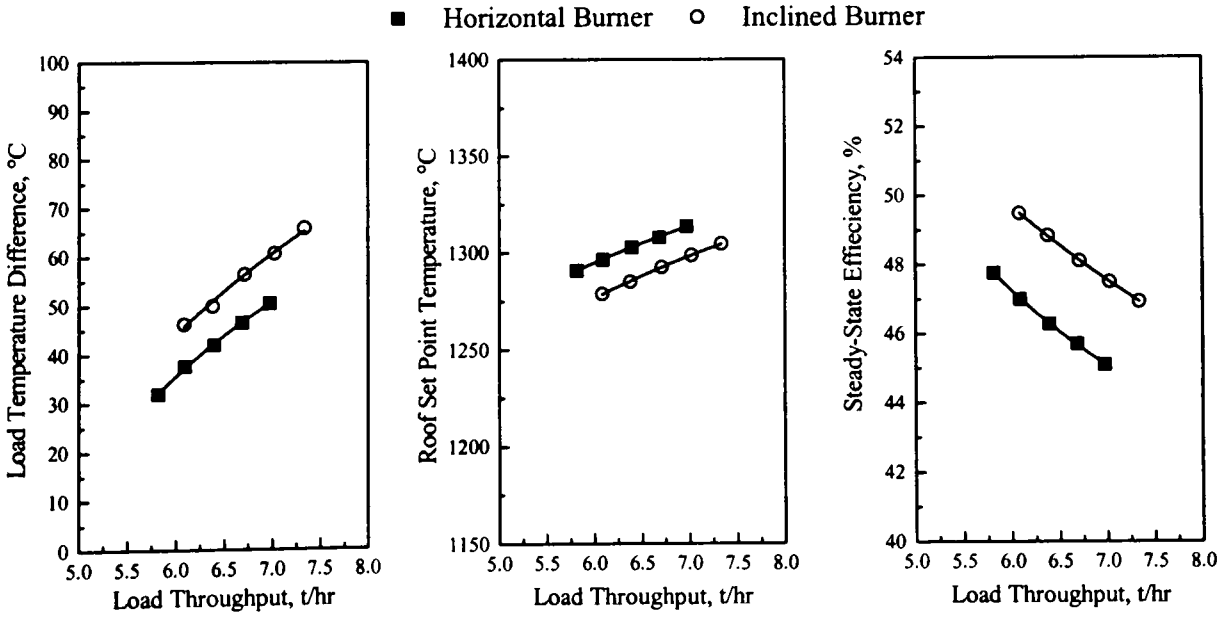

Figure 8.16 The Effect of Burner Orientation on the Overall Steady-State Furnace Performance (Discharge Surface Temperature=1250°C)

For both burner conditions larger temperature gradients in the bars are obtained at the higher productions rates because under these conditions conduction through the steel bars is limited by the short residence time for the load in the furnace despite the higher thermal inputs which were required to achieve the desired output condition. Load temperature top-to-bottom differentials are larger for the inclined burners. These result from the lower thermal inputs which are used in the inclined case to produce steel bars at the desired throughput, see Figure 8.17, and this leads to higher top-to-bottom temperature differences. Thus for the same production rates, the use of horizontal burners results in load temperature differences which are approximately 20% lower than those with inclined burners. The load temperature uniformity with the inclined burners can be improved by operating with a lower load throughput. Consequently, to discharge the load with a top-to-bottom difference of 50°C, the furnace throughput would need to be reduced to 6.3t/hr when compared with 7t/hr in the horizontal burner case.

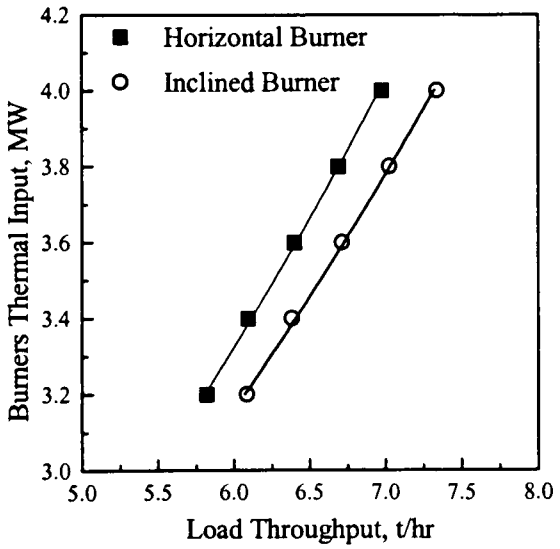

Figure 8.17 Variation of the Furnace Thermal Input with Load Throughput for the Two Burner Orientations

The lower thermal inputs which are required with the inclined burners result in lower temperatures in the enclosure particularly for the roof zones near the control sensor where relatively cool recirculated gases flow. This corroborates the trends in the transient predictions where the use of lower set point temperatures was also found for the inclined situation. Increasing the production rate results in all cases in increased temperatures for the roof surface acting as the control set point because under these conditions higher thermal inputs are required to achieve the load discharge condition.

Higher thermal efficiencies are achieved with inclined burners since less fuel is consumed at specific production rates. It is worth noting, however, that this improvement in energy utilisation is at the cost of greater non-uniformity in load temperature The efficiency decreases in both cases with increasing load throughput since higher thermal inputs are required.

The predictions of the steady-state model should be compared with those of the transient model following a long period of operation. Thus these models were compared in the horizontal burner case for two set point conditions. In the steady-state model the bottom of the load was allowed to lose heat to the hearth to more closely match the transient model conditions. Conduction through the furnace walls and roof was determined by calculating a one-dimensional steady-state heat loss through the refractory structure. The values for the discharge temperature and temperature differences in the load in the transient simulation were taken as those predicted at the end of the 20 hour production period, see Table 8.2.

Table 8.2 Comparison of the Predictions for the Steady-State and Transient Models

Simulation Type	Load Discharge Temperature (°C)		Load Temperature Difference (°C)		Specific Fuel Consumption (GJ/t)	
	STP=1300°C	STP=1380°C	STP=1300°C	STP=1380°C	STP=1300°C	STP=1380°C
Transient	1225	1325	60	50	0.68	0.82
Steady-State	1238	1339	50	42	0.64	0.78

Slightly higher surface temperatures at discharge are obtained with the steady-state simulation and this is probably because in the transient simulation the steady-state conditions have still not yet been fully reached since the wall surface temperatures are still gradually increasing. This effect is illustrated in Figure 7.22 where small increases in load discharge temperature are still observed towards the end of the simulation period. This is, however, less pronounced at the lower set point condition where lower output temperatures are predicted. Lower temperature top-to-bottom temperature differences were obtained for the load at discharge in the steady-state simulation. This may well be caused by the hearth not having reached thermal equilibrium in the transient predictions. Any resultant differences in the rate of conduction into the hearth will have a marked effect on the temperature of the under-surface of the bars. The higher load discharge temperature predicted in the steady-state model results in reduced

specific fuel consumption since in this case for similar throughput and firing conditions more heat is transfer to the load. The values for the transient model were obtained by calculating the specific fuel consumption over a one-hour period towards the end of the simulation. In addition higher heat losses to the "still transient" lining may also contributed to the predicted higher consumptions in the non-steady state models.

8.5.2 Changes in Furnace Length

The influence of the furnace length on the overall steady-state performance of the system was also investigated. In this study the overall furnace geometry was largely maintained and only the exhaust end of the system extended so that furnace capacity was increased. The 37 gas zone model was thus modified to include more zones at the charging end and consequently 38, 39 and 40 gas zone models were developed see Figure 8.18. This corresponds to the addition of one, two and three volume zones respectively to the original furnace geometry. The dimensions of each added volume zone were identical to those of the volume zone where the exhaust is placed in the 37 gas zone model and plug-flow was assumed in this zones.

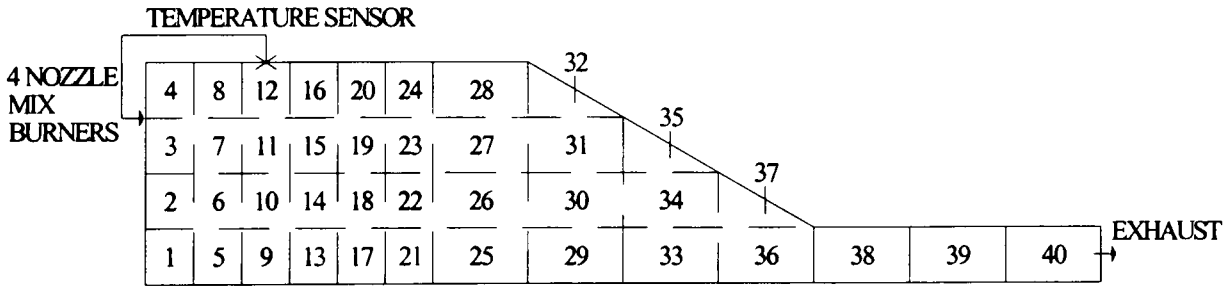

Figure 8.18 The 40 Gas Zone Model Arrangement

Figure 8.19 shows the effect of increasing the furnace length i.e. incorporation of stock preheating on the temperature history of load as it moves through the furnace for fixed throughput and thermal input. As expected, for a given throughput the longer the furnace, the higher the final load top surface temperature. This is because increasing the furnace length increases the load residence time. More energy is recovered from the hot combustion products before they leave in the exhaust. The heat fluxes along the furnace length reach a peak and subsequently decrease towards the exhaust. The heat fluxes at the discharge end decrease as the furnace length is increased as a result of the higher load temperatures at discharge.

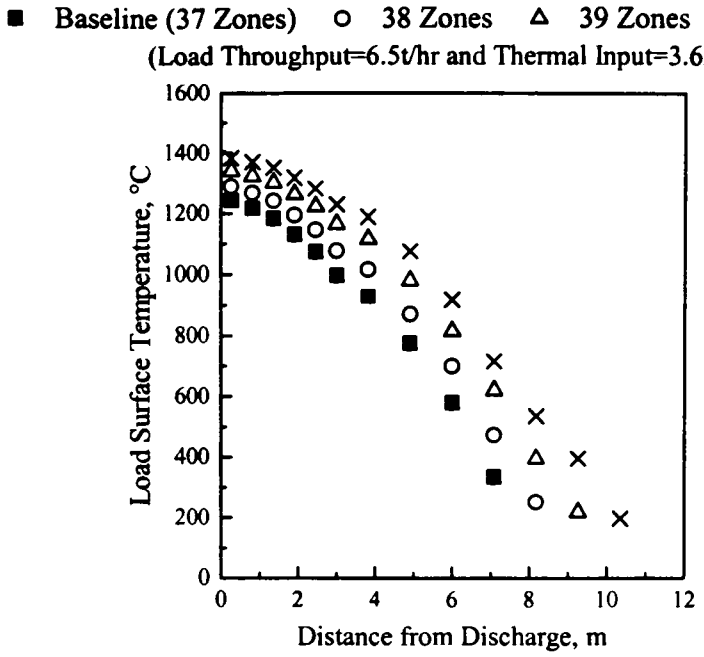

Figure 8.19 The Effect of Changes in the Furnace Length on the Load Surface Temperature and Heat Flux Profile

The performance of the different furnaces is compared in Figure 8.20, see also Table D.19, when producing steel bars at a surface discharge temperature of 1250°C. As the furnace length is increased the load residence time increases so that the load top-to-bottom temperature uniformity is improved. It can be seen that under similar throughput conditions temperature differences in the load decrease with an increase in furnace length.

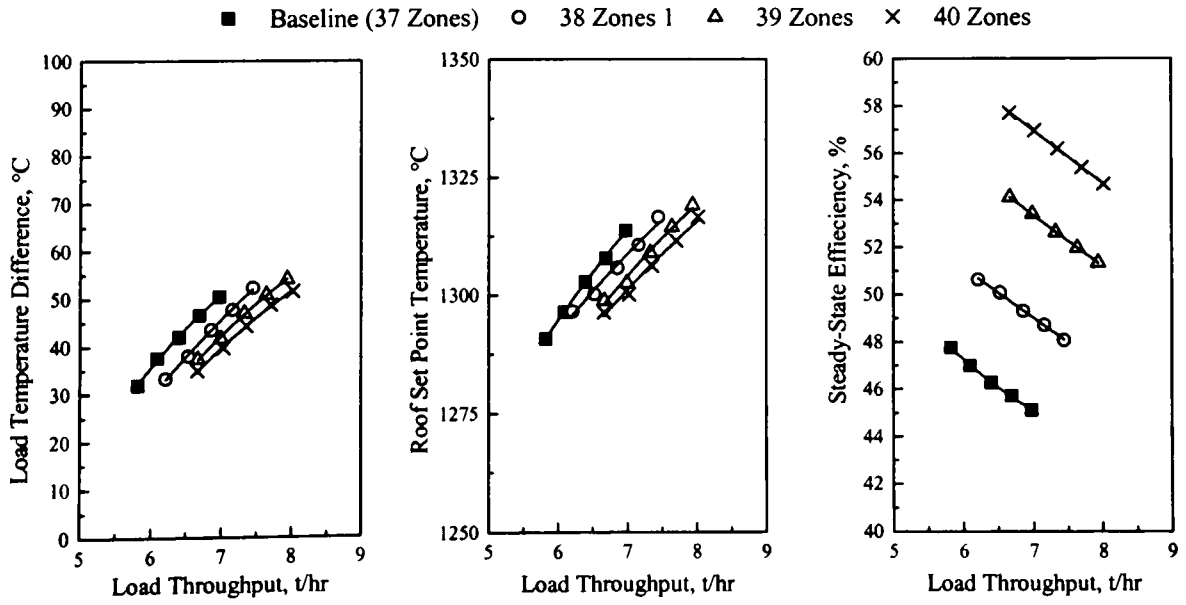

Figure 8.20 The Effect of Furnace Length on the Overall Steady-State Furnace Performance

As observed in Figure 8.19, the increase in furnace length results in high load surface temperatures so that for the same load throughputs, the thermal input to the burners must be reduced if the desired top temperatures are to be achieved, see Figure 8.21.

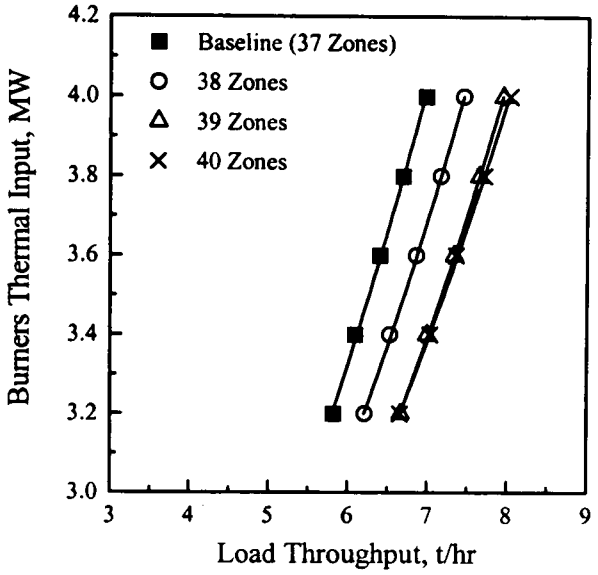

Figure 8.21 Variation of the Furnace Thermal Input with Load Throughput for Different Furnace Lengths (Load Discharge Temperature=1250°C)

Alternatively as the furnace length is increased similar temperature gradients in the load can ensue at higher throughputs for the same thermal input conditions. There is relatively little difference in the throughput which can be achieved with a specified thermal input once two additional volume zones have been added. This seems to suggest that further increases in the furnace length will not substantially affect the final temperature gradient.

Increasing the furnace length has little affect on the temperature of the roof surface acting as the control with the set point varying less than 1%. Slightly lower set point temperatures are predicted for the longer furnaces because of the lower thermal inputs used and this also leads to higher furnace efficiencies in these cases. The predicted efficiencies are shown to increase with increasing furnace length since in these systems stock preheating is an effective form of heat recovery from the combustion products. In all cases the efficiency is reduced at higher throughputs because under these conditions the input to the burners is increased and the furnace is "driven harder".

8.5.3 Position of the Control Sensor

Metal reheating furnaces are usually controlled by means of a thermocouple sensor(s) mounted at the hot face of the roof which adjusts the thermal input to the burners to maintain the furnace temperature at a specified set point. In this simulation the position of the control thermocouple was varied to determine the effect on the required set point temperature. Three different positions were considered with the sensor placed in the 2nd, 3rd and 4th roof downstream from the burners. Figure 8.22 and Table D.20 show that the predicted set point temperatures, required to produce bars at a discharge temperature of 1250°C, are significantly affected by the sensor position.

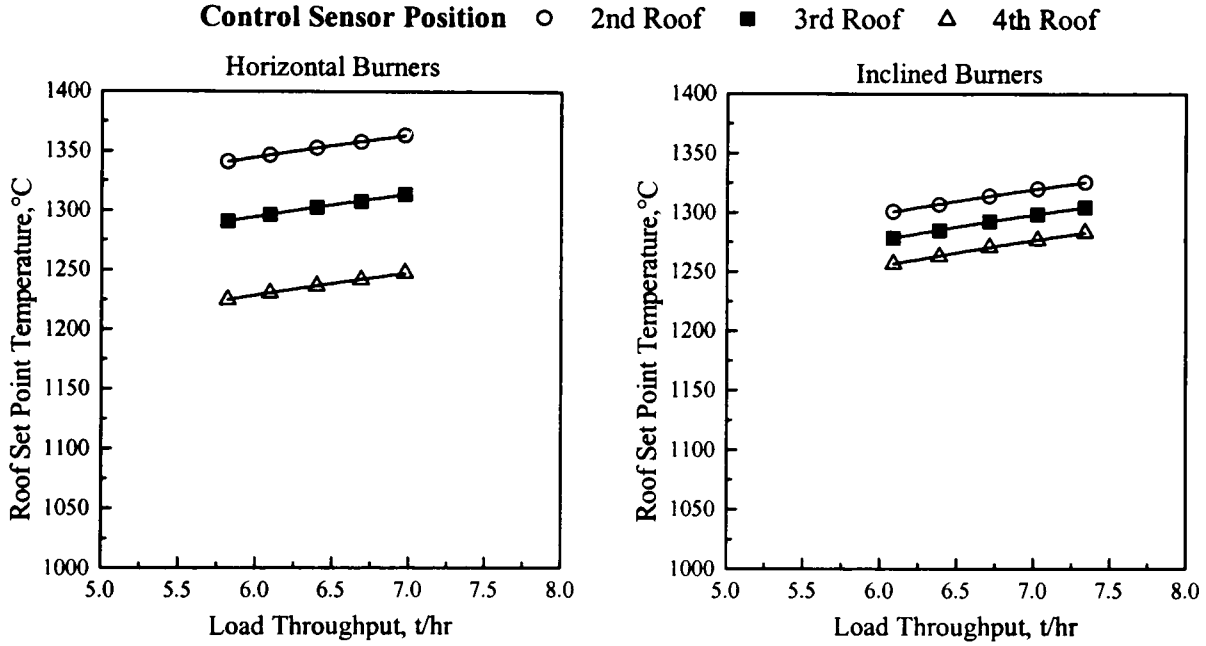

Figure 8.22 The Effect of Sensor Position on the Set Point Temperature at Different Load Throughputs

As indicated in this figure the further away the sensors are from the burners the lower the set points that would be required to produce steel bars at the desired discharge temperature of 1250°C. This is because of the lower temperatures of the upper gas and roof zones further downstream from the burners. Similar characteristics are observed for the inclined burners as the sensor position is varied. However the resultant different flow patterns in which relatively cool recirculated combustion products flow near the roof generally results in lower and more uniform temperatures for these surface zones so that differences in set point temperature for the three positions are reduced. Thus for the inclined burners displacement of the control sensor from the 2nd roof zone to the 4th

results in a set point temperature reduction of approximately 40°C whilst in the horizontal case the reduction is over 110°C. The results clearly indicate that the magnitude of the required set point temperature is dependent on the position of the control sensor with low roof set points required as we move downstream from the burners.

8.5.4 Variation of the Convective Heat Transfer Coefficient

In high temperatures furnaces convective heat transfer is comparatively unimportant (typically <5-10%) and predictions are usually carried out with a crude approximation for the heat transfer coefficient. To confirm the relative unimportance in this present case simulations were performed to assess the effect of different convective heat transfer coefficients on the overall furnace behaviour.

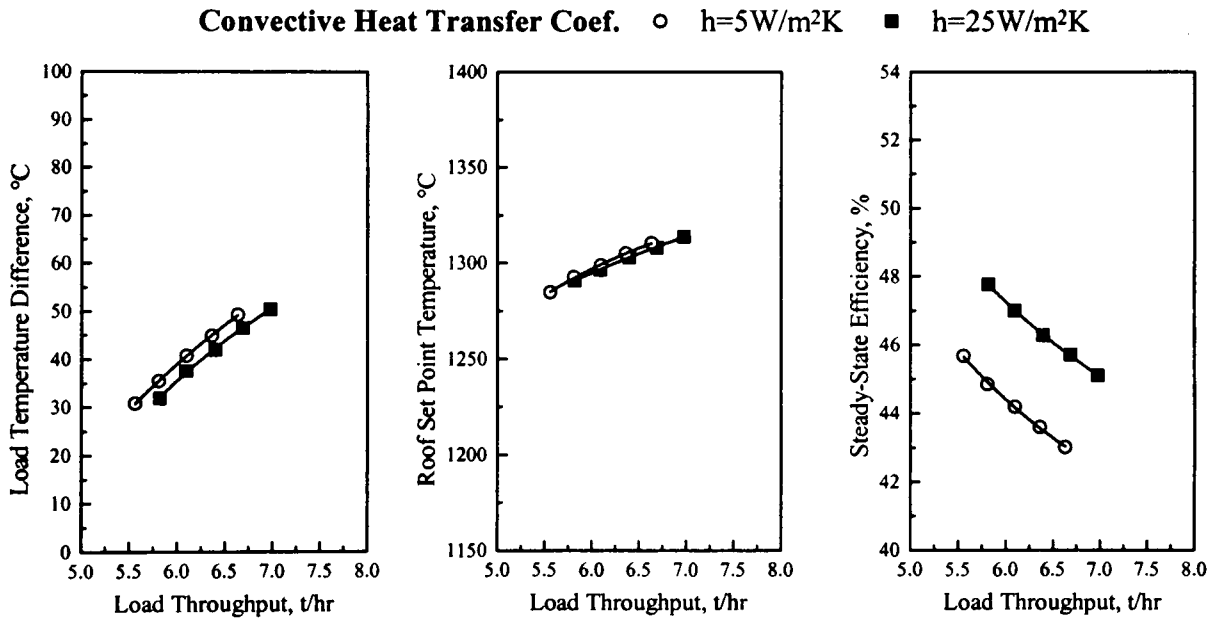

Figure 8.23 The Effect of the Convective Heat Transfer Coefficient on the Overall Steady-State Furnace Performance

The simulations were carried out for two different values, namely 5 and 25W/m^{2}K, which cover the likely range of values adopted in most mathematical models. Figure 8.23 and Table D.21 illustrate the results. The temperature differences in the load at discharge and the required set point temperature at a particular furnace throughput are relatively unaffected as the convective heat transfer coefficient is increased. Only slightly lower temperature differences are obtained with the higher convective heat transfer coefficient since under similar throughput conditions the total heat transfer to

the load is increased due to an increase in convection. This is illustrated in Figure 8.24 which plots the radiative and convective components of the heat transfer to the load along the furnace length. Comparing the two cases it can be seen that increasing the convective heat transfer coefficient produces small changes to the load radiative heat transfer profile with differences mainly for the zones close to discharge. This is because higher convective heat transfer coefficients result in lower flame temperatures for the same heat transfer rate.

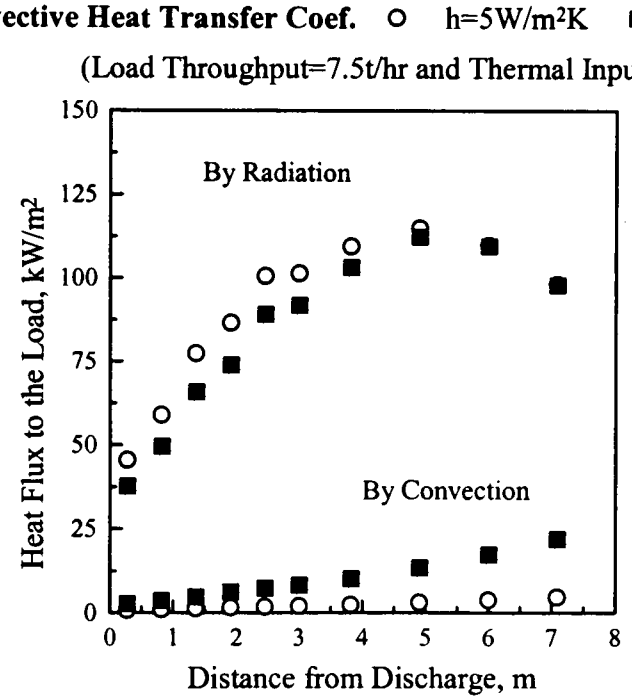

Figure 8.24 The Profile of the Radiative and Convective Heat Flux to the Load

Whilst the radiative fluxes are relatively unaffected, the profiles of the convective heat transfer to the load indicate substantial differences in this mode of heat transfer between the two cases particularly at the exhaust end of the furnace. In general increasing the convective heat transfer coefficient results in an increase of convection along the furnace length but close to the exhaust the predicted increase is more significant. This is a consequence of convection being more important at this "cool" end of the furnace. Overall only a slight increase in energy transfer to the load is predicted.

Variation of the convective heat transfer coefficient is shown to have virtually no effect on the predicted roof set point temperature since the control sensor is close to the burners and hence adjacent to higher gas temperature zones so that the overall heat transfer is not significantly altered. Higher efficiencies are, as expected, found with

higher convective heat transfer coefficients because of the lower fuel consumption in this case. The higher rates of heat transfer predicted with a higher coefficient means that lower burner thermal inputs will be required to provide the same heating rate. Thus in this case the potential gain in thermal efficiency when increasing the convective heat transfer coefficient from 5 to 25W/m^{2}K is about 2-3%. Overall the results seem to suggest that variation in the convective heat transfer coefficients have relatively little effect on the predicted load temperature gradient and roof set point but can be more important in predictions of fuel consumption and furnace efficiency. The improvements in efficiency are mainly due to increases in convective heat transfer particularly at the cooler end of the furnace where the effects were found to be more significant. There is perhaps scope here to look into techniques for promoting higher rates of convection such as the fitting of baffles to increase the velocity of the combustion products near these low temperature regions. In addition radiative heat transfer from the baffles would also improve energy utilisation.

8.5.5 Combustion Air Preheating

Air preheating has long been applied in metal reheating furnaces in an attempt to reduce energy losses in the exhaust gases. Considerable fuel savings can result from recovering some of the waste energy to preheat the incoming air which is supplied to the burners.

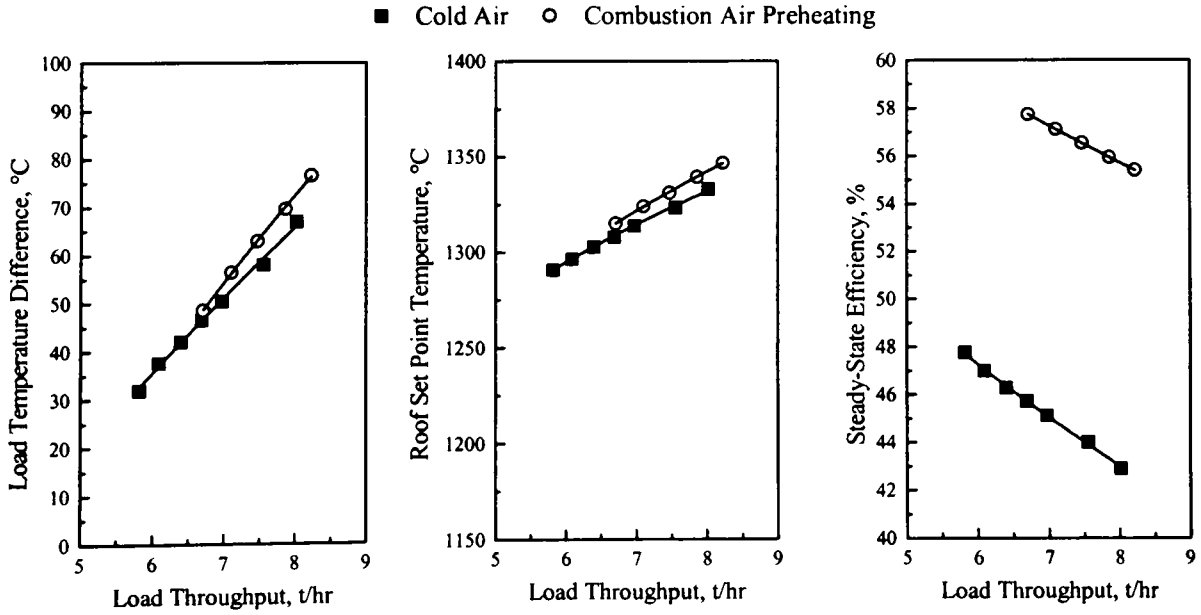

Figure 8.25 The Effect of Combustion Air Preheating on the Overall Steady-State Furnace Performance

The steady-state models were therefore employed to assess the overall advantages of this technique when the furnace is operating continuously to discharge load at a surface temperature of 1250°C. Combustion air preheating using a recuperator in the exhaust with an effectiveness of 30% is predicted to have only a small influence on the load temperature differences at discharge and on the temperature of the roof set point, see Figure 8.25 and Table D.22. This is because preheating results in a lower fuel input to the burners and has less affect on the overall pattern of heat distribution. Air preheating provides higher flame temperatures so that lower thermal inputs can be employed under similar throughput conditions to produce the same heating rates. Slightly lower load temperature gradients are predicted for the cold air burners at higher throughputs.

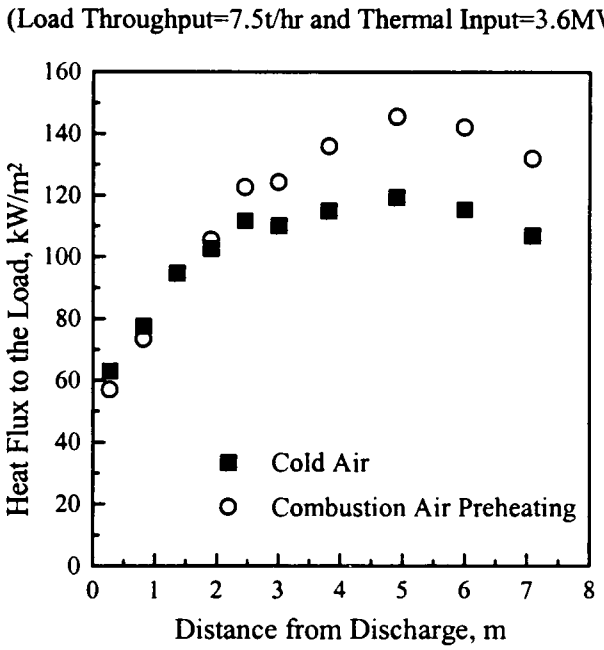

Figure 8.26 The Effect of Heat Recovery on Load Heat Flux Distribution

Figure 8.26 plots the load heat flux distribution along the furnace length and the enhancement is shown to be particularly important at the cooler end near the exhaust where the temperature difference between the gas zones and load surface is large. Because of the higher heat transfer rates and consequently lower thermal inputs for the same throughput conditions, a substantial increase in the steady-state efficiency is predicted when employing heat recovery. The predictions for heating the load to 1250°C with heat recovery suggest substantial efficiency increases. As previously seen the efficiency decreases with increases in throughput due to the higher thermal inputs required under these conditions.

The combined effects of combustion air preheating and increasing the length of the furnace on the efficiency was also assessed, see Figure 8.27 and Table D.23. This presents the predicted steady-sate efficiencies for the baseline furnace geometry and the longest case considered previously in section 8.5.2, i.e. adding a further 3 volume zones at the charge end.

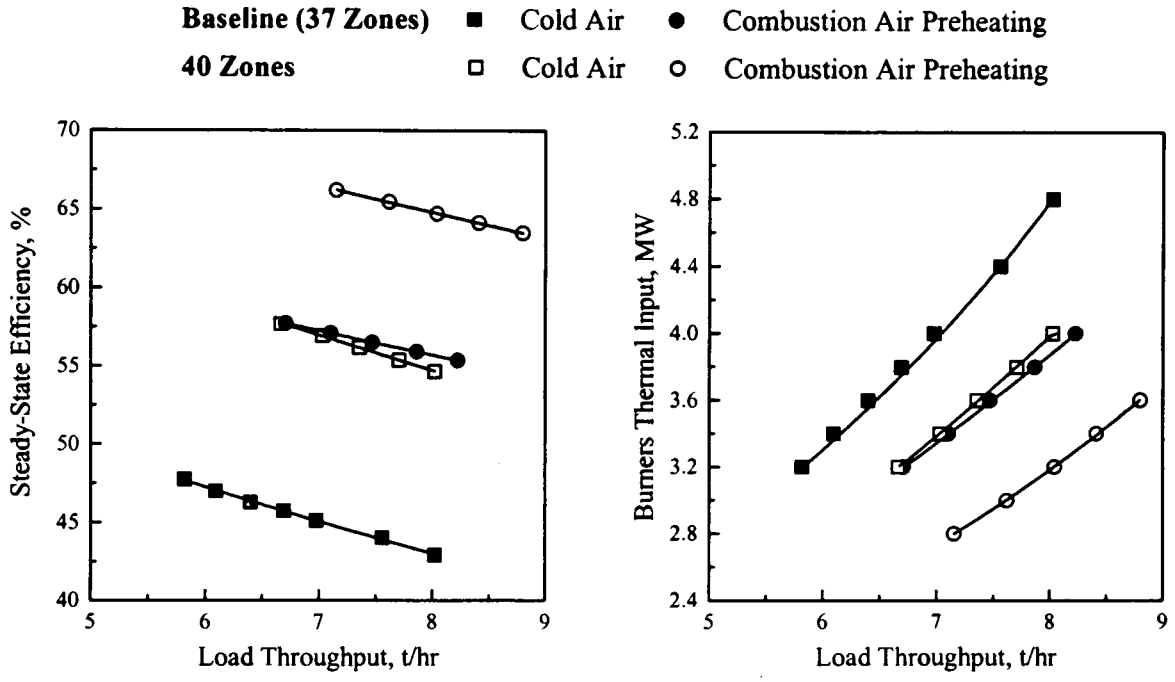

Figure 8.27 The Effect of Furnace Length and Combustion Air Preheating on the Predicted Efficiency

The potential improvements in efficiency due to combustion air preheating were found to be dependent on the furnace length. Thus the increase in efficiency due to heat recovery is smaller with the longer furnace. For example the predicted improvement in efficiency at a throughput of 7t/hr is approximately 18% for the longest furnace configuration in comparison with the 26% increase in the shortest furnace case. This is a consequence of the higher exhaust temperatures with the shortest baseline system. Since preheating of the combustion air is related to the temperature of the exhaust gases, an increase in this temperature results in higher preheat temperatures and hence greater reductions in fuel usage. Larger efficiency improvements are, therefore, expected in furnaces where the temperature of the exhaust combustion products is high. The results also demonstrate the important role played by load preheating in the longest furnace geometry. The benefit of greater load recuperation resultant from increasing the furnace length is comparable to employing air combustion preheating.

8.6 Conclusions

Steady-state zone models are much faster to run than transient versions and are adequate for predicting performance of furnaces operating continuously at constant throughput and thermal input. Initially comparisons were drawn between 2D models and LFMs to assess the differences arising from the use of the different models. These showed that 2D models are necessary when the flow of combustion products cannot be represented by a one-dimensional plug-flow. Sensitivity tests were then carried out to evaluate the effect of different 2D zoning arrangements on the overall steady-state model predictions. As a result a 37 gas zone model was employed to investigate the influence of operating parameters on the performance of a gas-fired furnace heating metal bars to a discharge temperature of 1250°C. The model demonstrated that changes in burner orientation have an effect on the furnace performance mainly because of differences in the flow patterns which affect the profile of heat transfer distribution. Increasing the furnace length was shown to yield significant improvements in the thermal efficiency because of the effects of load preheating. The necessary roof set point temperatures at any specific furnace throughput were found to be dependent on the position of the control sensor. Higher temperatures are required as the sensor is displaced closer to the burners and hence adjacent to a hotter gas zone. Variations in the assumed convection heat transfer coefficients were shown to mainly affect the furnace efficiency and the study has also highlighted the need to enhance convection at the cooler regions of the furnace. The benefits of combustion air preheating were shown to be significant in terms of fuel savings and it was further demonstrated that any potential enhancement in furnace efficiency from employing heat recovery is more important in applications with higher exhaust temperatures and hence lower efficiencies. In general predicted efficiency values for all cases studied in this chapter were somewhat higher than would occur in practice and this is probably due to the assumption of adiabatic refractory surfaces. This assumption, however, does not affect the conclusions that can be drawn with regard to furnace operation.

CHAPTER NINE

DIFFUSION FLAME MODELS

9.1 Introduction

The models described in previous chapters have all been developed for nozzle mix burners where combustion is assumed to be complete in the zone adjacent to the burner. The resultant intense mixing generally produces a short, compact non-luminous flame. In this case it is only necessary to represent the flow of combustion products within the furnace chamber and heat transfer for adequate prediction of the thermal behaviour. These mathematical models are, however, of limited use in furnaces which are end-fired by long diffusion flames. In this situation the lower rates of mixing produce a much longer flame with combustion and hence heat release occurring progressively along the furnace length. The furnace thus contains a hot flame core surrounded by regions of relatively cool recirculating combustion products. The two-dimensional zone models were modified to provide a more exact representation of a diffusion flame by treating the combusting jet and recirculated products as separate zones. An isothermal ambient CFD computation provided information regarding combustion heat release by simulating the air-fuel mixing process and assuming that "mixed-is-burnt". The models were then used to assess the effect of flame length and heat release profile on the heat flux distribution and thermal performance of the gas-fired metal reheating furnace.

9.2 Turbulent Diffusion Flames

Diffusion flames arise from the combustion of initially physically separated sources of fuel and oxidant which react as they mix. This can occur either in laminar or turbulent form and combustion takes place at the boundary between the fuel and oxidant. Since most combustion applications use turbulent flames it is this class which is of greater relevance. The modelling of turbulent diffusion flames often found in furnaces, boilers and other high temperature equipment is complex because with these flames energy release is primarily limited by the rates of mixing between the fuel and the oxidant. With poor mixing conditions the flame extends along the furnace downstream from the burners and heat is gradually released due to combustion. With oil flames poor mixing can result in the formation of large amounts of soot (small particles of carbon) which gives these flames their distinctive yellow colour and luminosity. However most natural gas diffusion flames are in effect non-luminous. The presence of soot also results in an increase of the emissivity of the flame. Therefore to successfully predict the rates and distribution of heat transfer from a turbulent diffusion flame it is essential to determine the mixing rate of the reactants and hence the flame length and the combustion heat release profile.

Combustion depends upon the rate of mixing between the combustion air and the fuel and this mixing process is markedly affected by the furnace aerodynamics so that these two phenomena are strongly coupled and must be determined simultaneously. There is, however, no direct method of obtaining this information within the simple zone models so that CFD models, physical modelling techniques and empirical correlations are often employed as alternatives to calculate the flame characteristics and flow patterns. The advantages and disadvantages of CFD models have already been discussed elsewhere in this thesis so that they will not be included here. It is, however important to emphasise that their use to simulate combustion processes is now reasonably developed and at the moment they can provide information on velocities, temperatures and concentration fields. However there is still uncertainty regarding the available combustion sub-models whose fundamentals are not yet fully understood and this greatly limits the applicability of these models. In addition CFD models require a high level of expertise by the user and are computationally expensive for practical design of industrial furnaces.

As an alternative in zone models, flow and combustion data can be estimated from empirical correlations or from isothermal physical modelling. Published correlations are based on the theory of mixing jets [1] and are fitted to observed and measured values taken from real plant or from model tests. Thus, an example, correlations exist to calculate the length of a flame. The flame length, which is a function of the mixing rate, defines the length in which combustion takes place so that it is possible to confine the heat release to a certain number of zones. Whilst most of these empirical expressions can adequately describe simple furnace geometries and firing systems, their representation may not be appropriate when modelling more complex configurations. In this case flow and combustion patterns can be determined using simple isothermal models.

Isothermal physical models have been employed to investigate overall flame characteristics by simulating the mixing process. Evidence suggests that isothermal flow studies without accounting for combustion and heat transfer can indeed provide reasonable replication of the combustion flow features [1]. One such method is the acid/alkali technique which simulates the mixing in the flame by using an acid and alkali to represent the air and the fuel respectively. When the acid and alkali mix, the coloured indicator becomes clear when neutralised after mixing so that a visual simulation of the diffusion flame is obtained. This technique is based on two concepts:

a) in a free expanding jet, velocities and concentrations are independent of the Reynolds number providing the flows remain turbulent.
b) combustion in a turbulent diffusion flame is governed by the mixing of air and fuel, the "mixed-is-burnt" concept.

Based on the same principles ambient isothermal CFD computations can simulate the flow and mixing process of a natural gas diffusion flame. In this case natural gas and air are injected separately into the model either through parallel nozzles or through concentric nozzles with the central jet carrying the fuel and the co-axial annular jet the air. Because simulations are isothermal appropriate scaling and similarity criteria must be considered in the model. The final model can therefore provide quantitative and visual information on flame length, shape, heat release and flow of the combustion products. This approach, although less common than a full CFD simulation, is considered adequate since the main interest here is to obtain complementary flow and combustion data to apply to the less complex zone models so that estimates of the transient behaviour of high temperature equipment can be made.

9.3 The Need to Represent Heat Release

It was demonstrated in Chapter 7 the importance of adequately representing the furnace flow patterns and the control system when simulating the transient performance of a gas-fired metal reheating furnace. While these previous models have all been developed under the assumption that combustion is complete at the point of injection, combustion in long diffusion flames extends throughout the enclosure so that a gradual release of energy occurs. It is therefore likely that the heat transfer characteristics in these systems will also be dependent on the flame combustion heat release. Consequently to assess its influence on the overall heat transfer of metal reheating furnaces, the zone models were modified to allow for combustion heat release to take place at each gas zone containing the flame. As previously mentioned, heat release patterns must be available as input to the zone models so that two distinct methods were employed to derived this information. In the preliminary zone models an exponential variation of the heat release, Q_{HR}, with axial distance, x, was assumed [2, 3]:

$$Q_{HR} = 1 - \exp\left\{-4.6\left(x / L_f\right)\right\} \text{x} \textit{Thermal Input in the Fuel} \qquad (9.1)$$

The constant 4.6 means that 99% of the heat release has occurred at the end of the flame i.e. when $x=L_f$. The length of the flame, L_f, can be determined either from existing correlations or by physical modelling. The objective of this initial study was to find the overall variation in furnace performance when energy release due to combustion is taken into account.

The 37 gas zone model employed in the nozzle mix burner studies was initially selected to describe the system. However the zoning system employed in the near burner region means that in the case of a long flame, the jet would be contained in a series of zones along the length and height. Since Equation 9.1 can only provide information on the axial heat release distribution it was decided to refine the near burner zones so that the flame jet is confined within the height of each axial zone. Consequently, a 46 gas zone model with a total of 128 surface zones was developed as shown in Figure 9.1.

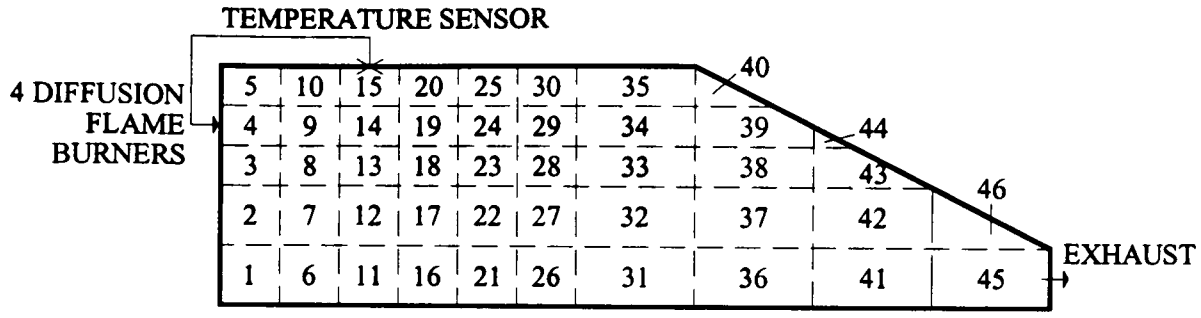

Figure 9.1 The 46 Gas Zone Arrangement

As previously mentioned it is important to know the flame length as this immediately restricts combustion to a specific number of zones. In these initial trials the flame length was not derived from any of the methods referred to previously but was assumed at a specific value. This is because initially the study concentrated on investigating the general effects of combustion heat release and not on modelling specific conditions. Assuming a maximum flame length of 4.36m, which corresponds to the boundaries of one of the axial zones, it is possible to allocate the fractional heat release due to combustion within the zones using Equation 9.1. The resultant distribution can be seen in Figure 9.2 with almost half of the total energy input released in the first zone immediately adjacent to the burners. The decay of heat release along the flame length is very rapid with 90% of combustion energy released in the first half of the flame.

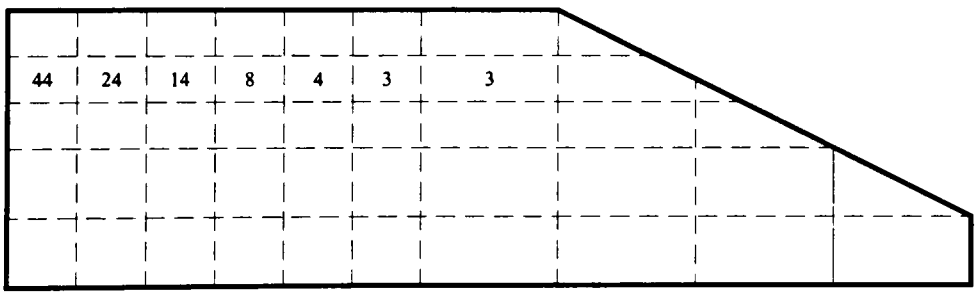

Figure 9.2 Exponential Heat Release Distribution (values are % heat release in a zone)

The simple diffusion flame zone model was then employed to assess the effect of combustion heat release on the behaviour of the metal reheating furnace following a cold start-up. The model predicted furnace start-up times and corresponding fuel consumptions and load temperatures when again heating 64mm thick mild steel bars to a nominal discharge temperature of 1250°C. The relative mass flows into and out of

each zone were determined, as before, using an isothermal ambient CFD computation, the details of which will be given in the next section. Comparisons of the predictions with a horizontal nozzle mix burner simulation for this 46 gas zone model are presented in Figure 9.3 and Table D.24 (see Appendix D) for different set point temperatures.

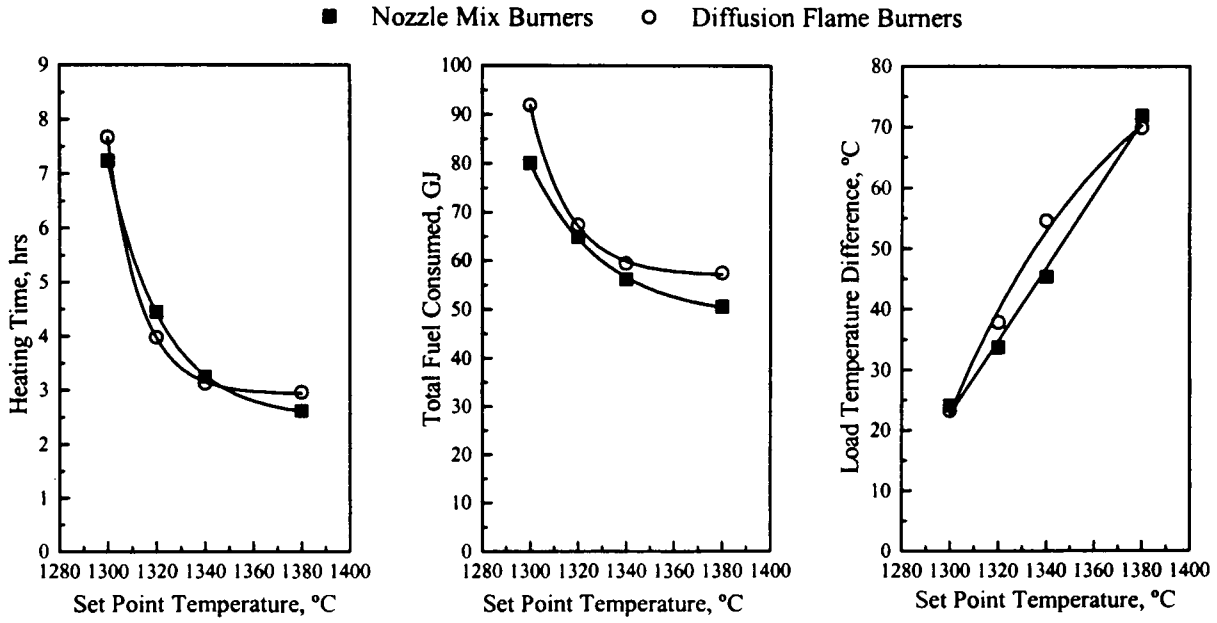

Figure 9.3 The Effect of Combustion Heat Release on the Overall Furnace Performance

As expected, the predicted start-up heating times for initial discharge of a hot bar increase as the set point is reduced due to modulation of the thermal input. The increase in start-up time is more significant with nozzle mix burners as indicated by the steeper profile of the curves in Figure 9.3. The burner modulation effect is therefore greater with this type of model suggesting that temperatures in the near burner region close to the control device are higher than the ones predicted by the diffusion flame model. Similar but less marked trends are predicted for the overall fuel consumption with nozzle mix models predicting lower values at all set points. Again illustrates the higher degree of burner modulation occurring with this type of burner. Profiles of temperature distribution within the load are consistent with the cases with longer predicted start-up times resulting in lower differentials between the top and bottom of the bars at discharge.

Despite the number of simplifications incorporated in the simple diffusion flame model, the results indicate that a furnace fitted with diffusion flame burners has different characteristics. It is known that the flow of combustion products influences the

mixing and hence the flame characteristics. In the current diffusion flame model the mixing and flow patterns were not related as the heat release pattern was given by an empirical expression and the flows determined from an isothermal CFD calculation. Thus it is likely that the overall heat transfer predictions will differ from reality. Nevertheless this preliminary exercise demonstrates that it is important to account for combustion heat release within the enclosure with diffusion flames. Therefore to accurately account for combustion energy release good representation of the mixing and flow patterns must be sought. Consequently 3D isothermal CFD simulations were used to provide the flow and mixing profiles inside the furnace chamber.

9.4 Isothermal CFD Simulations of Mixing in a Diffusion Flame

9.4.1 Geometry Definition

The overall furnace representation was based on the 50 blocks structure used in the nozzle mix burner simulations so that only half of the furnace geometry was considered. With this approach it is possible to increase the number of grid cells to improve the final solution while simultaneously minimising the overall computational requirements. While the exhaust set up characteristics remained the same as in the nozzle mix models, the fuel and air in this case were not premixed so that two separate inlets, one for the fuel and other for the air, were defined. Efforts initially concentrated on representing the co-axial injectors as circular nozzles. This, however, proved to be a difficult procedure within the geometry construction options of the pre-processor module so that it was decided to model the air inlet as a circular nozzle leaving the fuel inlet to be manually assigned. This means that it is possible to specify fuel inlet features such as the location, dimensions, fuel type, velocity, etc. by grouping individual cells of the grid into which the geometry was subdivided. The final model includes, therefore, an exhaust and two burners each consisting of a circular inlet for the air in which the middle cell was modelled as the natural gas nozzle, see Figure 9.4.

To ensure the CFD solution is independent of the grid design, the 50x36x20 grid used to model the nozzle mix burners was initially adopted. This grid arrangement, which is denser in the near burner region where large variations are expected to occur, was however too coarse to adequately represent the fuel inlet stream so that finer meshes were tried. The refinements aimed to reduce the fuel input area by increasing the number of subdivisions in the near burner regions so that increasingly smaller middle cells were obtained for the fuel inlet.

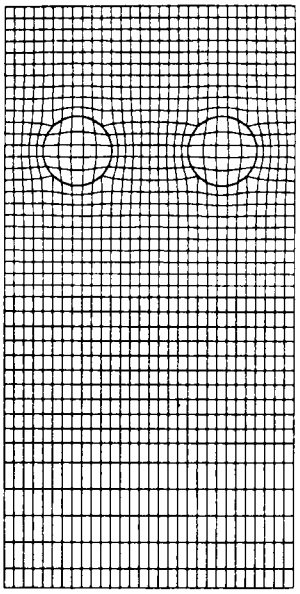

Figure 9.4 CFD Grid Representation of the Burner Inlets

In principle, the smaller the cell size the more accurate the solution becomes but this inevitably increases the computational effort. Therefore the level of refinement necessary to resolve the fuel burner geometry to compute the burner operating conditions was limited and only small improvements were possible. Consequently a final non-uniform grid of 50x41x30, see Figure 9.5, comprising a total of 61500 cells was selected i.e. an increase of more than 70% in the total number of cells. The final burner arrangement corresponds to an air inlet nozzle diameter of 0.12m where the middle cell which was defined to simulate the fuel nozzle corresponds to a diameter of 0.044m.

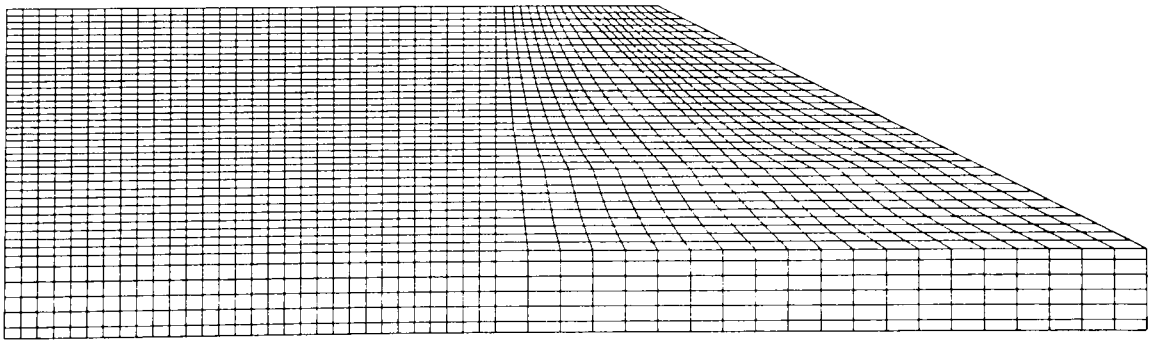

Figure 9.5 CFD Grid Arrangement for the Diffusion Flame

9.4.2 Model Description

As with the nozzle mix simulations a finite volume commercial code CFX 4.2 was used to simulate the 3D ambient isothermal mixing process between the air and the

natural gas. The standard k-ε model was used to model turbulence and boundary conditions were defined as in Chapter 4. The thermophysical properties for both air and fuel were obtained from the CFX fluid database. Since data was not available in this software for natural gas, the properties of its main constituent methane (CH_4) were used. The overall operating conditions for the baseline CFD mixing model are listed in Table 9.1. A typical CFX command file for the diffusion flame model is presented in Appendix C.

Table 9.1 Operating Conditions of the CFD Isothermal Mixing Model

Fluid	Air	Natural Gas
Temperature (°C)	20.0	20.0
u velocity (m/s)	79.5	100.0
v velocity (m/s)	0.0	0.0
k-ε turbulence model		
k (m^2/s^2)	12.6	20.0
Dissipation Length Scale (m)	0.095	0.063
Total Mass Flow per Burner (kg/h)	17245	942
Reynolds Number	$4x10^5$	$1.4x10^4$
Distorted Diameter (m)	0.26	0.07
Burner Angle	0°	
Excess Air (%)	10	

High velocities were used to ensure good mixing between the reactants so that combustion is complete within the enclosure. Convergence of the problem was very difficult so that to avoid divergence in the iterative solution various relaxation methods were employed during the course of the calculations to slow down changes between iterations. Normalised residuals, which test the error in the continuity equation, were of the order of 10^{-4}. Figure 9.6 shows the typical pattern of variation of the mass source residual with the progress of calculation for the CFD isothermal mixing model. Some oscillations are present in the beginning of the calculation but these eventually die out and convergence is finally achieved. The simulations were carried out on an SUN ULTRA-1, SPARC workstation. It was possible for calculations to be interrupted and restarted later with the values from the previous runs so that a total of 3000 iterations were performed. Typical overall convergence times were of the order of 15 hours.

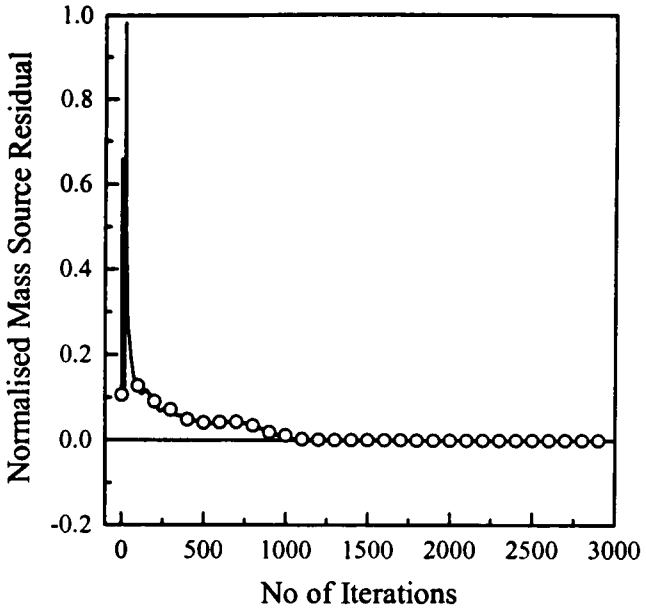

Figure 9.6 Variation of the Mass Source Residual

The model provided information on the furnace flow and mixing patterns inside the reheating furnace and a visual representation of the flame shape was possible. The effect of excess air on the mixing pattern and hence flame length was also studied.

9.4.3 Flow and Mixing Patterns

The predicted velocity vectors in the furnace are displayed in Figure 9.7 for three vertical planes normal to the wall containing the burners. The general flow arrangement, which is similar to the one described previously for the nozzle mix burners, is basically two-dimensional except in the vicinity of the burners where large variations occur. The main aerodynamic characteristic of the co-axial jet system of natural gas and air is a large recirculation zone in the central region of the enclosure below the jet. The recirculation causes the combined jet of fuel and air streams to deflect slightly upwards and attach over most of the roof and inclined surfaces. An outer smaller recirculation zone was also predicted in the roof region close to the burners as a consequence of entrainment of the surroundings into the jet. The CFD diffusion flame model with a different burner arrangement has produced flows which are somewhat different from the ones obtained with the nozzle mix model. The co-axial jets generated a larger central recirculation zone which extended through the length of the furnace whilst the single nozzle produced recirculation zones which surrounded the jet and rotated in opposite directions.

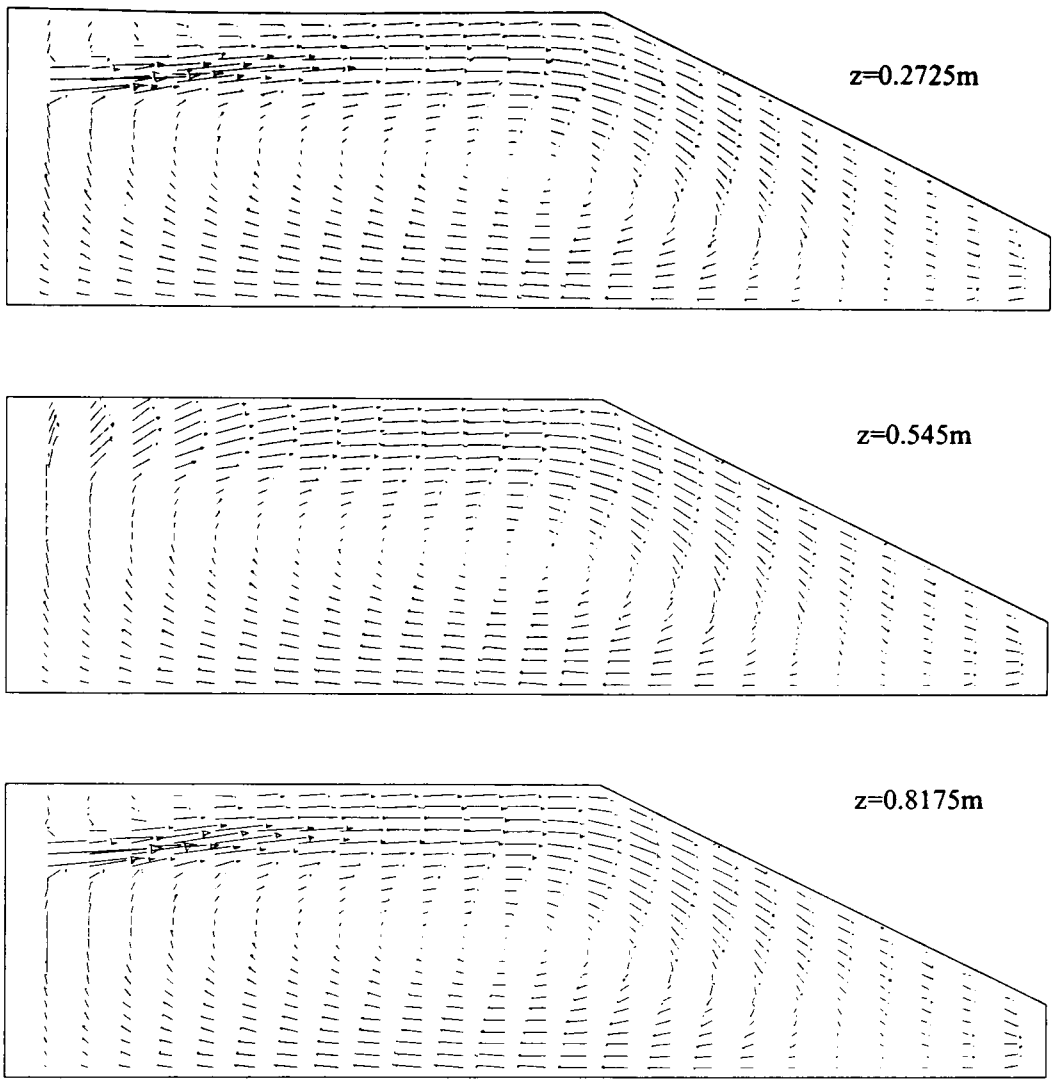

Figure 9.7 Furnace Flow Patterns for Diffusion Flame Burners

The mixing model was based on the "mixed is burnt" assumption i.e. combustion is complete when the fuel and oxidant are combined in stoichiometric proportions. The stoichiometric ratio for natural gas and air on a mass basis is equal to 0.06 [4] so that those values in excess of this quantity indicate fuel-rich regions whereas those below correspond to fuel-lean zones. Figure 9.8 shows the fuel mixture fraction distribution on the vertical planes at the axis of the burners. Only the contours of the fuel-rich areas are displayed for a better visualisation of the flame shape and hence location of zones with heat release.

It can be seen that combustion occurs relatively close to the burners. This is a consequence of the rapid rates of mixing generated by the high velocity levels of the inlet streams. However, the rate of mixing is found to decrease substantially along the length of the furnace and this is probably because of the recirculating flow induced by the jet bringing "combustion products" which are low in oxygen into the flame so that

combustion is hindered. As a result the flame is extended along the furnace length although only small amounts of fuel remain to be burnt.

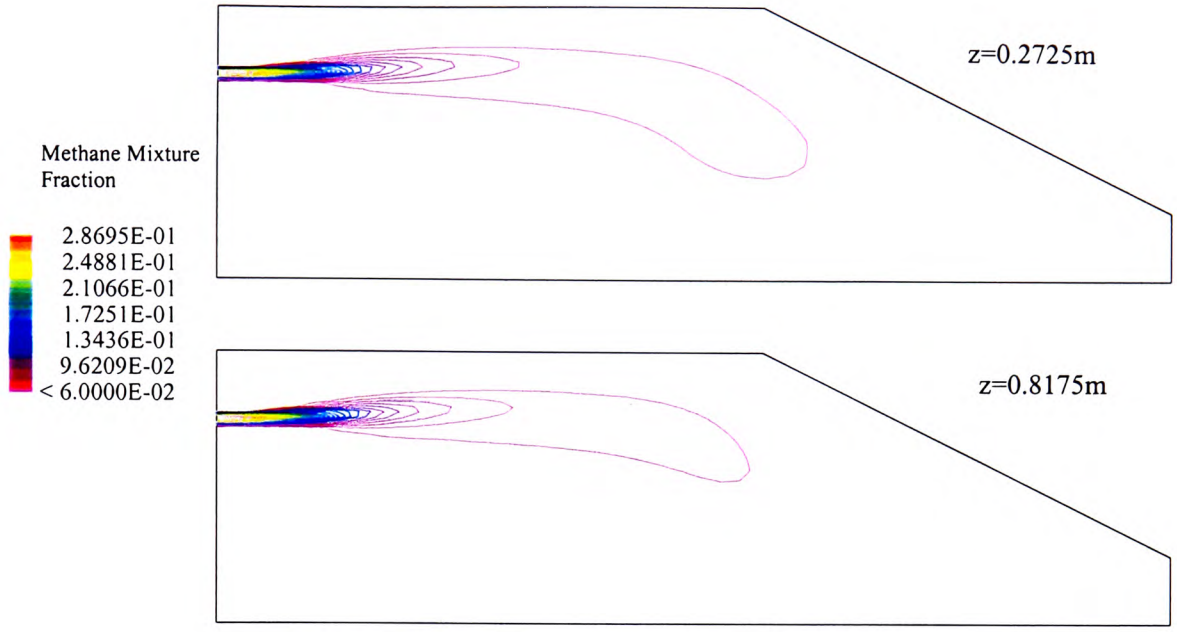

Figure 9.8 Methane Concentration Contours along the Central Plane of a Burner (Excess Air=10%)

As expected near the inclined roof the flame jet is deflected downwards as a result of downward flow in this region. The predicted flame length in Figure 9.8 was defined as the point combustion is 99% complete and is given by the outer contour. However turbulent diffusion flames are usually unsteady and flicker and therefore their length varies continuously to some extent. It can be seen that in the outer contours very little fuel is left to burn so that the flame length in our case must be in between the last two contours i.e. in the range of 3 to 4m long.

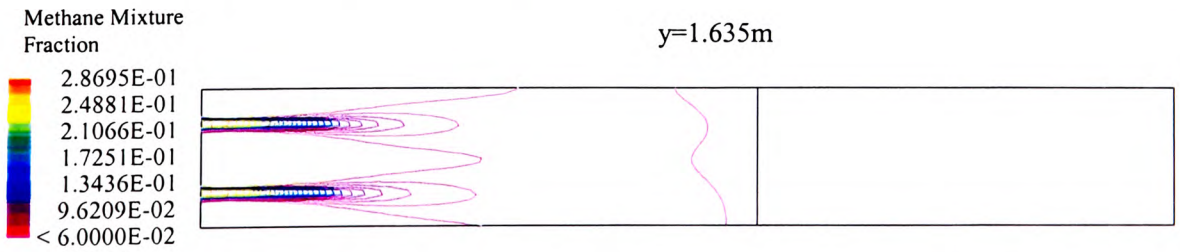

Figure 9.9 Methane Concentration Contours at the Burner Centreline (Excess Air=10%)

In the other two coordinate directions mixing is faster and combustion is seen to occur at the edges of the jet as Figure 9.9 and 9.11 illustrate. Contours along the axis of

the burners on a *x-z* plane, Figure 9.9, show clearly the shape of the flames for the two parallel burners. The flames are shown to have similar characteristics although slightly tighter outer contours at the inner flame suggest that better mixing of the reactants occurs in the middle region. For the outer burner, the side wall additionally confines the flow and increases entrainment into the jet so that fuel/oxidant mixing is delayed.

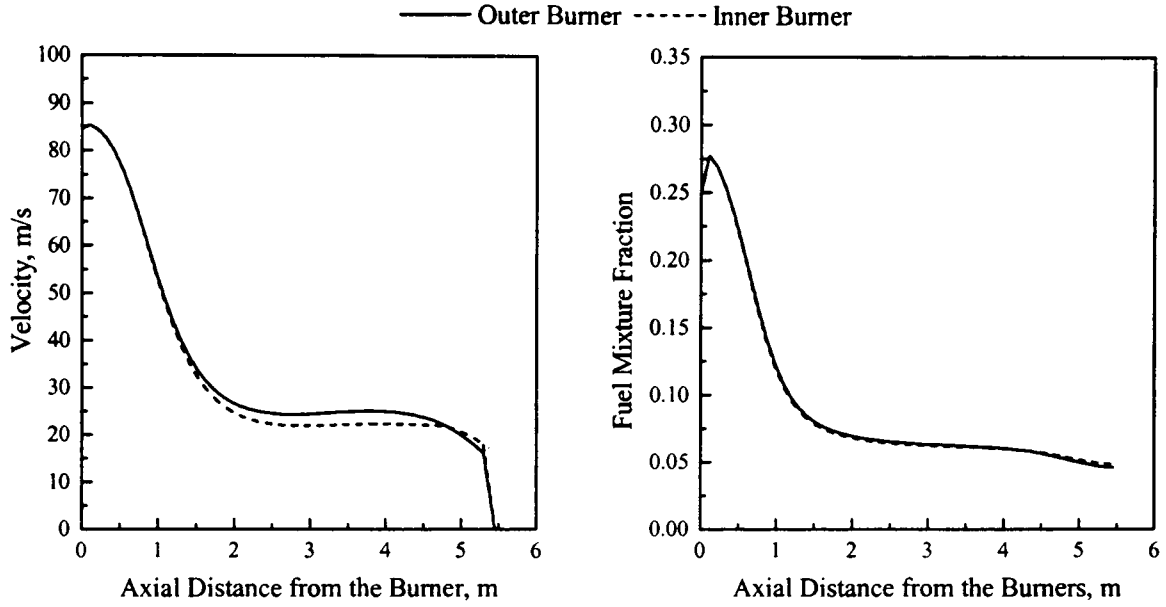

Figure 9.10 Decay of Velocity and Fuel Concentration at the Burners Centreline

Figure 9.10 shows a plot of the decay of velocity and fuel mixture fraction along the centreline of the burners. The decay in fuel concentrations are virtually identical, the decay in velocity for the inner burner is somewhat higher initially over the first 2m. As a result the rate of mixing in the inner flame close to the symmetry wall was increased and a shorter flame formed.

Figure 9.11 presents sectional profiles of velocity and fuel concentration at the burner centreline. As expected close to the burners high velocity and concentration peaks are found. The lateral variations, however, decrease rapidly as we move further from the burner nozzle and at x=2.725m approximately uniform velocity and fuel concentration profiles are achieved.

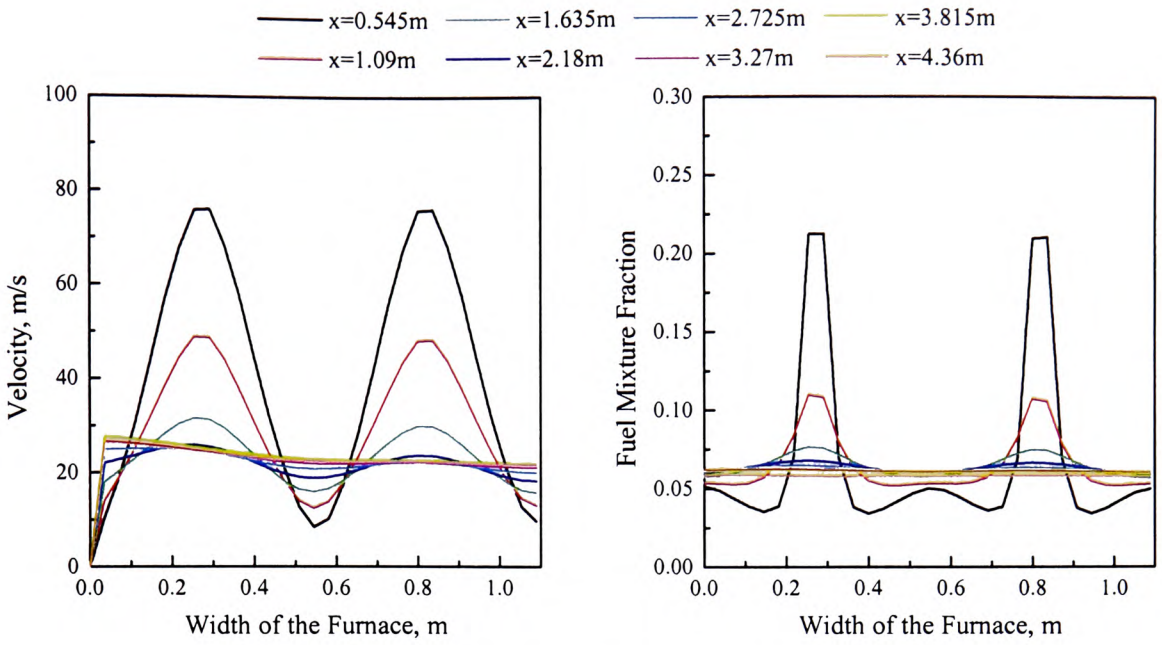

Figure 9.11 Sectional Profiles of Velocity and Fuel Concentration

It is well known that changes in the excess air used for combustion alter the flame characteristics. To test that the CFD produces "correct" trends it was decided to investigate the effect of varying the amount of excess air used for combustion. Two additional cases with 5 and 15% excess air were also studied and the results showed, as expected, that the flame length decreased significantly with increased excess air.

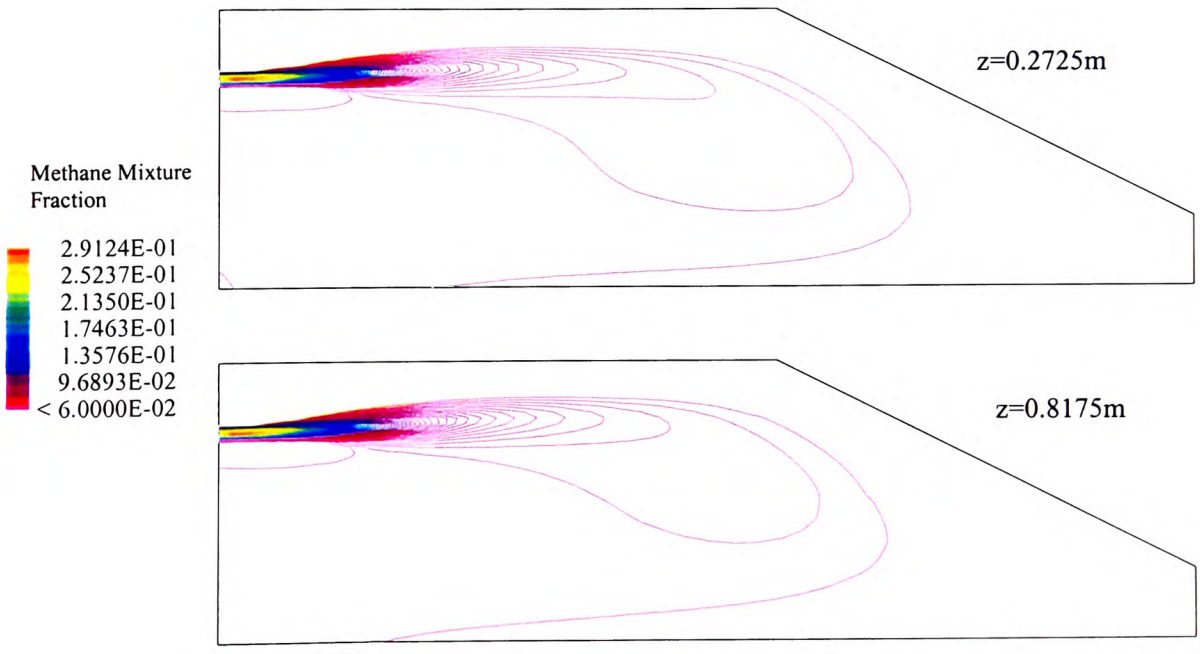

Figure 9.12 Methane Concentration Contours along the Centre Plane of a Burner (Excess Air=5%)

With only 5% excess air, longer flames are produced and this can be seen in the model where the fuel contours extended further downstream in the furnace, see Figure 9.12 which presents predicted contours in the plane of the burners. With this lower level of excess air mixing of the fuel and oxygen is delayed. The outer contour corresponding to the stoichiometric ratio of fuel and air is incomplete indicating that at these lower excess air levels combustion is also likely to be incomplete. Increasing the excess air level to 15% shortens the flame as Figure 9.13 and Table 9.2 indicate.

In this case the greater availability of oxygen in the combustion products speeds up the mixing between the fuel and the air and therefore leads to a reduction in the flame length.

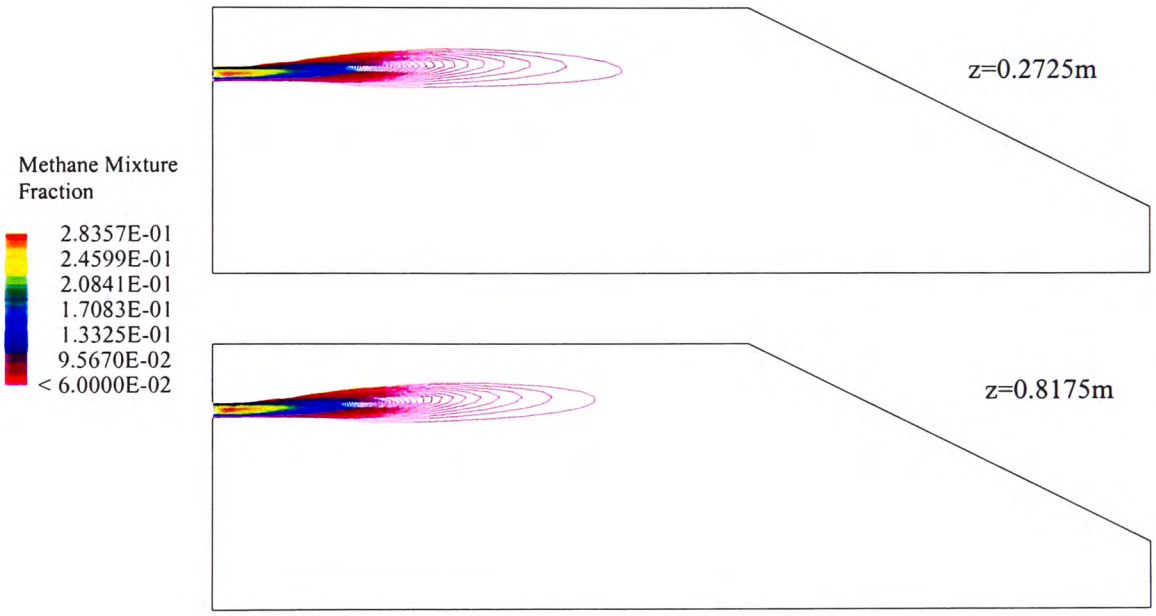

Figure 9.13 Methane Concentration Contours along the Centre Plane of a Burner (Excess Air=15%)

Table 9.2 Predicted CFD Flame Lengths

Excess Air (%)	Flame Length (m)
5	5.3
10	4.7
15	3.2

Figure 9.14 presents the decay of the burner centreline fuel concentration for the three excess air cases. As expected the decay is seen to depend on the amount of excess air supplied for combustion.

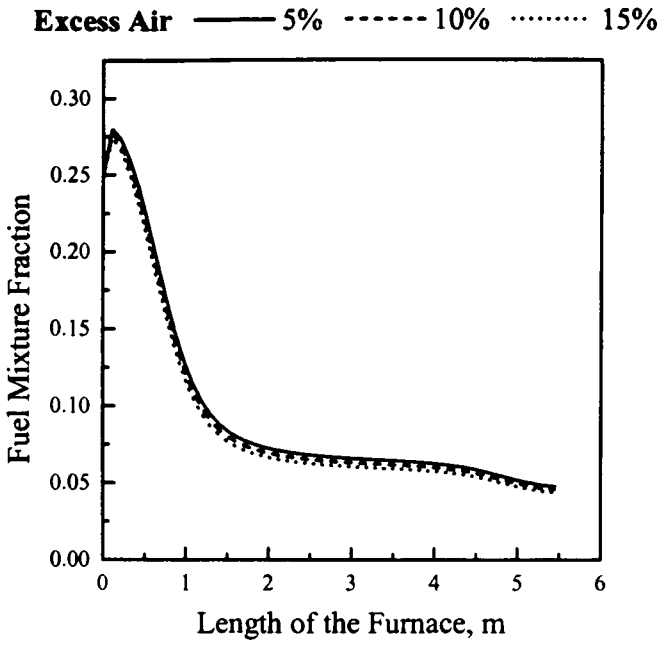

Figure 9.14 Decay of Burner Centreline Concentration for Three Levels of Excess Air

With higher levels of excess air the decay of fuel concentration on the axis is faster due to the high levels of oxygen present to complete combustion. In contrast low levels of excess air result in low rates of decay since under these conditions oxygen availability is reduced and mixing is delayed.

Chen and Ho [5] conducted isothermal studies to numerically simulate the combustion process in an existing steel reheating furnace. The furnace configuration and operating conditions were very similar to those in the present study and their model provided data on the flow field and mixing pattern inside the enclosure. In their model only the region between two neighbouring burners was considered and the inlet nozzles were square in shape as a result of combining mesh cells, see Figure 9.15.

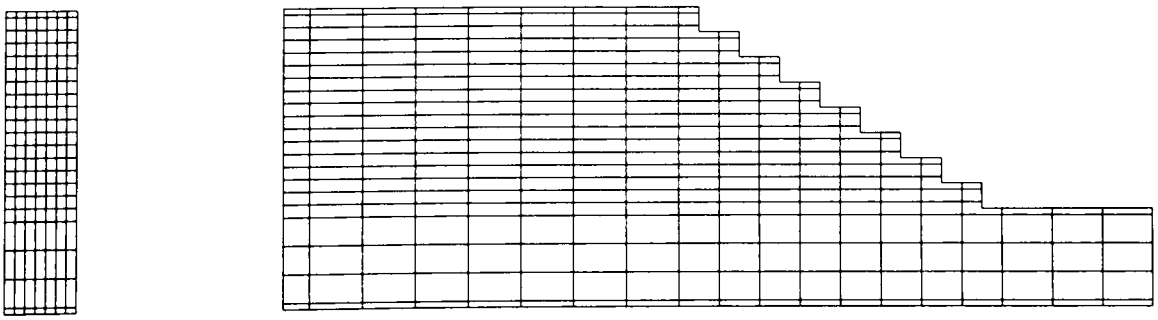

Figure 9.15 The CFD Grid Arrangement [5[

The resultant complicated flow and mixing patterns, see Figure 9.16, depicted the same characteristics found in the present study with a large recirculation area below the

jet. In the upper part of the jet their model predicted a smaller but longer recirculation rotating in the opposite direction and extending along the roof to the inclined section whilst in our case the jet attaches itself to the roof and shortens this recirculation area. The differences are possibly a result of the square nozzle arrangement adopted to simulate the burners in their study and this can alter the flow inside the furnace. In addition their furnace is not geometrically similar and is smaller.

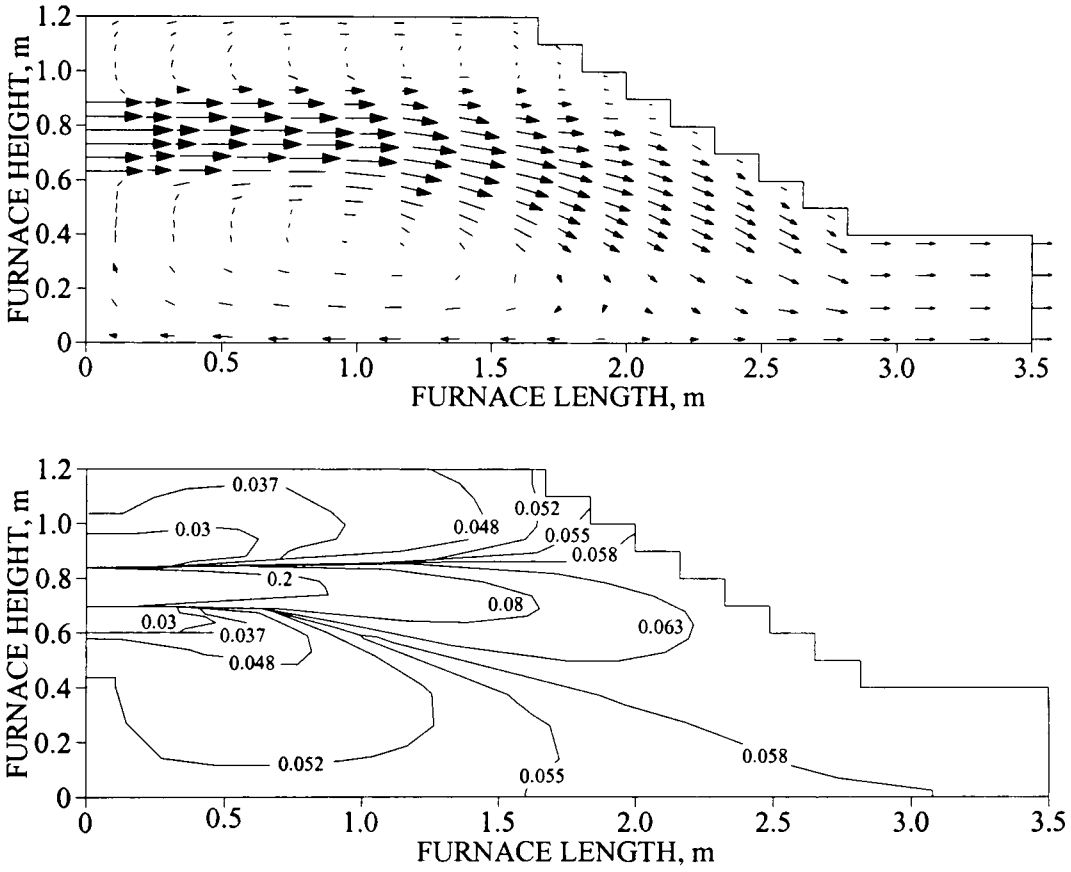

Figure 9.16 Flow and Mixing Patterns for a Reheating Furnace [5]

Their distribution of fuel concentration at different positions within the enclosure also bear close resemblance to the ones predicted in the present model with mixing taking place mostly at regions close to the burner exit. The predicted mixing rates were much slower along the length of the furnace in contrast with the other two coordinate directions where mixing was fast. Thus, despite the lack of experimental validation and limited comparisons available in the literature, it appears that CFD isothermal models may provide good representation of the flow and mixing patterns in the reheating furnace.

9.5 The Zone Models

As mentioned previously the model subdivided the furnace chamber into 46 volume zones and hence 118 refractory surface zones and 10 load surface zones. A finer subdivision was employed near the burners because of the steeper temperature and fuel concentration gradients in this region. The diffusion flame burners resulted in flows which were essentially two-dimensional except in the vicinity of the burner exits. As a consequence the furnace width was not subdivided and temperature and heat transfer rates were assumed to be uniformly distributed in this direction. As with the nozzle mix models, the diffusion flame models were employed to simulate the transient behaviour of the system during a start-up from ambient cold conditions. The overall structure of these models is similar to that presented in Chapter 4 for the nozzle mix models.

The energy balances for each zone in the diffusion flame model were drawn up taking into account the complex nature of radiation interchange between all zones as well as convective heat transport from appropriate hot gas zones to adjacent surface zones. In addition for each volume zone the energy balance takes into account energy release by combustion in the zones together with enthalpy transport into and out of the zones by the flow of combustion products.

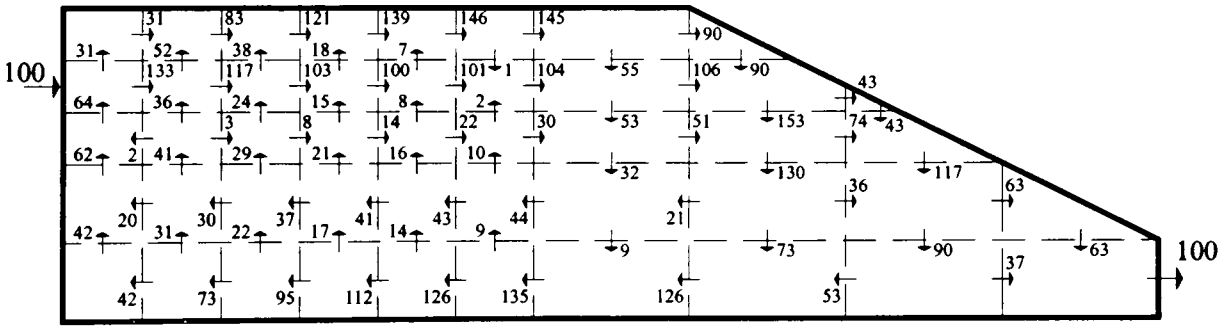

Figure 9.17 Inter-Zone Mass Flows For the Diffusion Flame Burners

Information on flow and mixing patterns were provided as previously mentioned by an ambient isothermal CFD simulation. The CFD models were able to compute velocities and concentration at each cell of the mesh which were then converted to inter-zone mass flows and heat release values in the zone. For the inter-zone mass flow rates, the velocities and hence volume flow rates were integrated at each gas zone boundary and normalised to the total input mass flow. Figure 9.17 shows the computed inter-zone mass flows for the diffusion flame burners in this 46 gas zone model. These relative inter-zone mass flows are identical for any level of excess air tested since under these

conditions the flows are turbulent and the flow patterns are therefore independent of burner velocity.

The energy release distribution was obtained by computing the total mass of unburnt fuel crossing each volume zone in which "combustion" occurred. At the boundaries of the gas zones containing the flame, values of air and fuel concentrations and velocities were found for each cell in the CFD grid. With these values it was possible to determine the fraction of fuel burnt at each cell by simply finding the ratio:

$$\varphi_i = \frac{A/F_{at\ cell\ i}}{A/F_{stoich}} \quad \text{where for} \begin{cases} \varphi_i \geq 1 & \textit{all the fuel was burnt, no heat release} \\ \varphi_i < 1 & \textit{heat release} \end{cases} \tag{9.2}$$

The overall amount of fuel burnt at each gas zone is then obtained by summing up the individual terms of the mass of unburnt fuel at each cell on the boundaries of the gas zone and determining the difference between the inlet and outlet fuel rates:

$$\text{Fuel Burnt in Gas Zone } j = \sum_{j=1}^{N_{\substack{Zone \\ Boundaries}}} \sum_{i=1}^{N_{cells}} \left(V_i A_i \rho_{Fuel} C_{Fuel,i} \left(1 - \varphi_i\right)\right) \tag{9.3}$$

where V is the cell velocity normal to the boundary of zone j, A is the cell cross-sectional area, ρ and C are the density and concentration of the fuel at cell i. Figure 9.18 presents the heat release distribution (normalised against the overall thermal input) inside the furnace chamber for two different levels of excess air namely 5 and 10%.

It can be seen that in both cases the sum of the heat release values does not completely add up to 100% and only approximately 97% of the total heat released has been allocated. As we move towards the inclined roof the percentage of fuel left to be burnt is small and is spread over a large number of zones, see for example Figure 9.12 in which the outer contour is not completely closed. It is difficult to predict the distribution of this remaining small amount of the energy input with reasonable accuracy. Any errors due to neglecting this heat release were small so that it was consequently neglected.

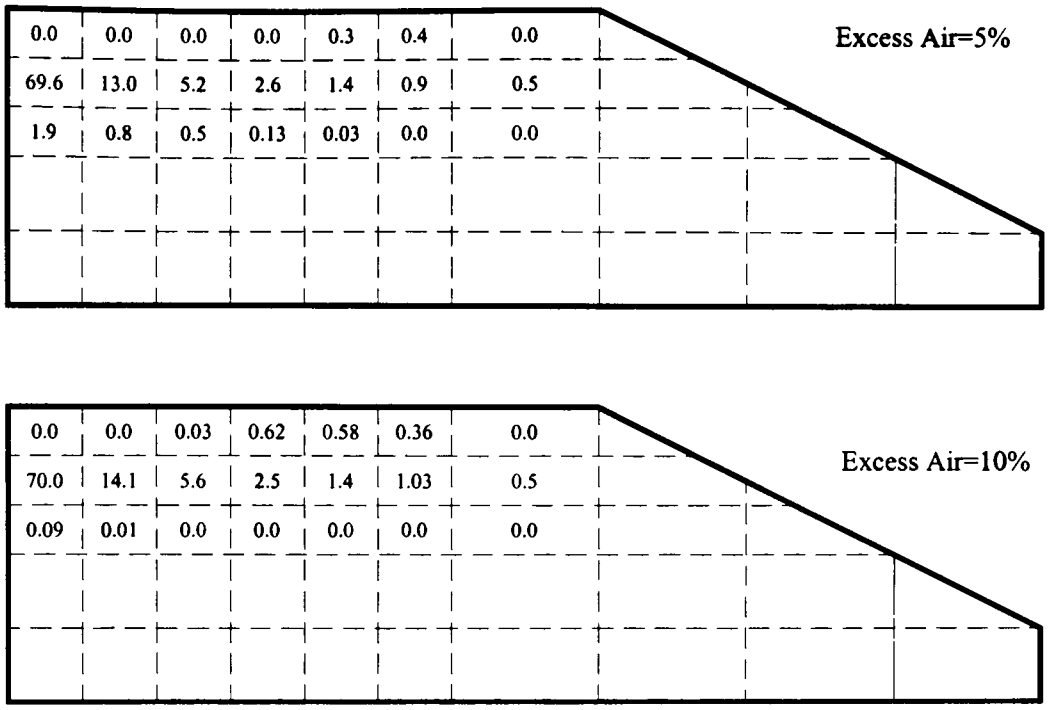

Figure 9.18 Heat Release Distribution for Two Flames (values are % heat release in a zone)

As mentioned previously, it was not possible to resolve the gas nozzle geometry to a diameter sufficiently small so that the overall maximum thermal input to the system (i.e. maximum rating of the burners) was identical to the 5.4MW used in the nozzle mix models. As a result in the diffusion flame isothermal CFD models the gas flow rate corresponded to a total of 60.6MW thermal input which is excessive for the reheating furnace considered. The air flows were correspondingly increased so that the appropriate air/fuel ratio was maintained. Air-fuel mixing is a function of the flow patterns which are themselves independent of burner velocity provided that the flow is turbulent. Consequently it can be assumed that the mixing and hence heat release patterns will be the same for the current 60.6MW case and the 5.4MW thermal input which is used in the diffusion flame zone model. The important consequence is that normalised flow and combustion patterns will remain the same and can be used to simulate an overall maximum thermal input of 5.4MW.

The diffusion burner zone model was therefore run for the conditions specified in Table 9.3 and simulated the period from a cold start-up to the discharge of the first billet which occurred when its top surface reached a temperature of 1250°C. The effect of different profiles of combustion heat release within the furnace enclosure were analysed by simulating two excess air conditions (5 and 10%). The set point value which controls

the temperature in the furnace was also varied to determine the influence of the control system on the overall performance of the reheating furnace.

Table 9.3 Diffusion Burner Model Conditions

Zoning Characteristics	
Number of Volume Zones and hence Simultaneous Equations which are Solved	46
Total Number of Surface Zones	128
of which	
Walls	98
Hearth	10
Roof	10
Load	10
Volume Zone Dimensions (m)	
Length	0.545/1.09
Height	0.545/0.363
Width	2.18
Model Conditions	
Load Dimensions (m)	
Thickness	0.0635
Width	1.83
Lining Thickness (m)	
Walls and Hearth	0.3
Roof	0.35
Burners	
Number	4
Type	Diffusion Flame
Fuel	Natural Gas
Max Thermal Input (MW gross)	5.4
Excess Air (%)	5, 10
Diameter (m)	
Air	0.12
Fuel	0.044
Location	Top, firing into gas zone 4
Inclination	0°
Combustion Products Representation	Weighted Sum of Grey Gases (1 clear + 2 grey)
Emissivities of the Materials	Steel Bars = 0.7; Ceramic Fibre Roof = 0.5; Refractory Walls and Hearth = 0.6
Enthalpy Flows & Combustion Patterns	3D Ambient Isothermal CFD Calculation
Convective Heat Transfer Coefficient (W/m^2K)	25
Initial Surface Temperatures (°C)	Ambient = 20
Conduction Through Surfaces	
Model	1D, Finite Difference, Fully Implicit
Number of Nodes	
Through the Thickness	
Load	11
Roof	8
Walls and Hearth	7

Thermal Contact Resistance Load-Hearth (m^2K/W)	0.002
Load Top Surface Discharge Temperature (°C)	1250
Set Point Temperature (°C)	1300, 1320, 1340, 1380
Sensor Location	3rd roof, hot face
Control System	
Type	Proportional
Error Band (°C)	±7.5
Turndown	0.2
Calculation Time Step (sec)	10

Comparisons where made with a nozzle mix simulation, where combustion is assumed to be complete at the zone of input, to assess the importance of including combustion heat release.

9.6 Results and Discussion

From the start-up simulations, see Figure 9.19 and Table D.25, it can be seen that the use of diffusion flame burners generally results in an increase in the time required to bring the load at discharge to a top temperature of 1250°C.

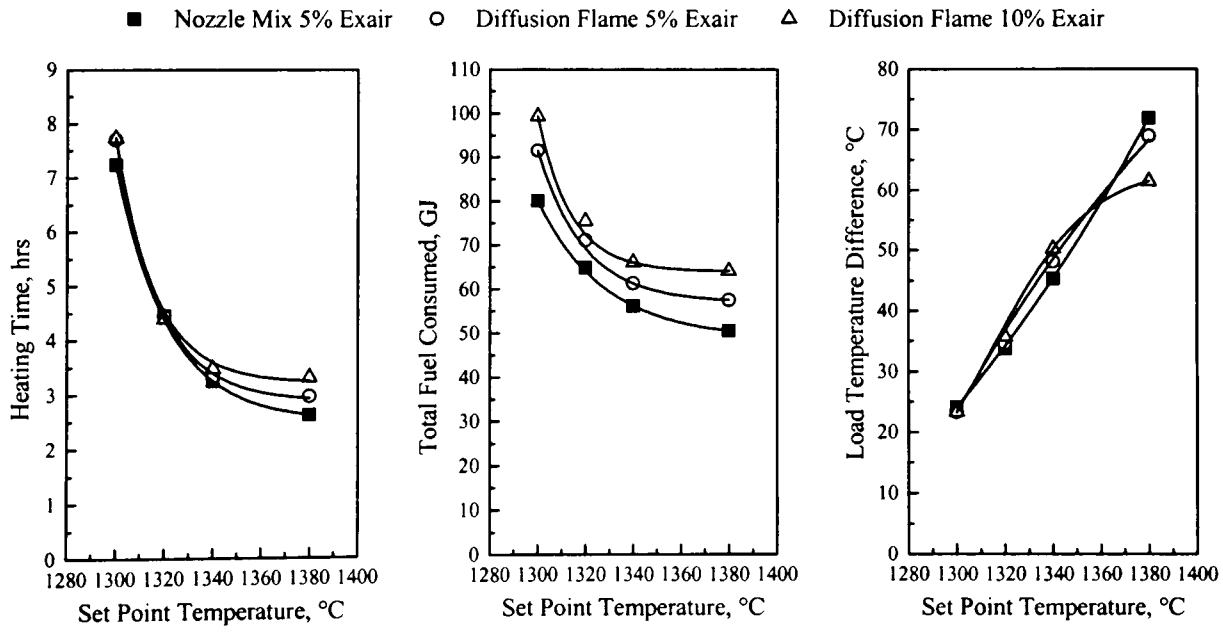

Figure 9.19 Comparison of Furnace Performance Between Different Burner Types

In contrast with nozzle mix burners where all the energy is released at the burner exit and hence confined to a small region, with the diffusion flame burners combustion progresses along the furnace and spreads over a much larger region. This gradual energy

release within the enclosure (which approximately corresponds to an exponential form along the burner centreline), see Figure 9.10, is likely to lead to lower peak temperatures in the near burner region and consequently to a reduction in the rate of heat transfer to the load near the discharge end so that longer heating times are required.

Figure 9.20 plots the temperature-time history of a so-called "flame region" and also the pattern of heat transfer to the load in gas zone 1 near discharge for the three different flames at various set points. The temperature of the flame region was taken as the average of the temperatures of the first 9 gas zones in the top half of the furnace close to the burners (i.e. zones 3, 4, 5, 8, 9, 10, 13, 14 and 15).

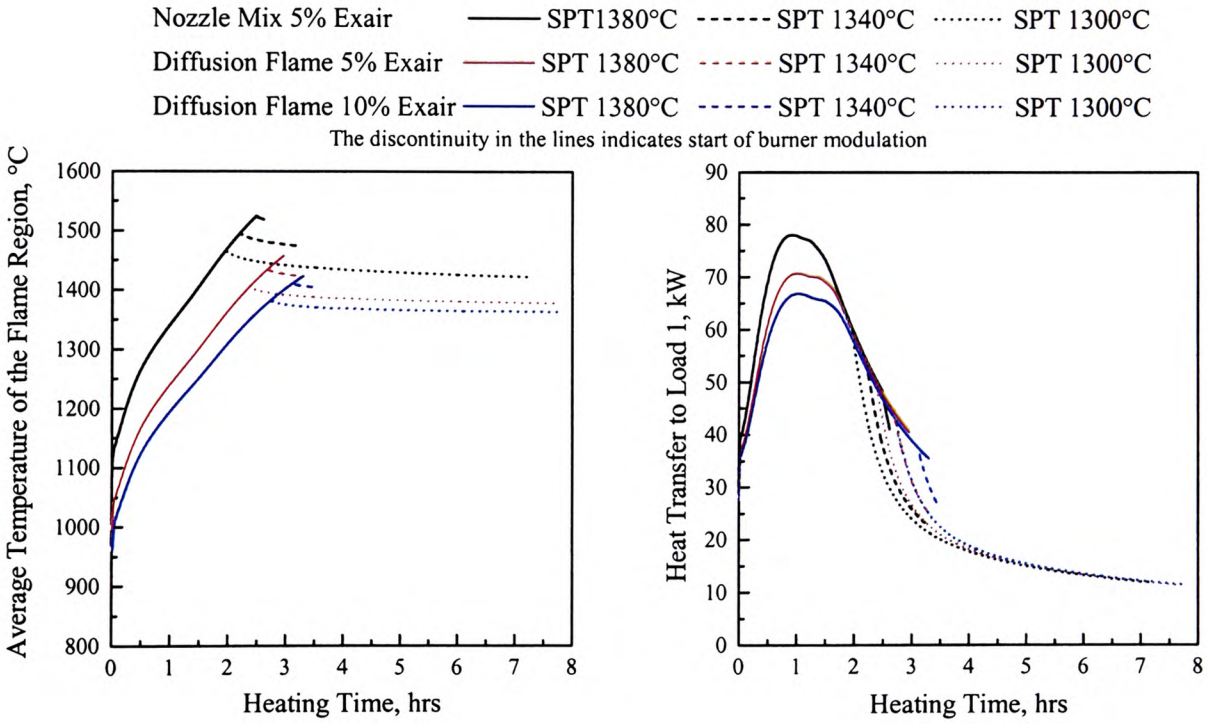

Figure 9.20 Comparison of Gas Temperature and Heat Transfer to the Load for Different Burner Types with Set Point Temperatures

It can be seen that the nozzle mix simulations always predict higher temperatures for this flame region under all set point conditions. The differences between the models is however reduced at lower set points so that for example at the end of the nozzle mix simulation the temperature difference is about 90°C at the highest set point whilst at 1300°C this value is reduced to 40°C. As a direct consequence of the higher temperatures predicted for the near burner and control system regions, burner modulation is greater in the nozzle mix case. Figure 9.20 also indicates that for the nozzle mix model modulation occurs at all set point temperatures as opposed to the

diffusion flame simulations where modulation occurs only at lower set points. As expected the heat transfer to the load is reduced in the diffusion flame case as a result of the overall reduction in flame temperature. The predicted start-up times were therefore greater with this type of flame.

Figure 9.19 shows that as the control temperature is reduced the heating time required to achieve the discharge temperature is increased. This is because at lower set points the control system modulates the thermal input and the burners operate at low firing conditions over longer periods. The increase is more significant with nozzle mix burners since their use results in higher temperatures in the gas zones adjacent to the control device as seen in Figure 9.20. With diffusion flame burners relatively cooler temperatures are predicted for the zones near the burners and the control system so that less modulation was necessary. In addition, the overall flame temperature was reduced with a consequent reduction in heat transfer to the load. Both these effects led to a longer start-up time at the lowest set point. Similar behaviour is predicted for the energy consumption profiles where longer heating times at lower set points result in higher fuel consumptions.

Temperature gradients in the load at discharge were also found to depend on the burner type and set point value. As the control temperature is reduced the predicted temperature differences in the load are also reduced with the model predicting almost identical differentials at the lowest set point. This is because at 1300°C more time is available for energy transfer by conduction to occur so that top-to-bottom temperature differences in the load are decreased. Increasing the set point to 1340°C results in lower temperature gradients for the nozzle mix simulation despite the slightly shorter heating period. With these models higher rates of heat transfer are predicted for the load near the discharge end so that the rate of conduction heat transfer is greater. Additionally the degree of burner modulation is higher in this case and leads to an extension of the start-up period so that the differences in heating times between the models are much less. For the highest set point greater temperature gradients are found with the nozzle mix simulation due to the shorter predicted heating times and moreover, in all cases, there is relatively little burner modulation. There is thus less time available for conduction to reduce temperature variations within the load in the nozzle mix case.

Increasing the excess air level in the diffusion flame model to 10% is, as expected, seen to decrease further the overall flame temperature and heat transfer to the load. Longer heating times are therefore predicted at all set points with differences decreasing

as the set point is reduced due to the greater burner modulation at low levels of excess air. With higher amounts of excess air cooler gas temperatures are predicted near the control system so that relatively little modulation ensues. Overall variations in energy usage and load temperature difference between the two diffusion flame models followed similar trends to the ones predicted for various excess air levels in the nozzle mix case, see section 7.3.5.

On the whole the present investigation indicates that there can be significant differences in predictions from the two types of burner with the diffusion flame model predicting overall lower temperatures in the furnace and hence higher heating times and fuel consumptions.

9.7 Summary

Most previously used zone models concentrate on simulating nozzle mix burners where combustion is more or less complete within the burner quarl. This representation is, however inappropriate for systems which are end fired by long diffusion flames where combustion energy is gradually released within the enclosure. Zone models have therefore been developed to extend the application of these models to diffusion flames by allocating the energy release in each zone where combustion takes place. A total of 46 gas zones were used to subdivide the furnace enclosure with finer subdivisions in the near burner region where variations in temperature and concentrations are likely to be steeper. Preliminary tests with an assumed flame length and combustion profile have shown that there are differences when compared to nozzle mix simulations. Consequently, isothermal CFD models were used to simulate the mixing process and hence obtain a more accurate representation of the heat release distribution so that an estimation of the flame length was possible. Due to computational time constraints the burner geometry was not fully resolved and the models simulated a much higher thermal input when compared with that originally specified for the reheating furnace. However, if the overall flow is turbulent the normalised flow and combustion patterns remain similar so that the mixing information can be used with a thermal input of 5.4MW. Simulation of nozzle mix and diffusion flame burners showed that significant differences arise in the transient operation of the metal reheating furnace. In general nozzle mix burners resulted in higher temperatures in the near burner region with consequent increases in heat flux to the load. The higher temperatures near the control device also result in greater modulation of the burners. The predictions have, therefore,

demonstrated the importance of adequately accounting for combustion heat release since it can lead to considerable distortion of the heat flux profile to the load and overall furnace behaviour. Changes to the set point temperature and level of excess air employed for combustion were also shown to affect the thermal performance of the furnace during the initial start-up from cold.

References

1. Beer, J.M., Chigier, N.A., *Combustion Aerodynamics*, 1972, London: Applied Science Pub.
2. Faber, A., Michelfelder, S., *A one-dimensional mathematical model for the calculation of heat flux distributions in furnaces with substantial external recirculation*, in *Report No. G 04/a/8.* 1976, IFRF: IJmuiden.
3. Rhine, J.M., Tucker, R.J., *Modelling of Gas-Fired Furnaces and Boilers and Other Industrial Heating Processes*, 1991, London: McGraw-Hill.
4. *Combustion Engineering and Gas Utilisation.* 3rd ed., 1992, London: Chapman and Hall.
5. Chen, J.D., Ho, T.Y., *Numerical analysis of isothermal flow fields in modelled reheating furnace.* in *Intl. Symp. Steel Reheat Furnace Technology,* p. 199-210. 1990. Ontario, Canada.

CHAPTER TEN

CONCLUSIONS AND FURTHER WORK

10.1 Conclusions

The zone method of radiation analysis treats radiation in an enclosure in a global manner so that reliable estimates of this mode of heat transfer can be obtained in systems such as gas-fired furnaces. The method provides the basis for mathematical models which can be used to simulate the behaviour of a range of industrial heating processes under both steady-state and transient operating conditions. However, the literature survey indicates that in many cases simplified, so called long furnace models have been employed for practical furnace design. This simplification, although justified in cases where simple plug-flow arrangements are encountered, is not necessarily appropriate in situations with considerably more complicated flow patterns including, for example, those where recirculation regions are set up near the burners. In addition, previous models have largely been developed for nozzle mix burners, where combustion is more or less complete within the burner, and consequently these have limited use in furnaces which are end-fired by long diffusion flames. However, this present study aimed to develop multi-zone mathematical models capable of improved simulations of the transient and steady-state performance of a high temperature gas-fired metal reheating furnace.

The following conclusions can be drawn:

1. Two-dimensional models were shown to provide improved results when compared against predictions from long furnace models under both transient and steady-state conditions. It was demonstrated that the simpler models can lead to substantial differences in the predictions of furnace performance particularly as a result of simplified representations of the control system and flow behaviour. Long furnace models are, therefore, less likely to predict accurately the influence of any changes in burner design and furnace control. In particular it appears that the LFM's tended to overpredict the furnace efficiency, or conversely underestimate the fuel input. These are major faults in any model since they would lead to undersizing of the furnace.

2. The importance of accurately zoning the furnace enclosure was investigated and the results indicated that the number of zones significantly affect the predicted thermal performance of both continuously and transiently operated gas-fired furnaces. The overall differences between the models with different degrees of complexity (ranging from a simple one-dimensional LFM to more sophisticated two-dimensional models) suggested that finer subdivision near the burner region could provide improved representation of the behaviour of a gas-fired furnace. The predictions of initial start-up period, fuel consumption and load temperature differences were all sensitive to the number of zones employed in the calculation. Consequently, in this study it was decided to apply a model with a 37 gas zone representation of the furnace enclosure.

3. The zone method requires as input a knowledge of the mass flows across each zone boundary in order to evaluate the enthalpy flows into and out of each volume zone. In this study an isothermal ambient CFD simulation of the flows in the furnace enclosure proved to be suited for this task since the model was able to predict the flow patterns resulting from changes in furnace design and operation. This approach was adopted since the use of small-scale, experimental near ambient models has been successfully employed in the past to investigate flow related behaviour of combustion systems providing the burner diameter is distorted to account for changes in density in the non-isothermal case.

4. Changes to the burner geometry, orientation and position were found to substantially affect the flow of combustion products so that it is important to realistically represent flow patterns in the furnace chamber. Burner inclination was found to result in hot combustion products near the load and relatively cool recirculated

combustion products near the roof whilst in contrast the flow from the horizontal burners resulted in relatively hot combustion gases near the roof and cooler zones near the load. Comparisons of flow predictions in the current investigation with previously published studies suggest that the CFD calculations can be used with confidence to provide reliable estimates of the flow patterns.

5. The transient models developed in this study were capable of predicting the effect of changes to the operating conditions and provided information regarding start-up times from cold, energy consumptions and load temperature profiles. The zone predictions have highlighted the importance of adequately representing the interaction between the heat transfer characteristics of the furnace and those of the control system (which modulates the thermal input to the burners) when simulating the transient operation of a pusher-type, gas-fired, metal reheating furnace. The burner characteristics were found to markedly affect the thermal performance of the system during both initial start-up from cold as well as over prolonged production periods. The thermal behaviour was also influenced by the magnitude of the furnace set point and position of the roof mounted thermocouple which acted as the control sensor. The use of low thermal mass ceramic fibre materials in the furnace provided benefits particularly when the whole of the furnace lining was constructed from these lightweight materials. The study has shown that potential energy savings can be made when employing heat recovery systems to preheat incoming combustion air. The models were easily applied to demonstrate the effect of adding more air than necessary to complete combustion. This section of the work illustrated how zone models can be used in practice.

6. For furnaces operating continuously at constant throughput and thermal input simplified steady-state zone models were shown to be adequate to evaluate the effect of alternative burner configurations as well as changes in furnace design. The model demonstrated that increasing the furnace length could improve significantly the thermal efficiency because of the effectiveness of load preheating. Variations in the assumed convection heat transfer coefficients were shown to affect mainly the furnace efficiency and the study has highlighted the need to enhance convection at the cooler regions of the furnace. The benefits of preheating the combustion air were shown to be significant in terms of fuel savings and it was further demonstrated that any potential enhancement in furnace efficiency from employing heat recovery is more important in shorter furnaces with high exhaust temperatures.

7. For systems end-fired by long diffusion flames additional information is necessary in the zone models to account for the energy release due to gradual combustion inside the furnace. Isothermal CFD models were employed to supply this information by simulating the mixing process in the enclosure. Comparison of the models with a nozzle-mix simulation showed that significant differences arise when investigating the transient operation of a metal reheating furnace. The diffusion flame models demonstrated the importance of adequately accounting for the combustion heat release since it can lead to considerable variation in the heat flux profile to the load and hence overall furnace behaviour. Changes to the set point temperature and level of excess air employed for combustion were also shown to affect the thermal performance of the furnace during the initial start-up from cold.

8. Overall the zone models were shown to have considerable potential to investigate furnace design and control. The zone models have relatively short computing times and provide sufficient detail to simulate the performance of a gas-fired metal reheating furnace under both transient and steady-state conditions. The flexibility of the models means they can easily be adapted to model different heating applications under various operating conditions.

10.2 Recommendations for Further Work

The improved zone models developed in course of this study have demonstrated the suitability of the technique to study overall furnace design and control. However, there is still scope for further improvements.

1. In any modelling exercise validation is an essential step to assess the accuracy and applicability of the simulations. In this study, validation of the both zone and CFD models was restricted to data available from closely related problems reported in the literature so that a full programme of experimental work should be undertaken on a production furnace for a range of operating conditions to produce reliable data for validation purposes.

2. The present study has demonstrated that isothermal non-combusting CFD simulations potentially can provide adequate information on flow and heat release patterns inside the furnace chamber. There is, however, a need to establish how the isothermal predictions compare with a non-isothermal simulation and in particular evaluate the impact of any differences on the zone model results.

3. In the present study, the flow of combustion products inside the furnace was considered to be essentially two-dimensional since the placement of four equally spaced burners across the furnace width resulted in relatively uniform flows in this direction over most of the furnace length. However, close to the burners the flow distribution is three-dimensional. Further investigations should therefore look at how these three-dimensional flows affect the overall model simulation.

4. In the present work RADEX, a Monte Carlo based computer code was employed to evaluate the exchange areas necessary to describe the radiation terms. The method although flexible enough to represent complex furnace configurations is limited by the zone specification method employed in the software. In here the zoning grid is set up by a series of (x,y) coordinates, each defining a pair of orthogonal grid lines which propagate throughout the entire enclosure. It is, therefore, not possible to define zones of varying size in different sections of the combustion system. While this restriction can be overcome by summing up the direct exchange areas to form the desired zoning arrangement this is time consuming so that a more flexible zoning option should be incorporated in the code.

5. RADEX could also be made more flexible by simplifying changes in the partial pressures of combustion products, for example, those which occur with oxygen enriched firing. This involves adding an extra option to the specification of the oxidant/fuel characteristics when defining the radiative properties of the furnace atmosphere. This will allow new values for the attenuation coefficients to be calculated corresponding to changes in the partial pressures of the radiating species.

6. This study has concentrated on developing improved zone models to simulate gas-fired furnaces mainly because the use of this fuel is widespread. There is, however, scope to extend the zone method to oil and other fuel types such as works arising low calorific value gases to evaluate, for example, the differences to a heating process resulting from fuel conversion.

7. In this study a rather simple representation of the furnace control system was employed since a proportional gas input controller was simulated. In this case the fuel input is continuously adjusted in linear proportion to deviations from a specified set point temperature. While for this type of control the temperature will settle somewhere within the proportional band, more sophisticated control systems are often employed

The models should therefore be improved to incorporate a better representation of a control system such as a PID controller.

8. The coupling of an isothermal CFD simulation with a zone model was shown to have advantages in terms of estimating the flow and mixing patterns. The method of extracting suitable inter-zone mass flow data is however complicated and very tedious so that further work should attempt to devise a more complete strategy that would combine the advantages of both types of model. A study should be carried out to compare the results of a combined zone/isothermal CFD model with predictions from a full CFD simulation. As an alternative to calculating isothermal CFD flows in every application consideration should be given to storing a database of realistic flow and mixing characteristics for a range of furnace geometries and operating conditions.

9. In the zone model, the assumption of grey radiation surfaces is acceptable in many cases. However recent work Jackson and Yen [1] have shown that refractories have highly wavelength-dependent emissivities. In this case the grey assumption is very crude so that it may be important to model the spectral radiative properties of the furnace surfaces. Extension of the standard zone model to allow for the spectral emissivity of the surfaces has been considered by Khan *et al.* [2] whose model also accounted for the spectral variation of the radiation properties of the combustion products. Although the so-called banded zone calculations have only been carried out for a simple, cubical furnace enclosure under steady-state conditions, the results showed that improvements to the heat transfer calculations can be significant. It is therefore recommended that the banded technique which allows for spectral variations in the radiative properties of the system should be applied to a multi-zone model of an industrial furnace. This will establish if the additional complications and computational effort are worthwhile in terms of the improvements in the accuracy of the predictions.

10. Over the last decade or so there has been increasing pressure to reduce pollutant emissions arising from combustion of fossil fuels. This has led to the development of models to predict NOx formation and these have been incorporated as a post-processor procedure into overall CFD models. Zone models should, therefore, be extended to include predictions of NOx emissions. Implementation in a gas-fired system involves modelling the so-called extended Zeldovich mechanism, which describe thermal NO formation [3]. This can be achieved by expressing the rate of NO formation as a function of the temperature, oxygen and nitrogen concentrations. In the zone model the

NO equation would be applied at each zone in the enclosure. From the knowledge of the residence time of the combustion products in each zone it possible to obtain the overall NO formed in the enclosure by summing up the individual contribution from each gas zone. Despite this very simple concept, the implementation of the model as a zone model post-processor NOx calculation is likely to provide overall trends of the emissions for a particular application. In diffusion flames where there are fuel-rich regions it would also be necessary to include appropriate NOx reduction mechanisms.

11. The absorption coefficients and temperature dependent weighting factors in the mixed grey gas models are determined by fitting the predicted emissivities and absorptivities to experimentally measured data. However much of the data was determined approximately 70 to 80 years ago by Hottel and his co-workers, see for example Hottel and Sarofim [4]. It would thus be appropriate to undertake an extensive experimental programme to provide more up-to-date information on the radiation properties of combustion products.

References

1. Jackson, J.D., Yen, C.C., *Measurement of total and spectral emissivities of some ceramic fibre insulation materials.* in *Ceramics in Energy Applications Conf.*, p. 159-174. 1994. London, UK.
2. Khan, Y.U., Lawson, D.A., Tucker, R.J., *Banded radiative heat transfer analysis.* Communications in Numerical Methods in Engineering, 1997. **13**: p. 803-813.
3. Zeldovich, J., Acta Physicochem, 1946. **21**: p. 577.
4. Hottel, H.C., Sarofim, A.F., *Radiative Transfer*, 1967, New York: McGraw-Hill.

THERMAL PROPERTIES

A.1 Properties of Natural Gas Combustion Products and of Air

The composition and properties of a natural gas from the North Sea are given in Table A.1 [1].

Table A.1 Properties of a Typical Natural Gas from the North Sea and of its Stoichiometric Products of Combustion

Composition (% by volume):						
CH_4	C_2H_6	C_3H_8	C_4H_{10}	C_5H_{12}	CO_2	N_2
94.4	3.22	0.6	0.2	0.07	0.05	1.46

Property:	
CV_{gross} (J/m^3)	38.69×10^6
CV_{net} (J/m^3)	34.91×10^6
Density, ρ_G^0 (kg/m^3)	0.719
Air/fuel ratio, R_s (m^3/m^3)	9.76
Combustion product/fuel ratio, P_s (m^3/m^3)	10.785
Adiabatic flame temperature (K)	2220

Combustion product composition (% by volume):		
CO_2	H_2O	N_2
9.627	18.753	71.617

For stoichiometric conditions the specific enthalpy of natural gas combustion products, $H_{g,s}(T)$, and of air, $H_a(T)$ were found using a fifth order polynomial of the form:

$$\Phi=a+bz+cz^2+dz^3+ez^4+fz^5 \qquad (A.1)$$

where $z=(T\text{-}1400)/200$ and the polynomial coefficients are given in Table A.2 [1]. T is in degrees Kelvin.

Table A.2 Polynomial Coefficients for the Properties of Stoichiometric Natural Gas Combustion Products and of Air Over the Temperature Range 400-2400K

Polynomial coefficients	*a*	*b*	*c*	*d*	*e*	*f*
Stoichiometric combustion products						
$H_{g,s}(T)$ (MJ/kg)	1.399955	0.28089	0.004526	0.000402	0.000224	0.000023
Air						
$H_a(T)$ (MJ/kg)	1.234164	0.243788	0.003322	-0.000059	0.000041	0.000006

The specific enthalpy of the combustion products, $H_g(T)$, at a given air/fuel ratio R_x and temperature T can be found by the expression:

$$H_g(T)=\{(R_s\rho_a^0+\rho_g^0)\,H_{g,s}(T)+(R_x-R_s)\,\rho_a^0\,H_a(T)\}/(R_x\rho_a^0+\rho_g^0) \quad \text{in MJ/kg} \qquad (A.2)$$

where ρ_a^0 and ρ_g^0 are the air and fuel density respectively and $H_a(T)$ is the specific enthalpy of air at temperature T [1].

A.2 Thermal Properties of Load and Insulating Materials

Thermal conductivity (λ), specific heat (C_p) and density (ρ) are presented for mild steel, ceramic fibre and dense refractory brick. The temperature variation of λ and C_p for these materials is given as polynomial expressions of the form (Rhine and Tucker, 1991):

$$\Phi=a+bz+cz^2+dz^3+ez^4+fz^5+gT^6 \qquad (A.3)$$

where T is in degrees Celcius and a, b, c, etc. are coefficients which are given in Table A.3.

Table A.3 Polynomial Coefficients for Thermal Conductivity and Specific Heat

Polynomial coefficients	*Mild Steel* $\rho=7800kg/m^3$		*Ceramic Fibre* $\rho=128kg/m^3$*	*Dense Refractory Brick* $\rho=2600kg/m^3$*
Thermal conductivity, λ (W/mK)	**0-800°C**	**>800°C**		
a	0.519059E+2	0.302492E+2	0.822297E-1	1.8406105E+0
b	-0.369417E-3	-0.155686E-1	-0.14283E-3	0.10118265E-3
c	-0.768098E-4	0.144759E-4	0.95429E-6	-0.516367E-7
d	-0.811310E-8	-0.982726E-8	-0.81346E-9	0.12338578E-9
e	0.212134E-9	0.159948E-10	0.38894E-12	-
f	-0.180744E-12	-0.936461E-14	-	-
g	-	0.148732E-17	-	-

Specific heat, C_p (J/kgK)	**0-750°C**	**750-900°C**	**>900°C**	
a	0.459389E+3	0.960497E+4	0.595783E+3	0.100164E+4
b	0.927605E+0	0.311055E+2	0.809290E+0	0.1583E+0
c	-0.892667E-2	-0.821919E-1	-0.172302E-2	-0.458133E-4
d	0.427170E-4	0.996642E-05	0.113957E-5	-
e	-0.823237E-7	-0.291067E-8	-0.946037E-10	-
f	0.617737E-10	0.166675E-9	-0.762604E-13	-
g	-0.885174E-14	-0.112167E-12		-

References

1. Rhine, J.M., Tucker, R.J., *Modelling of Gas-Fired Furnaces and Boilers and Other Industrial Heating Processes*, 1991, London: McGraw-Hill.

* Typical values only: density of these materials can vary widely

CENTRAL DIFFERENCE SCHEME

The central difference scheme is a numerical method which replaces the exact solution of the differential equation with discrete values. The discretised equations are usually derived by approximating the derivative in the differential equation by a truncated Taylor series development of the form:

$$\phi(x+\Delta x)=\phi(x)+\left(\frac{\partial\phi}{\partial x}\right)_x \Delta x+\left(\frac{\partial^2\phi}{\partial x^2}\right)_x \frac{\Delta x^2}{2}+\ldots \tag{B.1}$$

Using these expansions we can obtain approximate expressions for the first and higher derivatives at a point x, in terms of the function values at neighbouring points. For example let us consider the equally spaced one-dimensional grid shown in Figure B.1.

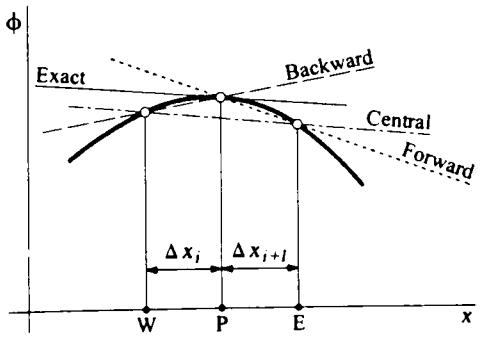

Figure B.1 Definition of Derivative and its Approximations

For grid point P, located midway between the grid points W and E, equation B.1 gives:

$$\phi_E = \phi_P + \left(\frac{\partial \phi}{\partial x}\right)_P \Delta x + \left(\frac{\partial^2 \phi}{\partial x^2}\right)_P \frac{\Delta x^2}{2} + \ldots \tag{B.2}$$

Truncating the series just after the second term we obtain:

$$\left(\frac{\partial \phi}{\partial x}\right)_P \approx \frac{\phi_E - \phi_P}{\Delta x} \tag{B.3}$$

The truncated terms are a measure of the accuracy of the approximation and determine the rate at which the error decreases as the spacing between grid points is reduced. Since the order of the term Δx^n indicates the order of the difference approximation, Equation B.1 is first order and can be write as:

$$\left(\frac{\partial \phi}{\partial x}\right)_P = \frac{\phi_E - \phi_P}{\Delta x} + O(\Delta x) \tag{B.4}$$

Since the derivative at point P is approximated by the slope of a line passing through point P and E (where $x_E > x_P$) is called forward difference. Similarly we can derive a backward difference formula for the derivative of point P by using point W:

$$\left(\frac{\partial \phi}{\partial x}\right)_P = \frac{\phi_P - \phi_W}{\Delta x} + O(\Delta x) \tag{B.5}$$

Equations B.4 and B.5 are both first order accurate and involve values at only two grid points. By subtracting the two equations a third formula is obtained:

$$\left(\frac{\partial \phi}{\partial x}\right)_P = \frac{\phi_E - \phi_W}{2\Delta x} + O(\Delta x^2) \tag{B.6}$$

The last equation uses the slope of a line passing through two grid points, W and E, lying in opposite sides to P and is called central difference formula. This formula is second order accurate and the quadratic dependence of the truncation error on the grid spacing means that the error decreases more rapidly with grid refinement.

CFX COMMAND FILE

A typical command file used by the CFX model to provide the flow characteristics of nozzle mix and diffusion flame burners is shown below.

C.1 Nozzle Mix Burner

```
>>CFX4
  >>OPTIONS
    THREE DIMENSIONS
    BODY FITTED GRID
    CARTESIAN COORDINATES
    TURBULENT FLOW
    ISOTHERMAL FLOW
    INCOMPRESSIBLE FLOW
    STEADY STATE
    USE DATABASE
>>MODEL DATA
  >>MATERIALS DATABASE
    >>SOURCE OF DATA
      PCP
    >>FLUID DATA
      FLUID 'AIR'
      MATERIAL TEMPERATURE
2.9315E+02
      MATERIAL PHASE 'GAS'
  >>PHYSICAL PROPERTIES
    >>TURBULENCE PARAMETERS
      >>TURBULENCE MODEL
        TURBULENCE MODEL 'K-
EPSILON'
>>SOLVER DATA
  >>PROGRAM CONTROL
    MAXIMUM NUMBER OF ITERATIONS
500
    OUTPUT MONITOR BLOCK 'BLOCK-
NUMBER-5'
    OUTPUT MONITOR POINT 3 12 5
    MASS SOURCE TOLERANCE
1.0000E-06
    ITERATIONS OF TURBULENCE
EQUATIONS 3
  >>DEFERRED CORRECTION
    K START 0
    K END 100
>>MODEL BOUNDARY CONDITIONS
  >>INLET BOUNDARIES
    PATCH NAME 'INLET1'
    U VELOCITY 1.0000E+00
    V VELOCITY 0.0000E+00
    K 2.0000E-03
    DISSIPATION LENGTH SCALE
1.5000E-01
  >>INLET BOUNDARIES
    PATCH NAME 'INLET2'
    U VELOCITY 1.0000E+00
    V VELOCITY 0.0000E+00
    K 2.0000E-03
    DISSIPATION LENGTH SCALE
1.5000E-01
```

```
  >>PRESSURE BOUNDARIES
    PATCH NAME 'PRESS1'
    PRESSURE 0.0000E+00
    STATIC PRESSURE SPECIFIED
>>OUTPUT OPTIONS
  >>FRONTEND PRINTING
    NO TOPOLOGY STRUCTURE
  >>PRINT OPTIONS
    >>WHAT
      U VELOCITY
    >>WHERE
      ALL I PLANES
      ALL BLOCKS
    >>WHEN
      FINAL SOLUTION
  >>PRINT OPTIONS
    >>WHAT
      V VELOCITY
    >>WHERE
      ALL J PLANES
      ALL BLOCKS
    >>WHEN
      FINAL SOLUTION
>>STOP
```

C.2 Diffusion Flame Burner

```
>>CFX4
  >>OPTIONS
    THREE DIMENSIONS
    BODY FITTED GRID
    CARTESIAN COORDINATES
    TURBULENT FLOW
    ISOTHERMAL FLOW
    INCOMPRESSIBLE FLOW
    STEADY STATE
    USE DATABASE
    MASS FRACTION EQUATIONS 2
>>MODEL TOPOLOGY
  >>CREATE PATCH
    PATCH NAME 'INLET1'
    BLOCK NAME 'BLOCK-NUMBER-5'
    PATCH TYPE 'INLET'
    PATCH LOCATION 1 1 13 13 8 8
    LOW I
    PATCH GROUP NUMBER 1
  >>CREATE PATCH
    PATCH NAME 'INLET2'
    BLOCK NAME 'BLOCK-NUMBER-26'
    PATCH TYPE 'INLET'
    PATCH LOCATION 1 1 13 13 8 8
    LOW I
    PATCH GROUP NUMBER 1
  >>CREATE PATCH
    PATCH NAME 'LOWER1'
    BLOCK NAME 'BLOCK-NUMBER-5'
    PATCH TYPE 'INLET'
    PATCH LOCATION 1 1 11 12 6 10
    LOW I
    PATCH GROUP NUMBER 2
  >>CREATE PATCH
    PATCH NAME 'LOWER2'
    BLOCK NAME 'BLOCK-NUMBER-26'
    PATCH TYPE 'INLET'
    PATCH LOCATION 1 1 11 12 6 10
    LOW I
    PATCH GROUP NUMBER 2
  >>CREATE PATCH
    PATCH NAME 'UPPER1'
    BLOCK NAME 'BLOCK-NUMBER-5'
    PATCH TYPE 'INLET'
    PATCH LOCATION 1 1 14 15 6
10
    LOW I
    PATCH GROUP NUMBER 2
  >>CREATE PATCH
    PATCH NAME 'SIDE11'
    BLOCK NAME 'BLOCK-NUMBER-5'
    PATCH TYPE 'INLET'
    PATCH LOCATION 1 1 13 13 6 7
    LOW I
    PATCH GROUP NUMBER 2
  >>CREATE PATCH
    PATCH NAME 'SIDE21'
    BLOCK NAME 'BLOCK-NUMBER-26'
    PATCH TYPE 'INLET'
    PATCH LOCATION 1 1 13 13 6 7
    LOW I
    PATCH GROUP NUMBER 2
  >>CREATE PATCH
    PATCH NAME 'SIDE22'
    BLOCK NAME 'BLOCK-NUMBER-26'
    PATCH TYPE 'INLET'
    PATCH LOCATION 1 1 13 13 9
10
    LOW I
    PATCH GROUP NUMBER 2
  >>CREATE PATCH
    PATCH NAME 'UPPER2'
    BLOCK NAME 'BLOCK-NUMBER-26'
    PATCH TYPE 'INLET'
    PATCH LOCATION 1 1 14 15 6
10
    LOW I
    PATCH GROUP NUMBER 2
  >>CREATE PATCH
    PATCH NAME 'SIDE12'
    BLOCK NAME 'BLOCK-NUMBER-5'
    PATCH TYPE 'INLET'
    PATCH LOCATION 1 1 13 13 9
10
    LOW I
    PATCH GROUP NUMBER 2
>>MODEL DATA
  >>DIFFERENCING SCHEME
    ALL EQUATIONS 'UPWIND'
  >>MATERIALS DATABASE
```

```
    >>SOURCE OF DATA
      PCP
    >>FLUID DATA
      FLUID 'AIR'
      MATERIAL TEMPERATURE
2.9315E+02
      MATERIAL PHASE 'GAS'
    >>SPECIES DATA
      MATERIAL TEMPERATURE
2.9315E+02
      MATERIAL PHASE 'GAS'
      MASS FRACTION1 'METHANE'
    >>SPECIES DATA
      MATERIAL TEMPERATURE
2.9315E+02
      MATERIAL PHASE 'GAS'
      MASS FRACTION2 'AIR'
  >>PHYSICAL PROPERTIES
    >>MASS TRANSFER PARAMETERS
      >>DIFFUSIVITIES
        ALL MASS FRACTIONS
1.0000E-05
    >>TURBULENCE PARAMETERS
      >>TURBULENCE MODEL
        TURBULENCE MODEL 'K-
EPSILON'
>>SOLVER DATA
  >>PROGRAM CONTROL
    MAXIMUM NUMBER OF ITERATIONS 1
    OUTPUT MONITOR BLOCK 'BLOCK-
NUMBER-5'
    OUTPUT MONITOR POINT 2 14 8
    MASS SOURCE TOLERANCE 1.0000E-
04
    ITERATIONS OF TURBULENCE
EQUATIONS 3
  >>SWEEPS INFORMATION
    >>MAXIMUM NUMBER
      PRESSURE 60
      K 10
      EPSILON 10
  >>UNDER RELAXATION FACTORS
    U VELOCITY 2.0000E-01
    V VELOCITY 2.0000E-01
    W VELOCITY 2.0000E-01
    PRESSURE 3.0000E-01
    VISCOSITY 3.0000E-01
    K 2.0000E-01
    EPSILON 2.0000E-01
    MASS FRACTION1 3.0000E-01
    MASS FRACTION2 3.0000E-01
>>MODEL BOUNDARY CONDITIONS
  >>INLET BOUNDARIES
    PATCH NAME 'INLET1'
    U VELOCITY 1.0000E+02
    V VELOCITY 0.0000E+00
    K 2.0000E+01
    DISSIPATION LENGTH SCALE
6.2630E-02
    MASS FRACTION1 1.0000E+00
    MASS FRACTION2 0.0000E+00
  >>INLET BOUNDARIES
    PATCH NAME 'INLET2'
    U VELOCITY 1.0000E+02
    V VELOCITY 0.0000E+00
    K 2.0000E+01
    DISSIPATION LENGTH SCALE
6.2630E-02
    MASS FRACTION1 1.0000E+00
    MASS FRACTION2 0.0000E+00
  >>INLET BOUNDARIES
    PATCH NAME 'LOWER1'
    U VELOCITY 7.9500E+01
    V VELOCITY 0.0000E+00
    K 1.2647E+01
    DISSIPATION LENGTH SCALE
9.5E-02
    MASS FRACTION1 0.0000E+00
    MASS FRACTION2 1.0000E+00
  >>INLET BOUNDARIES
    PATCH NAME 'LOWER2'
    U VELOCITY 7.9500E+01
    V VELOCITY 0.0000E+00
    K 1.2647E+01
    DISSIPATION LENGTH SCALE
9.5E-02
    MASS FRACTION1 0.0000E+00
    MASS FRACTION2 1.0000E+00
  >>INLET BOUNDARIES
    PATCH NAME 'UPPER1'
    U VELOCITY 7.9500E+01
    V VELOCITY 0.0000E+00
    K 1.2647E+01
    DISSIPATION LENGTH SCALE
9.5E-02
    MASS FRACTION1 0.0000E+00
    MASS FRACTION2 1.0000E+00
  >>INLET BOUNDARIES
    PATCH NAME 'SIDE11'
    U VELOCITY 7.9500E+01
    V VELOCITY 0.0000E+00
    K 1.2647E+01
    DISSIPATION LENGTH SCALE
9.5E-02
    MASS FRACTION1 0.0000E+00
    MASS FRACTION2 1.0000E+00
  >>INLET BOUNDARIES
    PATCH NAME 'SIDE21'
    U VELOCITY 7.9500E+01
    V VELOCITY 0.0000E+00
    K 1.2647E+01
    DISSIPATION LENGTH SCALE
9.5E-02
    MASS FRACTION1 0.0000E+00
    MASS FRACTION2 1.0000E+00
  >>INLET BOUNDARIES
    PATCH NAME 'SIDE22'
    U VELOCITY 7.9500E+01
    V VELOCITY 0.0000E+00
    K 1.2647E+01
    DISSIPATION LENGTH SCALE
9.5E-02
```

```
    MASS FRACTION1 0.0000E+00
    MASS FRACTION2 1.0000E+00
  >>INLET BOUNDARIES
    PATCH NAME 'UPPER2'
    U VELOCITY 7.9500E+01
    V VELOCITY 0.0000E+00
    K 1.2647E+01
    DISSIPATION LENGTH SCALE 9.5E-
02
    MASS FRACTION1 0.0000E+00
    MASS FRACTION2 1.0000E+00
  >>INLET BOUNDARIES
    PATCH NAME 'SIDE12'
    U VELOCITY 7.9500E+01
    V VELOCITY 0.0000E+00
    K 1.2647E+01
    DISSIPATION LENGTH SCALE 9.5E-
02
    MASS FRACTION1 0.0000E+00
    MASS FRACTION2 1.0000E+00
  >>PRESSURE BOUNDARIES
    PATCH NAME 'PRESS1'
    PRESSURE 0.0000E+00
    STATIC PRESSURE SPECIFIED
>>OUTPUT OPTIONS
  >>FRONTEND PRINTING
    NO FRONTEND PRINTING
    NO TOPOLOGY STRUCTURE
  >>PRINT OPTIONS
    >>WHAT
      ALL MASS FRACTIONS
    >>WHERE
      ALL J PLANES
      ALL BLOCKS
    >>WHEN
      FINAL SOLUTION
>>STOP
```

TABLE OF RESULTS

Table D.1 Variation of the Initial Heating Time with Burner Diameter (Figure 6.6)

ACTUAL BURNER DIAMETER (m)	HEATING TIME (hrs)	
	LFM (7 Gas Zones)	13 Gas Zones
0.14	1.99	1.56
0.19	1.88	1.57
0.28	1.75	1.6
0.42	1.67	1.85

Table D.2 The Effect of Set Point Temperature on the Performance of the LFM and 13 Gas Zone Model (Figure 6.9)

SET POINT TEMPERATURE (°C)	LFM (7 GAS ZONES)			13 GAS ZONES		
	Heating Time (hrs)	Total Fuel Consumed (GJ)	Load Temperature Difference (°C)	Heating Time (hrs)	Total Fuel Consumed (GJ)	Load Temperature Difference (°C)
1380	1.88	36.5	87.3	1.57	30.3	97.5
1360	1.88	36.5	87.3	1.57	30.3	97.5
1340	1.88	36.5	87.3	1.58	30.5	94.8
1320	1.92	37	79.1	1.67	31.7	77.8
1300	2.05	38.3	66.6	1.94	34.6	58.7

Table D.3 The Effect of Set Point Temperature on the Performance of the 25 and 37 Gas Zone Models (Figure 6.12)

SET POINT TEMPERATURE (°C)	25 GAS ZONES			37 GAS ZONES		
	Heating Time (hrs)	Total Fuel Consumed (GJ)	Load Temperature Difference (°C)	Heating Time (hrs)	Total Fuel Consumed (GJ)	Load Temperature Difference (°C)
1380	1.97	38.1	86.6	1.94	37.6	87.6
1360	1.97	38.1	86.6	1.94	37.6	87
1340	1.97	38.1	86.6	1.98	38.1	77.9
1320	2.02	38.8	75.6	2.17	40.1	61.5
1300	2.23	41.1	58.5	2.76	45.5	44.6

Table D.4a Variation of Heating Time with Burner Diameter (Figure 7.2)

ACTUAL BURNER DIAMETER (m)	HEATING TIME (hrs)			
	SPT=1380°C	SPT=1360°C	SPT=1340°C	SPT=1320°C
0.14	2.02	2.02	2.06	2.27
0.19	1.94	1.94	1.98	2.17
0.28	1.82	1.9	2.09	2.55
0.42	1.98	2.12	2.44	3.22

Table D.4b Variation of Total Fuel Consumption with Burner Diameter (Figure 7.2)

ACTUAL BURNER DIAMETER (m)	TOTAL FUEL CONSUMPTION (GJ)			
	SPT=1380°C	SPT=1360°C	SPT=1340°C	SPT=1320°C
0.14	39.1	39.1	39.7	41.8
0.19	37.6	37.6	38.1	40.1
0.28	35.3	36.2	38.1	42.2
0.42	38.1	39.5	42.3	48.2

Table D.4c Variation of Load Temperature Difference with Burner Diameter (Figure 7.2)

ACTUAL BURNER DIAMETER (m)	LOAD TEMPERATURE DIFFERENCE (°C)			
	SPT=1380°C	SPT=1360°C	SPT=1340°C	SPT=1320°C
0.14	85.2	85.2	75.7	59.2
0.19	87.6	87.6	77.9	61.5
0.28	90.7	77.3	62.4	48.1

0.42	82.6	67.7	53.5	40.5

Table D.5a Variation of Heating Time with Burner Firing Position (Figure 7.6)

SET POINT TEMPERATURE (°C)	HEATING TIME (hrs)		
	Upper Horizontal	Upper Inclined	Lower Horizontal
1380	1.94	1.68	2.15
1360	1.94	1.68	2.15
1340	1.98	1.68	2.19
1320	2.17	1.74	2.33
1300	2.76	1.91	2.71

Table D.5b Variation of Total Fuel Consumption with Burner Firing Position (Figure 7.6)

SET POINT TEMPERATURE (°C)	TOTAL FUEL CONSUMPTION (GJ)		
	Upper Horizontal	Upper Inclined	Lower Horizontal
1380	37.6	32.6	41.6
1360	37.6	32.6	41.6
1340	38.1	32.6	42
1320	40.1	33.3	43.6
1300	45.5	35.1	47

Table D.5c Variation of Load Temperature Difference with Burner Firing Position (Figure 7.6)

SET POINT TEMPERATURE (°C)	LOAD TEMPERATURE DIFFERENCE (°C)		
	Upper Horizontal	Upper Inclined	Lower Horizontal
1380	1380	87.6	96.5
1360	1360	87.6	96.5
1340	1340	77.9	96.2
1320	1320	61.5	82.9
1300	1300	44.6	66.3

Table D.6a Variation of Heating Time with Burner Thermal Input (Figure 7.7)

SET POINT TEMPERATURE (°C)	HEATING TIME (hrs)			
	4.6MW	5MW	5.4MW	5.8MW
1380	2.33	2.1	1.94	1.79
1360	2.33	2.1	1.94	1.79
1340	2.33	2.12	1.98	1.86

1320	2.47	2.3	2.17	2.05
1300	3.04	2.88	2.76	2.65

Table D.6b Variation of Total Fuel Consumption with Burner Thermal Input (Figure 7.7)

SET POINT TEMPERATURE (°C)	TOTAL FUEL CONSUMPTION (GJ)			
	4.6MW	5MW	5.4MW	5.8MW
1380	38.3	37.8	37.6	37.4
1360	38.3	37.8	37.6	37.4
1340	38.4	38.1	38.1	38.3
1320	39.9	39.9	40.1	40.4
1300	45	45.2	45.5	45.8

Table D.6c Variation of Load Temperature Difference with Burner Thermal Input (Figure 7.7)

SET POINT TEMPERATURE (°C)	LOAD TEMPERATURE DIFFERENCE (°C)			
	4.6MW	5MW	5.4MW	5.8MW
1380	75.2	81.9	87.6	94.1
1360	75.2	81.9	87.6	93.3
1340	73.8	76.4	77.9	79.2
1320	59.4	60.6	61.5	62.4
1300	43.2	44	44.6	45.2

Table D.7a Variation of Heating Time with Control Sensor Position for the Horizontal Burners (Figure 7.8)

SET POINT TEMPERATURE (°C)	HEATING TIME (hrs)		
	2nd Roof	3rd Roof	4th Roof
1380	1.94	1.94	1.98
1360	1.94	1.94	2.15
1340	1.98	1.94	2.65
1320	2.17	1.94	4.16
1300	2.76	1.94	8.29

Table D.7b Variation of Total Fuel Consumption with Control Sensor Position for the Horizontal Burners (Figure 7.8)

SET POINT TEMPERATURE (°C)	TOTAL FUEL CONSUMPTION (GJ)		
	2nd Roof	3rd Roof	4th Roof
1380	38	37.6	37.6
1360	40	37.6	37.6
1340	44.4	38.1	37.6
1320	55.2	40.1	37.6
1300	75.9	45.5	37.6

Table D.7c Variation of Load Temperature Difference with Control Sensor Position for the Horizontal Burners (Figure 7.8)

SET POINT TEMPERATURE (°C)	LOAD TEMPERATURE DIFFERENCE (°C)		
	2nd Roof	3rd Roof	4th Roof
1380	79.1	87.6	87.6
1360	62.8	87.6	87.6
1340	47.2	77.9	87.6
1320	32.8	61.5	87.6
1300	21.3	44.6	85.2

Table D.8a Variation of Heating Time with Control Sensor Position for the Inclined Burners (Figure 7.9)

SET POINT TEMPERATURE (°C)	HEATING TIME (hrs)		
	2nd Roof	3rd Roof	4th Roof
1380	1.68	1.68	1.68
1360	1.68	1.68	1.68
1340	1.71	1.68	1.68
1320	1.84	1.74	1.69
1300	2.18	1.91	1.78

Table D.8b Variation of Total Fuel Consumption with Control Sensor Position for the Inclined Burners (Figure 7.9)

SET POINT TEMPERATURE (°C)	TOTAL FUEL CONSUMPTION (GJ)		
	2nd Roof	3rd Roof	4th Roof
1380	1.68	1.68	1.68
1360	1.68	1.68	1.68
1340	1.71	1.68	1.68
1320	1.84	1.74	1.69
1300	2.18	1.91	1.78

Table D.8c Variation of Load Temperature Difference with Control Sensor Position for the Inclined Burners (Figure 7.9)

SET POINT TEMPERATURE (°C)	LOAD TEMPERATURE DIFFERENCE (°C)		
	2nd Roof	3rd Roof	4th Roof
1380	96.5	96.5	96.5
1360	96.5	96.5	96.5
1340	88.2	96.5	96.5
1320	71.4	82.9	92.6
1300	53.8	66.3	77.1

Table D.9a The Effect of Different Furnace Linings on the Heating Time for Horizontal Burners (Figure 7.10)

SET POINT TEMPERATURE (°C)	HEATING TIME (hrs)		
	Basecase	All Dense Refractory	All Ceramic Fibre
1380	1.94	2.43	0.79
1360	1.94	2.43	0.81
1340	1.98	2.43	0.85
1320	2.17	2.43	0.9
1300	2.76	2.43	0.97

Table D.9b The Effect of Different Furnace Linings on the Total Fuel Consumption for Horizontal Burners (Figure 7.10)

SET POINT TEMPERATURE (°C)	TOTAL FUEL CONSUMPTION (GJ)		
	Basecase	All Dense Refractory	All Ceramic Fibre
1380	37.6	47.1	15.2
1360	37.6	47.1	15.3
1340	38.1	47.1	15.5
1320	40.1	47.1	15.6
1300	45.5	47.2	15.8

Table D.9c The Effect of Different Furnace Linings on the Load Temperature Difference for Horizontal Burners (Figure 7.10)

SET POINT TEMPERATURE (°C)	LOAD TEMPERATURE DIFFERENCE (°C)		
	Basecase	All Dense Refractory	All Ceramic Fibre
1380	87.6	71.6	98.9
1360	87.6	71.6	83.5
1340	77.9	71.6	68.4
1320	61.5	71.6	53.9
1300	44.6	69.9	40

Table D.10a The Effect of Different Furnace Linings on the Heating Time for Inclined Burners (Figure 7.11)

SET POINT TEMPERATURE (°C)	HEATING TIME (hrs)		
	Basecase	All Dense Refractory	All Ceramic Fibre
1380	1.68	2.05	0.71
1360	1.68	2.05	0.73
1340	1.68	2.05	0.75
1320	1.74	2.05	0.79
1300	1.91	2.05	0.84

Table D.10b The Effect of Different Furnace Linings on the Total Fuel Consumption for Inclined Burners (Figure 7.11)

SET POINT TEMPERATURE (°C)	TOTAL FUEL CONSUMPTION (GJ)		
	Basecase	All Dense Refractory	All Ceramic Fibre
1380	32.6	39.7	13.7
1360	32.6	39.7	13.9
1340	32.6	39.7	14.1
1320	33.3	39.7	14.2
1300	35.1	39.7	14.4

Table D.10c The Effect of Different Furnace Linings on the Load Temperature Difference for Inclined Burners (Figure 7.11)

SET POINT TEMPERATURE (°C)	LOAD TEMPERATURE DIFFERENCE (°C)		
	Basecase	All Dense Refractory	All Ceramic Fibre
1380	32.6	39.7	13.7
1360	32.6	39.7	13.9
1340	32.6	39.7	14.1
1320	33.3	39.7	14.2
1300	35.1	39.7	14.4

Table D.11 The Effect of Combustion Air Preheating on Furnace Performance (Figure 7.12)

SET POINT TEMPERATURE (°C)	COLD AIR			COMBUSTION AIR PREHEATING		
	Heating Time (hrs)	Total Fuel Consumed (GJ)	Load Temperature Difference (°C)	Heating Time (hrs)	Total Fuel Consumed (GJ)	Load Temperature Difference (°C)
1380	1.94	37.6	87.6	1.44	27.7	114.2
1360	1.94	37.6	87.6	1.5	28.4	97.1
1340	1.98	38.1	77.9	1.63	29.5	79.5
1320	2.17	40.1	61.5	1.88	31.5	62.1
1300	2.76	45.5	44.6	2.56	36.3	44.6

Table D.12a Variation of Heating Time with Excess Air (Figure 7.14)

SET POINT TEMPERATURE (°C)	HEATING TIME (hrs)			
	5%	10%	15%	20%
1380	1.94	2.1	2.28	2.49
1360	1.94	2.1	2.28	2.49
1340	1.98	2.12	2.28	2.49
1320	2.17	2.27	2.39	2.55

1300	2.76	2.8	2.87	2.97

Table D.12b Variation of Total Fuel Consumption with Excess Air (Figure 7.14)

SET POINT TEMPERATURE (°C)	TOTAL FUEL CONSUMPTION (GJ)			
	5%	10%	15%	20%
1380	1.94	2.1	2.28	2.49
1360	1.94	2.1	2.28	2.49
1340	1.98	2.12	2.28	2.49
1320	2.17	2.27	2.39	2.55
1300	2.76	2.8	2.87	2.97

Table D.12c Variation of Load Temperature Difference with Excess Air (Figure 7.14)

SET POINT TEMPERATURE (°C)	LOAD TEMPERATURE DIFFERENCE (°C)			
	5%	10%	15%	20%
1380	87.6	80.9	74.5	68.4
1360	87.6	80.9	74.5	68.4
1340	77.9	77.2	74.5	68.4
1320	61.5	61.7	61.6	61.2
1300	44.6	45	45.3	45.4

Table D.13a Variation of Load Temperature Difference with Load Throughput for the 7 (LFM), 13 and 25 Zone Models (Figure 8.5)

LFM 7 GAS ZONES		13 GAS ZONES		25 GAS ZONES	
Load Throughput, t/hr	Load Temperature Difference, °C	Load Throughput, t/hr	Load Temperature Difference, °C	Load Throughput, t/hr	Load Temperature Difference, °C
7.4	86.2	7.2	74.3	6.8	51.8
7.1	81.1	6.9	69.1	6.6	47.5
6.8	75.3	6.6	63.5	6.3	43.7
6.4	69.9	6.3	57.0	6.0	39.0
6.2	63.5	6.0	51.7	5.8	34.1

Table D.13b Variation of Load Temperature Difference with Load Throughput for the 10 (LFM and 37 Zone Models (Figure 8.5)

LFM 10 GAS ZONES		37 GAS ZONES	
Load Throughput, t/hr	Load Temperature Difference, °C	Load Throughput, t/hr	Load Temperature Difference, °C
7.9	111.7	7.0	50.4
7.6	105.8	6.7	46.5

7.2	99.9	6.4	42.0
6.8	92.6	6.1	37.5
6.5	85.9	5.8	31.9

Table D.13c Variation of Load Temperature Difference with Load Throughput for the 14 (LFM and 50 Zone Models (Figure 8.5)

LFM 14 GAS ZONES		50 GAS ZONES	
Load Throughput, t/hr	Load Temperature Difference, °C	Load Throughput, t/hr	Load Temperature Difference, °C
8.1	115.2	7.1	52.2
7.8	109.3	6.8	47.8
7.4	102.6	6.5	43.5
7.0	95.4	6.2	39.2
6.7	89.3	5.9	34.7

Table D.14a Variation of the Set Point Temperature with Load Throughput for the 7 (LFM), 13 and 25 Zone Models (Figure 8.8)

LFM 7 GAS ZONES		13 GAS ZONES		25 GAS ZONES	
Load Throughput, t/hr	Load Temperature Difference, °C	Load Throughput, t/hr	Load Temperature Difference, °C	Load Throughput, t/hr	Load Temperature Difference, °C
7.4	1281.9	7.2	1316.5	6.8	1287.3
7.1	1275.7	6.9	1309.8	6.6	1282.6
6.8	1269.1	6.6	1303.4	6.3	1277.6
6.4	1261.7	6.3	1297.2	6.0	1271.7
6.2	1255.3	6.0	1291.2	5.8	1268.3

Table D.14b Variation of the Set Point Temperature with Load Throughput for the 10 (LFM and 37 Zone Models (Figure 8.8)

LFM 10 GAS ZONES		37 GAS ZONES	
Load Throughput, t/hr	Load Temperature Difference, °C	Load Throughput, t/hr	Load Temperature Difference, °C
7.9	1303.7	7.0	1313.7
7.6	1296.6	6.7	1307.9
7.2	1289.2	6.4	1302.8
6.8	1280.9	6.1	1296.4
6.5	1272.6	5.8	1290.8

Table D.14c Variation of the Set Point Temperature with Load Throughput for the 14 (LFM and 50 Zone Models (Figure 8.8)

LFM 14 GAS ZONES		50 GAS ZONES	
Load Throughput, t/hr	Load Temperature Difference, °C	Load Throughput, t/hr	Load Temperature Difference, °C
8.1	1308.6	7.1	1316.5
7.8	1301.9	6.8	1311.4
7.4	1294.1	6.5	1305.2
7.0	1285.6	6.2	1297.8
6.7	1278.0	5.9	1293.3

Table D.15a Variation of the Steady-State Efficiency with Load Throughput for the 7 (LFM), 13 and 25 Zone Models (Figure 8.10)

LFM 7 GAS ZONES		13 GAS ZONES		25 GAS ZONES	
Load Throughput, t/hr	Load Temperature Difference, °C	Load Throughput, t/hr	Load Temperature Difference, °C	Load Throughput, t/hr	Load Temperature Difference, °C
7.4	47.5	7.2	46.7	6.8	44.7
7.1	48.0	6.9	47.2	6.6	45.3
6.8	48.6	6.6	47.8	6.3	45.9
6.4	49.2	6.3	48.4	6.0	46.5
6.2	49.8	6.0	49.0	5.8	47.1

Table D.15b Variation of the Set Point Temperature with Load Throughput for the 10 (LFM and 37 Zone Models (Figure 8.10)

LFM 10 GAS ZONES		37 GAS ZONES	
Load Throughput, t/hr	Load Temperature Difference, °C	Load Throughput, t/hr	Load Temperature Difference, °C
7.9	49.1	7.0	45.1
7.6	49.7	6.7	45.7
7.2	50.3	6.4	46.3
6.8	51.0	6.1	47.0
6.5	51.6	5.8	47.8

Table D.15c Variation of the Set Point Temperature with Load Throughput for the 14 (LFM and 50 Zone Models (Figure 8.10)

LFM 14 GAS ZONES		50 GAS ZONES	
Load Throughput, t/hr	Load Temperature Difference, °C	Load Throughput, t/hr	Load Temperature Difference, °C
8.1	50.3	7.1	46.0
7.8	50.9	6.8	46.6
7.4	51.5	6.5	47.3
7.0	52.2	6.2	48.0
6.7	52.9	5.9	48.6

Table D.16a Comparison of Load Temperature Difference for the 2D Steady-State Zone Models (Figure 8.11)

13 GAS ZONES		25 GAS ZONES		37 GAS ZONES		50 GAS ZONES	
Load Throughput, t/hr	Load Temperature Difference, °C	Load Throughput, t/hr	Load Temperature Difference, °C	Load Throughput, t/hr	Load Temperature Difference, °C	Load Throughput, t/hr	Load Temperature Difference, °C
7.2	74.3	6.8	51.8	7.0	50.4	7.1	52.2
6.9	69.1	6.6	47.5	6.7	46.5	6.8	47.8
6.6	63.5	6.3	43.7	6.4	42.0	6.5	43.5
6.3	57.0	6.0	39.0	6.1	37.5	6.2	39.2
6.0	51.7	5.8	34.1	5.8	31.9	5.9	34.7

Table D.16b Comparison of Roof Set Point Temperature for the 2D Steady-State Zone Models (Figure 8.11)

13 GAS ZONES		25 GAS ZONES		37 GAS ZONES		50 GAS ZONES	
Load Throughput, t/hr	Set Point Temperature, °C	Load Throughput, t/hr	Set Point Temperature, °C	Load Throughput, t/hr	Set Point Temperature, °C	Load Throughput, t/hr	Set Point Temperature, °C
7.2	1316.5	6.8	1287.3	7.0	1313.7	7.1	1316.5
6.9	1309.8	6.6	1282.6	6.7	1307.9	6.8	1311.4
6.6	1303.4	6.3	1277.6	6.4	1302.8	6.5	1305.2
6.3	1297.2	6.0	1271.7	6.1	1296.4	6.2	1297.8
6.0	1291.2	5.8	1268.3	5.8	1290.8	5.9	1293.3

Table D.16c Comparison of the Steady-State Efficiency for the 2D Steady-State Zone Models (Figure 8.11)

13 GAS ZONES		25 GAS ZONES		37 GAS ZONES		50 GAS ZONES	
Load Throughput, t/hr	Steady-State Efficiency, %	Load Throughput, t/hr	Steady-State Efficiency, %	Load Throughput, t/hr	Steady-State Efficiency, %	Load Throughput, t/hr	Steady-State Efficiency, %
7.2	46.7	6.8	44.7	7.0	45.1	7.1	46.0
6.9	47.2	6.6	45.3	6.7	45.7	6.8	46.6
6.6	47.8	6.3	45.9	6.4	46.3	6.5	47.3
6.3	48.4	6.0	46.5	6.1	47.0	6.2	48.0
6.0	49.0	5.8	47.1	5.8	47.8	5.9	48.6

Table D.17 The Effect of Refractory Heat Losses on Furnace Performance (Figure 8.14)

NO REFRACTORY LOSSES				REFRACTORY LOSSES			
Load Throughput, t/hr	Load Temperature Difference, °C	Set Point Temperature, °C	Steady-State Efficiency, %	Load Throughput, t/hr	Load Temperature Difference, °C	Set Point Temperature, °C	Steady-State Efficiency, %
7.0	50.4	1313.7	45.1	6.1	44.3	1302.4	40.8
6.7	46.5	1307.9	45.7	5.8	38.9	1295.9	41.3
6.4	42.0	1302.8	46.3	5.5	35.0	1291.0	41.6
6.1	37.5	1296.4	47.0	5.3	28.0	1280.9	42.2
5.8	31.9	1290.8	47.8	5.0	23.5	1274.3	42.7

Table D.18 Variation of Furnace Performance with Burner Orientation for Steady-State Conditions (Figure 8.16)

HORIZONTAL BURNERS				INCLINED BURNERS			
Load Throughput, t/hr	Load Temperature Difference, °C	Set Point Temperature, °C	Steady-State Efficiency, %	Load Throughput, t/hr	Load Temperature Difference, °C	Set Point Temperature, °C	Steady-State Efficiency, %
7.0	50.4	1313.7	45.1	7.3	65.8	1304.6	46.9
6.7	46.5	1307.9	45.7	7.0	60.6	1298.6	47.5
6.4	42.0	1302.8	46.3	6.7	56.3	1292.5	48.1
6.1	37.5	1296.4	47.0	6.4	49.9	1284.9	48.8
5.8	31.9	1290.8	47.8	6.1	46.1	1278.6	49.5

Table D.19a The Variation of Load Temperature Difference with Furnace Length for Steady-State Conditions (Figure 8.20)

BASELINE (37 ZONES)		38 ZONES		39 ZONES		40 ZONES	
Load Throughput, t/hr	Load Temperature Difference, °C	Load Throughput, t/hr	Load Temperature Difference, °C	Load Throughput, t/hr	Load Temperature Difference, °C	Load Throughput, t/hr	Load Temperature Difference, °C
7.0	50.4	7.5	52.2	7.9	54.0	8.0	51.5
6.7	46.5	7.2	47.6	7.6	50.7	7.7	48.6
6.4	42.0	6.9	43.4	7.3	46.9	7.4	44.2
6.1	37.5	6.5	37.9	7.0	41.6	7.0	39.6
5.8	31.9	6.2	33.2	6.7	37.3	6.7	34.8

Table D.19b Variation of Set Point Temperature with Furnace Length for Steady-State Conditions (Figure 8.20)

BASELINE (37 ZONES)		38 ZONES		39 ZONES		40 ZONES	
Load Throughput, t/hr	Set Point Temperature, °C	Load Throughput, t/hr	Set Point Temperature, °C	Load Throughput, t/hr	Set Point Temperature, °C	Load Throughput, t/hr	Set Point Temperature, °C
7.0	1313.7	7.5	1316.5	7.9	1319.0	8.0	1316.5
6.7	1307.9	7.2	1310.6	7.6	1314.4	7.7	1311.5
6.4	1302.8	6.9	1305.8	7.3	1309.0	7.4	1306.2
6.1	1296.4	6.5	1300.2	7.0	1302.6	7.0	1300.2
5.8	1290.8	6.2	1296.6	6.7	1298.8	6.7	1296.3

Table D.19c Variation of Steady-State Efficiency with Furnace Length for Steady-State Conditions (Figure 8.20)

BASELINE (37 ZONES)		38 ZONES		39 ZONES		40 ZONES	
Load Throughput, t/hr	Steady-State Efficiency, %	Load Throughput, t/hr	Steady-State Efficiency, %	Load Throughput, t/hr	Steady-State Efficiency, %	Load Throughput, t/hr	Steady-State Efficiency, %
7.0	45.1	7.5	48.1	7.9	51.3	8.0	54.7
6.7	45.7	7.2	48.7	7.6	52.0	7.7	55.4
6.4	46.3	6.9	49.3	7.3	52.6	7.4	56.2
6.1	47.0	6.5	50.1	7.0	53.4	7.0	57.0
5.8	47.8	6.2	50.6	6.7	54.1	6.7	57.7

Table D.20 The Effect of Sensor Position on the Set Point Temperature at Different Load Throughput (Figure 8.22)

HORIZONTAL BURNERS				INCLINED BURNERS			
Load Throughput, t/hr	2nd Roof	3rd Roof	4th Roof	Load Throughput, t/hr	2nd Roof	3rd Roof	4th Roof
7.0	1313.7	1363.1	1247.4	7.3	1304.6	1325.7	1283.2
6.7	1307.9	1357.5	1241.4	7.0	1298.6	1320.0	1276.9
6.4	1302.8	1352.6	1236.5	6.7	1292.5	1314.0	1270.7
6.1	1296.4	1346.3	1230.4	6.4	1284.9	1306.8	1262.9
5.8	1290.8	1340.8	1224.6	6.1	1278.6	1300.8	1256.6

Table D.21 The Effect of the Convective Heat Transfer Coefficient on the Overall Steady-State Furnace Performance (Figure 8.23)

$H=25 W/m^2K$				$H=5 W/m^2K$			
Load Throughput, t/hr	Load Temperature Difference, °C	Set Point Temperature, °C	Steady-State Efficiency, %	Load Throughput, t/hr	Load Temperature Difference, °C	Set Point Temperature, °C	Steady-State Efficiency, %
7.0	50.4	1313.7	45.1	6.6	49.3	1310.3	43.0
6.7	46.5	1307.9	45.7	6.4	44.9	1305.0	43.6
6.4	42.0	1302.8	46.3	6.1	40.7	1298.7	44.2
6.1	37.5	1296.4	47.0	5.8	35.5	1292.7	44.8
5.8	31.9	1290.8	47.8	5.6	30.7	1284.7	45.7

Table D.22 The Effect of Combustion Air Preheating on the Overall Steady-State Furnace Performance (Figure 8.25)

COLD AIR				COMBUSTION AIR PREHEATING			
Load Throughput, t/hr	Load Temperature Difference, °C	Set Point Temperature, °C	Steady-State Efficiency, %	Load Throughput, t/hr	Load Temperature Difference, °C	Set Point Temperature, °C	Steady-State Efficiency, %
8.0	66.9	1333.1	42.9	8.2	76.5	1346.7	55.4
7.6	58.0	1323.1	44.0	7.9	69.6	1339.3	55.9
7.0	50.4	1313.7	45.1	7.5	62.9	1331.1	56.5
6.7	46.5	1307.9	45.7	7.1	56.3	1323.8	57.1
6.4	42.0	1302.8	46.3	6.7	48.5	1314.9	57.7
6.1	37.5	1296.4	47.0	-	-	-	-
5.8	31.9	1290.8	47.8	-	-	-	-

Table D.23 The Effect of Furnace Length and Combustion Air Preheating on the Steady-State Efficiency (Figure 8.27)

BASELINE FURNACE				LONGEST FURNACE			
Cold Air		Combustion Air Preheating		Cold Air		Combustion Air Preheating	
Load Throughput, t/hr	Steady-State Efficiency, %	Load Throughput, t/hr	Steady-State Efficiency, %	Load Throughput, t/hr	Steady-State Efficiency, %	Load Throughput, t/hr	Steady-State Efficiency, %
8.0	42.9	8.2	55.4	8.0	54.7	8.8	63.5
7.6	44.0	7.9	55.9	7.7	55.4	8.4	64.1
7.0	45.1	7.5	56.5	7.4	56.2	8.0	64.7
6.7	45.7	7.1	57.1	7.0	57.0	7.6	65.4
6.4	46.3	6.7	57.7	6.7	57.7	7.2	66.2
6.1	47.0	-	-	-	-	-	-
5.8	47.8	-	-	-	-	-	-

Table D.24 The Effect of Combustion Air Preheating on Furnace Performance (Figure 9.3)

SET POINT TEMPERATURE (°C)	NOZZLE MIX BURNERS			DIFFUSION FLAME BURNERS		
	Heating Time (hrs)	Total Fuel Consumed (GJ)	Load Temperature Difference (°C)	Heating Time (hrs)	Total Fuel Consumed (GJ)	Load Temperature Difference (°C)
1380	2.62	50.5	71.9	2.96	57.4	69.9
1340	3.25	56.2	45.3	3.13	59.4	54.6
1320	4.45	64.9	33.7	3.98	67.4	37.8
1300	7.24	80.1	24.1	7.67	91.9	23.2

Table D.25a Variation of Heating Time with Control Sensor Position for Different Burner Types (Figure 9.20)

SET POINT TEMPERATURE (°C)	HEATING TIME (hrs)		
	Nozzle Mix (5% Exair)	Diffusion Flame (5% Exair)	Diffusion Flame (10% Exair)
1380	2.62	2.96	3.31
1340	3.25	3.32	3.47
1320	4.45	4.45	4.39
1300	7.24	7.7	7.73

Table D.25b Variation of Total Fuel Consumption with Control Sensor Position for Different Burner Types (Figure 9.20)

SET POINT TEMPERATURE (°C)	TOTAL FUEL CONSUMPTION (GJ)		
	Nozzle Mix (5% Exair)	Diffusion Flame (5% Exair)	Diffusion Flame (10% Exair)
1380	50.5	57.5	64.1
1340	56.2	61.3	66
1320	64.9	71.1	75.4
1300	80.1	91.5	99.3

Table D.25c Variation of Load Temperature Difference with Control Sensor Position for Different Burner Types (Figure 9.20)

SET POINT TEMPERATURE (°C)	LOAD TEMPERATURE DIFFERENCE (°C)		
	Nozzle Mix (5% Exair)	Diffusion Flame (5% Exair)	Diffusion Flame (10% Exair)
1380	71.9	68.9	61.4
1340	45.3	48.1	50.2
1320	33.7	34.5	35.7
1300	24.1	23.3	23.3

Published papers arising from this study

1. Ward J., Correia, S.A.C., Sousa, J.L.V.A, Nov. 1999, "The Application of Multi-Zone Thermal Radiation Models to Investigate the Energy Efficiency of a Metal Reheating Furnace Under Start-Up Conditions", *Proc. of the ASME*, AES-Vol. 39, pp 621-626, Nashville, USA.

2. Correia, S.A.C., Ward, J., Sousa, J.L.V.A., Sept. 2000," Application of a Multi-Zone Two-Dimensional Thermal Radiation for Control of a Metal Reheating Furnace Under Transient Conditions", Proc. *3rd European Thermal Sciences Conf.*, vol 1, pp 599-604, Heidelberg, Germany.

3. Ward, J. and Sousa, J.L.V.A., Nov. 2000, "Numerical Prediction of the Transient Operation of a Gas-Fired Reheating Furnace", *Proc. of the ASME*, HTD-vol 367, pp 87-94,Orlando, USA.

Abstracts sent for publication

1. Correia, S.A.C., Ward, J., Sousa, J.L.V.A., April 2002,"The Application of a Range of Zone Models to Predict the Thermal Behaviour of a Continuously Operated Metal Reheating Furnace", accepted for presentation at the *6th European Conference on Industrial Furnaces and Boilers*, Lisbon, Portugal.

2. Correia, S.A.C., Ward, J., Sousa, J.L.V.A., Aug. 2002,"Comparison of the Use of a Range of Multi-Zone Models of a Continuously Operated Metal Reheating Furnace", accepted for presentation at the *12th Int. Heat Transfer Conference*, Grenoble, France.